Wrocław University
of Science and Technology

Faculty of Fundamental Problems of Technology
Department of Biomedical Engineering

Doctoral dissertation

ASSESSMENT OF CEREBRAL COMPLIANCE BASED ON ANALYSIS OF THE SHAPE OF INTRACRANIAL PRESSURE PULSE WAVEFORM

Agnieszka Kazimierska, MSc

Supervisors

Magdalena Kasprowicz, PhD, DSc
Wrocław University of Science and Technology, Poland

Prof. Marek Czosnyka, PhD, DSc
University of Cambridge, United Kingdom

Wrocław 2022

Acknowledgements

This dissertation is the result of numerous studies that I have done over several years. As with most journeys, some of it was easy; some of it was not. Luckily, I did not have to make that journey alone.

First and foremost, I would like to thank my supervisors, Professor Magdalena Kasprowicz and Professor Marek Czosnyka, for their guidance, continuous encouragement, and endless patience. Their knowledge and experience have been invaluable in making this dissertation happen and I couldn't be more grateful for the opportunities that I have been offered.

I would like to thank the Biomedical Signal Processing Group at Wroclaw University of Science and Technology, especially the BrainLab team, for all the time we spent working together and all the fun we had in the meantime.

I would also like to thank the Brain Physics Lab at the University of Cambridge whom I had the pleasure to visit during my PhD studies for showing me new and exciting research directions as well as a great time in Cambridge.

Finally, I would like to thank my parents and my friends who have supported me tirelessly, always encouraged my passion for learning, and never stopped believing in me.

Contents

Summary

Patient management in modern neurocritical care units relies heavily on brain multimodal monitoring, including secondary indices describing the homeostasis of the nervous and circulatory systems. Interdisciplinary approaches combining the field of medicine with technological advances play a crucial role in improving patient care through development of novel diagnostic tools, predictive models, and therapeutic strategies. Still, despite decades of study, our understanding of the pressure–volume relationships in the intracranial space, and consequently, available management approaches for treatment of intracranial pathologies, remain incomplete. Since Lundberg's seminal 1965 paper on continuous intracranial pressure (ICP) monitoring, various attempts have been made to precisely characterise traumatic brain injury (TBI) patients and predict impending deterioration of their condition. Cerebrospinal compliance, defined as the ratio of change in volume to change in pressure and describing the cerebrospinal system's ability to buffer changes in volume without potentially threatening increases in pressure, is often considered as a promising tool to improve patient care. Diminished compliance indicates that even a relatively small volume increment may produce disproportionately large increase in ICP. In turn, ICP elevation is a hazardous condition as it may lead to restricted cerebral blood flow or mechanical damage to the brain. Therefore, identification of TBI patients at risk of increases in ICP before a hypertension episode occurs could allow for early therapeutic intervention and help prevent the adverse effects from taking place, in contrast to currently employed protocols where ICP elevation is managed rather than averted. Compliance could also complement the current methods of assessing cerebrospinal fluid dynamics in hydrocephalus, as in this group evaluation of the patient's volume–pressure compensation is included in the decision process for shunt implantation.

However, none of the methods of compliance estimation suggested to date have been successfully incorporated into routine clinical practice. The earliest proposed approaches, dating back to the 1970s, are based on manipulation of intracranial volume through either bolus injection or constant rate infusion of fluid. Although these techniques remain the primary method of direct compliance assessment, their clinical applicability is limited due to the fact that they are additionally invasive, can only be performed intermittently, and may be too dangerous in patients already at risk of uncontrolled ICP elevation. Imaging techniques such as magnetic resonance imaging can be used to measure changes in intracranial volume without external manipulation, but they cannot be employed in continuous monitoring, and the measurements are still relatively expensive. On the other hand, it has been shown in the 1980s that information on cerebrospinal compliance may be derived indirectly through analysis of the ICP pulse waveform, i.e. the shape of the signal over a single cardiac cycle. In normal conditions, the waveform contains three characteristic local maxima, called peaks P1, P2, and P3. As compliance decreases and

ICP increases, the height of the second peak increases to a greater extent than the other two. Therefore, it has been suggested that the height ratio of the first two peaks may be used to estimate compliance. However, the ICP pulse waveform presents a large variety of complex shapes, changing both over time and between subjects, which makes peak detection a highly challenging task. The solutions proposed so far have not gained widespread acceptance or been introduced to clinical practice, and the validity of the peak ratio as a measure of compliance has never been conclusively proven. Moreover, it has been shown that at very high ICP the pulse waveform becomes rounded and the peaks are no longer distinguishable, which causes peak detection to fail. More recently, a different approach was proposed. In this technique, four characteristic shapes of the ICP pulse waveform, roughly reflecting the changing configuration of peaks associated with changes in compliance, were described using radial basis function approximation and classified using an artificial neural network. A study in hydrocephalus patients showed that automatic morphological classification is a promising new tool for indirect compliance estimation, although further results using this method have not been published.

Building upon the groundwork laid down in previous studies, this dissertation addresses the problem of compliance estimation through analysis of the shape of ICP pulse waveform. Firstly, the peak ratio approach is compared with other known methods of compliance estimation during controlled changes in mean ICP in order to confirm the validity of using ICP pulse morphology as an indirect measure of cerebrospinal compliance. Secondly, the existing body of knowledge on compliance-related changes in ICP pulse waveform morphology is integrated with new developments in the field of machine learning in order to propose a novel solution for continuous monitoring of compliance. As ICP measurement in TBI patients is usually performed over several days, producing recordings that contain hundreds of thousands of individual pulses, assessment of ICP pulse morphology is already a challenging task due to the sheer volume of generated data. Taking that difficulty into account, the abovementioned pulse shape classification approach is combined for the first time with deep learning algorithms that rose to prominence in recent years as a tool for big data analysis. A deep neural network model, capable of classifying characteristic shapes of the ICP pulses and simultaneously detecting artefactual waveforms is developed, and a new index describing the ICP pulse morphology, termed pulse shape index (PSI), is introduced. It is demonstrated through a series of studies in patients with intracranial pathologies that features of the ICP pulse waveform can be used to monitor cerebrospinal volume compensation continuously and that assessment of the shape of the ICP pulse waveform using deep learning has the potential to improve neurocritical care management of TBI patients.

The studies presented in this dissertation were conducted as part of two research projects: National Science Centre (Poland) OPUS grant no UMO-2019/35/B/ST7/00500 (*Development of brain compliance monitoring methods by means of intracranial pressure pulse waveform analysis in traumatic brain injury*) and the National Agency for Academic Exchange (Poland) International Academic Partnerships programme (*Physics and engineering for future electronic, optical and medical technologies*; international collaboration with University of Cambridge, Cambridge, UK).

Selected results were published in the following papers:

- **Kazimierska, A.**, Kasprowicz, M., Czosnyka, M., Placek, M. M., Baledent, O., Smielewski, P., and Czosnyka, Z. (2021). Compliance of the cerebrospinal space: comparison of three methods. *Acta Neurochirurgica*, 163(7):1979–1989.
- Mataczyński, C.*, **Kazimierska, A.***, Uryga, A., Burzyńska, M., Rusiecki, A., and Kasprowicz, M. (2022). End-to-end automatic morphological classification of intracranial pressure pulse waveforms using deep learning. *IEEE Journal of Biomedical and Health Informatics*, 26(2):494–504. *joint first authorship
- **Kazimierska, A.**, Uryga, A., Mataczyński, C., Burzyńska, M., Ziółkowski, A., Rusiecki, A., and Kasprowicz, M. (2021). Analysis of the shape of intracranial pressure pulse waveform in traumatic brain injury patients. In *Annual International Conference of the IEEE Engineering in Medicine and Biology Society*, pages 546–549, Mexico. IEEE.

and are part of unpublished works:

- **Kazimierska, A.**, Uryga, A., Mataczyński, C., Pelah, A., Czosnyka, M., Kasprowicz, M., and the CENTER-TBI high resolution sub-study participants and investigators. The shape of intracranial pressure pulse waveform in traumatic brain injury: a CENTER-TBI study. Submitted to *Scientific Reports* journal in March 2022.
- Mataczyński, C., **Kazimierska, A.**, Uryga, A., Kasprowicz, M., and the CENTER-TBI high resolution sub-study participants and investigators. Intracranial pressure pulse morphology-based definition of life-threatening intracranial hypertension episodes. Accepted for publication at the *44th Annual International Conference of the IEEE Engineering in Medicine and Biology Society* (planned date: 11–15 July 2022, Glasgow, UK).

This dissertation includes six chapters.

Chapter 1 presents a review of ICP monitoring and the pressure–volume relationships in the cerebrospinal space, including the relevant physiology and clinical significance of compliance assessment, as well as an overview of the estimation methods proposed so far with emphasis on analysis of the ICP pulse waveform.

In Chapter 2, the aims of this thesis and the research hypotheses are outlined.

Chapter 3 discusses a comparison study in hydrocephalus patients between the 'gold standard' method of compliance estimation based on external manipulation of the intracranial volume and two indirect methods: an approach based on analysis of characteristic features of the ICP pulse waveform and another based on evaluation of changes in ICP pulse pressure in relation to changes in cerebral blood volume. The results of this study confirm the validity of using the P1/P2 ratio of the ICP pulse waveform as a measure of relative changes in compliance.

In Chapter 4, the feasibility of using deep learning to automatically classify characteristic shapes of the ICP pulse waveform, and therefore overcome the need for precise peak identification, is discussed. A residual neural network is proposed as a tool for morphological classification of individual ICP pulses and used to assess the potential clinical usefulness of this approach in long-term recordings obtained from TBI patients. The results show that it is possible to classify the ICP pulse waveform using deep neural networks with high accuracy and good generalisation.

Chapter 5 continues the investigation into ICP pulse waveform classification as a potential tool for continuous monitoring of the cerebrospinal volume compensation. A new index describing the ICP pulse waveform, PSI, is introduced and investigated in a large, multi-centre cohort of TBI patients. The relationship between PSI and other ICP-derived metrics is discussed in relation to the pressure–volume relationships in the cerebrospinal space. The results also show the link between the shape of ICP pulse waveform and outcome after TBI as well as the presence of mass lesions in the brain.

Conclusions of this dissertation along with suggestions for further investigations are presented in Chapter 6.

List of figures

List of tables

List of abbreviations

ABP	Arterial blood pressure [mm Hg]
AmpICP	Pulse amplitude of intracranial pressure [mm Hg]
AMP–P	Amplitude–pressure relationship (characteristic)
aSAH	Aneurysmal subarachnoid haemorrhage
CBF	Cerebral blood flow [ml/s]
CBFV	Cerebral blood flow velocity [cm/s]
CBV	Cerebral blood volume [ml]
CPP	Cerebral perfusion pressure [mm Hg]
CSF	Cerebrospinal fluid
CT	Computed tomography
EVD	External ventricular drain
GCS	Glasgow Coma Scale
GOS	Glasgow Outcome Scale
GOSE	Glasgow Outcome Scale Extended
HFC	High frequency centroid [Hz]
HHC	Higher harmonics centroid [no of harmonic]
ICP	Intracranial pressure [mm Hg]
IH	Intracranial hypertension
MOCAIP	Morphological clustering and analysis of continuous intracranial pressure (method of analysis and software package)
NPH	Normal pressure hydrocephalus
NCCU	Neurointensive care unit
P–V	Pressure–volume relationship (curve)
PRx	Pressure reactivity index [arbitrary units]
PSI	Pulse shape index [arbitrary units]
PVI	Pressure–volume index [ml]
RAP	Index of cerebrospinal compensatory reserve [arbitrary units]
ResNet	Residual neural network
TBI	Traumatic brain injury
TCD	Transcranial Doppler ultrasonography
VPR	Volume–pressure response [mm Hg/ml]

Chapter 1

Review of physiological foundations of cerebrospinal pressure–volume compensation

1.1 Anatomy and physiology of cerebral circulation

In adult humans, the skull is viewed as a rigid, non-distensible box containing a fixed volume of approximately 1500 ml. This space is filled with three major volume components: brain tissue (approx. 80%), cerebrospinal fluid (CSF), and cerebral blood (approx. 10% each) (Heldt et al., 2019). The cerebrospinal compartment, enclosed by a boundary with severely limited ability to deform, presents unique biomechanical conditions for the functioning of the central nervous system, with a high degree of coupling between several biological subsystems. Furthermore, under normal conditions, brain tissue remains settled with the bounds set by the skull, but both CSF and cerebral blood circulate continuously, influencing the intracranial pressure–volume relationships.

Cerebrospinal fluid circulation Normal CSF is a clear, colourless fluid, similar in composition to blood plasma (although with different ion concentrations and not as rich in proteins), that fills the cavities of the ventricular system and flows around the external surfaces of the brain (Morrison, 2009). The role of CSF is twofold: firstly, it provides physical support for the brain by acting as a cushion against mechanical trauma and equalising potential pressure gradients within the brain; secondly, it contributes to brain homeostasis through distribution of biologically active substances and removal of metabolic waste products (Noback et al., 2005).

CSF is secreted continuously at the rate of approximately 0.4 ml/min, primarily in the choroid plexus lining the inner surfaces of the ventricles (Morrison, 2009). From there is travels (mostly by bulk flow, although evidence of pulsatile and bidirectional flow has also been presented) through the ventricular system into the subarachnoid space where it is resorbed into venous blood by the arachnoid granulations (Hartman, 2009). In healthy subjects, the rates of production and resorption are assumed to be equal, and the entire CSF volume is replaced several times a day (Morrison, 2009). Despite making up a relatively low proportion of the total intracranial volume, the presence of CSF is essential for the central nervous system. Most notably, disturbances in CSF circulation are the underlying source of hydrocephalus (Noback et al., 2005).

Cerebral blood flow The arterial supply to the brain is provided by two pairs of trunk arteries: the vertebral arteries and the internal carotid arteries (Noback et al., 2005). The vertebral arteries, supplying the brainstem and posterior brain, unite to form the basilar artery which in turn bifurcates into the paired posterior cerebral arteries. Each of the internal carotid arteries supplying the anterior brain divides into an anterior cerebral artery and a middle cerebral artery, and they join to form the anterior communicating artery. The two cerebral arterial systems, carotid and vertebral, although essentially independent, contain a number of anastomotic connections and are collectively known as the circle of Willis. In the event of vessel occlusion within the circle of Willis, the interconnections serve as a safety valve, providing collateral blood supply to counteract blood flow impairment. Blood supply within the substance of the brain is provided by an extensive system of smaller arteries and capillaries. The venous drainage points are comprised of a network of anastomotic veins and dural sinuses, with most of cerebral venous volume draining into the internal jugular vein at the base of the skull.

Despite its low mass relative to the rest of the human body, the brain accounts for nearly 20% of the arterial blood flow from the heart, with roughly 800 ml of blood flowing through the brain every minute (Noback et al., 2005). Unlike other cells, neurons cannot survive anaerobically, and almost always die within minutes if deprived of oxygen. This requirement for continuous oxygen supply, combined with a high metabolic demand, makes the brain very sensitive to hypoperfusion. Consequently, blood flow in the intracranial space is tightly regulated by a mechanism called cerebral autoregulation which works to maintain approximately stable blood supply adequate to the brain's needs (Gomes and Bhardwaj, 2009). Regulation of cerebral blood flow (CBF) is achieved via either contraction or dilation of small arteries and arterioles in response to variations in cerebral perfusion pressure (CPP). The changes in vessel diameter alter cerebrovascular resistance which increases linearly with CPP, thus modifying CBF. The effective range of cerebral autoregulation is estimated in normal subjects at 50 mm Hg to 150 mm Hg (Panerai, 1998). Outside that range, vascular resistance is no longer dependent on CPP; in particular, at very low CPP resistance increases due to collapse of small arterial vessels.

1.2 Intracranial pressure

Intracranial pressure (ICP) is the pressure exerted by the components of the intracranial compartment, determined by their individual volumes, circulation of cerebral blood and CSF, and in case of pathologies, additional space-occupying lesions (Gomes and Bhardwaj, 2009). In adults resting in the horizontal position, the range of normal ICP is usually specified as 5 mm Hg to 15 mm Hg. Certain variations in ICP are associated with factors such as age, body position, respiration, and systemic blood pressure. Each of the components of the intracranial space may also undergo volume changes, and thus alter ICP, in the course of different pathologies (Gomes and Bhardwaj, 2009). The indications for ICP measurement vary between centres. In traumatic brain injury (TBI), ICP monitoring and management is recommended by established guidelines (Carney et al., 2017). It also serves as a common diagnostic tool in hydrocephalus and idiopathic intracranial

hypertension (Marmarou et al., 2005; Nakajima et al., 2021). Moreover, it may be used, if the potential clinical benefits outweigh the cost and danger associated with placing the sensor, in conditions such as intracerebral or subarachnoid haemorrhage, ischaemic stroke, and encephalitis (Zweifel et al., 2011).

The criteria for raised ICP also vary between specific disorders. For instance, in patients suspected of hydrocephalus, ICP over 15 mm Hg may already be considered elevated (Czosnyka et al., 2017). In TBI, clinical guidelines recommend ICP-lowering treatment over 20 mm Hg (Bratton et al., 2007); recently revised to 22 mm Hg (Carney et al., 2017). Common symptoms of elevated ICP include headaches, vision impairment, vomiting, problems with respiration and movement, and behavioural changes (Timofeev, 2008). Intracranial hypertension (IH) is also one of the most dangerous complications in TBI, associated with higher mortality and worse outcomes (Badri et al., 2012). This is explained through two pathophysiological links (Harary et al., 2018). Firstly, CPP is defined as the difference between mean arterial blood pressure (ABP) and ICP; increased ICP can therefore effectively lower brain perfusion, potentially leading to ischemia. Secondly, elevated ICP may induce herniation of brain structures, which in turn may cause damage to the brain stem.

1.2.1 Intracranial pressure monitoring

Although several non-invasive methods of ICP estimation have been proposed to date, they are not yet widely used in clinical practice, and invasive measurement remains the current standard (Evensen and Eide, 2020). Historically, ICP measurement via lumbar puncture dates back to the 19th century, and foundations for the modern catheter-based sensors were laid down in the early 20th century (Heldt et al., 2019). Over the years, various techniques were tested, including epidural, subdural, subarachnoid, parenchymal, and ventricular sensor placement, but most were abandoned due to insufficient reliability; today, two main approaches to ICP measurement in the neurocritical care unit (NCCU) remain: external ventricular drains (EVDs) and intraparenchymal microsensors (Heldt et al., 2019). ICP recording via lumbar puncture also remains in use, but it is most commonly employed in the management of hydrocephalus and idiopathic intracranial hypertension, with rare applications in the NCCU (Czosnyka et al., 2017). Fluid-filled catheters connected to external fluid pressure sensors are often considered the 'gold standard' as they are placed into the ventricles and therefore not dependent on pressure gradients, providing direct ICP measurement. Implantable sensors most commonly take the form of fibre optic or strain gauge microtransducers placed into the brain tissue, measuring local pressure at the site. They are potentially prone to errors due to the fact that pressure in the intracranial compartment is not uniform (Evensen and Eide, 2020).

However, the choice of monitoring approach is primarily dependent on the patient's needs and the protocols of each clinical centre. All methods of invasive ICP measurement require surgical procedures to position the sensor, and as such are associated with the risk of haemorrhages, infection, and misplacement (Tavakoli et al., 2017). Implantable sensors may produce misleading results due to the tissue pressure gradients, but ventricular puncture required to introduce an EVD is considered more invasive with higher

risk of complications (Evensen and Eide, 2020). Intraparenchymal probes lack the major advantage of EVDs as they cannot be simultaneously used in therapy to lower ICP through drainage of fluid, and they cannot be recalibrated or zeroed once placed, which may lead to loss of accuracy over time (Heldt et al., 2019). On the other hand, brain swelling and compression of ventricles in brain injury patients may make placement of an EVD impossible, leaving intraparenchymal probes as the more viable option (Zweifel et al., 2011). All of these factors need to be considered while choosing an appropriate measurement approach.

1.2.2 Components of the intracranial pressure signal

Over the years various researches have pointed out that despite the widespread use of mean ICP value in the clinical setting, ICP is in fact 'more than a number', and detailed analysis of the signal can provide much more information than simple time average (Kirkness et al., 2000; Czosnyka et al., 2007; Wagshul et al., 2011). In the time domain, the signal consists of three overlapping components superimposed on the fluctuations in mean ICP level. These components are separated in the frequency domain into slow waves, respiratory waves, and the pulse waveform (Czosnyka et al., 2007).

Plateau waves (or A waves; see Figure 1.1a) were first characterised by Lundberg et al. (1965). This term describes rapid increases in ICP up to 100 mm Hg evoked by intrinsic vasomotor changes in cerebral blood volume (CBV) and associated with a phenomenon called 'vasodilatory cascade' in which cerebral vasodilation initiates a positive feedback loop of changes in CBV and ICP, leading to further vasodilation and eventually a crisis (Rosner and Becker, 1984). Plateau waves are a common occurrence in TBI patients and they usually terminate spontaneously after several minutes; however, the substantial increase in ICP is accompanied by a loss of cerebral autoregulation and a decrease in CPP which may lead to ischemia, and plateau waves lasting longer than 30 minutes are correlated with worse outcome in TBI (Castellani et al., 2009).

The B waves (Figure 1.1b) are characterised as repeating increases in ICP (by 10–20 mm Hg) occurring at 0.5–2 cycles/min (Martinez-Tejada et al., 2019). They present varying shapes, most commonly divided into symmetrical and asymmetrical, and may also include a plateau phase. Although B waves are usually linked with vasogenic activity and cerebral dysfunction, their clinical usefulness, particularly in predicting the response to shunting in hydrocephalus patients, has been disputed (Stephensen et al., 2005). C waves occur at 4–8 cycles/min, synchronously with oscillations in ABP and with much smaller amplitude than B waves (Smith, 2008). They are considered to not have any meaningful diagnostic significance.

Respiratory waves (8–20 cycles/min) are induced by changes in CBV related to variations in intrathoracic pressure occurring with inspiration and expiration (Czosnyka et al., 2007; Kasprowicz et al., 2016). Some studies examined the relationship between the respiratory waves and CSF dynamics (Foltz et al., 1990; Momjian et al., 2004), but they are arguably more useful in assessment of cerebral autoregulation during slow, metronome-controlled breathing (Diehl et al., 1995; Reinhard et al., 2003).

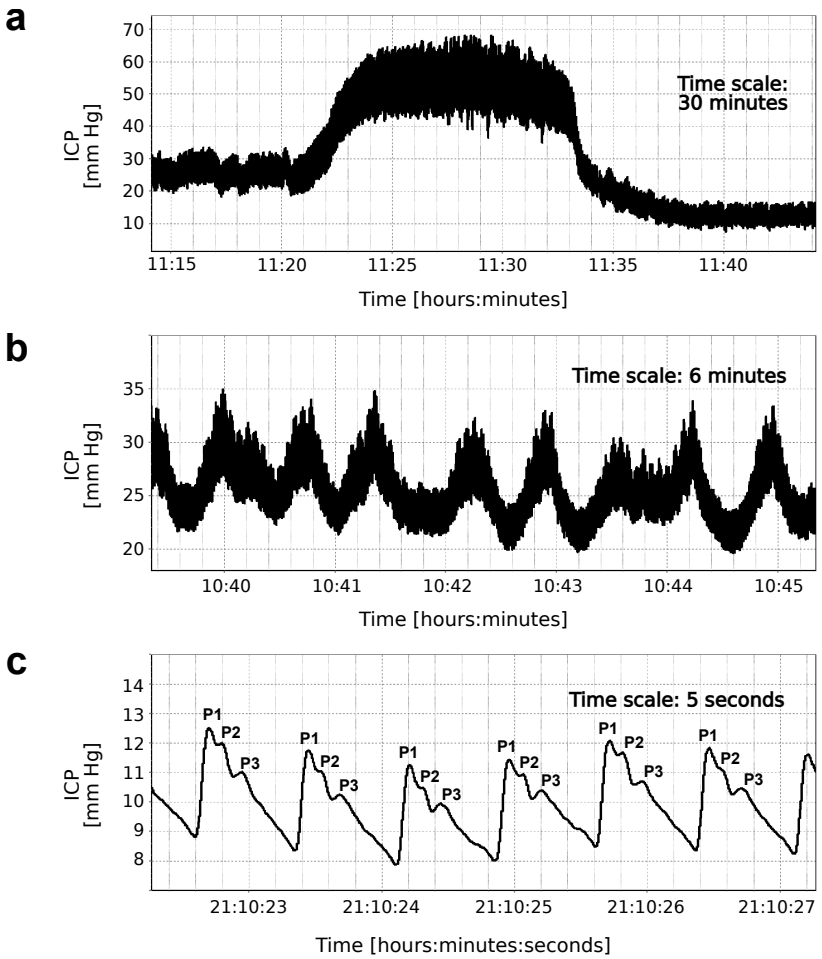

Figure 1.1. Illustrative examples of characteristic components of the intracranial pressure (ICP) signal: a) plateau wave, b) B waves, c) ICP pulse waveforms with annotated peaks P1, P2, and P3.

Finally, the ICP pulse waveform (40–160 cycles/min; see Figure 1.1c) is associated with fluctuations in CBV occurring naturally with each heartbeat. During each cardiac cycle, arterial blood inflow and subsequent venous outflow produce short-term changes in intracranial blood volume, and consequently, rhythmic instability of the ICP signal synchronised with heart rate (Ambarki et al., 2007). The ICP pulse waveform usually exhibits three distinct local maxima, or peaks, denoted P1 ('percussion wave'), P2 ('tidal wave'), and P3 ('dicrotic wave'), with P2 and P3 separated by the dicrotic notch (Germon, 1988). The precise origin of the waveform remains a subject of debate, but the overall waveform shape is associated with a combination of vascular factors and the intracranial pressure–volume relationships (Czosnyka and Czosnyka, 2020). The earliest peak, P1, is synchronous with the systolic peak of the ABP pulse and associated with the propagation of the arterial pulse and immediate distention of the arterial walls (Fan et al., 2008; Carrera et al., 2010). Peaks P2 and P3 are linked to the interaction between changes in CBV and the volume compensation mechanism (see Section 1.3.1), with P2 shown to be synchronous with the maximum of the estimated cerebral arterial blood volume pulse (Carrera et al., 2010). Some authors reputedly associate P3 with the dicrotic notch or second peak of the ABP pulse (Czosnyka et al., 2017).

Under normal conditions, specifically at low mean ICP, the ICP pulse waveform presents the three characteristic peaks arranged in a descending saw-tooth pattern, with P1 as the dominant peak (Germon, 1988). As mean ICP increases, the amplitude of the ICP pulse also increases, and the peaks gradually become less defined, the waveform eventually taking a 'rounded' or 'monotonic' shape. This observation led to a number of studies aiming to use the features of the ICP pulse waveform as a tool in ICP monitoring. The analysis methods proposed so far are discussed in detail in Section 1.4.2.

1.3 Volume–pressure relationships in the intracranial space

1.3.1 Pressure–volume curve

According to a theoretical description called the Monro–Kellie doctrine (first proposed in the works of Monro (1783) and Kellie (1824) and later refined by Cushing (1926), in normal circumstances the three volume components of the intracranial space exist in a state of equilibrium such that increases in the volume of one component are balanced by decreases in the volume of another (Noback et al., 2005). As neither of the intracranial components is particularly compressible, volume compensation mostly occurs through downward migration of venous blood and displacement of CSF into the lumbar space (Germon, 1988). Within the range permitted by the compensatory mechanisms, addition of volume into the intracranial space is accompanied by relatively small changes in ICP,

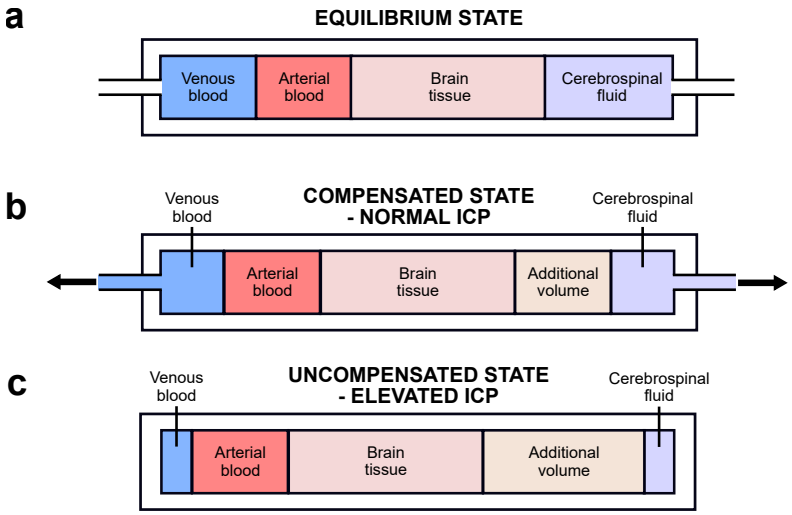

Figure 1.2. Schematic representation of the volume compensation mechanisms in the intracranial space. a) Equilibrium state with normal volume of intracranial components. b) Volume compensation working to accommodate additional volume without increases in pressure through displacement of cerebrospinal fluid and venous blood. c) Exhaustion of the compensatory mechanisms and intracranial pressure (ICP) elevation due to additional volume exceeding the intracranial compensatory reserve. Adapted from (Oswal and Toma, 2020). Proportions between volumes of individual components are not preserved.

but after the compensatory reserve is exhausted, further volume expansion results in ICP elevation. Consequently, at each time instant ICP depends on the balance between the intracranial compartments and the ability of the craniospinal system to buffer variations in volume. A schematic representation of the volume compensation mechanism is presented in Figure 1.2.

The relationship between volume and pressure in the intracranial space is mathematically expressed by a model called the pressure–volume (P–V) curve (Figure 1.3) (Ryder et al., 1953; Lofgren et al., 1973). It should be noted that the P–V curve is not a fundamental property of the intracranial environment, but rather an approximation based on observational studies (Wagshul et al., 2011). This model can be divided into three regions. At low intracranial volume (region A in Figure 1.3), with working compensatory mechanisms, increases in volume produce little to no changes in pressure. In the steep exponential portion (region B), as intracranial volume increases and the compensatory reserve is gradually depleted, even small volume increments result in disproportionate, progressively larger changes in pressure. The third part (region C) corresponds to a breakpoint in the P–V curve observed at extremely elevated ICP where the volume–pressure relationship is disturbed by collapse of cerebral blood vessels and derangement of cerebrovascular reactivity (Steiner and Andrews, 2006).

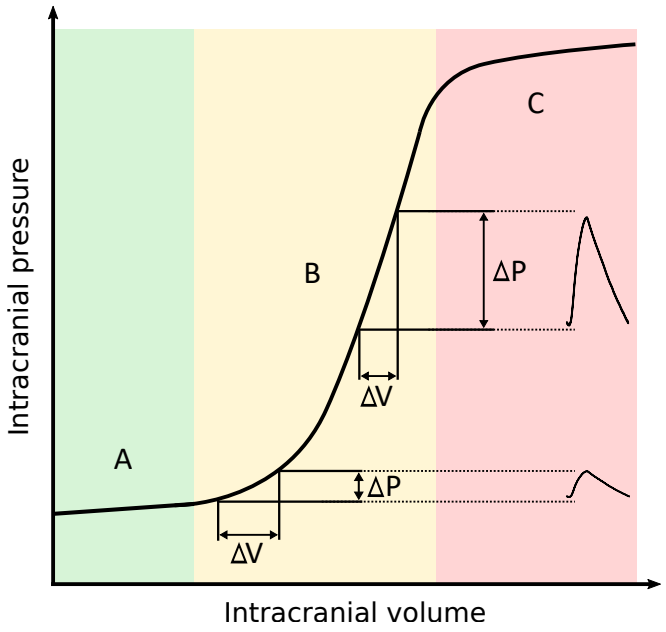

Figure 1.3. The relationship between pressure (P) and volume (V) in the intracranial space with schematic representation of changes in the intracranial pressure pulse. Region A: Baseline intracranial volume with high compliance and good compensatory reserve. Region B: Gradual reduction of compliance and depletion of the compensatory reserve accompanying increase in intracranial volume and corresponding increase in intracranial pressure. Region C: Collapse of cerebral vasculature at critically high intracranial pressure. Adapted from (Wagshul et al., 2011).

As noted in Section 1.2.2, the ICP pulse waveform is associated with short-term oscillations in CBV occurring naturally with each heartbeat. Taking into account the P–V curve, cardiac-related oscillations in CBV are expected to produce progressively larger changes in ICP as the compensatory mechanisms are diminished, manifested as increased ICP pulsatility. Accordingly, it has been shown that the pulse pressure of ICP rises concomitantly with the mean value (Szewczykowski et al., 1977; Avezaat et al., 1979).

1.3.2 Cerebrospinal compliance

Cerebrospinal compliance (C) is a measure derived from the P–V curve, expressed as the inverse slope of the curve (Marmarou et al., 1975):

$$C = \frac{\Delta V}{\Delta P}, \tag{1.1}$$

where ΔV is the change in intracranial volume and ΔP is the change in ICP. This parameter describes quantitatively the ability of the craniospinal space to adapt to changes in volume (Figure 1.4). If the change in pressure produced by given increase in volume is small, the system is characterised by high compliance. As the compensatory reserve decreases and the pressure response to a volume increment becomes larger, a reduction in

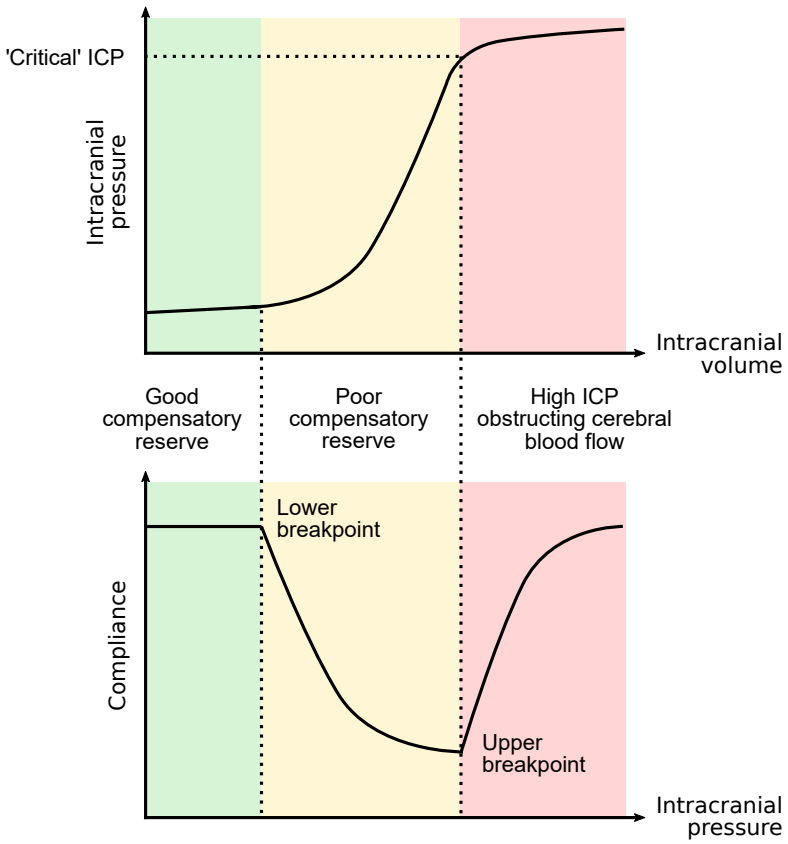

Figure 1.4. Schematic representation of the relationship between the pressure–volume curve and changes in cerebrospinal compliance. Adapted from (Czosnyka, 2021).

compliance is observed. Finally, after the breakpoint associated with cessation of cerebral blood flow due to vessel collapse, the severe disruption of the volume equilibrium results in a non-physiological increase in compliance.

Although often presented as a single parameter, total brain compliance is in fact a combination of the compliances of the components of the intracranial space: CSF and venous pool (Czosnyka and Citerio, 2012). In literature, compliance is variously termed 'brain' or 'cerebral', 'intracranial', or 'cerebrospinal'. One has to keep in mind that those names usually stand for compliance of the low-pressure compartments, combining the CSF and venous pools, a parameter substantially different from the compliance of the high-pressure arterial bed. Separate analysis of compartmental compliances is a relatively recent concept explored mainly in imaging (Alperin et al., 2005, 2006) and modelling studies (Kim et al., 2009b, 2012). In this dissertation the term 'compliance' is used exclusively to refer to cerebrospinal, and not arterial compliance.

1.3.3 Clinical significance of monitoring the volume–pressure relationship

In the clinical setting, ICP is usually characterised by its mean value averaged over a longer period of time (Czosnyka et al., 2007). For instance, internationally accepted guidelines for the management of TBI patients in the NCCU recommend monitoring of mean ICP and CPP and maintaining them within the safety range below 22 mm Hg (for ICP) and between 60 mm Hg and 70 mm Hg (for CPP) (Carney et al., 2017). However, despite its widespread use in clinical practice, the utility of ICP monitoring, particularly with one general treatment threshold for the whole population, remains the subject of controversy (Czosnyka et al., 2007; Lavinio and Menon, 2011; Chesnut et al., 2014; Hawthorne and Piper, 2014), and the recommendation is still based only on level II ('moderate degree of certainty') evidence (Carney et al., 2017).

Some authors attribute the limitations of the current approach to the missing information on the cerebrospinal buffering capacity (Heldt et al., 2019). As shown by the P–V curve, high ICP is by itself an indicator of decreased compliance, and upon detection of ICP elevation appropriate ICP-lowering strategies should be introduced to reduce it to a safe level. However, normal ICP alone cannot be regarded as a sign of sufficient compensatory reserve. Within the margin of volume compensation, ICP may still be relatively low, but significant amounts of volume may have already been displaced and further increases may not be tolerated. As elevated mean ICP may signify that adverse effects on the brain have already occurred, in order to introduce therapeutic strategies at a sufficiently early point in time—therefore shifting from a reactive approach based on mitigating damage that already exists to preventing it from happening in the first place—clinical protocols should include not only monitoring of mean ICP but also the state of cerebral compensatory reserve to identify in advance patients at risk of ICP elevation due to reduced buffering capacity.

TBI in particular is a multifactorial condition where the primarily insult is often followed by complications leading to changes in intracranial volume (Stocchetti et al., 2017). The CSF compartment may expand due to disturbances in the CSF flow pathways. Cere-

bral blood may accumulate within the intracranial space both intravenously, as a result of increased arterial inflow or decreased venous outflow, or in the form of hemorrhage-related lesions. Brain tissue may swell in the presence of injury due to evolving brain oedema. While in non-traumatic hydrocephalus the deterioration of the intracranial pressure–volume equilibrium is more gradual, in TBI patients the intracranial volume changes may occur at a rapid rate, and the state of volume compensation needs to be monitored continuously in order to detect them in time.

1.4 Assessment of cerebrospinal compliance and compensatory reserve

1.4.1 Volume–pressure tests

The early methods of compliance estimation date back to the 1970s. Given the definition expressed by Eq. 1.1, direct assessment of compliance requires simultaneous measurement of changes in volume (i.e. the stimulus) and pressure (i.e. the system's response). Miller et al. (Miller and Garibi, 1972; Miller et al., 1973) introduced a metric called the volume–pressure response (VPR), defined as the change in ICP induced by 1 ml addition or withdrawal of fluid from the CSF space. VPR expresses cerebrospinal elastance, which is the inverse of compliance, and VPR greater than 5 mm Hg/ml is thought to reflect a reduction in the volume buffering capacity (Miller et al., 1973). Studies in neurosurgical patients showed that VPR is significantly correlated with mean ICP level, as expected on the basis of the P–V curve, and may provide information on the intracranial volume–pressure relationship complementary to mean ICP (Miller et al., 1973) as well as reflect the degree of volume decompensation caused by midline shift (Miller and Pickard, 1974).

Marmarou et al. (1975) in turn proposed an approach where the pressure response is measured following the injection of a known volume into the CSF space and the injected volume is subsequently plotted against the decadic logarithm of ICP, producing a straight line whose slope is called the pressure–volume index (PVI). PVI expresses the volume necessary to increase the pressure tenfold, and compliance can be calculated by multiplying PVI by a factor of 0.4343 and dividing it by the mean ICP level at which the parameter was estimated. Normal PVI is estimated at approximately 26 ml (Shapiro et al., 1980); a decrease down to 18 ml signifies a reduction in compliance, with 13 ml considered the critical level indicating exhaustion of the compensatory reserve (Tans and Poortvliet, 1983). Notably, low PVI has been shown to correlate with outcome in TBI (Maset et al., 1987; Pillai et al., 2004).

The infusion study is a different type of volume–pressure test, first proposed by Katzmann and Husey in the 1970s (Katzman and Husey, 1970) and now usually performed in a modernised form, called the computerised infusion test (Børgesen et al., 1992). In this approach, volumetric manipulation is performed in a slow, continuous manner by adding known volumes of fluid to the CSF space at a constant rate (usually 1–1.5 ml/min) rather than through bolus injection. The infusion test is routinely performed in patients with symptoms of normal pressure hydrocephalus (NPH) to assess cerebral compensatory pa-

rameters (including cerebrospinal compliance) or the function of ventricular shunts based on the patient's pressure response to controlled changes in intracranial volume (Eklund et al., 2007). The analysis is based on Marmarou's model of CSF dynamics (Marmarou, 1973) which can be solved analytically for constant rate infusion, providing a model curve that is fitted to the full ICP recording. This model is described in detail in Chapter 3.

Compliance estimation based on addition of fluid to (or withdrawal from) the cerebrospinal space is still the established 'gold standard' method and the only technique capable of measuring absolute values of compliance. However, the requirement for external volume manipulation remains its major drawback and the likely reason for the limited use of compliance in clinical management. In order to assess compliance using either of the methods described above, one has to obtain pressure recordings at different volume levels. As a result, the measurement can only be performed intermittently, making it unsuitable for routine monitoring in the NCCU (Robertson et al., 1989). The Spiegelberg Brain Compliance Monitor (Piper et al., 1999) was an attempt to translate this approach for continuous use with a periodically expanding intraventricular balloon, but it has not been introduced to standard practice, presumably due to unsatisfactory performance (Heldt et al., 2019). Additionally, the changes in volume required by the 'gold standard' method may result in unintentional, potentially dangerous increases in ICP, which is of particular importance in TBI patients already at risk of uncontrolled IH, and external manipulation carries the risk of introducing infection due to the invasive nature of the procedure (Chopp and Portnoy, 1980; Robertson et al., 1989).

1.4.2 Analysis of intracranial pressure pulse waveform

In contrast to the volume–pressure tests based on controlled, externally induced changes in intracranial volume, various contemporary studies on compliance estimation in both humans and experimental animals attempted to analyse the pressure response to naturally occurring volume changes in the form of the ICP pulse waveform. Due to the unknown extent of volume change in each heartbeat, compliance estimators derived from the ICP pulse waveform cannot be translated to absolute measures obtained with the volume–pressure tests (Czosnyka and Citerio, 2012). However, a number of methods proposed so far showed the potential to allow for continuous assessment, and thus overcome the major disadvantage of the 'gold standard' approach, with the only limitation being the need for invasive placement of the ICP sensor.

ICP pulse amplitude The application of pulse pressure analysis in compliance assessment was proposed in the late 1970s. Szewczykowski et al. (1977) investigated the changes in pulse amplitude of ICP (AmpICP) associated with alterations in mean ICP to estimate cerebrospinal elastance. Based on the simplifying assumption that the cerebral fraction of cardiac stroke volume is constant in each heartbeat, and therefore AmpICP differs from intracranial elastance only by the constant factor $1/\mathrm{d}V$, the authors proposed to analyse elastance by calculating the slope of the amplitude–pressure (AMP–P) characteristic which describes changes in AmpICP as a function of mean ICP (Figure 1.5). The study showed that the AMP–P plot consists of two regions. The initial part represents

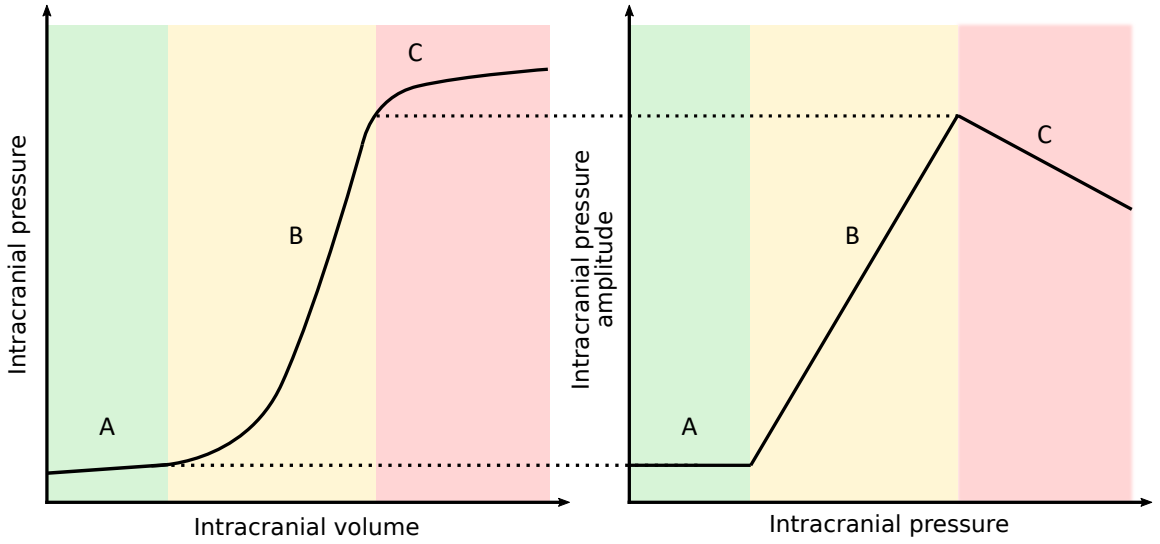

Figure 1.5. Schematic representation of the relationship between the pressure–volume curve (left) and the amplitude–pressure plot (right). Region A: Baseline intracranial volume, low intracranial pressure (ICP) with pulse amplitude (AmpICP) independent of mean ICP. Region B: Gradual increase in AmpICP accompanying the increase in intracranial volume and corresponding increase in ICP. Region C: Decrease in AmpICP following the collapse of cerebral vessels and derangement of cerebrovascular reactivity at critically high mean ICP.

the baseline state of nearly constant elastance associated with low mean ICP while the second part corresponds to gradual increase in elastance. It has since been established that the AMP–P plot may include one more region where at very high mean ICP, following a breakpoint associated with the collapse of cerebral blood vessels, AmpICP decreases again (Czosnyka et al., 1996a).

Around the same time, a study by Avezaat et al. (1979) compared the changes in AmpICP and VPR at different mean ICP levels. The authors observed that AmpICP increases linearly with mean ICP up to the level of 60 mm Hg, reflecting the changes in VPR. This led to the conclusion that the cerebral fraction of stroke volume can be assumed to be constant in that range and AmpICP can be used as a measure of cerebrospinal elastance. However, the study also showed that over 60 mm Hg VPR remains constant while AmpICP continues to increase at a steeper rate. This observation was attributed to a failure of autoregulation at highly elevated ICP, suggesting that in non-autoregulating patients AmpICP may be a better clinical indicator than the volume–pressure test. It should be noted that this study was performed in dogs and the level over which VPR and AmpICP diverge may be different in humans, as ICP of 60 mm Hg is considered severely elevated and may already exceed with the upper breakpoint of the AMP–P characteristic.

AmpICP is arguably the most frequently studied feature of the pulse waveform, with more than half a century of studies showing changes in AmpICP in conditions such as hydrocephalus (Eide and Brean, 2006; Czosnyka et al., 2008; Eide, 2016), TBI (Czosnyka et al., 1996a; Holm and Eide, 2008; Hall and O'Kane, 2016), and subarachnoid haemorrhage (Eide and Sorteberg, 2006; Eide et al., 2011). Some authors propose to estimate AmpICP directly in the time domain, as the peak-to-nadir value of the ICP

pulse waveform (Eide, 2006), while others employ spectral analysis to calculate AmpICP as the amplitude of the fundamental component of the signal's Fourier spectrum (Czosnyka et al., 1988). The two approaches have been said to produce strongly correlated results (Pearson correlation coefficient $R = 0.97$) (Czosnyka et al., 2007), although Holm and Eide (Holm and Eide, 2008) suggested that the frequency domain approach underestimates AmpICP when the ICP pulse waveforms undergoes pathological changes with ICP elevation. Nevertheless, neither technique has been conclusively proven to offer more clinical benefit (Wagshul et al., 2011). Moreover, the validity of using elevated AmpICP as an indicator of reduced compliance has been called into question (Wilkinson et al., 1979), and it has been shown to be strongly influenced by vascular factors (Kaczmarska et al., 2021).

RAP index The RAP index, proposed by Czosnyka et al. (1988), incorporates the information contained in the P–V and AMP–P characteristics. The parameter is defined as the moving Pearson correlation coefficient between mean ICP and AmpICP calculated over longer periods of time, usually 5 minutes. Its name is derived from the common symbol for the correlation coefficient (R) and the words 'amplitude' and 'pressure'. Positive values of RAP close to 0 suggest good compensatory reserve as the changes in AmpICP are not driven by oscillations in mean ICP. Values close to 1 represent decreased compensatory reserve, with changes in mean ICP producing corresponding changes in AmpICP. Finally, negative values are associated with disturbed cerebrovascular reactivity following the upper breakpoint of the P–V curve. While not a direct estimate of cerebrospinal compliance, RAP index serves as an indicator of the patients 'working point' on the P–V

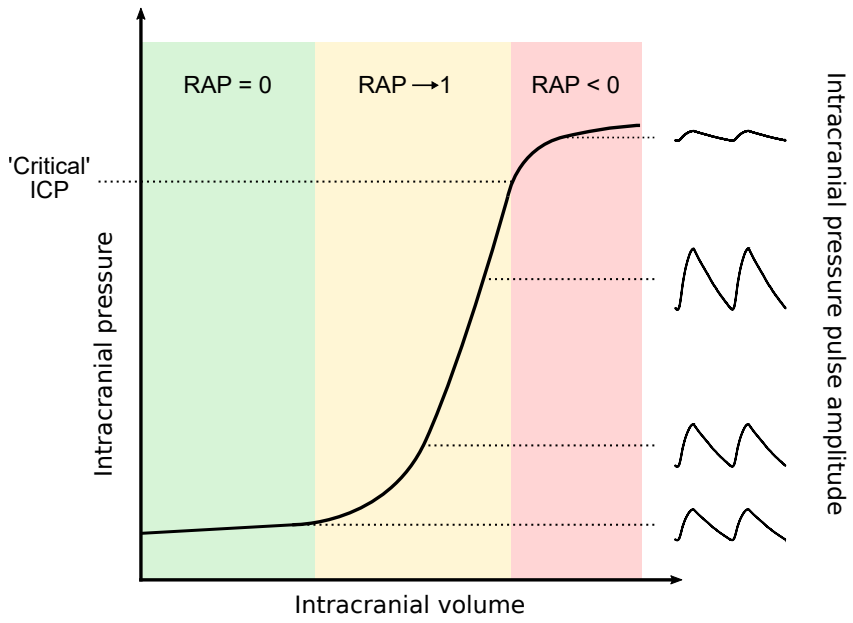

Figure 1.6. Interpretation of the RAP index. Values close to 0 indicate the initial region of the pressure–volume curve (green), values close to 1 suggest reduced compensatory reserve (yellow), and negative values correspond to deranged cerebrovascular reactivity occurring at critically elevated ICP (red). Adapted from (Czosnyka et al., 1996a).

curve (Figure 1.6) and can be calculated continuously, therefore allowing for identification of patients with exhausted volume compensation.

Since its introduction, RAP index has been studied in both hydrocephalus (Kim et al., 2009a; Weerakkody et al., 2011) and TBI (Czosnyka et al., 1994, 1996a; Balestreri et al., 2004; Steiner et al., 2005; Timofeev et al., 2008; Zeiler et al., 2018). In TBI, the superiority of RAP index over other measures, primarily AmpICP, has been disputed (Howells et al., 2012; Hall and O'Kane, 2016). However, its usefulness has been shown, for instance, in RAP-weighted mean ICP (defined as $\mathrm{ICP} \cdot (1 - \mathrm{RAP})$ and sometimes termed 'true ICP') outperforming standard mean ICP in prediction of outcome after TBI (Czosnyka et al., 2005; Calviello et al., 2018; Zeiler et al., 2019).

Spectral analysis In addition to providing an alternative method of calculating AmpICP, spectral analysis based on the Fourier transform was used for more detailed description of the changes the ICP pulse waveform undergoes at different mean ICP levels. Chopp and Portnoy (1980) proposed a systems analysis approach to characterise the ICP pulse waveform in relation to the ABP pulse, with the latter treated as the input and the former as the output of the cerebrospinal system. Based on the transfer function approach, the authors reported enhanced transfer from ABP to ICP with increased mean ICP, suggesting that cerebral vasodilation which accompanies ICP elevation diminishes the ability of the arterioles to attenuate the arterial pulse, leading to increased transmission in a dysautoregulated system. These results were later confirmed by Takizawa et al. (1987) who postulated that the pulse transmission from ABP to ICP is influenced by a combination of intracranial compliance and cerebral vasomotor reactivity. The authors investigated further the shape of the ICP pulse waveform through analysis of the signal's Fourier spectrum, showing that at higher mean ICP, the higher harmonics of ICP are reduced compared to the fundamental wave, and so is the distortion factor describing the degree of dissimilarity between the ICP waveform and simple sine wave. This finding was in line with the previously reported rounding of the pulse wave observed with increased ICP in the time domain.

This avenue of study was also explored in research on the high frequency centroid (HFC), defined as the frequency centroid (i.e. centre of mass) of the ICP power spectrum in the range 4–15 Hz (Robertson et al., 1989). Bray et al. (1986) examined the changes in HFC in relation to PVI and showed that HFC around 7 Hz is considered normal whereas an increase up to 9 Hz corresponds to a reduction in PVI to approximately 13 ml and signifies exhausted compensatory reserve. Later studies using HFC as a tool for continuous monitoring in TBI patients showed that increased HFC correlates with higher mortality and occurrence of IH (Robertson et al., 1989), and opposite direction of changes in HFC can differentiate transient from refractory IH episodes (Contant et al., 1995). More recently, focus has shifted to a different spectral centroid, called the higher harmonics centroid (HHC) (Zakrzewska et al., 2021). In contrast to HFC, which is calculated in the same range regardless of the fundamental cardiac frequency, HHC attempts to take into account the variations in heart rate by defining the range in harmonic numbers rather than Hz. HHC calculated from the 2nd through 10th harmonic was shown to be positively

correlated with mean ICP in TBI patients and to decrease significantly during ICP plateau waves (Zakrzewska et al., 2021).

However, it should be noted that the use of the Fourier transform requires that the signal in question satisfies the stationarity condition. During continuous monitoring, with frequent changes related to, for instance, cardiac arrhythmia, this requirement may not always be fulfilled, potentially making this approach imprecise for ICP analysis.

ICP pulse waveform morphology ICP pulse waveform morphology refers to the shape of the ICP signal observed during a single cardiac cycle. As mentioned in Section 1.2.2, under normal conditions the ICP pulse waveform exhibits three distinct local maxima, called peaks P1, P2, and P3, whereas at elevated ICP, in addition to increased AmpICP, the waveform becomes more 'rounded' or 'monotonic', with the peaks gradually disappearing (Germon, 1988). In 1983, Cardoso et al. (1983) investigated the changes in the configuration of the characteristic peaks during alterations in mean ICP caused by different manoeuvres. The authors noted that in addition to the previously known influence on AmpICP, hyperventilation-induced ICP reduction has a profound effect on the ICP pulse contour in the form of decreasing prominence of peak P2. They suggested that since hyperventilation influences cerebral bulk volume (and with it, cerebrospinal compliance) through vasoconstriction of arterioles, the relative height of the first two characteristic peaks may provide an indirect measure of compliance.

Based on those observations, other researches proposed to use the P2/P1 ratio in prediction of impending rises in ICP. Studies in TBI patients demonstrated that the ratio is indeed higher in patients who exhibit IH episodes compared to those who do not (Fan et al., 2008) and P2 elevation may be predictive of increased frequency of IH episodes (Mitchell et al., 1997). Yet when used with a prediction threshold of 0.8, this approach showed low specificity, leading to the conclusion that elevated P2/P1 ratio alone is not a reliable indicator of impending increases in mean ICP as it was also present in the comparison data (Fan et al., 2008). Notably, however, the studies did not attempt to validate the peak ratio approach against other methods of cerebrospinal compliance assessment and the proposed threshold appears to have been chosen arbitrarily. A P2/P1 ratio of 0.8 corresponds to a waveform with dominating peak P1 and slightly lower P2, which may still be considered normal; peak P2 can only be clearly said to dominate when the ratio exceeds 1 (see Figure 1.7). One could therefore argue that the method's apparent failure as a tool for IH prediction could be rectified by a more in-depth investigation of what constitutes an appropriate peak ratio threshold.

Meanwhile, various studies aimed to refine morphological analysis in order to replace visual assessment of the waveform shape with automated tools. Hu et al. (2009) developed an algorithm called Morphological Clustering and Analysis of Continuous Intracranial Pressure (MOCAIP) capable of assessing a number of pulse shape metrics, including peak height, latency, and curvature. Proposed as a generalised method of ICP pulse waveform analysis, MOCAIP-derived metrics have been used to investigate cerebrovascular phenomena (Hu et al., 2010a; Asgari et al., 2011a,b), ICP slow waves (Kasprowicz et al., 2010) and response to shunting (Hamilton et al., 2016), predict ICP elevation (Hamilton et al., 2009; Hu et al., 2010b) and identify artefactual pulses (Megjhani et al.,

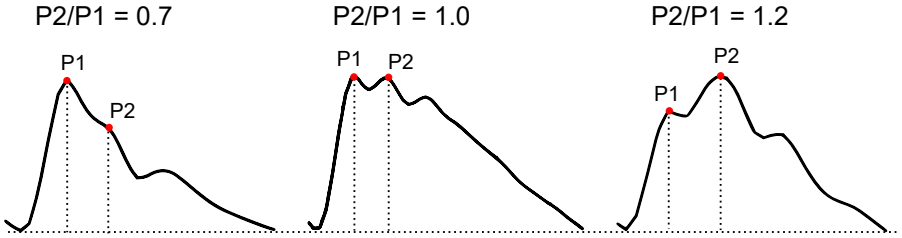

Figure 1.7. Illustrative examples of intracranial pressure pulse waveforms with different ratio of peaks P1 and P2.

2019), and the same group introduced different improvements to this technique (Scalzo et al., 2009, 2010; Asgari et al., 2009). In a small group of four patients with slit ventricle syndrome, increase in MOCAIP-based P2/P1 ratio was shown to correlate with enlargement of the lateral ventricles (Hu et al., 2008). Various other attempts to solve the task of peak designation have also been reported (Elixmann et al., 2012; Scalzo et al., 2012; Calisto et al., 2013; Lee et al., 2016). Still, analysis of ICP pulse waveform morphology is yet to transition beyond the realm of research. The ICP signal is intricate, highly variable, and the changes it undergoes occur both over time and between patients (Ellis et al., 2005). The computational algorithms proposed to date demonstrate varying levels of accuracy, and their technical complexity leads to limited understanding and acceptance in the medical community.

Recently, a different approach based on machine learning was presented where peak detection was substituted with easy to interpret visual criteria for overall pulse waveform morphology. Nucci et al. (2016) isolated four classes of ICP pulse shapes reflecting the changing configuration of characteristic peaks in hydrocephalus patients and proposed an artificial neural network capable of classifying ICP pulse waveforms with 88% accuracy. The categories ranged from normal waveforms with three peaks arranged in a descending saw-tooth pattern to fully rounded pathological waveforms with only one defined maximum. Using the proposed classification model, the authors compared the dominant ICP pulse waveform class with parameters describing CSF circulation obtained from analysis of controlled changes in mean ICP caused by infusion of fluid into the CSF space. The results showed that pathologically altered pulse waveform morphology at baseline is indicative of disturbances in intracranial elastance revealed by the infusion test, suggesting the predictive potential of this method of ICP pulse analysis. However, at the time of writing this dissertation, further results utilising this approach have not been reported.

Chapter 2

Aims and hypotheses

Monitoring of mean ICP is one the cornerstones of modern neurocritical care. While it has long been shown that information on the cerebrospinal system's ability to buffer changes in volume could potentially complement established mean ICP-based management of TBI patients, current methods of assessing cerebrospinal compliance and compensatory reserve are not very well suited to this scenario. The morphology of the ICP pulse waveform, i.e. the shape of the signal during a single cardiac cycle, has been proposed as an indicator of compliance almost four decades ago, but despite promising early reports and a certain degree of interest over the years, it has not been examined in much detail and this method still awaits introduction to standard medical practice.

The aim of this dissertation was to further explore the information encoded in the features of the ICP pulse waveform and its potential for improving clinical management of patients with intracranial pathologies. The following research hypotheses were formulated:

1. Changes in the shape of intracranial pressure pulse waveform, expressed by the ratio of characteristic peaks P1 and P2, are correlated with compliance assessed during volumetric manipulation (Chapter 3).

2. Deep neural networks can be used to automatically classify ICP pulse waveform shapes in traumatic brain injury patients (Chapter 4).

3. Changes in the shape of intracranial pressure pulse waveform expressed by pulse waveform classification are associated with outcome after traumatic brain injury (Chapter 5).

Chapter 3

Cerebrospinal compliance estimation based on the shape of intracranial pressure pulse waveform

The results presented in this chapter were published in:

Kazimierska, A., Kasprowicz, M., Czosnyka, M., Placek, M. M., Baledent, O., Smielewski, P., and Czosnyka, Z. (2021). Compliance of the cerebrospinal space: comparison of three methods. *Acta Neurochirurgica*, 163(7):1979–1989.

Full text of the paper can be found in Appendix A.

3.1 Introduction

Over the years, features of the ICP pulse waveform have served as the basis of various indices of cerebral compensatory reserve, including AmpICP and the AMP–P slope (Szewczykowski et al., 1977; Avezaat et al., 1979), RAP index (Czosnyka et al., 1988, 1996a), and HFC (Bray et al., 1986; Robertson et al., 1989). The ratio of characteristic peaks P1 and P2, despite promising early reports, has not been investigated in much detail. In their 1983 study, Cardoso et al. (1983) showed that changes in the relative height of peaks P1 and P2 reflect hyperventilation-induced decrease in mean ICP and corresponding increase in compliance. Other researchers attempted to use the P2/P1 ratio as a predictor of dangerous IH episodes (Mitchell et al., 1997; Fan et al., 2008). Still, this approach has never been explicitly validated against other methods of compliance estimation.

The aim of this chapter was to assess the feasibility of using the P1/P2 ratio as a measure of cerebrospinal compliance during controlled increases in mean ICP by comparing it firstly to the 'gold standard' method of direct volumetric manipulation and secondly, to a different indirect approach based on evaluation of changes in CBV using non-invasive transcranial Doppler (TCD) ultrasonography measurement of cerebral blood flow velocity (CBFV). If proven to be linked to the 'gold standard' compliance, estimates based on the ICP pulse waveform or changes in CBV would allow for continuous monitoring of compliance, thereby overcoming the major limitation of the volume–pressure tests. Results of this study offer new insights into the indirect methods of compliance monitoring.

3.2 Material

3.2.1 Data collection

Data used in this study were selected retrospectively from infusion test recordings collected in NPH patients at Addenbrooke's Hospital (Cambridge, UK) between 1993 and 1998. The infusion test was executed via a pre-implanted Ommaya reservoir using two hypodermic needles (25 gauge): one for ICP measurement and one for fluid infusion. The first needle was connected to a pressure transducer via a saline-filled tube connected in turn to a pressure amplifier (Simonsen & Will, Sidcup, UK). The second needle was connected to an infusion pump. The full recording consisted of three phases: baseline (approximately 10 minutes), increase in ICP, and plateau. If the patient did not reach the plateau phase by the time ICP approached the maximum acceptable level of 40 mm Hg, the infusion was stopped due to safety concerns. Following the end of infusion, the recording was collected until ICP returned to baseline. The rate of infusion was chosen based on the patient's baseline ICP level: 1.5 ml/min for baseline ICP below 15 mm Hg and 1 ml/min above that threshold (Czosnyka et al., 1996b).

CBFV was simultaneously monitored in the middle cerebral artery using a TCD unit (Neuroguard; MedaSonics, Fremont, CA, USA) with 2-MHz probes fixed in a stable position at the temporal acoustic window using a commercially available fixation system. In a subset of patients, ABP was also measured non-invasively using a photopletysmographic system (Finapres; Finapres Medical Systems, the Netherlands) in the middle finger of the left hand held at heart level. Data from pressure monitors and the TCD unit was collected via an analogue-to-digital converter (DT 2814; Data Translation, Marlboro, USA) connected to an IBM AT laptop computer (Amstrad ALT 386 SX; Amstrad, Brentwood, UK) with custom software for waveform recording (WREC; W. Zabolotny, Warsaw University of Technology, Warsaw, Poland). Sampling frequency ranged from 30 Hz to 50 Hz.

As part of routine clinical management of hydrocephalus patients, the infusion tests alone did not require separate ethical agreement. Local Ethics Committee approval was obtained for simultaneous TCD recording of CBFV (no 08/H0306/103).

3.2.2 Data selection

In this study only recordings of ICP measured via a pre-implanted Ommaya reservoir with simultaneous monitoring of CBFV were used. In standard clinical practice, the infusion test is more commonly performed via lumbar puncture instead of the Ommaya reservoir. However, the ICP recorded via lumbar puncture is not strictly the same as observed with ventricular or intraparenchymal probes (Behrens et al., 2013), and existing reports on ICP pulse morphology have been based on the ICP waveform recorded intracranially (Cardoso et al., 1983; Fan et al., 2008; Hu et al., 2009; Nucci et al., 2016). Furthermore, lumbar recording places the measurement sites of ICP and CBFV, the latter of which is measured in large cerebral arteries, at a considerable distance. As this study included also the calculation of compliance estimates based on the CBFV signal, lumbar recordings were excluded to enable more accurate comparison.

72 recordings were initially considered for analysis. Further selection was made on the basis of good quality of both ICP and CBFV signals and the visibility of peaks P1 and P2 in the ICP pulse waveform. 20 recordings were excluded due to low quality of either the ICP or the CBFV signal. 16 recordings were excluded due to pathological rounding of the pulse waveform, even at baseline, which made identification of both characteristic peaks impossible. Finally, 36 recordings were included in the study, out of which 26 included also the ABP signal. Figure 3.1 shows an illustrative example of full recording from a single patient.

Mean age in the selected group was 54 years (range: 27–76 years). Based on the bicaudate index assessed by a clinician using computed tomography (CT) exams with age-dependent thresholds (Little et al., 2008), the patients showed signs of ventricular dilation (mean bicaudate index: 0.27, range: 0.14–0.39), and 14% showed evidence of white matter ischemia.

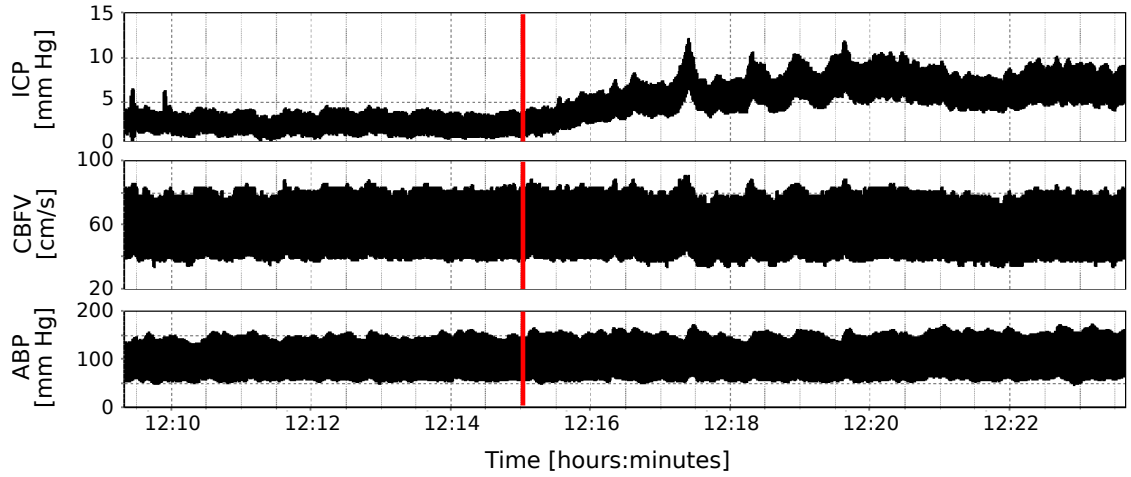

Figure 3.1. Illustrative example of infusion test recording of (from top to bottom) intracranial pressure (ICP), cerebral blood flow velocity (CBFV), and arterial blood pressure (ABP) for a single patient. Vertical red lines indicate the start of constant rate infusion.

3.3 Methods

3.3.1 Assessment of cerebrospinal compliance

In order to assess the validity of using indirect methods of compliance estimation, the infusion test recordings were analysed using three approaches: based on the model of CSF dynamics (the 'gold standard' method of volumetric manipulation); based on the height ratio of characteristic peaks P1 and P2 of ICP pulse waveform; and based on evaluation of changes in arterial CBV. Unless explicitly stated otherwise, all analyses were performed using programs custom written in Python 3.7.

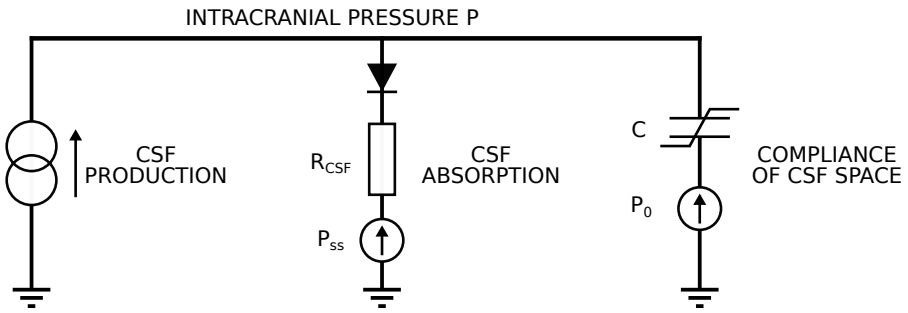

Figure 3.2. Electrical circuit equivalent of Marmarou's compartmental model of cerebrospinal fluid (CSF) circulation. R_{CSF}—resistance to CSF outflow, P_{SS}—pressure in the sagittal sinuses, C—cerebrospinal compliance, P_0—reference pressure. Adapted from (Marmarou, 1973).

Model of cerebrospinal fluid dynamics The mathematical model of CSF dynamics in the intracranial space was first proposed by Marmarou (1973) to describe the relationship between different compartments of the CSF circulatory system. It is commonly depicted using an electrical equivalent (Figure 3.2) comprised of the following elements: a current source (corresponding to CSF formation), a resistor and diode branch (corresponding to CSF absorption), and a non-linear capacitor (corresponding to compliance of the CSF space).

Under normal conditions, the components of CSF circulation balance each other, as described by the following equation:

$$\text{CSF production} = \text{CSF storage} + \text{CSF reabsorption}. \tag{3.1}$$

The rate of CSF production (I_{P}) is assumed to be constant. The rate of CSF storage (I_{S}) is proportional to cerebrospinal compliance (C):

$$I_{\mathrm{S}} = C\,\frac{\mathrm{d}P}{\mathrm{d}V}, \tag{3.2}$$

where P is the CSF pressure. The rate of CSF reabsorption (I_{R}) depends on the gradient between CSF pressure P and pressure in the sagittal sinuses (P_{SS}):

$$I_{\mathrm{R}} = \frac{P - P_{\mathrm{SS}}}{R_{\mathrm{CSF}}}, \tag{3.3}$$

where R_{CSF} is a parameter called resistance to CSF outflow (unit: mm Hg/(ml/min)).

Compliance C is inversely proportional to the gradient between CSF pressure P and reference pressure P_0:

$$C = \frac{1}{E \cdot (P - P_0)}, \tag{3.4}$$

where E represents cerebrospinal elastance (unit: ml^{-1}). This relationship is considered valid above certain pressure level termed 'lower breakpoint pressure' (Figure 3.3) above which the P–V curve becomes exponential. Below that point the P–V curve is assumed to be linear, and compliance is approximately constant.

To describe the conditions present during the infusion test, a fourth term, representing the rate of external volume addition ($I(t)$), is added to Eq. (3.1). Combined with Eqs (3.2)–(3.4), Eq. (3.1) can be rewritten as:

$$\frac{1}{E \cdot (P - P_0)} \frac{\mathrm{d}P}{\mathrm{d}t} + \frac{P - P_\mathrm{b}}{R_\mathrm{CSF}} = I(t), \tag{3.5}$$

where P_b is the baseline pressure approximating P_SS. The solution to Eq. (3.5) for constant rate infusion, with the assumption that $P(0) = P_\mathrm{b}$, $I(t) = 0$ for $t < 0$ and $I(t) = I_\mathrm{inf}$ for $t > 0$, where I_inf is the constant rate of infusion, is expressed as:

$$P(t) = \frac{\left(1 + \frac{P_\mathrm{b} - P_0}{R_\mathrm{CSF} \cdot I_\mathrm{inf}}\right) \cdot (P_\mathrm{b} - P_0)}{\frac{P_\mathrm{b} - P_0}{R_\mathrm{CSF} \cdot I_\mathrm{inf}} + \exp\left(-E_1 \left(1 + \frac{P_\mathrm{b} - P_0}{R_\mathrm{CSF} \cdot I_\mathrm{inf}}\right) \cdot t \cdot I_\mathrm{inf}\right)} + P_0. \tag{3.6}$$

In this study, ICP recordings collected during the infusion test were processed using the built-in infusion test analysis module of ICM+ software (Cambridge Enterprise Ltd., Cambridge, UK) to obtain the parameters describing CSF dynamics from Eq. (3.6) (namely, E, R_CSF, and P_0 for each patient. An example of analysis results produced by ICM+ is presented in Figure 3.4. The time course of changes in compliance was subsequently calculated using Eq. (3.4). This compliance estimate is henceforth denoted as C_CSF (from 'CSF dynamics').

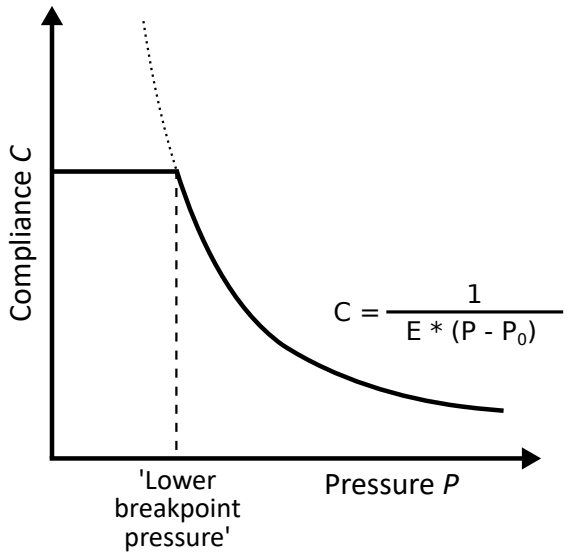

Figure 3.3. The relationship between compliance (C), elastance (E) and pressure (P) in the intracranial space in the cerebrospinal fluid dynamics model. Below the 'lower breakpoint pressure' (P_0) compliance is approximately constant, and the P–V curve is linear. Above the threshold compliance decreases with increasing pressure as described by Eq. (3.4) and the P–V curve becomes exponential. Adapted from (Czosnyka et al., 1997b).

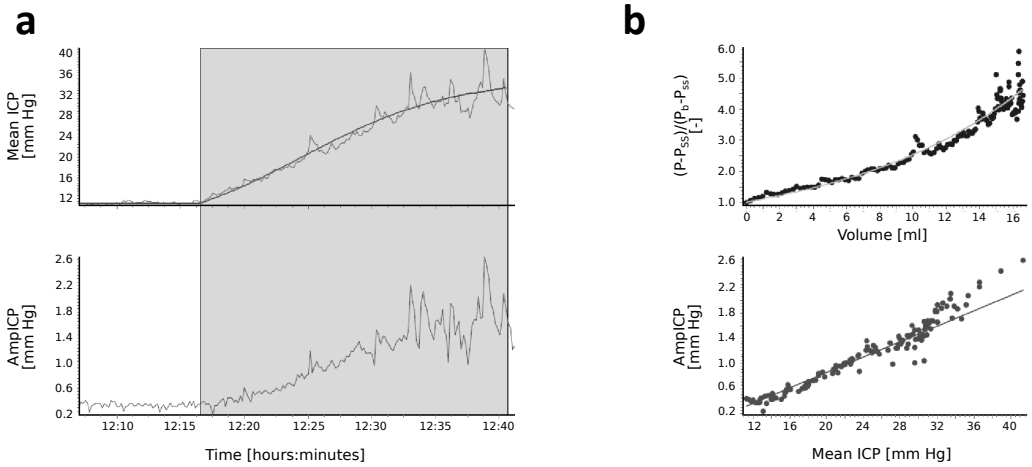

Figure 3.4. Illustrative example of constant rate infusion test results for a single patient obtained using the analysis module of ICM+ software. a) Upper plot: intracranial pressure (ICP) recording with model curve according to Eq. (3.6). Lower plot: spectral ICP pulse amplitude (AmpICP) recording. Grey background indicates the period of infusion. b) Upper plot: pressure–volume curve obtained from the ICP recording. Lower plot: amplitude–pressure plot obtained from the ICP and AmpICP recordings. Modified from (Kazimierska et al., 2021c).

Height ratio of peaks P1 and P2 According to the observations reported by Cardoso et al. (1983), decreased cerebrospinal compliance manifests as relative elevation of the characteristic peak P2 of the ICP pulse waveform over peak P1. In this study, the height ratio of P1 to P2 was used as an estimator of cerebrospinal compliance. Some studies used the inverse, P2 to P1 (Mitchell et al., 1997; Fan et al., 2008); however, there is no validated standard for this method of ICP pulse waveform analysis, and unlike the P2/P1 ratio, the changes in P1/P2 should theoretically be consistent with other compliance estimates, i.e. show a decrease with increasing mean ICP.

Prior to analysis, ICP and CBFV signals (and ABP, where available) were low-pass filtered with cutoff frequency of 10 Hz in order to reduce the high frequency noise, primarily in the ICP signal which is prone to distortions. The cutoff frequency was selected based on previous analyses showing that the power of the ICP signal is mostly contained in the range below 8 Hz (Dai et al., 2020). Individual pulse onset points were automatically marked in the ICP signal using the modified Scholkmann algorithm previously validated for use with neuroscience data such as the ICP signal (Bishop and Ercole 2018); corresponding sections of CBFV (and ABP, where available) were extracted based on ICP pulses. Each pulse was independently normalised to interval 0–1 and linearly detrended.

Peaks P1 and P2 were annotated pulse-by-pulse using a semi-automated algorithm for detection of local maxima custom-written specifically for this study. Initial P1 and P2 candidates were identified based on the shape of CBFV and ABP signals. Previous studies have noted that the position of P1 corresponds to the systolic maximum of ABP (Fan et al., 2008; Carrera et al., 2010). In some patients, due to unavailability of the ABP signal, CBFV was used instead as the systolic part of both waveforms is similar. In turn, P2 roughly correlates with the local maximum of pulsatile changes in cerebral

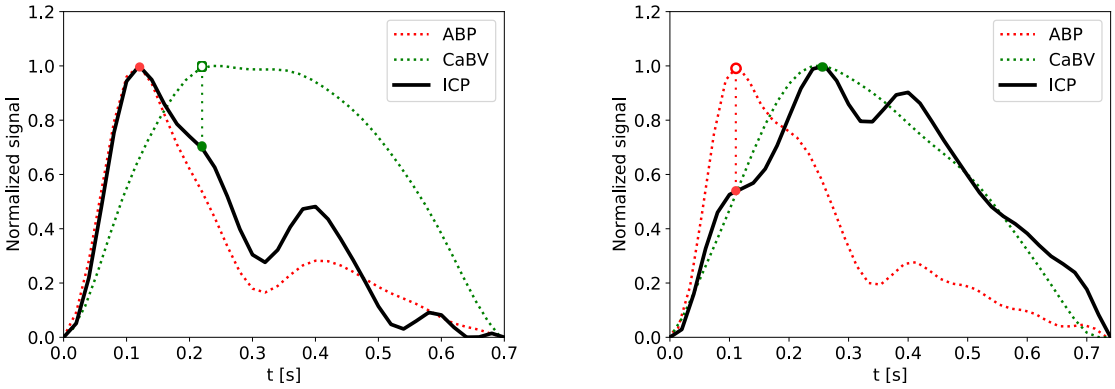

Figure 3.5. Illustrative examples of individual intracranial pressure (ICP) pulse waveforms with peak annotations (red dots: P1, green dots: P2) and supplementary signals: arterial blood pressure (ABP) and change in cerebral arterial blood volume (CaBV). Dotted vertical lines show the relationship between ICP pulse waveform and local maxima in the ABP and CaBV signals (red and green circle, respectively). Modified from (Kazimierska et al., 2021a).

arterial blood volume (C_aBV; see the next section for detailed description of the method of obtaining this signal) (Carrera et al., 2010). In order to use the information contained in the supplementary signals, ICP and CBFV pulses (and ABP, where available) were aligned with regard to the pulse onset point to eliminate the phase shift resulting from distance between measurement sites (i.e. between peripheral signal ABP and cranial signals ICP and CBFV), and the P1, P2 candidates were marked automatically. Each pair of peak candidates was then manually checked and corrected if necessary to ensure that the P1/P2 ratio was estimated as reliably as possible and not subject to errors in the peak designation method. Pulses with distorted ICP waveform or unidentifiable P1 or P2 were excluded from further analyses. Illustrative examples of ICP pulses with peak annotations and supplementary signals are presented in Figure 3.5.

In each pulse the peak-based compliance estimate (denoted $C_{P1/P2}$) was calculated as the ratio of the height of peaks P1 and P2 with peak height calculated as the vertical difference between the peak and pulse onset point. As the peak heights are expressed in mm Hg, the resulting value is dimensionless and cannot be calibrated in units of ml/mm Hg like in the 'gold standard' method.

Changes in cerebral arterial blood volume The fluctuations in cerebral arterial blood volume (C_aBV) occurring in each cardiac cycle, which contribute to the oscillations in ICP registered as the ICP pulse waveform, are governed by cerebral blood inflow (CBF_{in}) and simultaneous venous outflow (CBF_{out}). Both CBF components are characterised as pulsatile, and their differing waveforms generate changes in C_aBV (ΔC_aBV).

According to the description proposed based on experimental studies by Avezaat and van Eijndhoven (1984), ΔC_aBV over a single cardiac cycle can be expressed as:

$$\Delta C_aBV(t) = \int_{t_0}^{t} (CBF_{in}(x) - CBF_{out}(x))\,dx, \tag{3.7}$$

where t_0, t are the beginning and end of the cardiac cycle, respectively, CBF_{in} is the cerebral arterial inflow, CBF_{out} is the venous outflow, and x is the variable of integration. CBF_{out} is assumed to have low pulsatility compared to CBF_{in} (Stoquart-Elsankari et al., 2009). Consequently, venous outflow can be approximated by constant flow equal to mean arterial inflow:

$$CBF_{out}(t) = \text{mean}CBF_{in}. \tag{3.8}$$

In general, blood flow can be expressed as blood flow velocity multiplied by the cross-sectional area of the vessel (Kim et al., 2009b). Assuming that the vessel diameter remains constant during the measurement (see the Limitations section for discussion on this assumption), CBF can be expressed as:

$$CBF = CBFV \cdot S_a, \tag{3.9}$$

where S_a is the cross-sectional area of the vessel (units: cm^2), and Eq. (3.7) for discrete values of CBFV obtained with finite sampling frequency can be rewritten as:

$$\Delta C_aBV(n) = S_a \cdot \sum_{i=1}^{n} (CBFV(i) - \text{mean}CBFV)\,\Delta t(i), \tag{3.10}$$

where n is the number of samples from the beginning of the cardiac cycle and Δt is the time difference between two consecutive samples. An example of ΔC_aBV produced by Eq. (3.10) is presented in Figure 3.6.

Cerebrospinal compliance can be estimated based on pulsatile changes in CBV and corresponding changes in ICP (this estimate is denoted C_{C_aBV}) as:

$$C = \frac{\text{Amp}C_aBV}{\text{AmpICP}}, \tag{3.11}$$

where $\text{Amp}C_aBV$, AmpICP are the amplitudes of the fundamental (i.e. cardiac-related) components of ΔC_aBV and ICP, respectively. In this study, both $\text{Amp}C_aBV$ and AmpICP were calculated pulse-by-pulse in the time domain as the peak-to-nadir value of each waveform. Unlike the 'gold standard' C_{CSF}, C_{C_aBV} obtained with TCD CBFV recordings is expressed in cm/mm Hg rather than ml/mm Hg due to the unknown value of S_a. It may be interpreted as compliance per unit (cm^2) of net cross-sectional area of arterial blood inflow bed.

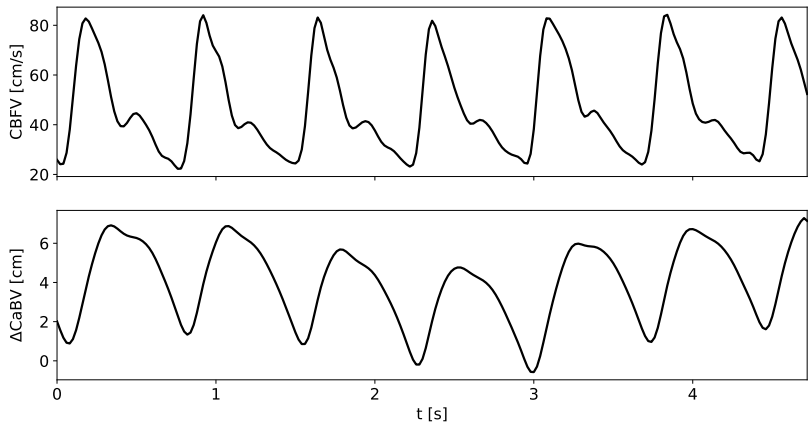

Figure 3.6. Illustrative example of changes in cerebral arterial blood volume (ΔC_aBV; lower plot) calculated from cerebral blood flow velocity (CBFV; upper plot) recording for a single patient using Eq. (3.10).

3.3.2 Statistical analysis

Normality of all analysed variables was tested using the Shapiro–Wilk test with significance level of 0.05 and the normality hypothesis was rejected for the majority of variables. Accordingly, non-parametric methods were selected to investigate the relationships between compliance estimates and related metrics. The significance level of 0.05 was assumed in all statistical tests.

The relationships between the time courses of compliance estimates (compared with each other in pairs) and between each compliance estimate and mean ICP were assessed using the Spearman correlation coefficient. Considering the difference in time scales used in calculations (particularly the pulse-by-pulse approach employed in estimation of C_{C_aBV} and $C_{P1/P2}$ compared to analysis of whole recording in case of C_{CSF}), 30-pulse moving averages were used instead of 'raw' values. The correlations were assessed individually between the time courses of each parameter for a single patient and then averaged over the whole group.

Compliance estimates at baseline (low pressure) and plateau (high pressure) phase of the infusion test, corresponding to 'high' and 'low' compliance conditions, were compared using averages of manually selected 1-minute-long fragments of the recording. In recordings where the signals at baseline were significantly distorted the initial stage of infusion was used as baseline. Two patients were excluded from this part of the analysis due to unavailability of baseline values resulting either from low signal quality or the lower breakpoint limit used in estimation of C_{CSF}. In the remaining 34 patients, the significance of changes in compliance estimates as well as changes in P1 and P2 height, $AmpC_aBV$, AmpICP, and pulse amplitude of CBFV (AmpCBFV) between the baseline and plateau phase was examined with the Wilcoxon signed rank test. As C_aBV cannot be compared directly between patients, changes in $AmpC_aBV$ were expressed in %, with baseline $AmpC_aBV$ taken as 100% individually for each patient.

All group-averaged results are presented as median [first–third quartile].

3.4 Results

3.4.1 Changes in physiological signals and derived indices

Between the baseline and plateau phase of the infusion test (Table 3.1), statistically significant increases were observed in mean ICP, peak-to-peak AmpICP, and $AmpC_aBV$ while mean CBFV and AmpCBFV both slightly decreased.

The rise in mean ICP during infusion resulted in significant elevation of both characteristic peaks ($p \ll .001$). Larger degree of changes was registered for the height of P2 (from 3.5 [2.4–4.5] mm Hg at baseline to 6.2 [4.4–8.3] mm Hg during plateau) compared to P1 (from 2.5 [1.4–3.6] mm Hg to 4.2 [2.7–4.7] mm Hg). In all patients the time courses of both heights were significantly correlated with mean ICP with slightly stronger correlation observed for P2 (group-averaged correlation coefficient: 0.98 [0.93–0.99]) than P1 (0.95 [0.82–0.96]). An illustrative example of changes in mean ICP and peak heights for a single patient is presented in Figure 3.7.

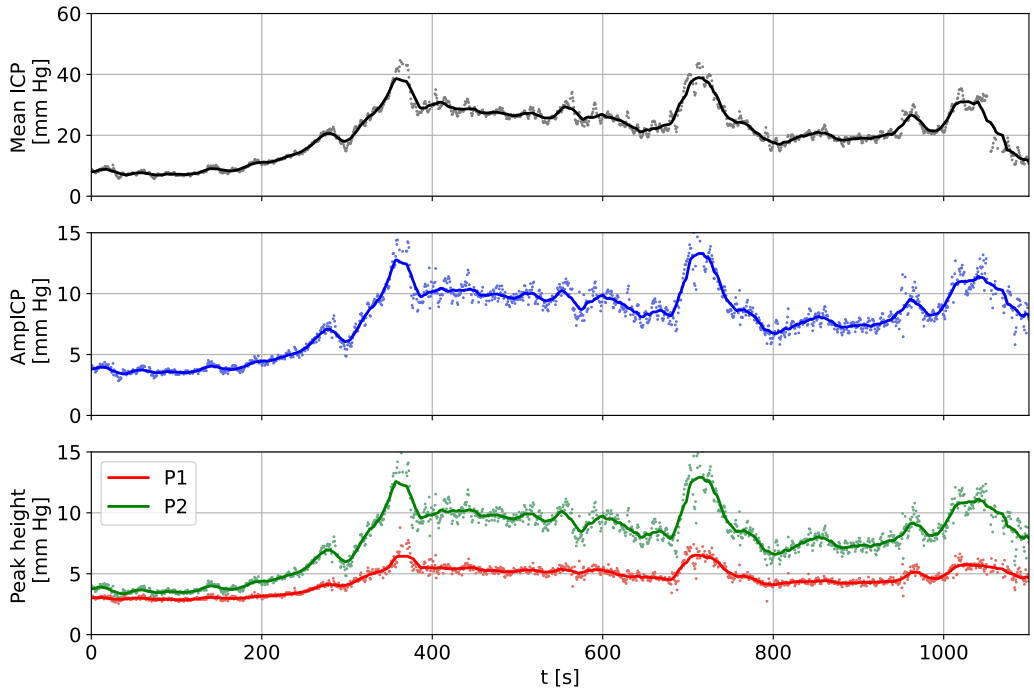

Figure 3.7. Illustrative example of changes in a) mean intracranial pressure (ICP), b) peak-to-peak pulse amplitude of ICP, and c) height of peak P1 (red symbols) and P2 (green symbols) during constant rate infusion for a single patient. Full pulse-by-pulse time courses are presented with dots and 30-pulse moving averages are presented with solid lines. Modified from (Kazimierska et al., 2021a).

Table 3.1. Comparison of physiological signals and calculated indices between the baseline and plateau phase of the infusion test with Wilcoxon signed rank test p value. Data are presented as median [first–third quartile].

Parameter	**Baseline**	**Plateau**	***p* value**
Mean ICP [mm Hg]	13.4 [9.5–16.5]	22.6 [18.7–28.1]	$\ll .001$
Mean CBFV [cm/s]	53.0 [39.4–59.1]	48.9 [39.6–57.5]	$< .001$
AmpICP [mm Hg]	3.9 [2.6–4.8]	6.4 [4.7–8.6]	$\ll .001$
AmpCBFV [cm/s]	38.3 [31.1–49.8]	38.0 [31.9–51.8]	.002
AmpC_aBV [%]	100 [100–100]	105 [99–116]	$< .001$

3.4.2 Comparison of cerebrospinal compliance estimates

All three compliance estimates decreased between the baseline and plateau phase of the infusion test (Table 3.2). The largest change relative to baseline value of 100% was observed for C_{CSF} (46 [37–65] %), smaller for $C_{\mathrm{C_aBV}}$ (41 [31–48] %), and the smallest for $C_{\mathrm{P1/P2}}$ (16 [7–28] %). The time courses of compliance estimates were strongly and significantly ($p < .05$) correlated with each other: 0.94 [0.88–0.97] for C_{CSF} vs $C_{\mathrm{C_aBV}}$, 0.77 [0.63–0.91] for C_{CSF} vs $C_{\mathrm{P1/P2}}$ and 0.68 [0.48–0.91] for $C_{\mathrm{C_aBV}}$ and $C_{\mathrm{P1/P2}}$. Furthermore, both $C_{\mathrm{C_aBV}}$ and $C_{\mathrm{P1/P2}}$ showed strong inverse correlation with mean ICP (C_{CSF} was not compared with mean ICP as it is directly calculated from this parameter): -0.82 [-0.71–-0.86] and -0.71 [-0.46–-0.79], respectively. An illustrative example of changes in mean ICP and compliance estimates for a single patient is presented in Figure 3.8.

Table 3.2. Comparison of compliance estimates between the baseline and plateau phase of the infusion test with Wilcoxon signed rank test p value. Data are presented as median [first–third quartile]; a.u.—arbitrary units.

Compliance estimate	**Baseline**	**Plateau**	***p* value**
C_{CSF} [ml/mm Hg]	0.67 [0.37–1.16]	0.27 [0.17–0.51]	$\ll .001$
$C_{\mathrm{P1/P2}}$ [a.u.]	0.69 [0.58–0.90]	0.57 [0.46–0.74]	$\ll .001$
$C_{\mathrm{C_aBV}}$ [cm/mm Hg]	1.16 [0.71–1.75]	0.72 [0.50–1.00]	$\ll .001$

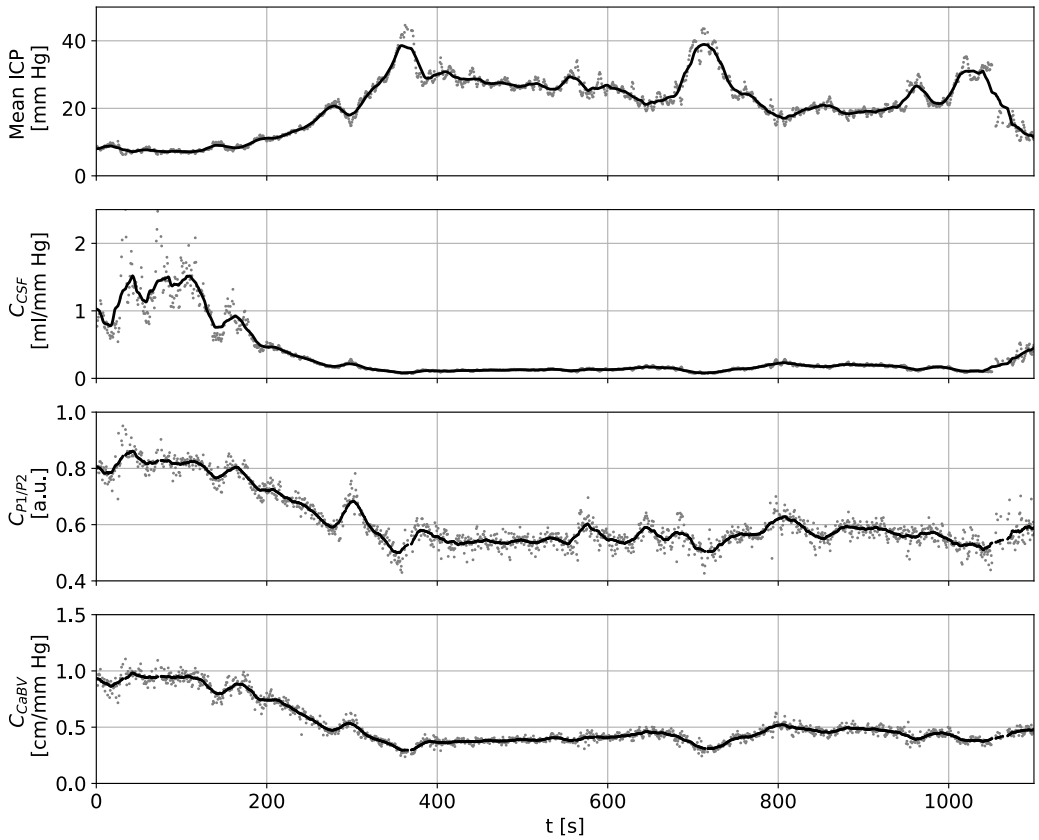

Figure 3.8. Illustrative example of changes in a) mean intracranial pressure (ICP) and compliance estimates obtained with b) the model of cerebrospinal fluid dynamics (C_{CSF}), c) P1/P2 ratio of ICP pulse waveform ($C_{\mathrm{P1/P2}}$), d) evaluation of changes in cerebral arterial blood volume ($C_{\mathrm{C_aBV}}$) during constant rate infusion test for a single patient. Full pulse-by-pulse time courses are presented with dots and 30-pulse moving averages are presented with solid lines. a.u.—arbitrary units. Modified from (Kazimierska et al., 2021a).

3.5 Discussion

The aim of this study was to assess the possibility of monitoring cerebrospinal compliance using the information contained in the shape of the ICP pulse waveform. Three methods of compliance estimation were used to examine the changes produced by external volumetric manipulation in the form of constant rate infusion in NPH patients. Firstly, compliance was calculated using a model of CSF dynamics in the intracranial space, which is considered the 'gold standard' method. Secondly, the P1/P2 height ratio of individual ICP pulse waveforms was assessed over the entire recordings, and finally, a model of arterial CBV changes was used to compare changes in pulse amplitudes of CBV and ICP.

All three compliance estimates showed a marked decrease at elevated mean ICP. While the results produced by each of the methods varied greatly in terms of value, all three allowed for statistically significant differentiation between the 'high' and 'low' compliance

level, corresponding to low (baseline phase) and high (plateau phase) mean ICP. Individual time courses of $C_{\mathrm{P1/P2}}$ and $C_{\mathrm{C_aBV}}$ followed the 'gold standard' C_{CSF} closely, with median correlation coefficient of 0.77 and 0.94, respectively, suggesting a strong relationship. These results provide validation to the long-held belief that the configuration of characteristic peaks of the ICP pulse waveform reflects variations in cerebrospinal compliance. As noted by Cardoso et al. (1983), while progressive changes in intracranial volume and corresponding changes in compliance can be observed as variations in the overall pulse amplitude, they primarily affect the second peak. Accordingly, although the heights of both the first and second peak were strongly correlated with the time course of mean ICP, peak P2 showed a more pronounced increase with reduced compliance than peak P1, leading to diminished P1/P2 ratio. Additionally, performed analysis proved the validity of using model-based $C_{\mathrm{C_aBV}}$ to monitor cerebrospinal compliance, as postulated by previous studies (Kim et al., 2009b, 2012).

However, it should be noted that the three analysed estimates have certain inherent differences. Most importantly, only C_{CSF} is a direct approach producing absolute values of compliance expressed in ml/mm Hg. CBFV, measured in cm/s, serves as a surrogate for CBF with the assumption that the diameter of insonated vessel remains constant during the measurement (see the Limitations subsection). As a result, $C_{\mathrm{C_aBV}}$ has the units of cm/mm Hg instead of ml/mm Hg and cannot be directly compared between patients, allowing instead for monitoring of relative changes over time. $C_{\mathrm{P1/P2}}$ as the ratio of peak heights expressed in mm Hg is dimensionless. Peak ratios can theoretically be compared between patients, as similar P1/P2 ratio indicates similar configuration of the first two peaks even if the specific shape of the waveform varies, but each patient may exhibit different baseline level and the cerebral fraction of stroke volume contributing to the pulse waveform is unknown in this method. Therefore, absolute value of $C_{\mathrm{P1/P2}}$ must be interpreted with caution and taking into account the patient's reference point.

The three estimates are also calculated using different time scales, which could explain certain dissimilarity between their time courses. The CSF dynamics model relies on the trend in mean ICP both in initial estimation of model parameters and later in calculation of compliance, and the time course of C_{CSF} is obtained retrospectively from the analysis of the entire recording. On the other hand, both of the indirect methods produce results in a pulse-by-pulse manner, independent of the preceding and subsequent values. This difference in time scales was only partially alleviated by the use of 30-pulse averages in correlation analysis. Moreover, while C_{CSF} and $C_{\mathrm{P1/P2}}$ are based solely on the ICP signal, $C_{\mathrm{C_aBV}}$ also takes into account CBFV, which is recorded synchronously with ICP but is fundamentally a different modality.

The separate CBFV measurement can be considered a limitation of the $C_{\mathrm{C_aBV}}$ approach as TCD monitoring cannot be performed if the acoustic window in the skull cannot be accessed (which may concern 10–20% of patients (Baumgartner, 2006)) and continuous recording over many hours is only possible if the probe is fixed in a stable position; the latter can be easily disturbed, for instance, by the need to move the patient. Conversely, the P1/P2 approach can be applied as long as the ICP signal is recorded with sufficiently high sampling frequency to examine the pulse waveform in detail. This method, however, is strongly dependent on precise peak identification. The aim of this study was to vali-

date the proposed peak ratio method against the 'gold standard' rather than introduce a new tool for morphological analysis. Consequently, peak detection was performed using a semi-automated algorithm with supplementary signals and the results were manually verified in order to minimise the influence of erroneous annotations. In order to employ this technique in continuous monitoring, a fully automated peak identification tool would have to be proposed. This task was undertaken by numerous groups over the years with varying degree of success (Hu et al., 2009; Elixmann et al., 2012; Calisto et al., 2013; Lee et al., 2016). Moreover, delineation of local maxima in the pulse contour becomes impossible in pathologically rounded waveforms that appear at elevated mean ICP. In this study, 16 recordings (22% of the initial group) were excluded from analysis due to the inability to distinguish P1 even at baseline. While pathologically altered, nearly sinusoidal pulses could potentially be identified separately and used as a form of 'low compliance indicator', this problem further complicates the technical side of the P1/P2 approach.

Nevertheless, strong correlation between the 'gold standard' method and peak analysis supports the application of the latter technique in continuous monitoring of relative changes in cerebrospinal compliance without the need for volumetric manipulation. To date only a limited number of studies focused on this approach, especially in TBI patients in whom compliance assessment offers the most potential benefits but externally induced changes in intracranial volume can be too hazardous (Robertson et al., 1989). In addition to the early observations by Cardoso et al. (1983), the peak ratio (expressed in this case as P2/P1) was shown to differ in TBI patients who exhibited disproportionately increased ICP and those who did not (Fan et al., 2008), even though P2/P1 higher than 0.8 was not an independent predictor of such episodes (Mitchell et al., 1997; Fan et al., 2008). However, P2/P1 ratio of 0.8 roughly corresponds to P1/P2 of 1.2; in this study all patients presented baseline $C_{\mathrm{P1/P2}}$ below that level. On the one hand, NPH and TBI are different clinical entities and patients in both groups may exhibit different pattern of changes in cerebrospinal compliance due to different underlying pathologies. On the other hand, a revised threshold may improve the performance of peak ratio in identification of patients at risk of potentially threatening ICP elevations. Further investigation into the relationship between the shape of the ICP pulse waveform and the status of the patient is required in order to employ the P1/P2 ratio as an indicator of volume decompensation in the clinical setting. Interestingly, between the publication (Kazimierska et al., 2021a) and the time of writing of this dissertation, there appeared some renewed interest in this approach, with a study in decompressive craniectomy patients showing the link between P2/P1 ratio and loss of skull integrity (Brasil et al., 2021). Analysis of the P1/P2 ratio was also continued in a co-authored study on relative changes in the ICP and CBFV pulse waveform shapes (Ziółkowski et al., 2021) which demonstrated that in NPH patients the P1/P2 ratio estimated at baseline before infusion is significantly correlated with intracranial elasticity (Spearman correlation coefficient $R = -0.42$, $p = .018$) and the RAP index ($R = -0.38$, $p = .040$), suggesting its potential to reveal disturbances in CSF dynamics without external volumetric manipulation.

3.5.1 Limitations

This study was conducted as a retrospective analysis of recordings selected from the existing database of infusion studies performed at Addenbrooke's Hospital (Cambridge, UK). As transcranial Doppler measurement is not part of routine clinical procedure in hydrocephalus patients, these data constitute a unique set of simultaneously recorded ICP and CBFV signals, with ICP monitored via pre-implanted Ommaya reservoirs rather than the more common lumbar puncture. Repeated collection of the same type of data could be regarded as a wasteful misuse of time and resources. However, as the recordings were not originally collected with the explicit purpose of analysing the ICP and CBFV pulse waveform in detail and the patient group was limited, a relatively high number of cases were excluded due to insufficient quality of either signal (28%). The exclusion rate was further increased by the presence of pathologically rounded waveforms that did not allow for identification of peaks P1 and P2 (22%).

Secondly, the use of peak height ratio and evaluation of changes in C_aBV in compliance assessment is based on the assumption that the cerebral fraction of stroke volume is constant during the infusion test. As the fraction of stroke volume is not measured simultaneously, the indirect compliance estimates cannot be translated to absolute values expressed in ml/mm Hg. Moreover, the C_aBV evaluation method uses the CBFV signal as a surrogate for CBF with the assumption that the diameter of insonated vessel remains unchanged during the measurement and CBFV differs from CBF only by a constant factor representing the cross-sectional area of the artery. This approach also assumes a lack of pulsatility in cerebral venous outflow which is in fact pulsatile, albeit to a smaller extent than arterial inflow. Analysis of the validity of these assumptions has been conducted in one of the previous studies on the C_aBV evaluation model (Kim et al., 2009b) and the authors concluded it should not introduce significant errors to compliance estimation based on TCD measurement in the middle cerebral artery.

Chapter 4

Morphological classification of intracranial pressure pulse waveforms using deep neural networks

The results presented in this chapter were published in:

- Mataczyński, C.*, Kazimierska, A.*, Uryga, A., Burzyńska, M., Rusiecki, A., and Kasprowicz, M. (2022). End-to-end automatic morphological classification of intracranial pressure pulse waveforms using deep learning. *IEEE Journal of Biomedical and Health Informatics*, 26(2):494–504. *joint first authorship
- Kazimierska, A., Uryga, A., Mataczyński, C., Burzyńska, M., Ziółkowski, A., Rusiecki, A., and Kasprowicz, M. (2021). Analysis of the shape of intracranial pressure pulse waveform in traumatic brain injury patients. In: *Annual International Conference of the IEEE Engineering in Medicine and Biology Society (EMBC 2021)*, pages 546–549, Mexico. IEEE.

Full text of the papers can be found in Appendix A.

4.1 Introduction

As shown in Chapter 3, the ICP pulse waveform contains information about cerebrospinal compliance encoded in the ratio of local maxima P1 and P2 and the indirect measure produced by waveform analysis allows for reliable monitoring of relative changes in compliance. However, accurate peak detection is a complex task due to the wide variety of pulse waveform shapes observed in the clinical setting (including distorted waveforms considered as artefacts but not easily distinguished from valid pulses) and existing approaches have not gained universal acceptance outside research. Taking into account the difficulties associated with precise peak identification and the occurrence of pathologically changed, rounded waveforms with no distinguishable peaks, Nucci et al. (2016) proposed a set of visual criteria for classification of ICP pulse waveforms observed in hydrocephalus patients. In this approach, instead of denoting the peaks P1, P2, and P3, the overall shape of the signal is inspected visually and assigned to one of four possible categories which roughly correspond to different peak configurations. Class 1 ('normal') represents

the saw-tooth shape with three identifiable peaks arranged in a descending pattern, with P1 as the dominant peak. Class 2 ('potentially pathological') encompasses waveforms with increased prominence of the middle peak P2 but P1 still dominating over P3 while class 3 ('likely pathological') includes pulses where P2 and P3 significantly exceed the first peak. Finally, class 4 ('pathological') is used to identify rounded or triangular waveforms that do not permit peak annotation. In their study, Nucci et al. developed a method of automatic classification of ICP pulse waveforms using a shallow artificial neural network taking a radial basis function approximation of the pulse as input; this approach was reported to have 88.3% accuracy compared to an expert examiner in an additional set of pulses not included in training (Nucci et al., 2016), but it was not tested in data derived from different patient groups. The authors suggested that in hydrocephalus patients, pulse shape classification could reveal the disruption of cerebral volume–pressure equilibrium without the need for external volumetric manipulation.

This technique, however, has never been applied to continuous, long-term (i.e. lasting several days and therefore much longer than the infusion test performed over approximately half an hour) ICP recordings obtained in TBI patients. In this group, previous efforts to employ artificial neural networks focused generally on distinguishing valid from artefactual patterns (Lee et al., 2019), detection of long-term trends (Mariak et al., 2000), and predicting ICP elevation (Swiercz et al., 2000; Quachtran et al., 2016; Lee et al., 2021). Meanwhile, the advancements in the field of machine learning in recent years brought to light the potential of a relatively new type of models, the deep neural networks, to recognise data patterns (Ganapathy et al., 2018; Rim et al., 2020), including various types of blood pressure pulses (Li et al., 2019). Therefore, the aim of this study was to propose a method for automatic classification of different ICP pulse waveform shapes reflecting changes in cerebrospinal compliance based on deep neural networks with simultaneous detection of invalid artefactual pulses. If proven to be successful, this approach would offer the possibility of indirect continuous monitoring of cerebrospinal compliance not burdened by the need for precise peak identification.

4.2 Material

Data used in this study were collected between 2014 and 2019 in patients admitted to the NCCU of Wrocław University Hospital (Wrocław, Poland). The study was approved by the Ethics Committee at Wrocław Medical University (approvals no KB-624/2014 and KB-134/2014) and conducted in adherence to the Declaration of Helsinki. ICP was measured invasively with intraparenchymal sensors inserted into the frontal cortex (Codman MicroSensor ICP Transducer; Codman & Shurtleff, Randolph, MA, USA). ABP was measured with standard monitoring kits (Baxter Healthcare, CardioVascular Group, Irvine, CA, USA) in the radial or femoral artery. The signals were recorded simultaneously using ICM+ software (Cambridge Enterprise Ltd, Cambridge, UK) with sampling frequency of 50 Hz or higher (up to 300 Hz; all signals were later resampled to 50 Hz in order to reduce computation time taking into account earlier studies on recommended minimum sampling rate for ICP pulse waveform analysis (Holm and Eide, 2009). Monitoring commenced on

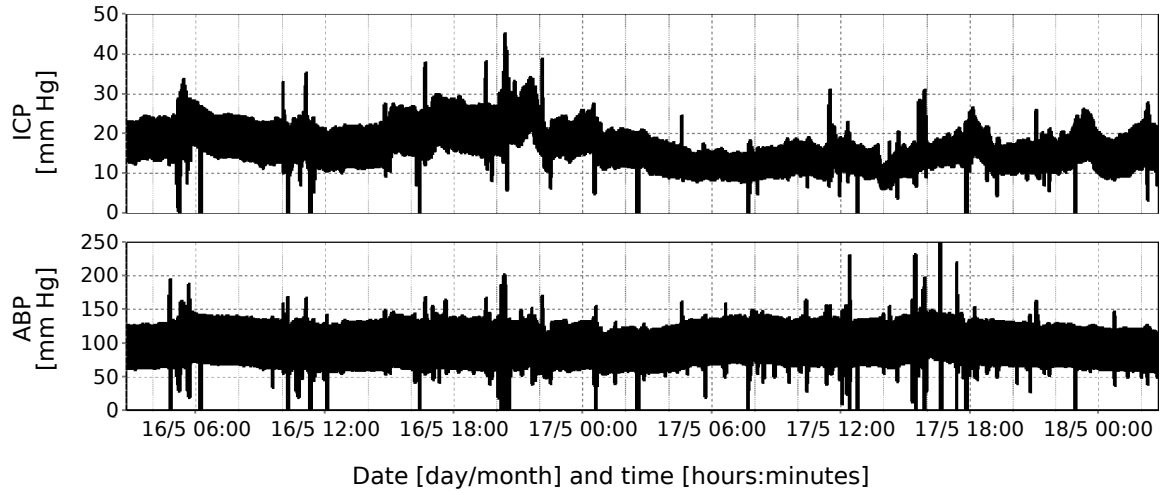

Figure 4.1. Illustrative example of a long-term intracranial pressure (ICP; top panel) and arterial blood pressure (ABP; bottom panel) recording spanning approximately two days. Note that the recording of both signals contains a number of short-term disturbances visible as sharp drops and spikes which may have been caused e.g. by movement of the patient, tracheal suction, arterial blood sampling etc.

day 1 or day 2 after admission to the hospital (depending on the time of surgery), with admission occurring in most cases on the day of injury. Patients were monitored throughout their NCCU stay until medical indications prompted the decision to remove the ICP sensor (average monitoring time: 5 ± 3 days). Patient condition in the NCCU was assessed using the Glasgow Coma Scale (GCS) (Teasdale and Jennet, 1974; Teasdale et al., 2014). Outcome was assessed three months after discharge from the hospital using the Glasgow Outcome Scale (GOS) (Jennet and Bond, 1975; McMillan et al., 2016). An illustrative example of long-term ICP and ABP recording is presented in Figure 4.1.

The patients included in retrospective analysis were selected based on availability and sufficient quality of the ICP signal. The full dataset of 50 patients consisted of two groups with different clinical diagnosis: TBI or aneurysmal subarachnoid haemorrhage (aSAH). TBI patients ($n = 39$) were treated according to the American Brain Trauma Foundation guidelines applicable at the time of admission (Bratton et al., 2007; Carney et al., 2017). Patients with confirmed aSAH ($n = 11$) were treated according to the American Heart Association/American Stroke Association guidelines (Connolly et al., 2012). While TBI and aSAH are separate clinical entities with distinct pathophysiology, both are linked with disturbance of the volume equilibrium in the intracranial space and consequently, both are expected to produce changes in the ICP pulse waveform. Previous studies have sometimes combined data from different pathologies to increase the number of available recordings during development of computational tools (Hu et al., 2009; Scalzo et al., 2009). In this study, the two groups formed separate datasets used for training/validation and testing of the proposed neural network, respectively (see Section 4.3.3 for details).

Clinical characteristics of the TBI cohort are summarised in Table 4.1 and presented in detail in (Mataczyński, Kazimierska et al., 2022).

Table 4.1. Clinical characteristics of the traumatic brain injury cohort (39 patients). Data are presented as number of occurrences (% of total group) or as median [first–third quartile]. GCS—Glasgow Coma Scale, GOS—Glasgow Outcome Scale; n—number of occurrences, $Q1$—first quartile, $Q3$—third quartile. Modified from (Mataczyński, Kazimierska et al., 2022).

Parameter	**Value**
Age [years] mean & range	mean: 43, range: 20–85
Sex n (%)	male: 27 (69%), female: 12 (31%)
GCS median [$Q1$–$Q3$]	6 [5–8]
GOS at discharge median [$Q1$–$Q3$]	3 [2–3]
30-days mortality n (%)	4 (10%)
GOS after 3 months median [$Q1$–$Q3$]	3 [1–4]

4.3 Methods

4.3.1 Problem formulation

The aim of this study was to design a comprehensive solution for classification of ICP pulse waveforms in long term ICP recordings obtained from NCCU patients. In particular, the algorithm was expected to accept a raw, unprocessed ICP signal and produce final results without human intervention during the pre-processing or analysis stages (i.e. an end-to-end approach). The problem could therefore be stated to encompass two separate tasks: pulse onset detection followed by classification of individual waveforms (including both valid waveforms and simultaneously identified artefacts) and described as obtaining a mapping from the full-length ICP signal to a set of values containing the location of each pulse and its detected class.

An overview of the proposed analysis pipeline is presented in Figure 4.2. In addition to the four classes introduced by Nucci et al. (2016), a fifth class representing artefactual waveforms was included to simultaneously identify distorted waveforms resulting from disturbances either at the signal collection stage (e.g. patient movement, sensor displacement, tracheal suction, etc.) or individual pulse detection stage (i.e. incorrectly marked pulse onset points). This change was made in order to avoid adding a separate artefact removal algorithm to the pipeline while still reducing the influence of invalid waveforms on final results.

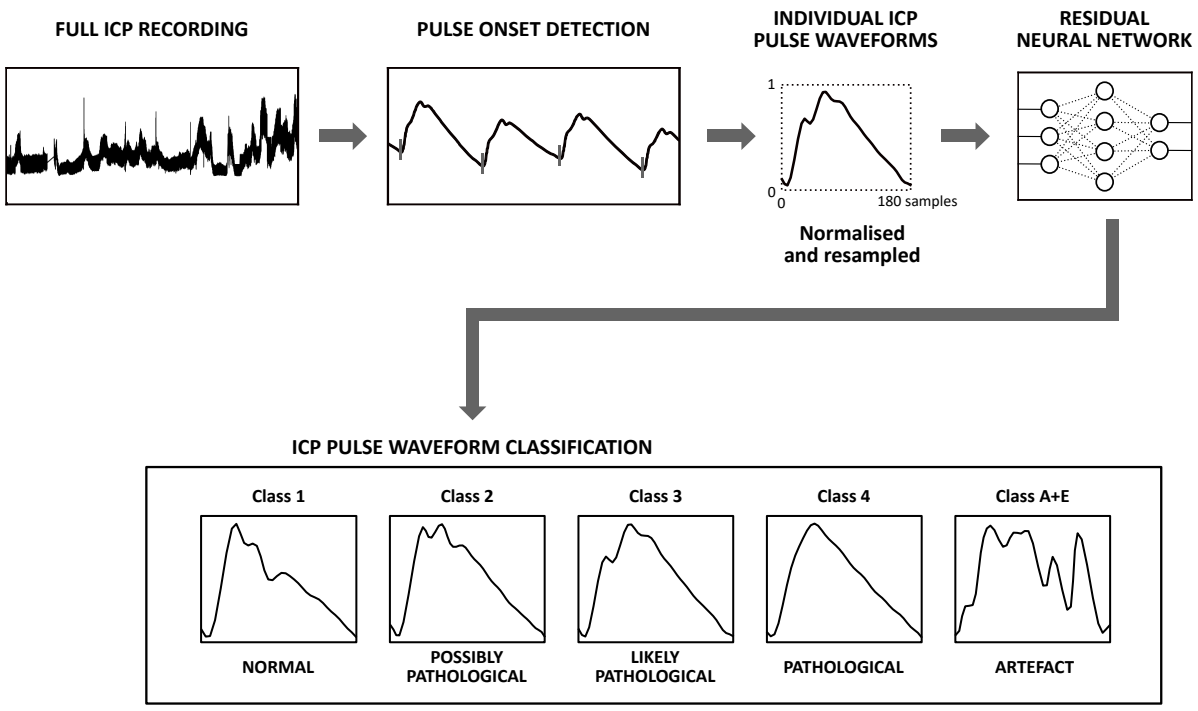

Figure 4.2. Overview of the proposed approach to intracranial pressure (ICP) pulse waveform classification with illustrative examples of waveforms from each class.

4.3.2 Individual pulse detection and processing

The modified Scholkmann algorithm, previously validated for use with neuroscience data such as the ICP signal (Bishop and Ercole, 2018), was used for pulse onset detection. Pulse detection was performed in full long-term recordings low-pass filtered with the cutoff frequency of 10 Hz, taking into account studies that showed that the power of the ICP signal is mostly contained in the frequency range below 8 Hz (Dai et al., 2020).

In order to remove the effect of differences in pulse length and amplitude on classification results, the latter of which is strongly correlated with mean ICP and could vary between patients despite comparable pulse shape, the pulses were scaled to an interval from 0 to 1 and resampled to uniform length of 180 samples using cubic resampling. One dimensional (1-D) vectors of normalised signal samples were used as input to the classification model. Other types of data representations were tested but did not improve classification accuracy and were rejected (see Section 4.4.3).

4.3.3 Classification datasets

The recordings from 39 TBI patients were the source of the training/validation dataset while the data from 11 aSAH patients formed a separate testing dataset used to assess the ability of the proposed model to generalise to different data distributions. In both cases a number of individual ICP pulse waveforms was selected randomly from full-length recordings and manually assigned a waveform class by an expert researcher.

In the training/validation dataset, 21390 ICP pulses were selected. Corresponding fragments of the ABP signal were extracted simultaneously to aid in manual classification

as it has been shown previously that the systolic part of the ABP pulse correlates with the position of peak P1 in ICP pulse and the slopes of both signals become increasingly divergent with more pathological waveform shape (Carrera et al., 2010). Each example was then annotated by an expert researcher. It was noted that pulses from the same patient within one waveform class show a high degree of similarity. In order to prevent that similarity from influencing the model's generalisation ability, the patients were divided into non-overlapping training and validation groups. A simple binary genetic algorithm was used to separate pulses with approximately 2:1 ratio of training to validation examples in each class. This resulted in a split into the training dataset with 14578 pulses and the validation dataset with 6812 pulses. Pulses exhibiting features of two adjacent classes or lacking agreement between the experts' assessment were assigned two labels: 'primary class' and a secondary 'possible class'. This step was introduced in acknowledgement of the fact that a four-category scale is inherently unable to capture the full range of ICP shapes observed in the clinical setting.

In the testing dataset formed of aSAH patients, 650 pulses were selected in the abovedescribed manner. The examples were manually annotated by a panel of three expert researchers. Inter-rater agreement between the experts' primary type annotations was tested with the Fleiss κ test (Artstein and Poesio, 2008) with significance level of 0.05 and showed statistically significant substantial agreement in the reference classification ($\kappa = 0.700$, 95% CI 0.672–0.728, $p < .001$).

The distribution of pulse examples between classes in all three datasets is presented in Figure 4.3.

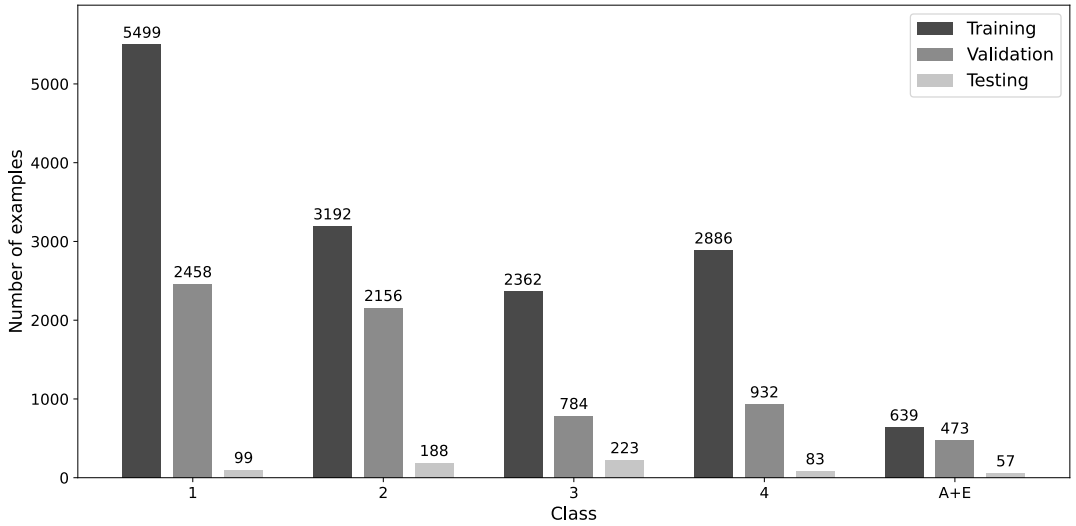

Figure 4.3. Distribution of examples between waveform classes in the training (total number of pulses: 14578), validation (total number of pulses: 6812), and testing dataset (total number of pulses: 650). Modified from (Mataczyński, Kazimierska et al., 2022).

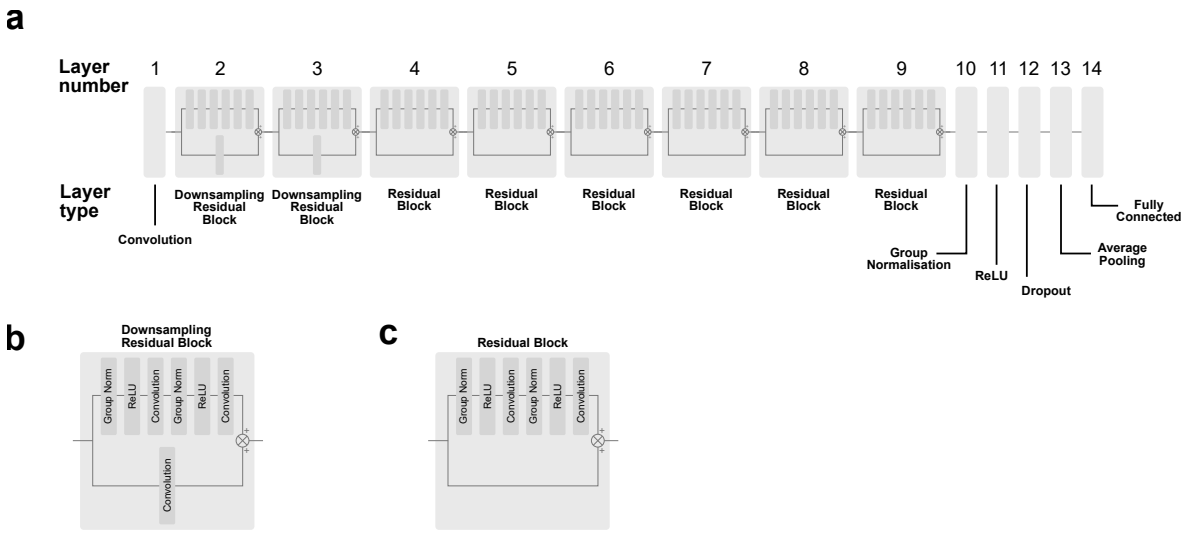

Figure 4.4. Architecture of used residual network: a) full architecture, b) detailed representation of the Downsampling Residual Block, c) detailed representation of the Residual Block. Modified from (Mataczyński, Kazimierska et al., 2022).

4.3.4 Classification model and its evaluation

A number of different neural network models were investigated to achieve the highest classification accuracy; this section describes the best performing model while the rejected configurations are presented in Section 4.4.3.

The best performing model in terms of classification accuracy was a 1-D Residual Neural Network (ResNet) whose architecture and hyperparameters are presented in Figure 4.4 and Table 4.2, respectively. The convolution nodes are all 1-D convolution. The Residual and Downsampling Residual blocks are standard residual blocks with convolutions of size 3 and group normalisation with 32 groups. The Downsampling block is also scaling the input by adding stride 2 to the first convolution in the main branch and adding size 1 convolution with stride 2 and the same number of filters as the main branch to the skip connection branch. The initial Downsampling blocks are used to reduce the size of the processed tensors.

The hyperparameters were chosen through the empirical choice method across multiple experiments. Training was performed for 100 epochs optimised by stochastic gradient descent with Nesterov momentum of 0.95 and starting learning rate of 0.01 and using cross entropy loss. Learning rate was lowered to 0.001 on epoch 33 and to 0.0001 on epoch 66. Classification accuracy was evaluated based only on primary class annotations (standard single-label accuracy, denoted 'strict accuracy') as well as both primary and possible class. In the latter approach (denoted 'best accuracy'), the prediction was considered correct if the predicted class matched either of the manual annotations. The second scoring method was introduced to test the model's performance in cases where the experts allowed the possibility of assigning the waveform to more than one class.

Table 4.2. Hyperparameters of the residual network presented in Figure 4.4. Reproduced from (Mataczyński, Kazimierska et al., 2022).

Layer number	**Layer type**	**Hyperparameters**
1	1-D Convolution	Filters = 64, Window = 3, Stride = 1
2–3	Downsampling Residual Block	Filters = 64, Stride = 2
4–9	Residual Block	Filters = 64, Stride = 1
10	Group Normalisation	Groups = 32, Channels = 64
11	ReLU	Not applicable
12	Average Pooling	Adaptive to size 1
13	Dropout	0.6 probability during training
14	Fully Connected	64 inputs, 5 neurons

4.3.5 Potential for real-time processing

In order to test the best performing model's potential to be employed in near real-time analysis of the ICP recording in the clinical setting, a single illustrative recording was processed in 10-second chunks and the computation times for pulse onset detection and pulse classification were recorded. The recording was presented to the algorithm in chunks because the pulse detection stage cannot be performed on individual signals samples, and short fragments of the signal can be said to approximate continuous monitoring. The test was performed on a machine with AMD Ryzen 99 3900XT (3.8–4.7 GHz) 12 core CPU and Nvidia GeForce RTX 3090 GPU with 24 GB of VRAM.

4.3.6 The relationship between waveform class and other derived indices

Full classification results were obtained in 35 TBI patients. Four patients from the initial group used to develop the model were excluded from further analysis as their ICP recordings included large gaps (lasting more than several hours and likely related to procedures performed as part of clinical management) that had no effect on single pulse classification but could impact the analysis of the relationship between ICP pulse waveform class and other metrics.

Additionally, each patient was characterised by metrics calculated over the full recordings: mean ICP, pulse amplitude of ICP (AmpICP), and RAP index. Both mean ICP and AmpICP were calculated in 10-second windows as the average ICP value and the amplitude of the fundamental component in the signal's Fast Fourier Transform spectrum (frequency range 0.6–3 Hz), respectively. RAP index was calculated as the Pearson correlation coefficient between mean ICP and AmpICP in 5-minute windows shifted every 10 seconds. The interpretation of the RAP index is presented in Section 1.4.2 of Chap-

ter 1. Each pulse was then assigned a corresponding mean ICP, AmpICP, and RAP value and each patient was characterised by mean ICP, AmpICP, and RAP averaged over all pulses of given class.

Statistical analysis was performed using Statistica software (v13.1, Tibco, Palo Alto, Ca, USA) and Python 3.7. Significance level of 0.05 was assumed in all analyses. Data distributions were tested for normality using the Shapiro–Wilk test and the normality of most of analysed variables was rejected. The relationships between waveform class and other ICP-derived metrics (mean ICP, AmpICP, and RAP index) were assessed using partial correlation coefficient between analysed variables.

4.4 Results

4.4.1 Model performance

Table 4.3 outlines the overall classification accuracy of the selected best performing ResNet model. In the validation dataset comprised of TBI patients, the network achieved strict accuracy of 93%, and in the independent testing dataset of aSAH patients, almost 82%. The use of best accuracy score resulted in improved performance in both sets, with increase up to 95% and up to 86% in the validation and testing dataset, respectively.

As shown by the confusion matrices (Figure 4.5), in both datasets classification errors for the non-artefactual classes primarily occurred between adjacent classes (e.g. class 1 and 2), with a small number of cases where a normal waveform was marked as fully pathological or vice versa. One exception was a relatively high number of mislabelled examples between classes 2 and 4. Furthermore, in the validation dataset a large percentage of incorrect class assignments concerned the artefact class (A+E).

Interestingly, detailed classification scores for each of the waveform classes (Table 4.4) revealed additional differences between the validation and testing datasets. Only class 1 retained consistently high scores across both sets, with comparable precision, recall, and specificity. In the validation set, the other four classes showed similar F_1 scores, but class 2 exhibited higher precision balanced by lower recall, an inverse relationship than classes 3, 4, and A+E. Class 2 was also characterised by the lowest specificity. Conversely, in the testing dataset specificity was visibly decreased for class 4 and so was recall, leading to a markedly smaller F_1 score. Moreover, the relationship between precision and recall for classes 2 and A+E was reversed compared to the other dataset.

Table 4.3. Overall classification accuracy of the residual network model in different datasets. N—total number of pulses in dataset. Modified from (Mataczyński, Kazimierska et al., 2022).

Parameter	**Training set** ($N = 14578$)	**Validation set** ($N = 6812$)	**Testing set** ($N = 650$)
Strict accuracy [%]	97.8	93.0	81.9
Best accuracy [%]	98.5	95.2	86.0

Table 4.4. Detailed classification scores of the residual network model in the validation and testing dataset. N—total number of pulses in dataset. Reproduced from (Mataczyński, Kazimierska et al., 2022).

Validation set ($N = 6812$)

Score	**Class 1**	**Class 2**	**Class 3**	**Class 4**	**Class A+E**
Precision	0.95	0.94	0.75	0.76	0.73
Recall	0.95	0.72	0.90	0.93	0.99
F_1	0.95	0.82	0.82	0.84	0.84
Specificity	0.97	0.88	0.99	0.99	0.99

Testing set ($N = 650$)

Score	**Class 1**	**Class 2**	**Class 3**	**Class 4**	**Class A+E**
Precision	0.95	0.76	0.73	0.98	0.91
Recall	0.90	0.93	0.93	0.55	0.74
F_1	0.93	0.84	0.82	0.70	0.82
Specificity	0.98	0.98	0.97	0.88	0.97

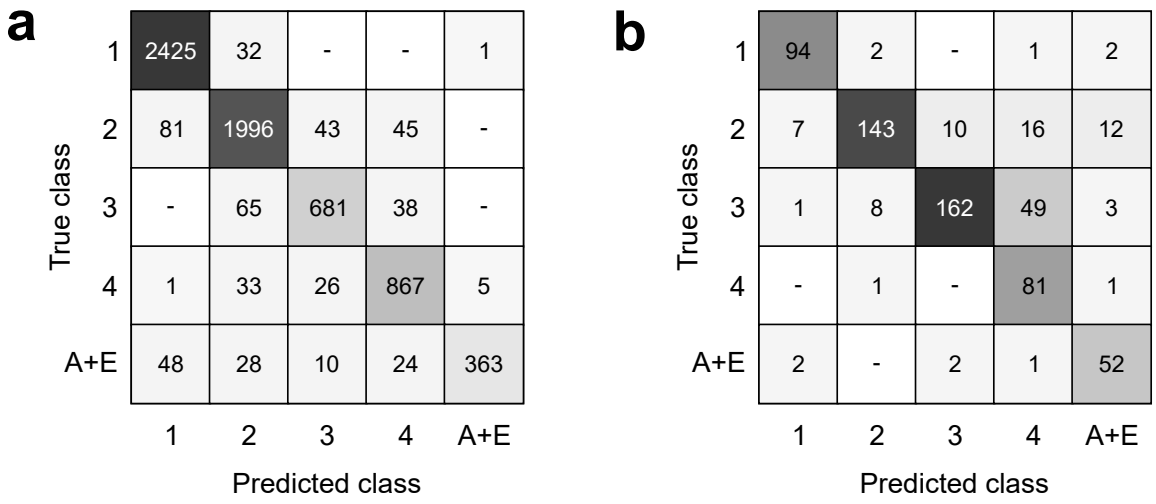

Figure 4.5. Confusion matrices of the residual network model for the a) validation dataset (total number of pulses: 6912) and b) testing dataset (total number of pulses: 650). The number in each tile shows how many examples with given true label were assigned to given predicted class. The darker the tile, the higher the percentage of all pulses it represents. Modified from (Mataczyński, Kazimierska et al., 2022).

4.4.2 Potential for real-time analysis

The average processing time in a subset of 1000 10-seconds-long chunks of the ICP signal was 0.027 [0.026–0.029] seconds per pulse. The average time of pulse detection was 0.020 [0.019–0.021] seconds per pulse and the average time of pulse waveform classification was 0.0075 [0.0070–0.0080] seconds per pulse, making up approximately 73% and 27% of the full analysis time, respectively.

4.4.3 Rejected approaches to ICP pulse waveform classification

Different types of neural networks A fully connected network was used as a baseline for comparison. The ResNet that proved to have the highest accuracy was selected as a type of convolutional neural network capable of extracting morphological features using both the given sample and the neighbouring samples with more stable error propagation. While the proposed approach was intended for short signals (i.e. single pulses approximately one second long), and therefore not expected to require the modelling of long-term dependencies, a long-short term memory fully convolutional network was selected to test the possibility that those dependencies are more relevant to the classification problem. Additionally, models based on long-short term memory cells, gated recurrent unit cells, and shallow convolutional neural networks with different configurations were examined. The baseline fully connect network showed strict accuracy of 74% in the validation dataset and 69% in the testing dataset. None of the other modifications resulted in improved accuracy compared to the ResNet model, with the second-best performing option (long-short term memory fully convolutional network) achieving 89% and 78% accuracy in the validation and testing dataset, respectively.

Different data representations In addition to the 1-D vectors of signal samples that proved to be the most effective, different representations of the ICP pulse waveform were investigated: Fourier transform coefficients, spectrograms, orthogonal Chebyshev polynomials, empirical mode decomposition, radial basis function coefficients (as used by Nucci et al. (2016)), as well as signal conversion into a representative two-dimensional image (previously used in classification of valid vs artefactual pulses (Lee et al., 2019)). None of them showed improvement over the normalised 1-D vector, and the additional approximation steps could potentially lead to a loss of information on the ICP pulse morphology, so the alternative approaches were rejected. Another test included foregoing of the normalisation step in favour of presenting the pulses to the model with their original amplitudes. However, this reduced the generalisation ability of the model, suggesting the shape of the waveform is not directly connected to the pulse amplitude.

Furthermore, given the relationship between the ICP and ABP pulse, particularly the increasing dissimilarity of the waveforms associated with rounding of the ICP pulse, the possibility of using ABP as a second input to the model was tested. However, neither attaching the signal as a second input channel to the convolutional layers nor training a shared weights model of two univariate feature extractors had a positive effect on classification accuracy.

Multi-label classification The multi-label approach was used with the same type of networks but with separate sigmoids (classification threshold: 0.5) as output instead of a softmax block. The results were comparable to single-label classification (e.g. ResNet with a multi-label output achieved best accuracy of 95.6% compared to 95.2% in the standard approach), and this option was rejected as it introduces an additional level of complexity to the algorithm without a significant benefit in terms of accuracy.

4.4.4 The relationship between ICP pulse waveform class and other ICP-derived indices

Both mean ICP and AmpICP increased with higher waveform class (Figure 4.6), with partial correlation coefficients of 0.63 ($p < .001$) and 0.61 ($p < .001$), respectively, although AmpICP levelled off for class 3 and 4. RAP index rose with the change in waveform class from 1 to 3, but then presented a breakpoint with subsequent decrease for class 4, leading to a much smaller (although still statistically significant) partial correlation coefficient of 0.26 ($p = .004$).

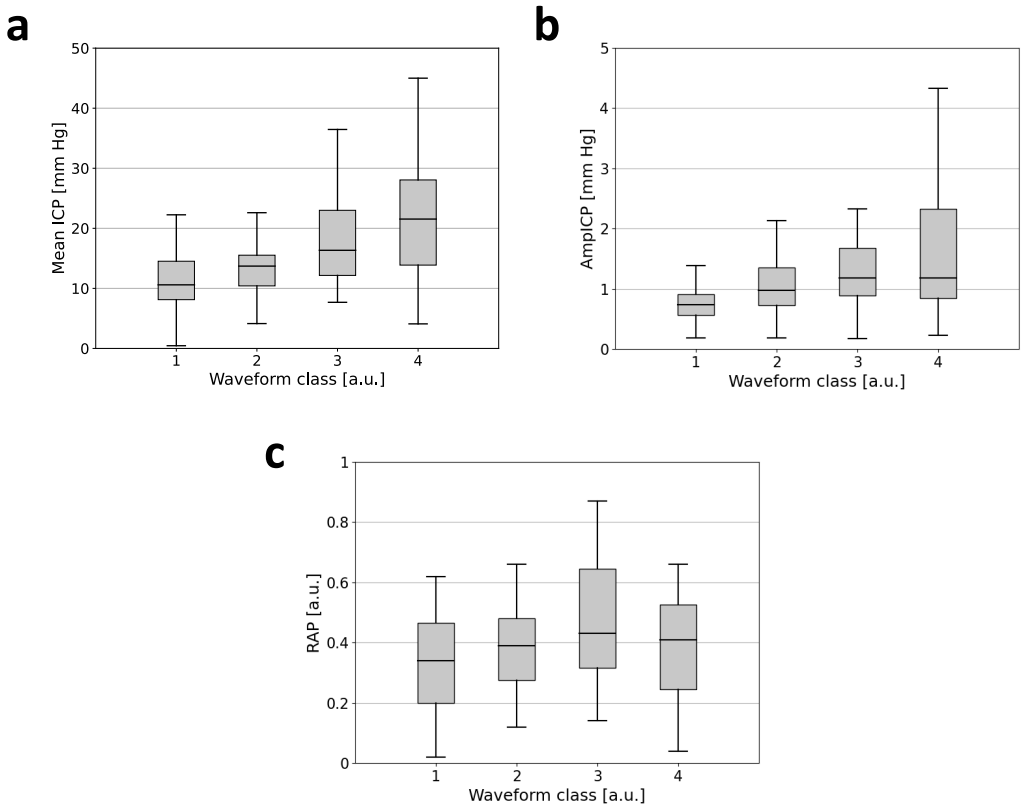

Figure 4.6. The relationship between intracranial pressure (ICP) pulse waveform class and derived parameters: a) mean ICP, b) spectral pulse amplitude of ICP (AmpICP), and c) index of compensatory reserve (RAP). Grey boxes represent the interquartile range, central line represents the median value and whiskers extend to extreme values not including outliers. a.u.—arbitrary units. Modified from (Kazimierska et al., 2021b).

4.5 Discussion

The primary aim of this study was to assess the feasibility of using deep neural networks to classify characteristic shapes of the ICP pulse waveform. The ResNet taking as input 1-D vectors of normalised signal samples was identified as the best performing model, capable of classifying the ICP pulse waveforms in the validation set with 93% accuracy (compared to 88% reported previously by Nucci et al. (2016)). The model also showed good accuracy of 82% in the independent testing dataset. As the testing examples were not only kept separate from the training and validation set but selected from a different group of patients, they represent a distinct data distribution which produced different classification scores for some of the analysed classes. Therefore, relatively high overall accuracy in the testing dataset proves good generalisation ability of the model and shows the possibility of applying it to other patient cohorts without a substantial degradation of performance. This is further supported by the fact that the classification was carried out at single pulse level and does not require information about the waveform's position in the full recording, making this approach robust to varying length of the recordings.

Moreover, the proposed algorithm was constructed as an end-to-end solution that encompasses both identification of individual pulses in full recordings and their classification, without the need for human intervention at any stage. The pulses are presented to the model with minimal pre-processing (i.e. only resampling and normalisation) which reduces the potential data loss associated with using techniques such as polynomial approximation or the Fourier transform. As invalid pulses constitute a separate waveform class, errors in pulse onset detection and artefacts in collected signals (e.g. spikes, drops, or waveform deformation) can also be marked simultaneously with valid waveforms and excluded from any further analyses, potentially reducing the number of false positive alarms during continuous monitoring. It has been shown previously that artefacts are a significant source of alarms in the clinical setting (Imhoff and Kuhls, 2006) and their removal improves the performance of various metrics used in the management of TBI patients (Lee et al., 2019). By treating those invalid pulses as a different waveform type, the proposed algorithm removes the need for an additional artefact detection step, reducing the overall complexity. In its current form, assuming sufficient hardware configuration, this approach could work in near real-time, with the computation time for a 10-second fragment of the signal shown to be much lower than 10 seconds. As long as the recording is presented in chunks rather than as individual samples, therefore making pulse onset detection possible, classification results could be obtained with only a slight delay.

However, it should be noted that in all datasets the use of best accuracy as a more relaxed metric allowing for two classes to be considered correct for a given example improved the model's performance. It increased the accuracy up to 95% and up to 86% for the validation and testing dataset, respectively. Combined with the fact that the majority of classification errors occurred between adjacent classes, this could suggest that a four-category scale is an imperfect and too coarse representation of the gradual changes in the ICP pulse waveform, and a number of pulses exhibit the features of more than one class. This problem could potentially be rectified by introducing a more fine-grained classification or a more balanced training set. On the other hand, even though every wrong

label leads to a decrease in overall classification accuracy, from the standpoint of clinical interpretation a one-class error is less severe than inaccurately labelling a normal pulse as pathological or vice versa, especially given the ambiguity of certain waveform shapes observed by the experts performing manual annotations. A simple four-category scale, although inherently unable to capture all the possible waveform shapes that manifest in real-life recordings, is easy to comprehend while still representing the major changes in ICP pulse morphology.

This is supported by the observation that the increase in ICP pulse waveform class was accompanied by increases in both mean ICP and AmpICP. According to the P–V curve (Marmarou et al., 1975) and the AMP–P characteristic (Szewczykowski et al., 1977), at elevated mean ICP the pulse pressure is expected to rise while compliance is expected to decrease, reflecting the underlying changes in intracranial volume. Higher mean ICP and AmpICP observed for pulses assigned to higher waveform classes are in accordance with the model of pressure–volume relationship in the cerebrospinal space. On the other hand, the markedly lower degree of correlation between waveform class and the RAP index, resulting from a non-linear relationship, could suggest that although both RAP and ICP pulse class provide information on the state of the intracranial space, they do in fact assess different aspects of the system, with RAP representing the patient's cerebrospinal compensatory reserve associated with their position on the P–V curve (Czosnyka and Citerio, 2012). With such interpretation, waveform class roughly reflects the information on cerebrospinal compliance expressed by the P1/P2 ratio (Nucci et al., 2016).

Interestingly, although higher waveform classes were generally associated with increased mean ICP and AmpICP, they also occurred at ICP levels below the clinical intervention threshold of 20 mm Hg (Carney et al., 2017), as shown by the range of extremes in Figure 4.6a. This is especially pronounced in class 4 which is characterised by the largest dispersion of mean ICP values. While the incidence of pathologically altered waveforms at elevated ICP is not by itself alarming on the basis of the P–V curve, it can be seen that they are also present at relatively low mean ICP (even below 10 mm Hg). This observation in particular suggests that the shape of the ICP pulse waveform is not strictly dependent on mean ICP level but contains additional information on the state of the intracranial space, and diminished cerebrospinal compliance detected before ICP increases may be an early indicator for the medical personnel that the patient is at risk of volume decompensation and should be closely monitored. Measurement of the ICP signal is already recommended by internationally accepted guidelines for the management of TBI (Carney et al., 2017), and currently available measurement systems generally permit high enough sampling frequency to analyse the ICP pulse morphology in detail (Holm and Eide, 2009). As the pulse waveform classification approach does not require manipulation of the intracranial volume, is not additionally invasive, and overcomes the major limitations of the peak detection method when combined with a neural network with sufficiently high accuracy, this technique offers the potential to track such changes in cerebrospinal volume compensation continuously, at the same time as the routinely monitored mean ICP. In order to test this hypothesis, the assessment of clinical significance of ICP pulse waveform morphology in TBI was continued in large, multi-centre study presented in Chapter 5.

4.5.1 Limitations

This study was conducted as retrospective analysis of a relatively small number of recordings collected in a single medical centre. Evaluation of the relationship between ICP pulse waveform class and other ICP-derived indices was restricted to a homogenous cohort of TBI patients treated according to the same management guidelines and characterised by comparable clinical status scores. Moreover, the analysis was performed using parameters averaged over the whole recordings and without any length restrictions. Patients with continuous episodes of elevated mean ICP were not separated from those with highly unstable ICP, and no information on whether ICP-lowering interventions were introduced in any cases was included. Consequently, the results of this study represent global trends rather than short-term changes, and the performed analysis does not allow for differentiating patients with gradual transition from normal to pathological pulse morphology from those in whom the shape of the waveform was already pathologically altered when the monitoring started. The latter can potentially explain the wide range of mean ICP values associated with pathological waveforms of class 4 and should be investigated in more detail.

Finally, while the accuracy scores of the selected neural network model generally suggest a good ability to distinguish between different waveform classes, the algorithm is not perfect, and the final results are likely to be influenced to a certain degree by classification errors.

Chapter 5

The index of intracranial pressure pulse waveform shape in traumatic brain injury

The results presented in this chapter were submitted for publication as:
Kazimierska, A., Uryga, A., Mataczyński, C., Pelah, A., Czosnyka, M., Kasprowicz, M., and the CENTER-TBI high resolution sub-study participants and investigators. The shape of intracranial pressure pulse waveform in traumatic brain injury: a CENTER-TBI study. As of April 2022, the manuscript is under peer review in *Scientific Reports* journal.

5.1 Introduction

The results presented in Chapter 4 support the potential of using deep neural networks to automatically classify characteristic shapes of the ICP pulse waveform. The preliminary small, single-centre study also hinted at the relationship between ICP pulse morphology and clinical outcome of TBI patients, as patients with good outcome generally presented higher incidence of normal waveforms and lower incidence of pathological waveforms (Mataczyński, Kazimierska et al., 2022) as well as higher dominant waveform class (Kazimierska et al., 2021b). However, a major limitation of the straightforward classification approach is the coarse, four-category scale. On the one hand, it removes the requirement for precise peak delineation in the ICP pulse contour in favour of easy to interpret visual criteria. On the other hand, the changes in the ICP pulse waveform are gradual rather than step-like and a wide variety of shapes is observed in clinical recordings, not all of them falling neatly into the predefined categories. Consequently, classification of individual waveforms is not particularly well suited to monitoring of changes over time as an alteration of the pulse shape will only become visible if the change exceeds one full class, and instantaneous waveform shape does note reliably characterise the state of the cerebrospinal system. It is possible to analyse the dominant class (i.e. the most frequently occurring one) in a moving window (e.g. 5 minutes), but this approach still leads to loss of information on pulse shape variability.

Taking that drawback into account, the aim of the final part of this dissertation was to propose a new index describing the ICP pulse waveform based on automatic morphological classification, called the pulse shape index (PSI). This metric is calculated in 5-minute

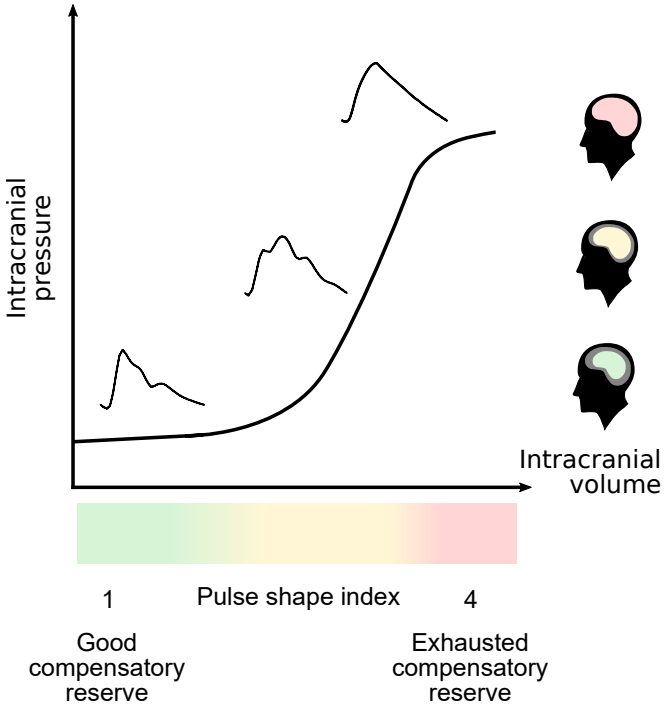

Figure 5.1. Proposed interpretation of the pulse shape index in relation to changes in the intracranial pressure–volume balance.

windows (shifted every 10 seconds) as the weighted sum of class numbers, with weights corresponding to the fraction of non-artefactual pulses assigned to given class. Proposed interpretation of the index in relation to the P–V curve is presented in Figure 5.1. In contrast to plain class numbers, PSI would change gradually with the occurrence of different waveform shapes, allowing for a more precise characterisation of the trends in the ICP signal. At the same time, it retains a simple interpretation, with values close to 1 indicating normal pulse morphology (mostly waveforms of class 1) and values close to 4 indicating pathological changes (mostly waveforms of class 4), and the ability to remove artefacts prior to analysis, potentially improving the reliability of calculated indices. In this work, PSI was evaluated in a large, multi-centre cohort of TBI patients from the CENTER-TBI project in order to compare the results of the previous small, single-centre study (Mataczyński, Kazimierska et al., 2022; Kazimierska et al., 2021b) with a more diverse group and further examine the potential usefulness of this approach in neurocritical care, including the relationship between PSI and other ICP-derived indices of cerebral pressure—volume compensation and cerebrovascular pressure reactivity which have been shown to correlate with outcome in TBI patients (Holm and Eide, 2008; Badri et al., 2012; Sorrentino et al., 2012). Moreover, the link between PSI and mortality after TBI and between PSI and the presence of mass lesions in CT scans was investigated.

5.2 Material

Data used in this work were collected as part of the high resolution sub-study of the CENTER-TBI project, a large European study on TBI epidemiology and management (Maas et al., 2015), and used with permission from the CENTER-TBI committee (approval no 359). The CENTER-TBI study (EC grant 602150) was conducted in accordance with all relevant laws of the EU if directly applicable or of direct effect and all relevant laws of the country where the Recruiting sites were located, including but not limited to, the relevant privacy and data protection laws and regulations (the "Privacy Law"), the relevant laws and regulations on the use of human materials, and all relevant guidance relating to clinical studies from time to time in force including, but not limited to, the ICH Harmonised Tripartite Guideline for Good Clinical Practice (CPMP/ICH/135/95) ("ICH GCP") and the World Medical Association Declaration of Helsinki entitled "Ethical Principles for Medical Research Involving Human Subjects". Informed Consent by the patients and/or the legal representative/next of kin was obtained, accordingly to the local legislations, for all patients recruited in the Core Dataset of CENTER-TBI and documented in the e-CRF. Ethical approval was obtained for each recruiting site and the list of approvals is available on https://www.center-tbi.eu/project/ethical-approval.

In the CENTER-TBI high resolution sub-study, ICP was monitored using intraparenchymal strain gauge probes (Codman ICP MicroSensor; Codman & Shurtleff Inc., Raynham, MA, USA) or parenchymal fibre optic pressure sensors (Camino ICP Monitor; Integra Life Sciences, Plainsboro, NJ, USA). ABP was measured via radial or femoral arterial lines connected to pressure transducers (Baxter Healthcare Corp. CardioVascular Group, Irvine, CA, USA). The signals were recorded using ICM+ software (Cambridge Enterprise Ltd., Cambridge, UK) and/or Moberg CNS Monitor (Moberg Research Inc., Ambler, PA, USA) with sampling frequency of 100 Hz or higher. Data for the CENTER-TBI project were collected through the Quesgen e-CRF (Quesgen Systems Inc., USA), hosted on the INCF platform and extracted via the INCS Neurobot tool (INCF, Sweden). In this study, version CENTER Core 3.0 of the CENTER-TBI dataset was used.

The high resolution sub-study dataset was comprised of 282 patients; 203 were selected for final analysis. The exclusion process is outlined in Figure 5.2. Patients below the age of 16 were excluded to limit the analysis to adult TBI. Patients with EVDs were excluded because the ICP pulse waveform is unavailable during drainage periods. Patients who underwent decompressive craniectomy before the start of monitoring were excluded due to the disturbance of the intracranial pressure–volume relationships caused by removal of a part of the skull. However, recordings from patients who had the procedure while monitoring was already in progress were still included up to the date of surgery. Patients with CPP below 40 mm Hg or ICP over 50 mm Hg were excluded to eliminate evidently terminal data. Furthermore, all included recordings were truncated to seven days post injury as previous studies have shown that the predictive power of ICP-derived metrics is limited to that period (Adams et al., 2017). Average monitoring time (median [first–third quartile]) was 115 [66–157] hours.

The clinical status of the patients at admission was assessed using the GCS scores. Mortality was assessed after six months using the Glasgow Outcome Scale Extended

(GOSE) (Wilson et al., 1998), with patients separated into deceased (GOSE score 1) and surviving (GOSE scores 2–8). Presence of mass lesions in CT scans (defined as mass volume > 25 cc) was analysed in scans taken within the first seven days post injury and the patients were divided into those who did or who did not exhibit mass lesions in that period. Summary characteristics of the patient cohort are presented in Table 5.1.

Table 5.1. Clinical characteristics of the CENTER-TBI patient cohort (203 patients). Data are presented as number of occurrences (% of total group) or as median [first–third quartile] unless otherwise indicated. GCS—Glasgow Coma Scale, GOS—Glasgow Outcome Scale, ICU—intensive care unit; n—number of occurrences, $Q1$—first quartile, $Q3$—third quartile, NA—data not available.

Parameter	**Value**
Age [years] mean & range	mean: 48, range: 16–85
Sex n (%)	male: 156 (77%), female: 47 (23%)
GCS at admission median [$Q1$–$Q3$]	7 [3–11]
6-months mortality n (%)	survived: 148 (80%), deceased: 36 (20%), NA: 19
Mass lesions in CT scans n (%)	absent: 100 (60%), present: 67 (40%), NA: 36

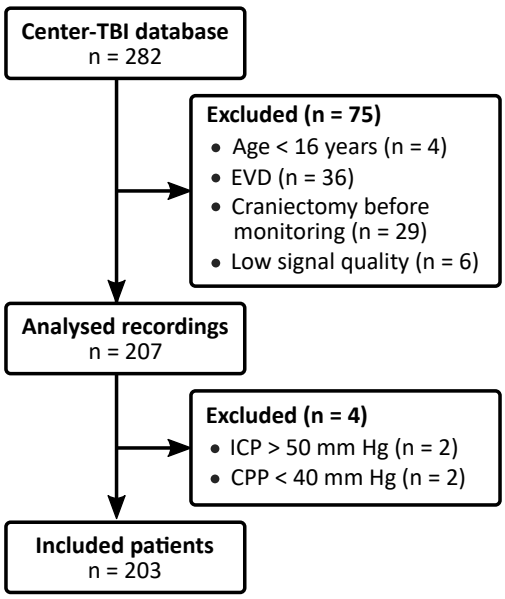

Figure 5.2. Selection criteria for the final patient dataset included in analysis. EVD—external ventricular drain, ICP—intracranial pressure, CPP—cerebral perfusion pressure.

5.3 Methods

5.3.1 Pulse shape index and other ICP-derived parameters

All steps of the analysis were performed using programs custom-written in Python 3.7. The basis of PSI calculation was formed by the algorithm for ICP pulse waveform classification using a ResNet model described in detail in Chapter 4. First, all individual pulses were identified in long-term recordings and classified into one of five classes: normal (class 1), possibly pathological (class 2), likely pathological (class 3), pathological (class 4), or artefacts. Prior to further analyses all pulses marked as artefacts were excluded from the recordings. Then, the following parameters were calculated: occurrence of different waveform classes, dominant class, and PSI. Occurrence of each of the four non-artefactual classes was expressed as the percentage of all pulses assigned to given class in the whole analysis period, with all valid pulses making up 100%. Dominant class was determined as the class occurring most frequently in the recording. These two metrics represent the global characteristics of the ICP pulse shape for each patient.

In turn, PSI was calculated in 5-minute windows shifted every 10 seconds using the following equation:

$$\mathrm{PSI} = \sum_{i=1}^{4} i \cdot p_i, \tag{5.1}$$

where i is the class number, $i \in \{1, 2, 3, 4\}$, and p_i is the fraction of pulses assigned to given class i expressed on a scale from 0 to 1. Occurrence of each waveform class in each PSI analysis window was again estimated after artefact exclusion, i.e. with non-artefactual pulses making up 100%. In contrast to pulse class percentages and the dominant class, PSI reflects gradual changes in the ICP pulse shape in a shorter time scale. An overview of the algorithm to obtain PSI as an extension of the ICP pulse classification pipeline is presented in Figure 5.3.

Mean ICP and AmpICP were calculated in 10-second windows as the average and peak-to-nadir value of the ICP signal, respectively. Cerebrovascular pressure reactivity index (PRx) was calculated in 5-minute windows (window shift: 10 seconds) as the moving Pearson correlation coefficient between mean ICP and mean ABP (Czosnyka et al., 1997a). PRx is an indirect measure of cerebral autoregulation that reflects the ability of cerebral blood vessels to constrict or dilate in response to changes in ABP. As changes in vessel diameter affect CBV, and in turn ICP, negative values of PRx indicate good pressure reactivity. PRx below 0 implies that changes in ABP produce an opposite reaction in ICP, indicating that an increase in mean ABP is followed by a decrease in CBV, and consequently a decrease in mean ICP (or vice versa, a decrease in mean ABP is accompanied by increases in CBV and mean ICP). Conversely, positive PRx suggests a pressure-passive system with non-reactive vessels and changes in ABP and ICP occurring in the same direction. In TBI patients, PRx above 0.3 is considered a predictor of mortality (Sorrentino et al., 2012).

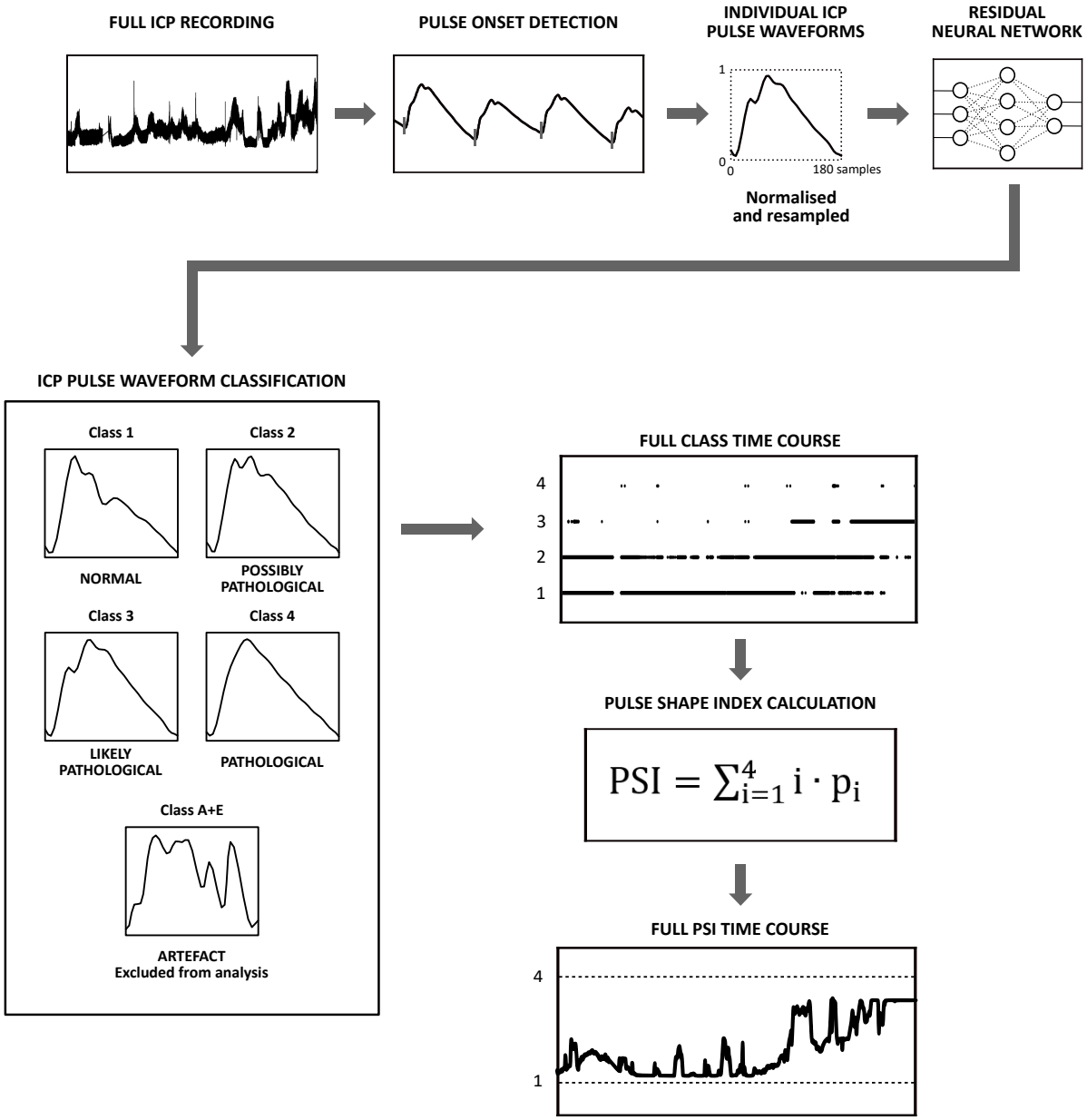

Figure 5.3. Overview of the proposed approach to calculate the pulse shape index (PSI) as an extension of the intracranial pressure (ICP) pulse waveform classification pipeline.

Finally, each patient was characterised by a PSI, mean ICP, AmpICP, and PRx value averaged over the whole analysis period as well as metrics computed globally: dominant waveform class and occurrence of each of the non-artefactual classes. An illustrative example of changes in calculated metrics for a single patient is presented in Figure 5.4.

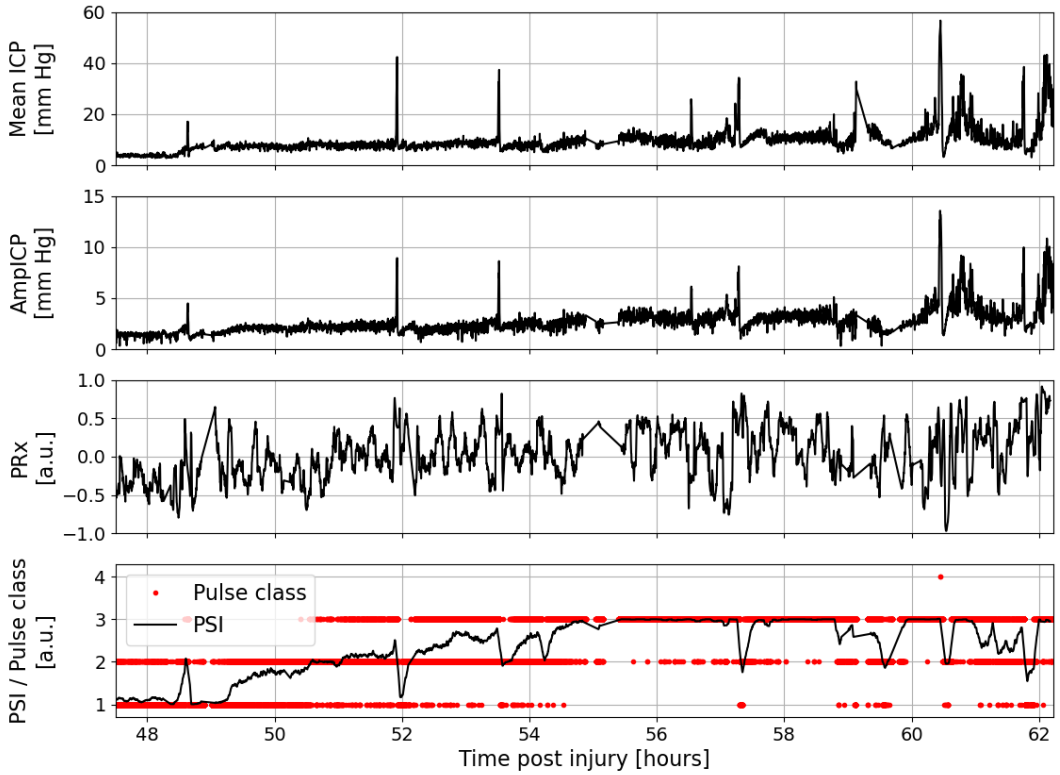

Figure 5.4. Illustrative example of the time course of derived parameters (from top to bottom): mean intracranial pressure (ICP), peak-to-peak pulse amplitude of ICP (AmpICP), pressure reactivity index (PRx), and pulse shape index (PSI; black line) overlaid on classification result of individual ICP pulse waveforms (red dots).

5.3.2 Statistical analysis

Statistical analysis was performed using Statistica software (v13.1, Tibco, Palo Alto, Ca, USA) and Python 3.7. Significance level of 0.05 was assumed in all analyses. Data distributions were tested for normality using the Shapiro–Wilk test and the normality of most analysed variables was rejected. The relationship between PSI and other derived indices was examined visually using boxplots over values grouped into bins of width 7.5 mm Hg, 5 mm Hg, and 0.2 for mean ICP, AmpICP, and PRx, respectively. Only bins containing more than 1% of the data or more than 1 patient (whichever was larger) were included in analysis. Similarly, the relationship between mean ICP and the remaining parameters in different outcome groups was studied using boxplots over mean ICP bins (bin width: 7.5 mm Hg). The Mann–Whitney U test was used to assess the differences between the deceased and surviving group as well as between patients with or without mass lesions in CT scans.

5.4 Results

5.4.1 The relationship between PSI and other ICP-derived indices

Figure 5.5 presents the relationship between PSI and derived indices: mean ICP, AmpICP, and PRx. With the exception of the first bin, PSI generally rose non-linearly with increases in all other parameters. In all cases the changes in PSI started at approximately 2–2.5, indicating the presence of possibly pathological waveforms, and progressed towards likely pathological waveforms of class 3, suggesting that even at low mean ICP the incidence of pathologically altered waveforms was higher than that of normal pulse morphology. However, while the range of PSI values for low mean ICP (< 15 mm Hg) and low PRx (< 0) did not greatly exceed 2.5, for low AmpICP (< 5 mm Hg) both low and high PSI were observed, as shown by the large dispersion of values compared to the other bins. On the other hand, average PSI values approaching 4 were not observed even with high mean ICP.

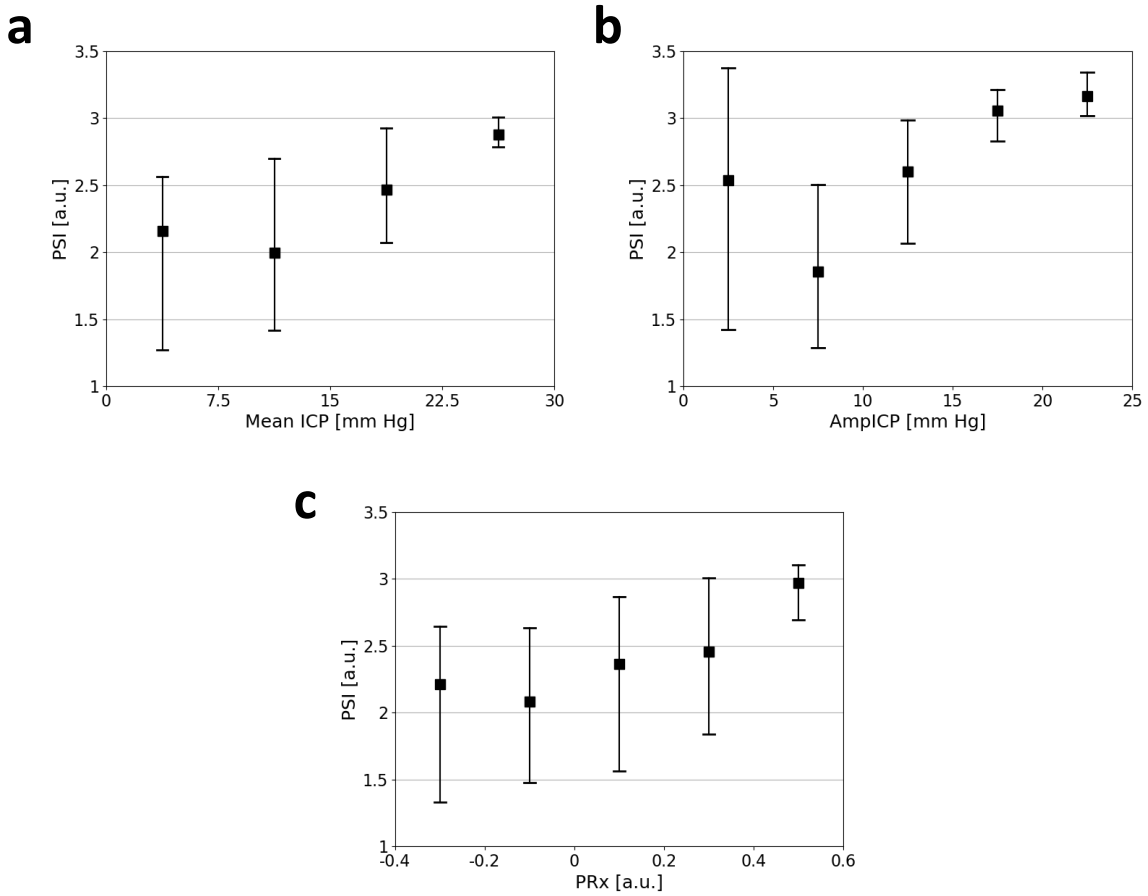

Figure 5.5. The relationship between pulse shape index (PSI) and other derived parameters: a) mean intracranial pressure (ICP), b) peak-to-peak pulse amplitude of intracranial pressure (AmpICP), and c) pressure reactivity index (PRx). Black squares represent the median of each bin and whiskers (bar) represent the interquartile range. a.u.—arbitrary units.

5.4.2 The relationship between ICP pulse waveform class, other derived indices, and outcome

Table 5.2 presents the occurrence of different waveform classes in two outcome groups. Patients who survived exhibited increased occurrence of normal (class 1) and possibly pathological (class 2) waveforms compared to patients who died, although only the difference for class 1 reached statistical significance. In contrast, deceased patients showed a significantly higher incidence of both likely pathological (class 3) and pathological (class 4) waveforms. In the surviving group, most of the pulses were assigned to classes 1 to 3, and the occurrence of pathological waveforms was very low, with the average below 1%. On the other hand, in patients who died the majority of pulses were classified as likely pathological, and the incidence of classes 1 and 2 was markedly lower than class 3.

Table 5.2. Group-averaged occurrence of intracranial pressure pulse waveform classes (expressed as % of all non-artefactual pulses) in the deceased and surviving patient group. Results are presented as median [first–third quartile] with Mann–Whitney U test p value. n—number of patients in group, n.s.—result not statistically significant.

Parameter	**Deceased** ($n = 36$)	**Survived** ($n = 148$)	***p* value**
Class 1 [%]	0.4 [0.0–19.5]	19.3 [1.7–63.7]	$< .001$
Class 2 [%]	12.6 [1.4–38.1]	22.7 [7.5–45]	n.s.
Class 3 [%]	41.5 [18.8–82.6]	15.4 [1.9–55.3]	.008
Class 4 [%]	3.6 [0.0–17.1]	0.2 [0.0–3.9]	.015

Table 5.3. Pulse shape index (PSI), mean intracranial pressure (ICP), peak-to-peak pulse amplitude of ICP (AmpICP), and pressure reactivity index (PRx) in the deceased and surviving patient group. Results are presented as median [first–third quartile] with Mann–Whitney U test p value. n—number of patients in group, a.u.—arbitrary units.

Parameter	**Deceased** ($n = 36$)	**Survived** ($n = 148$)	***p* value**
PSI [a.u.]	2.8 [2.3–3.0]	2.2 [1.5–2.8]	$< .001$
Dominant class [a.u.]	3 [2–3]	2 [1–3]	.003
Mean ICP [mm Hg]	15.6 [11.7–18.9]	12.6 [9.6–15.5]	.003
AmpICP [mm Hg]	12.0 [10.1–15.9]	8.6 [7.0–10.8]	$\ll .001$
PRx [a.u.]	0.10 [0.01–0.32]	-0.02 [-0.12–0.08]	$< .001$

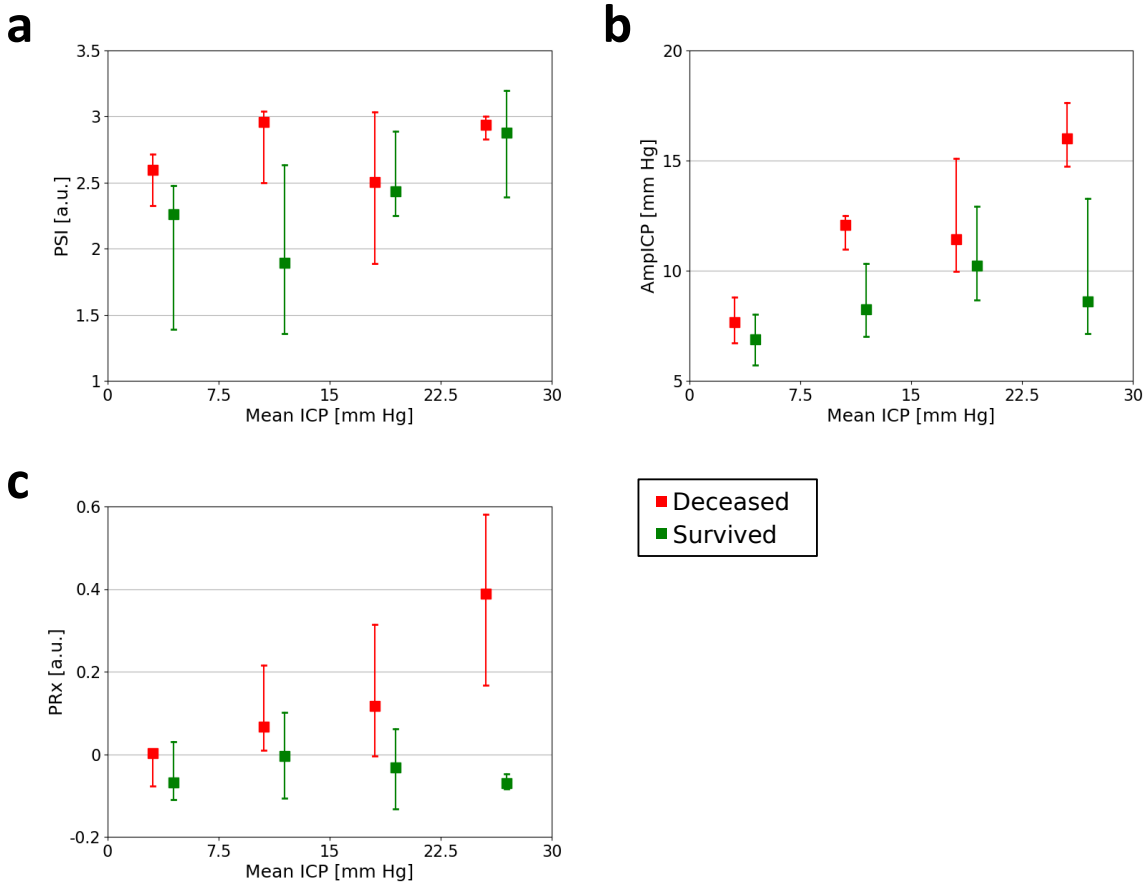

Figure 5.6. The relationship between mean intracranial pressure (ICP) and derived indices: a) pulse shape index (PSI), b) peak-to-peak pulse amplitude of ICP (AmpICP), and c) pressure reactivity index (PRx) separated into the deceased (red symbols) and surviving (green symbols) patient group. Squares represent the median of each bin and whiskers (bar) represent the interquartile range. a.u.—arbitrary units.

All of the other parameters were significantly increased in patients who died compared to those who survived (Table 5.3). As shown in Figure 5.6a, deceased patients exhibited increased PSI (around 2.5 and higher) even at relatively low ICP, with no consistent trend of changes in PSI with rising mean ICP. Conversely, in patients who survived PSI generally increased with increasing mean ICP, with a pronounced change between lower (below 15 mm Hg) and higher (over 15 mm Hg) mean ICP range. AmpICP (Figure 5.6b) was slightly higher for patients who died than those who survived at all mean ICP levels and in both groups mostly rose with increasing mean ICP, but presented a breakpoint in the last bin for patients who survived. PRx also behaved differently in deceased and surviving patients (Figure 5.6c). In patients who survived, it remained at a similar level in all bins, with values around 0 or slightly negative. In patients who died, it was approximately 0 at very low mean ICP, but rose with increasing mean ICP up to approximately 0.4.

5.4.3 The relationship between ICP-derived indices and presence of mass lesions

Patients who exhibited mass lesions in CT scans showed increased PSI compared to patients who did not (median [first–third quartile]: 2.5 [2.0–3.0] vs 1.9 [1.2–2.6], $p \ll .001$) as well as slightly elevated mean ICP (14.2 [11.0–16.5] vs 12.1 [8.7–15.6], $p = .007$) while no significant differences were observed for AmpICP and PRx. Distribution of PSI values for patients with mass lesions was visibly shifted towards higher values (Figure 5.7b) but still wider than for patients who died (Figure 5.7a), suggesting higher incidence of lower PSI in this group.

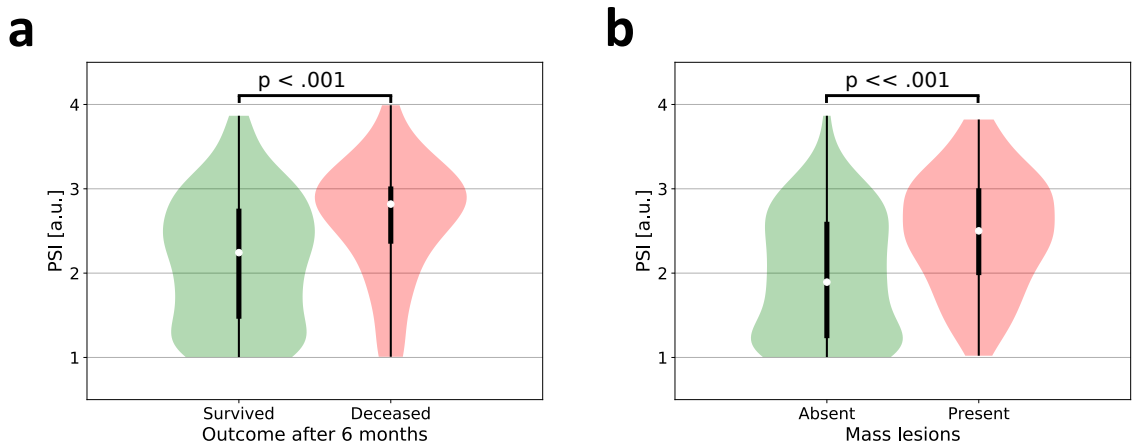

Figure 5.7. Distribution of pulse shape index (PSI) values in a) patients who survived (green plot) vs patients who died (red symbols) and b) patients who exhibited mass lesions in CT scans (red plot) vs patients who did not (green plot). Central white dots represent medians, black rectangles represent the interquartile ranges, and vertical lines extend to the extreme values. Brackets above the plots show the p values of Mann–Whitney U test (all differences statistically significant).

5.5 Discussion

In this chapter, a new index describing the ICP pulse waveform morphology, called PSI, was proposed, and its potential usefulness in neurocritical care was investigated in a large, multi-centre cohort of TBI patients. As shown in Chapter 4, the use of deep neural networks allows for automatic classification of characteristic shapes of the ICP pulse waveform with satisfyingly high accuracy. However, while the classification approach itself uses easily interpretable visual criteria for pulse morphology and is independent of precise peak detection (and therefore does not require that pathologically rounded pulses are excluded from analysis), it is not very well suited to tracking changes over time due to its discrete four-category scale. PSI is an attempt to overcome this limitation by performing the calculations in a moving 5-minute window and describing the pulse shape as a weighted sum of class numbers, incorporating the information on class incidence in given analysis period, thus producing a metric more appropriate for continuous monitoring. Unlike the

percentages of each waveform class, it does not require simultaneous tracking of four different parameters, and is presented on a continuous scale in contrast to the categorical dominant class which can only assume a limited number of values.

Results of this investigation confirm the observations from the previous small, single-centre study (Mataczyński, Kazimierska et al., 2022; Kazimierska et al., 2021b) that patients with worse outcome exhibit pathological waveforms more frequently than the good outcome group. Accordingly, patients who died also showed significantly increased PSI, indicating more pathologically changed waveform shape and therefore reduced volume compensation compared to those who survived. Interestingly, the difference in PSI was more pronounced at mean ICP levels below the clinical threshold for ICP-lowering interventions (Carney et al., 2017). While elevated ICP itself is linked with worse outcome in TBI (Badri et al., 2012), the contrasting PSI values for deceased and surviving patients at low ICP suggest that the disturbance of intracranial volume equilibrium may be observed earlier than changes in mean ICP and patients at risk of worse outcome may be identified in advance. It also supports the view that ICP pulse morphology is not solely dependent on mean ICP (Ellis et al., 2005), and the compensatory mechanisms of CSF and cerebral blood displacement may already be compromised while ICP remains normal (Heldt et al., 2019). Moreover, the trend of changes in PSI with increasing mean ICP in the two outcome groups was clearly different. Taking into account the relationship modelled by the P–V curve, cerebrospinal compliance is high at low mean ICP and low intracranial volume, with small volume increments producing small changes in pressure, but progressively reduced as the curve becomes exponential. As high PSI is considered an indirect measure of diminished compliance, it is expected to increase with rising mean ICP. Here, patients who survived did in fact show PSI mostly increasing with mean ICP, although the relationship was non-linear, suggesting that the metric cannot be considered strictly as an inverse on mean ICP. Patients who died, however, exhibited no consistent trend, with high PSI regardless of the mean ICP level.

Conversely, AmpICP was significantly elevated in deceased patients, but its relationship with mean ICP was similar for both groups, with higher AmpICP accompanying higher mean ICP. According to the AMP–P plot, AmpICP is expected to rise with mean ICP up to the breakpoint associated with the collapse of cerebral blood vessels at critically elevated ICP. Therefore, the general trend observed in this study is in line with previous investigations (Szewczykowski et al., 1977; Avezaat et al., 1979), as is the link between large AmpICP and worse outcome in TBI (Holm and Eide, 2008). Interestingly, PSI was non-linearly related with AmpICP, with higher PSI occurring even with low AmpICP. While AmpICP is not a direct estimate of compliance due to the unknown stroke volume contributing to the ICP pulse, it has been used as a surrogate measure (Szewczykowski et al., 1977; Avezaat et al., 1979). The non-linear relationship with PSI suggests that the two metrics reflect different aspects of the cerebrospinal system. Accordingly, one previous study reported that in TBI patients AmpICP depends more on changes in CBV during the cardiac cycle than on mean ICP, implying strong influence of vascular factors (Carrera et al., 2010), while pulse waveform classification used to obtain PSI is based on compliance-related changes in peak configuration as described in Chapter 4.

The difference between PSI and AmpICP could also be seen in patients who did or did not exhibit mass lesions in CT scans, as only PSI and mean ICP were significantly different between those two groups. Increased PSI in patients who developed mass lesions confirms the link between ICP pulse morphology and the volume equilibrium in the intracranial space, with pathologically altered waveforms occurring more frequently in patients in whom that balance is disturbed by additional volume. Moreover, it is in line with the association between PSI and worse outcome, as the occurrence of lesions may lead to potentially life-threatening complications related to the mass effect on the brain (Stocchetti et al., 2017). However, more in-depth examination is required to determine if PSI is capable of predicting impeding changes before they become visible in CT scans or if it corresponds to the extent of volume imbalance, e.g. the degree of midline shift which was shown to correlate with elastance assessed by the VPR (Miller and Pickard, 1974).

Finally, increases in PSI were also associated with disturbed cerebrovascular pressure reactivity reflected by increased PRx. The connection between PRx and outcome in TBI has been investigated in various previous studies (Czosnyka et al., 1997a; Sorrentino et al., 2012; Adams et al., 2017; Ai Åkerlund et al., 2020). In accordance with those earlier studies, in patients who died PRx rose substantially with mean ICP, indicating progressive disruption of cerebral autoregulation, while in patients who survived it remained consistently below or around 0. The relationship with PSI also suggests that diminished vessel reactivity and reduced effectiveness of buffering cardiac changes in CBV affect the ICP pulse shape. Based on analysis of the transfer function between ABP and ICP, Chopp and Portnoy (1980) concluded that cerebral vasodilation that accompanies increases in mean ICP is reflected in increased AmpICP due to decreased ability of the cerebral vessels to attenuate the arterial pulse. The results of this study indicate that this effect is visible not only in pulse pressure but also in its morphology. Moreover, the links between PSI, mean ICP, AmpICP, and PRx highlight the need for multiparametric assessment in TBI patients, as the intracranial volume–pressure relationship and CBF dynamics are unquestionably strongly interconnected.

The latter observation was also explored in a co-authored paper on the relationship between IH episodes and mortality in TBI (Mataczyński et al., 2022b) (accepted for publication). Recently, a study by Lee et al. (2021) showed the application of machine learning in prediction of life-threatening IH, a subset of IH episodes defined as elevated ICP (indicated by increased pressure–time dose (Kahraman et al., 2010) rather than a single set threshold) with simultaneous compromised cerebrovascular reactivity (indicated by positive PRx value). The authors demonstrated that the occurrence of these life-threatening IH events is correlated with mortality in TBI, thus introducing a new concept to ICP monitoring. In (Mataczyński et al., 2022b), we combined the definition proposed by Lee et al. with assessment of ICP pulse morphology using the classification model described in Chapter 4 and compared the incidence of different types of life threatening IH episodes (i.e. defined only based on ICP pressure–time dose, on pressure–time dose and PRx, or on pressure–time dose and ICP pulse waveform class) in the CENTER-TBI database. The study showed that pathological ICP waveforms of class 4 are present during ICP increases almost only in patients who died, as 42% of deceased patients developed at least one such episode during the analysis period compared to only 6% in the much larger surviving

group. The morphology-based definition of life-threatening IH also outperformed the previous PRx-based one in terms of mortality prediction, suggesting again the potential of using the ICP pulse waveform shape analysis in TBI management.

5.5.1 Limitations

This work was conducted as a retrospective analysis of data compiled during the CENTER-TBI project. While the high resolution dataset was collected with the purpose of analysing the ICP pulse waveform and recorded with sufficiently high sampling frequency, evaluation of ICP pulse waveform morphology was not the primary objective of the study reflected in the original study protocol. Furthermore, in this study outcome after TBI was expressed as mortality after six months based on available clinical records. As TBI is a complex, multifactorial condition, outcome after six months depends on a number of factors, not all of which will be reflected as changes in the shape of the ICP pulse waveform. The prognostic value of PSI should be assessed in prospectively collected data, taking into account clinical metrics with known association with long-term outcome after TBI, such as age and GCS. The link between presence of mass lesions and ICP pulse waveform morphology should also be studied in more detail as in this work this relationship was examined based only on a binary description of the patients' CT scans.

Secondly, calculation of PSI as a weighted sum of class numbers in a moving window partially overcomes the limitations of the discrete four-category scale used in ICP pulse waveform classification as gradual changes in pulse shape can be captured more easily by PSI than by simple class numbers. However, this approach still relies on the underlying neural network which is characterised by high but not perfect accuracy. Therefore, classification errors cannot be avoided and may influence PSI estimation.

Chapter 6

Conclusions and direction of future studies

Continuous monitoring of mean ICP has been an essential part of neurocritical care for more than half a century. In the 1980s, studies suggested that short-term variations in the ICP signal over a single cardiac cycle may provide additional information on the state of the intracranial pressure–volume compensation and improve the management of intracranial pathologies, but interest in this approach waned in the following decades. However, the advent of novel signal processing methods and machine learning approaches in recent years offered new possibilities for ICP pulse waveform analysis. The work presented in this dissertation was undertaken to revisit the concept of ICP pulse waveform morphology as a measure of cerebrospinal compliance and propose a new method of monitoring cerebrospinal volume compensation, taking those technological advances into account. Firstly, it was demonstrated that the ratio of characteristic peaks P1 and P2 of the ICP pulse waveform provides information on relative changes in cerebrospinal compliance in good agreement with the 'gold standard' method based on volumetric manipulation. This study proved for the first time that the P1/P2 peak ratio can be considered as an indirect measure of compliance (Hypothesis 1). In order to overcome the requirement for precise peak identification that could limit the applicability of this method in continuous monitoring, a neural network model was developed to classify characteristic shapes of the ICP pulse waveform reflecting the changes in peak configuration. In contrast to previously suggested methods, the proposed algorithm does not include peak delineation and it takes advantage of the benefits offered by deep neural networks as the ICP signal is presented to the model with minimal pre-processing. The model achieved high accuracy and good generalisation in data obtained from long-term recordings of TBI patients, proving Hypothesis 2. The initial single-centre study conducted in a small number of TBI patients also suggested that occurrence of pathologically changed waveforms is linked to clinical outcome after TBI. However, as a categorical variable taking only one of four possible values, the dominant waveform class used in that investigation was found to be ill-suited for continuous monitoring of changes in ICP pulse morphology. Therefore, further studies were performed in order to propose a more appropriate measure and assess its clinical

significance in the management of TBI. This led to introduction of a new index, called PSI, which describes the shape of the ICP pulse waveform based on the results of pulse classification but is presented on a continuous scale and is suitable for tracking changes in ICP pulse morphology over time. A study in a large, multi-centre cohort of TBI patients showed that PSI is strongly correlated with outcome after TBI, which proved Hypothesis 3.

The work presented in this dissertation was aimed at combining the existing body of knowledge on compliance-related changes in the shape of the ICP pulse waveform with advances in the field of machine learning. The belief that assessment of cerebrospinal compliance could aid in the management of TBI patients, especially as a tool for predicting impending decompensation and potentially life-threatening episodes of elevated ICP, was expressed by numerous authors over the years, some of them quite recently, even though the various direct and indirect measures of compliance proposed to date have not yet found their place in standard clinical practice. The use of a validated index of cerebrospinal volume compensation as a secondary modality describing brain homeostasis would be strongly in line with the multimodal monitoring protocols common in modern neurocritical care units.

The evidence presented in this dissertation may lead to renewed interest in continuous monitoring of cerebrospinal compliance by means of morphological analysis of the ICP pulse waveform and result in more effective management of patients with intracranial pathologies, as there remain a number of avenues to explore in future studies. The presented studies showed that pathologically changed ICP pulse waveforms may appear even in the absence of ICP elevation, contradicting the view that compliance is strictly dependent on mean ICP. Further investigation of temporal changes in ICP pulse morphology compared to mean ICP will be conducted to assess if the former can be used as an indicator of imminent hypertensive episodes, again making use of the potential of deep learning algorithms as they have shown good performance in various forecasting tasks but so far found limited application in ICP analysis. A well-performing model for early prediction of ICP elevation remains one of the missing, and potentially crucial, elements of neurocritical care in TBI. The shape of the ICP pulse waveform assessed using PSI will also be studied during clinically significant events such as ICP plateau waves or controlled hypocapnia to add new insights on the pressure–volume compensation mechanisms in different scenarios. Moreover, it remains to be seen if changes in ICP pulse shape are correlated with known measures derived from imaging studies, such as midline shift or ventricular dilation, as the relationship between ICP pulse morphology and presence of mass lesions explored here suggests the former's potential importance in assessing the changes in brain structure.

The ICP pulse waveform classification approach will also be explored further with regard to the relationship between ICP pulse morphology and the shapes of ABP and CBFV pulses. As the cerebrospinal system can be (to a certain extent) regarded as converting blood pressure pulsations to pulsatile blood flow and further to the ICP pulse waveform, it stands to reason that changes in ABP and CBFV pulse morphology may influence the ICP waveform. Deep learning algorithms, shown in this dissertation to be capable of successfully differentiating various ICP pulse shapes, will be used to propose a

complementary model for ABP pulse classification. This, in turn, will provide the means for concurrent evaluation of both pressure waveforms in the large, multi-centre database of long-term recordings from TBI patients that is not burdened by the assumptions and limitations of the previously applied Fourier transform-based systems analysis.

Finally, while this dissertation focused on the significance of monitoring the ICP pulse waveform morphology in TBI patients, it can also be studied in hydrocephalus, as indicated in the original study by Nucci et al. Currently, hydrocephalus patients usually undergo infusion tests in order to evaluate the state of CSF dynamics or shunt function. Automatic classification of ICP pulse shapes could complement the standard protocol or reduce the need for external volumetric manipulation if ICP pulse morphology is proven to contain meaningful information on cerebrospinal volume–pressure relationship in this group.

References

Adams, H., Donnelly, J., Czosnyka, M., Kolias, A. G., Helmy, A., Menon, D. K., Smielewski, P., and Hutchinson, P. J. (2017). Temporal profile of intracranial pressure and cerebrovascular reactivity in severe traumatic brain injury and association with fatal outcome: An observational study. *PLoS Medicine*, 14(7):e1002353.

Ai Åkerlund, C., Donnelly, J., Zeiler, F. A., Helbok, R., Holst, A., Cabeleira, M., Güiza, F., Meyfroidt, G., Czosnyka, M., Smielewski, P., Stocchetti, N., Ercole, A., and Nelson, D. W. (2020). Impact of duration and magnitude of raised intracranial pressure on outcome after severe traumatic brain injury: A CENTER-TBI high-resolution group study. *PLoS ONE*, 15(12):e0243427.

Alperin, N., Mazda, M., Lichtor, T., and Lee, S. H. (2006). From cerebrospinal fluid pulsation to noninvasive intracranial compliance and pressure measured by MRI flow studies. *Current Medical Imaging Reviews*, 2(1):117–129.

Alperin, N., Sivaramakrishnan, A., and Lichtor, T. (2005). Magnetic resonance imaging–based measurements of cerebrospinal fluid and blood flow as indicators of intracranial compliance in patients with chiari malformation. *Journal of Neurosurgery*, 103(1):46–52.

Ambarki, K., Baledent, O., Kongolo, G., Bouzerar, R., Fall, S., and Meyer, M.-E. (2007). A new lumped-parameter model of cerebrospinal hydrodynamics during the cardiac cycle in healthy volunteers. *IEEE Transactions on Biomedical Engineering*, 54(3):483–491.

Artstein, R. and Poesio, M. (2008). Inter-coder agreement for computational linguistics. *Computational Linguistics*, 34(4):555–596.

Asgari, S., Bergsneider, M., Hamilton, R., Vespa, P., and Hu, X. (2011a). Consistent changes in intracranial pressure waveform morphology induced by acute hypercapnic cerebral vasodilatation. *Neurocritical Care*, 15(1):55–62.

Asgari, S., Vespa, P., Bergsneider, M., and Hu, X. (2011b). Lack of consistent intracranial pressure pulse morphological changes during episodes of microdialysis lactate/pyruvate ratio increase. *Physiological Measurement*, 32(10):1639–1651.

Asgari, S., Xu, P., Bergsneider, M., and Hu, X. (2009). A subspace decomposition approach toward recognizing valid pulsatile signals. *Physiological Measurement*, 30(11):1211–1225.

Avezaat, C. J. J. and van Eijndhoven, J. H. (1984). *Cerebrospinal fluid pulse pressure and craniospinal dynamics: a theoretical, clinical and experimental study.* PhD thesis, Erasmus University Rotterdam.

Avezaat, C. J. J., van Eijndhoven, J. H., and Wyper, D. J. (1979). Cerebrospinal fluid pulse pressure and intracranial volume-pressure relationships. *Journal of Neurology, Neurosurgery and Psychiatry*, 42(8):687–700.

Badri, S., Chen, J., Barber, J., Temkin, N. R., Dikmen, S. S., Chesnut, R. M., Deem, S., Yanez, N. D., and Treggiari, M. M. (2012). Mortality and long-term functional outcome associated with intracranial pressure after traumatic brain injury. *Intensive Care Medicine*, 38(11):1800–1809.

Balestreri, M., Czosnyka, M., Steiner, L. A., Schmidt, E., Smielewski, P., Matta, B., and Pickard, J. D. (2004). Intracranial hypertension: what additional information can be derived from ICP waveform after head injury? *Acta Neurochirurgica*, 146(2):131–141.

Baumgartner, R. W. (2006). Transcranial insonation. *Frontiers of Neurology and Neuroscience*, 21:105–116.

Behrens, A., Lenfeldt, N., Qvarlander, S., Koskinen, L. O., Malm, J., and Eklund, A. (2013). Are intracranial pressure wave amplitudes measurable through lumbar puncture? *Acta Neurologica Scandinavica*, 127(4):233–241.

Bishop, S. M. and Ercole, A. (2018). Multi-scale peak and trough detection optimised for periodic and quasi-periodic neuroscience data. *Acta Neurochirurgica Supplement*, 126:189–195.

Børgesen, S. E., Albeck, M. J., Gjerris, F., Czosnyka, M., and Laniewski, P. (1992). Computerized infusion test compared to steady pressure constant infusion test in measurement of resistance to CSF outflow. *Acta Neurochirurgica*, 119(1-4):12–16.

Brasil, S., Fontoura Solla, D. J., de Carvalho Nogueira, R., Jacobsen Teixeira, M., Sa Malbouisson, L. M., and Silva Paiva, W. (2021). Intracranial compliance assessed by intracranial pressure pulse waveform. *Brain Sciences*, 11(8):971.

Bratton, S. L., Chestnut, R. M., Ghajar, J., Mcconnell Hammond, F. F., Harris, O. A., Hartl, R., Manley, G. T., Nemecek, A., Newell, D. W., Rosenthal, G., Schouten, J., Shutter, L., Timmons, S. D., Ullman, J. S., Videtta, W., Wilberger, J. E., and Wright, D. W. (2007). Guidelines for the management of severe traumatic brain injury. VIII. Intracranial pressure thresholds. *Journal of Neurotrauma*, 24(Suppl 1):S55–58.

Bray, R. S., Sherwood, A. M., Halter, J. A., Robertson, C., and Grossman, R. G. (1986). Development of a clinical monitoring system by means of ICP waveform analysis. In Miller, J. D., Teasdale, G. M., Rowan, J. O., Galbraith, S. L., and Mendelow, A. D., editors, *Intracranial Pressure VI*, pages 260–264, Berlin, Heidelberg. Springer.

Calisto, A., Galeano, M., Serrano, S., Calisto, A., and Azzerboni, B. (2013). A new approach for investigating intracranial pressure signal: filtering and morphological features extraction from continuous recording. *IEEE Transactions on Biomedical Engineering*, 60(3):830–837.

Calviello, L., Donnelly, J., Cardim, D., Robba, C., Zeiler, F. A., Smielewski, P., and Czosnyka, M. (2018). Compensatory-reserve-weighted intracranial pressure and its association with outcome after traumatic brain injury. *Neurocritical Care*, 28(2):212–220.

Cardoso, E. R., Rowan, J. O., and Galbraith, S. (1983). Analysis of the cerebrospinal fluid pulse wave in intracranial pressure. *Journal of Neurosurgery*, 59(5):817–821.

Carney, N., Totten, A. M., O'Reilly, C., Ullman, J. S., Hawryluk, G. W. J., Bell, M. J., Bratton, S. L., Chesnut, R., Harris, O. A., Kissoon, N., Rubiano, A. M., Shutter, L., Tasker, R. C., Vavilala, M. S., Wilberger, J., Wright, D. W., and Ghajar, J. (2017). Guidelines for the management of severe traumatic brain injury, fourth edition. *Neurosurgery*, 80(1):6–15.

Carrera, E., Kim, D.-J., Castellani, G., Zweifel, C., Czosnyka, Z., Kasprowicz, M., Smielewski, P., Pickard, J. D., and Czosnyka, M. (2010). What shapes pulse amplitude of intracranial pressure? *Journal of Neurotrauma*, 27(2):317–324.

Castellani, G., Zweifel, C., Kim, D.-J., Carrera, E., Radolovich, D. K., Smielewski, P., Hutchinson, P. J., Pickard, J. D., and Czosnyka, M. (2009). Plateau waves in head injured patients requiring neurocritical care. *Neurocritical Care*, 11(2):143–150.

Chesnut, R., Videtta, W., Vespa, P., Le Roux, P., and Participants in the International Multidisciplinary Consensus Conference on Multimodality Monitoring, G. (2014). Intracranial pressure monitoring: fundamental considerations and rationale for monitoring. *Neurocritical Care*, 21(2):64–84.

Chopp, M. and Portnoy, H. D. (1980). Systems analysis of intracranial pressure. Comparison with volume-pressure test and CSF-pulse amplitude analysis. *Journal of Neurosurgery*, 53(4):516–527.

Connolly, E. S., Rabinstein, A. A., Carhuapoma, J. R., Derdeyn, C. P., Dion, J., Higashida, R. T., Hoh, B. L., Kirkness, C. J., Naidech, A. M., Ogilvy, C. S., Patel, A. B., Thompson, B. G., and Vespa, P. (2012). Guidelines for the management of aneurysmal subarachnoid hemorrhage: a guideline for healthcare professionals from the American Heart Association/American Stroke Association. *Stroke*, 43(6):1711–1737.

Contant, C. F., Robertson, C. S., Crouch, J., Gopinath, S. P., Narayan, R. K., and Grossman, R. G. (1995). Intracranial pressure waveform indices in transient and refractory intracranial hypertension. *Journal of Neuroscience Methods*, 57(1):15–25.

Cushing, H. (1926). *Studies in intracranial physiology & surgery: the third circulation, the hypophysis, the gliomas*. Oxford University Press, London.

Czosnyka, M. (2021). Brain physics in 30 short lectures (not only for engineers). https://www.neurosurg.cam.ac.uk/research-groups/brain-physics-lab/brain-physics-lectures/ [Accessed: 19 April 2022].

Czosnyka, M. and Citerio, G. (2012). Brain compliance: the old story with a new 'et cetera'. *Intensive Care Medicine*, 38(6):925–927.

Czosnyka, M. and Czosnyka, Z. (2020). Origin of intracranial pressure pulse waveform. *Acta Neurochirurgica*, 162(8):1815–1817.

Czosnyka, M., Guazzo, E., Whitehouse, M., Smielewski, P., Czosnyka, Z., Kirkpatrick, P., Piechnik, S., and Pickard, J. D. (1996a). Significance of intracranial pressure waveform analysis after head injury. *Acta Neurochirurgica*, 138(5):531–542.

Czosnyka, M., Pickard, J. D., and Steiner, L. A. (2017). Principles of intracranial pressure monitoring and treatment. *Handbook of Clinical Neurology*, 140:67–89.

Czosnyka, M., Piechnik, S., Richards, H. K., Kirkpatrick, P., Smielewski, P., and Pickard, J. D. (1997a). Contribution of mathematical modelling to the interpretation of bedside tests of cerebrovascular autoregulation. *Journal of Neurology Neurosurgery and Psychiatry*, 63(6):721–731.

Czosnyka, M., Price, D. J., and Williamson, M. (1994). Monitoring of cerebrospinal dynamics using continuous analysis of intracranial pressure and cerebral perfusion pressure in head injury. *Acta Neurochirurgica*, 126(2-4):113–119.

Czosnyka, M., Smielewski, P., Kirkpatrick, P., Laing, R. J., Menon, D., and Pickard, J. D. (1997b). Continuous assessment of the cerebral vasomotor reactivity in head injury. *Neurosurgery*, 41(1):11–19.

Czosnyka, M., Smielewski, P., Timofeev, I., Lavinio, A., Guazzo, E., Hutchinson, P., and Pickard, J. D. (2007). Intracranial pressure: more than a number. *Neurosurgical Focus*, 22(5):E10.

Czosnyka, M., Steiner, L., Balestreri, M., Schmidt, E., Smielewski, P., Hutchinson, P. J., and Pickard, J. D. (2005). Concept of "true ICP" in monitoring and prognostication in head trauma. *Acta Neurochirurgica Supplement*, 95:341–344.

Czosnyka, M., Whitehouse, H., Smielewski, P., Simac, S., and Pickard, J. D. (1996b). Testing of cerebrospinal compensatory reserve in shunted and non-shunted patients: A guide to interpretation based on an observational study. *Journal of Neurology, Neurosurgery and Psychiatry*, 60(5):549–558.

Czosnyka, M., Wollk-Laniewski, P., Batorski, L., and Zaworski, W. (1988). Analysis of intracranial pressure waveform during infusion test. *Acta Nerochirurgica*, 93(3-4):140–145.

Czosnyka, Z., Keong, N., Kim, D.-J., Radolovich, D., Smielewski, P., Lavinio, A., Schmidt, E. A., Momjian, S., Owler, B., Pickard, J. D., and Czosnyka, M. (2008). Pulse amplitude of intracranial pressure pulse waveform in hydrocephalus. *Acta Neurochirurgica Supplement*, 102:137–140.

Dai, H., Jia, X., Pahren, L., Lee, J., and Foreman, B. (2020). Intracranial pressure monitoring signals after traumatic brain Injury: a narrative overview and conceptual data science framework. *Frontiers in Neurology*, 11:959.

Diehl, R. R., Linden, D., Lucke, D., and Berlit, P. (1995). Phase relationship between cerebral blood flow velocity and blood pressure. A clinical test of autoregulation. *Stroke*, 26(10):1801–1804.

Eide, P. K. (2006). A new method for processing of continuous intracranial pressure signals. *Medical Engineering and Physics*, 28(6):579–587.

Eide, P. K. (2016). The correlation between pulsatile intracranial pressure and indices of intracranial pressure-volume reserve capacity: results from ventricular infusion testing. *Journal of Neurosurgery*, 125(6):1493–1503.

Eide, P. K., Bentsen, G., Sorteberg, A. G., Marthinsen, P. B., Stubhaug, A., and Sorteberg, W. (2011). A randomized and blinded single-center trial comparing the effect of intracranial pressure and intracranial pressure wave amplitude-guided intensive care management on early clinical state and 12-month outcome in patients with aneurysmal subarachnoid hemo. *Neurosurgery*, 69(5):1105–1115.

Eide, P. K. and Brean, A. (2006). Intracranial pulse pressure amplitude levels determined during preoperative assessment of subjects with possible idiopathic normal pressure hydrocephalus. *Acta Neurochirurgica*, 148(11):1151–1156.

Eide, P. K. and Sorteberg, W. (2006). Intracranial pressure levels and single wave amplitudes, Glasgow Coma Score and Glasgow Outcome Score after subarachnoid haemorrhage. *Acta Neurochirurgica*, 148(12):1267–1275.

Eklund, A., Smielewski, P., Chambers, I., Alperin, N., Malm, J., Czosnyka, M., and Marmarou, A. (2007). Assessment of cerebrospinal fluid outflow resistance. *Medical & Biological Engineering & Computing*, 45(8):719–735.

Elixmann, I. M., Hansinger, J., Goffin, C., Antes, S., Radermacher, K., and Leonhardt, S. (2012). Single pulse analysis of intracranial pressure for a hydrocephalus implant. In *2012 Annual International Conference of the IEEE Engineering in Medicine and Biology Society*, pages 3939–3942, San Diego, CA, USA. IEEE.

Ellis, T., McNames, J., and Goldstein, B. (2005). Residual pulse morphology visualization and analysis in pressure signals. In *2005 IEEE Engineering in Medicine and Biology Society 27th Annual Conference*, pages 3966–3969, Shanghai, China. IEEE.

Evensen, K. B. and Eide, P. K. (2020). Measuring intracranial pressure by invasive, less invasive or non-invasive means: limitations and avenues for improvement. *Fluids and Barriers of the CNS*, 17(1):34.

Fan, J.-Y., Kirkness, C., Vicini, P., Burr, R., and Mitchell, P. (2008). Intracranial pressure waveform morphology and intracranial adaptive capacity. *American Journal of Critical Care*, 17(6):545–554.

Foltz, E. L., Blanks, J. P., and Yonemura, K. (1990). CSF pulsatility in hydrocephalus: respiratory effect on pulse wave slope as an indicator of intracranial compliance. *Neurological Research*, 12(2):67–74.

Ganapathy, N., Swaminathan, R., and Deserno, T. M. (2018). Deep learning on 1-D biosignals : a taxonomy-based survey. *Yearbook of Medical Informatics*, 27(1):98–109.

Germon, K. (1988). Interpretation of ICP pulse waves to determine intracerebral compliance. *Journal of Neuroscience Nursing*, 20(6):344–351.

Gomes, J. A. and Bhardwaj, A. (2009). Normal intracranial pressure physiology. In Irani, D. N., editor, *Cerebrospinal fluid in clinical practice*, chapter 4, pages 18–25. Saunders Elsevier, Philadelphia, PA, USA.

Hall, A. and O'Kane, R. (2016). The best marker for guiding the clinical management of patients with raised intracranial pressure—the RAP index or the mean pulse amplitude? *Acta Neurochirurgica*, 158(10):1997–2009.

Hamilton, R., Fuller, J., Baldwin, K., Vespa, P., Hu, X., and Bergsneider, M. (2016). Relative position of the third characteristic peak of the intracranial pressure pulse waveform morphology differentiates normal-pressure hydrocephalus shunt responders and nonresponders. *Acta Neurochirurgica Supplement*, 122:339–345.

Hamilton, R., Xu, P., Asgari, S., Kasprowicz, M., Vespa, P., Bergsneider, M., and Hu, X. (2009). Forecasting intracranial pressure elevation using pulse waveform morphology. In *Annual International Conference of the IEEE Engineering in Medicine and Biology Society*, pages 4331–4334, Minneapolis, MN, USA. IEEE.

Harary, M., Dolmans, R. G. F., and Gormley, W. B. (2018). Intracranial pressure monitoring—review and avenues for development. *Sensors (Switzerland)*, 18(2):465.

Hartman, A. L. (2009). Normal anatomy of the cerebrospinal fluid compartment. In Irani, D. N., editor, *Cerebrospinal fluid in clinical practice*, chapter 2, pages 5–10. Saunders Elsevier, Philadelphia, PA, USA.

Hawthorne, C. and Piper, I. (2014). Monitoring of intracranial pressure in patients with traumatic brain injury. *Frontiers in Neurology*, 5:121.

Heldt, T., Zoerle, T., Teichmann, D., and Stocchetti, N. (2019). Intracranial pressure and intracranial elastance monitoring in neurocritical care. *Annual Review of Biomedical Engineering*, 21:523–549.

Holm, S. and Eide, P. K. (2008). The frequency domain versus time domain methods for processing of intracranial pressure (ICP) signals. *Medical Engineering and Physics*, 30(2):164–170.

Holm, S. and Eide, P. K. (2009). Impact of sampling rate for time domain analysis of continuous intracranial pressure (ICP) signals. *Medical Engineering and Physics*, 31(5):601–606.

Howells, T., Lewen, A., Skold, M. K., Ronne-Engstrom, E., and Enblad, P. (2012). An evaluation of three measures of intracranial compliance in traumatic brain injury patients. *Intensive Care Medicine*, 38(6):1061–1068.

Hu, X., Glenn, T., Scalzo, F., Bergsneider, M., Sarkiss, C., Martin, N., and Vespa, P. (2010a). Intracranial pressure pulse morphological features improved detection of decreased cerebral blood flow. *Physiological Measurement*, 31(5):679–695.

Hu, X., Xu, P., Asgari, S., Vespa, P., and Bergsneider, M. (2010b). Forecasting ICP elevation based on prescient changes of intracranial pressure waveform morphology. *IEEE Transactions on Biomedical Engineering*, 57(5):1070–1078.

Hu, X., Xu, P., Lee, D. J., Paul, V., and Bergsneider, M. (2008). Morphological changes of intracranial pressure pulses are correlated with acute dilatation of ventricles. *Acta Neurochirurgica Supplement*, 102:131–136.

Hu, X., Xu, P., Scalzo, F., Vespa, P., and Bergsneider, M. (2009). Morphological clustering and analysis of continuous intracranial pressure. *IEEE Transactions on Biomedical Engineering*, 56(3):696–705.

Imhoff, M. and Kuhls, S. (2006). Alarm algorithms in critical monitoring. *Anesthesia and Analgesia*, 102(5):1525–1537.

Jennet, B. and Bond, M. (1975). Assessment of outcome after severe brain damage. *The Lancet*, 1(7905):480–484.

Kaczmarska, K., Smielewski, P., Kasprowicz, M., **Kazimierska, A.**, Grzanka, A., Czosnyka, Z., and Czosnyka, M. (2021). Analysis of intracranial pressure pulse–pressure relationship: experimental validation. *Acta Neurochirurgica Supplement*, 131:279–282.

Kahraman, S., Dutton, R. P., Hu, P., Xiao, Y., Aarabi, B., Stein, D. M., and Scalea, T. M. (2010). Automated measurement of "pressure times time dose" of intracranial hypertension best predicts outcome after severe traumatic brain injury. *Journal of Trauma and Acute Care Surgery*, 69(1):110–118.

Kasprowicz, M., Asgari, S., Bergsneider, M., Czosnyka, M., Hamilton, R., and Hu, X. (2010). Pattern recognition of overnight intracranial pressure slow waves using morphological features of intracranial pressure pulse. *Journal of Neuroscience Methods*, 190(2):310–318.

Kasprowicz, M., Lalou, D. A., Czosnyka, M., Garnett, M., and Czosnyka, Z. (2016). Intracranial pressure, its components and cerebrospinal fluid pressure–volume compensation. *Acta Neurologica Scandinavica*, 134(3):168–180.

Katzman, R. and Husey, F. (1970). A simple constant-infusion manometric test for measurement of CSF absorption. I. Rationale and method. *Neurology*, 20(6):534–544.

Kazimierska, A., Kasprowicz, M., Czosnyka, M., Placek, M. M., Baledent, O., Smielewski, P., and Czosnyka, Z. (2021a). Compliance of the cerebrospinal space: comparison of three methods. *Acta Neurochirurgica*, 163(7):1979–1989.

Kazimierska, A., Uryga, A., Mataczyński, C., Burzyńska, M., Ziolkowski, A., Rusiecki, A., and Kasprowicz, M. (2021b). Analysis of the shape of intracranial pressure pulse waveform in traumatic brain injury patients. In *Annual International Conference of the IEEE Engineering in Medicine and Biology Society*, pages 546–549, Mexico. IEEE.

Kazimierska, A., Ziółkowski, A., Kasprowicz, M., Lalou, D. A., Czosnyka, Z., and Czosnyka, M. (2021c). Mathematical modelling in hydrocephalus. *Neurology India*, 69 (Supplement):S275–S282.

Kellie, G. (1824). An account of the appearances observed in the dissection of two of three individuals presumed to have perished in the storm of the 3rd, and whose bodies were discovered in the vicinity of Leith on the morning of the 4th November 1821; with some reflections on the pathology of the brain. *Transactions. Medico-Chirurgical Society of Edinburgh*, 1:84–122.

Kim, D.-J., Czosnyka, Z., Kasprowicz, M., Smielewski, P., Balédent, O., Guerguerian, A.-M., Pickard, J. D., and Czosnyka, M. (2012). Continuous monitoring of the Monro-Kellie doctrine: is it possible? *Journal of Neurotrauma*, 29(7):1354–1363.

Kim, D.-J., Czosnyka, Z., Keong, N., Radolovich, D. K., Smielewski, P., Sutcliffe, M. P. F., Pickard, J. D., and Czosnyka, M. (2009a). Index of cerebrospinal compensatory reserve in hydrocephalus. *Neurosurgery*, 64(3):494–501.

Kim, D. J., Kasprowicz, M., Carrera, E., Castellani, G., Zweifel, C., Lavinio, A., Smielewski, P., Sutcliffe, M. P., Pickard, J. D., and Czosnyka, M. (2009b). The monitoring of relative changes in compartmental compliances of brain. *Physiological Measurement*, 30(7):647–659.

Kirkness, C. J., Mitchell, P. H., Burr, R. L., March, K. S., and Newell, D. W. (2000). Intracranial pressure waveform analysis: clinical and research implications. *Journal of Neuroscience Nursing*, 32(5):271–277.

Lavinio, A. and Menon, D. K. (2011). Intracranial pressure: why we monitor it, how to monitor it, what to do with the number and what's the future? *Current Opinion in Anaesthesiology*, 24(2):117–123.

Lee, H.-J., Jeong, E.-J., Kim, H., Czosnyka, M., and Kim, D.-J. (2016). Morphological feature extraction from a continuous intracranial pressure pulse via a peak clustering algorithm. *IEEE Transactions on Biomedical Engineering*, 63(10):2169–2176.

Lee, H.-J., Kim, H., Kim, Y.-T., Won, K., Czosnyka, M., and Kim, D.-J. (2021). Prediction of life-threatening intracranial hypertension during the acute phase of traumatic brain injury using machine learning. *IEEE Journal of Biomedical and Health Informatics*, 25(10):3967–3976.

Lee, S.-B., Kim, H., Kim, Y.-T., Zeiler, F. A., Smielewski, P., Czosnyka, M., and Kim, D.-J. (2019). Artifact removal from neurophysiological signals: impact on intracranial and arterial pressure monitoring in traumatic brain injury. *Journal of Neurosurgery*, 132(6):1952–1960.

Li, G., Watanabe, K., Anzai, H., Song, X., Qiao, A., and Ohta, M. (2019). Pulse-wave-pattern classification with a convolutional neural network. *Scientific Reports*, 9(1):14930.

Little, A. S., Zabramski, J. M., Peterson, M., Goslar, P. W., Wait, S. D., Albuquerque, F. C., McDougall, C. G., and Spetzler, R. F. (2008). Ventriculoperitoneal shunting after aneurysmal subarachnoid hemorrhage: analysis of the indications, complications, and outcome with a focus on patients with borderline ventriculomegaly. *Neurosurgery*, 62(3):618–627.

Lofgren, J., von Essen, C., and Zwetnow, N. N. (1973). The pressure-volume curve of the cerebrospinal fluid space in dogs. *Acta Neurologica Scandinavica*, 49(5):557–574.

Lundberg, N., Troupp, H., and Lorin, H. (1965). Continuous recording of the ventricular-fluid pressure in patients with severe acute traumatic brain injury. A preliminary report. *Journal of Neurosurgery*, 22(6):581–590.

Maas, A. I. R., Menon, D. K., Steyerberg, E. W., Citerio, G., Lecky, F., Manley, G. T., Hill, S., Legrand, V., Sorgner, A., participants, C.-T., and investigators, G. (2015). Collaborative European neurotrauma effectiveness research in traumatic brain injury (CENTER-TBI): A prospective longitudinal observational study. *Neurosurgery*, 76(1):67–80.

Mariak, Z., Swiercz, M., Krejza, J., Lewko, J., and Lyson, T. (2000). Intracranial pressure processing with artificial neural networks: classification of signal properties. *Acta Neurochirurgica*, 142(4):407–412.

Marmarou, A. (1973). *A theoretical model and experimental evaluation of the cerebrospinal fluid system*. PhD thesis, Drexel University.

Marmarou, A., Black, P., Bergsneider, M., Klinge, P., Relkin, N., and International NPH Consultant Group, G. (2005). Guidelines for management of idiopathic normal pressure hydrocephalus: Progress to date. *Acta Neurochirurgica Supplement*, 95:237–240.

Marmarou, A., Shulman, K., and LaMorgese, J. (1975). Compartmental analysis of compliance and outflow resistance of the cerebrospinal fluid system. *Journal of Neurosurgery*, 43(5):523–534.

Martinez-Tejada, I., Arum, A., Wilhjelm, J. E., Juhler, M., and Andresen, M. (2019). B waves: A systematic review of terminology, characteristics, and analysis methods. *Fluids and Barriers of the CNS*, 16(1):33.

Maset, A. L., Marmarou, A., Ward, J. D., Choi, S., Lutz, H. A., Brooks, D., Moulton, R. J., DeSalles, A., Muizelaar, J. P., Turner, H., and Young, H. F. (1987). Pressure-volume index in head injury. *Journal of Neurosurgery*, 67(6):832–840.

Mataczyński, C., **Kazimierska, A.**, Uryga, A., Burzyńska, M., Rusiecki, A., and Kasprowicz, M. (2022a). End-to-end automatic morphological classification of intracranial pressure pulse waveforms using deep learning. *IEEE Journal of Biomedical and Health Informatics*, 26(2):494–504. Joint first authorship of C. Mataczyński and A. Kazimierska.

Mataczyński, C., **Kazimierska, A.**, Uryga, A., Kasprowicz, M., and CENTER-TBI high resolution sub-study participants and investigators (2022b). Intracranial pressure pulse morphology-based definition of life-threatening intracranial hypertension episodes. Accepted for publication at the 44th Annual International Conference of the IEEE Engineering in Medicine and Biology Society (11–15 July 2022, Glasgow, UK).

McMillan, T., Wilson, L., Ponsford, J., Levin, H., Teasdale, G., and Bond, M. (2016). The Glasgow Outcome Scale-40 years of application and refinement. *Nature Reviews Neurology*, 12(8):477–485.

Megjhani, M., Alkhachroum, A., Terilli, K., Ford, J., Rubinos, C., Kromm, J., Wallace, B. K., Connolly, E. S., Roh, D., Agarwal, S., Claassen, J., Padmanabhan, R., Hu, X., and Park, S. (2019). An active learning framework for enhancing identification of non-artifactual intracranial pressure waveforms. *Physiological Measurement*, 40(1):015002.

Miller, J. D. and Garibi, J. (1972). Intracranial volume/pressure relationships during continuous monitoring of ventricular fluid pressure. In Brock, M. and Dietz, H., editors, *Intracranial Pressure*, pages 270–274, Berlin, Heidelberg. Springer.

Miller, J. D., Garibi, J., and Pickard, J. D. (1973). Induced changes of cerebrospinal fluid volume. Effects during continuous monitoring of ventricular fluid pressure. *Archives of Neurology*, 28(4):265–269.

Miller, J. D. and Pickard, J. D. (1974). Intracranial volume pressure studies in patients with head injury. *Injury*, 5(3):265–268.

Mitchell, P. H., Kirkness, C., Burr, R., March, K. S., and Newell, D. W. (1997). Waveform predictors: adverse response to nursing care. In Marmarou, A., Bullock, R., Avezaat, C. J. J., Baethmann, A., Becker, D., Brock, M., Hoff, J., Nagai, H., Reulen, H.-J., and Teasdale, G., editors, *Intracranial Pressure and Neuromonitoring in Brain Injury:*

Proceedings of the Tenth International ICP Symposium, page 420, Williamsburg, VA, USA. Springer.

Momjian, S., Czosnyka, Z., Czosnyka, M., and Pickard, J. D. (2004). Link between vasogenic waves of intracranial pressure and cerebrospinal fluid outflow resistance in normal pressure hydrocephalus. *British Journal of Neurosurgery*, 18(1):56–61.

Monro, A. (1783). *Observations on the structure and functions of the nervous system*. Creech and Johnson, Edinburgh.

Morrison, B. M. (2009). Physiology of cerebrospinal fluid secretion, recirculation, and resorption. In Irani, D. N., editor, *Cerebrospinal fluid in clinical practice*, chapter 3, pages 11–17. Saunders Elsevier, Philadelphia, PA, USA.

Nakajima, M., Yamada, S., Miyajima, M., Ishii, K., Kuriyama, N., Kazui, H., Kanemoto, H., Suehiro, T., Yoshiyama, K., Kameda, M., Kajimoto, Y., Mase, M., Murai, H., Kita, D., Kimura, T., Samejima, N., Tokuda, T., Kaijima, M., Akiba, C., Kawamura, K., Atsuchi, M., Hirata, Y., Matsumae, M., Sasaki, M., Yamashita, F., Aoki, S., Irie, R., Miyake, H., Kato, T., Mori, E., Ishikawa, M., Date, I., Arai, H., and Research committe of idiopathic normal pressure hydrocephalus, G. (2021). Guidelines for management of idiopathic normal pressure hydrocephalus (Third edition): Endorsed by the Japanese Society of Normal Pressure Hydrocephalus. *Neurologia Medico-Chirurgica*, 61(2):63–97.

Noback, C. L., Strominger, N. L., Demarest, R. J., and Ruggiero, D. A. (2005). *The human nervous system. Structure and function*. Humana Press, Totowa, NJ, USA, 6th edition.

Nucci, C. G., De Bonis, P., Mangiola, A., Santini, P., Sciandrone, M., Risi, A., and Anile, C. (2016). Intracranial pressure wave morphological classification: automated analysis and clinical validation. *Acta Neurochirurgica*, 158(3):581–588.

Oswal, A. and Toma, A. K. (2020). Intracranial pressure and cerebral haemodynamics. *Anaesthesia & Intensive Care Medicine*, 21(6):317–321.

Panerai, R. B. (1998). Assessment of cerebral pressure autoregulation in humans - A review of measurement methods. *Physiological Measurement*, 19(3):305–338.

Pillai, S., Praharaj, S. S., Rao, G. S. U., and Kolluri, V. R. S. (2004). Cerebral perfusion pressure management of severe diffuse head injury: effect on brain compliance and intracranial pressure. *Neurology India*, 52(1):67–71.

Piper, I., Spiegelberg, A., Whittle, I., Signorini, D., and Mascia, L. (1999). A comparative study of the Spiegelberg compliance device with a manual volume-injection method: a clinical evaluation in patients with hydrocephalus. *British Journal of Neurosurgery*, 13(6):581–586.

Quachtran, B., Hamilton, R., and Scalzo, F. (2016). Detection of intracranial hypertension using deep learning. In *23th International Conference on Pattern Recognition*, volume 2016, pages 2491–2496, Cancun, Mexico. IEEE.

Reinhard, M., Müller, T., Guschlbauer, B., Timmer, J., and Hetzel, A. (2003). Transfer function analysis for clinical evaluation of dynamic cerebral autoregulation - a comparison between spontaneous and respiratory-induced oscillations. *Physiological Measurement*, 24(1):27–43.

Rim, B., Sung, N.-J., Min, S., and Hong, M. (2020). Deep learning in physiological signal data: A survey. *Sensors (Switzerland)*, 20(4):969.

Robertson, C. S., Narayan, R. K., Contant, C. F., Grossman, R. G., Gokaslan, Z. L., Pahwa, R., Caram Jr, P., Bray Jr, R. S., and Sherwood, A. M. (1989). Clinical experience with a continuous monitor of intracranial compliance. *Journal of Neurosurgery*, 71(5 Pt 1):673–680.

Rosner, M. J. and Becker, D. P. (1984). Origin and evolution of plateau waves. Experimental observations and a theoretical model. *Journal of Neurosurgery*, 60(2):312–324.

Ryder, H. W., Espey, F. F., Kimbell, F. D., Penka, E. J., Rosenauer, A., Podolsky, B., and Evans, J. P. (1953). The mechanism of the change in cerebrospinal fluid pressure following an induced change in the volume of the fluid space. *Journal of Laboratory & Clinical Medicine*, 41(3):428–435.

Scalzo, F., Asgari, S., Kim, S., Bergsneider, M., and Hu, X. (2010). Robust peak recognition in intracranial pressure signals. *Biomedical Engineering Online*, 9:61.

Scalzo, F., Asgari, S., Kim, S., Bergsneider, M., and Hu, X. (2012). Bayesian tracking of intracranial pressure signal morphology. *Artificial Intelligence in Medicine*, 54(2):115–123.

Scalzo, F., Xu, P., Asgari, S., Bergsneider, M., and Hu, X. (2009). Regression analysis for peak designation in pulsatile pressure signals. *Medical & Biological Engineering & Computing*, 47(9):967–977.

Shapiro, K., Marmarou, A., and Shulman, K. (1980). Characterization of clinical CSF dynamics and neural axis compliance using the pressure-volume index: I. The normal pressure-volume index. *Annals of Neurology*, 7(6):508–514.

Smith, M. (2008). Monitoring intracranial pressure in traumatic brain injury. *Anesthesia and Analgesia*, 106(1):240–248.

Sorrentino, E., Diedler, J., Kasprowicz, M., Budohoski, K. P., Haubrich, C., Smielewski, P., Outtrim, J. G., Manktelow, A., Hutchinson, P. J., Pickard, J. D., Menon, D. K., and Czosnyka, M. (2012). Critical thresholds for cerebrovascular reactivity after traumatic brain injury. *Neurocritical Care*, 16(2):258–266.

Steiner, L. A. and Andrews, P. J. D. (2006). Monitoring the injured brain: ICP and CBF. *British Journal of Anaesthesia*, 97(1):26–38.

Steiner, L. A., Balestreri, M., Johnston, A. J., Coles, J. P., Smielewski, P., Pickard, J. D., Menon, D. K., and Czosnyka, M. (2005). Predicting the response of intracranial pressure to moderate hyperventilation. *Acta Neurochirurgica*, 147(5):477–483.

Stephensen, H., Andersson, N., Eklund, A., Malm, J., Tisell, M., and Wikkelsö, C. (2005). Objective B wave analysis in 55 patients with non-communicating and communicating hydrocephalus. *Journal of Neurology Neurosurgery and Psychiatry*, 76(7):965–970.

Stocchetti, N., Carbonara, M., Citerio, G., Ercole, A., Skrifvars, M. B., Smielewski, P., Zoerle, T., and Menon, D. K. (2017). Severe traumatic brain injury: targeted management in the intensive care unit. *Lancet Neurology*, 16(6):452–464.

Stoquart-Elsankari, S., Lehmann, P., Villette, A., Czosnyka, M., Meyer, M. E., Deramond, H., and Balédent, O. (2009). A phase-contrast MRI study of physiologic cerebral venous flow. *Journal of Cerebral Blood Flow and Metabolism*, 29(6):1208–1215.

Swiercz, M., Mariak, Z., Krejza, J., Lewko, J., and Szydlik, P. (2000). Intracranial pressure processing with artificial neural networks: prediction of ICP trends. *Acta Nerochirurgica*, 142(4):401–406.

Szewczykowski, J., Śliwka, S., Kunicki, A., Dytko, P., and Korsak-Śliwka, J. (1977). A fast method of estimating the elastance of the intracranial system. *Journal of Neurosurgery*, 47(1):19–26.

Takizawa, H., Gabra-Sanders, T., and Miller, J. D. (1987). Changes in the cerebrospinal fluid pulse wave spectrum associated with raised intracranial pressure. *Neurosurgery*, 20(3):355–361.

Tans, J. T. and Poortvliet, D. C. (1983). Intracranial volume-pressure relationship in man. Part 2: Clinical significance of the pressure-volume index. *Journal of Neurosurgery*, 59(5):810–816.

Tavakoli, S., Peitz, G., Ares, W., Hafeez, S., and Grandhi, R. (2017). Complications of invasive intracranial pressure monitoring devices in neurocritical care. *Neurosurgical Focus*, 43(5):E6.

Teasdale, G. and Jennet, B. (1974). Assessment of coma and impaired consciousness. A practical scale. *The Lancet*, 2(7872):81–84.

Teasdale, G., Maas, A., Lecky, F., Manley, G., Stocchetti, N., and Murray, G. (2014). The Glasgow Coma Scale at 40 years: Standing the test of time. *The Lancet Neurology*, 13(8):844–854.

Timofeev, I. (2008). The intracranial compartment and intracranial pressure. In Gupta, A. K. and Gelb, A. W., editors, *Essentials of Neuroanesthesia and Neurointensive Care*, chapter 4, pages 26–31. W.B. Saunders.

Timofeev, I., Czosnyka, M., Nortje, J., Smielewski, P., Kirkpatrick, P., Gupta, A., and Hutchinson, P. (2008). Effect of decompressive craniectomy on intracranial pressure and cerebrospinal compensation following traumatic brain injury. *Journal of Neurosurgery*, 108(1):66–73.

Wagshul, M. E., Eide, P. K., and Madsen, J. R. (2011). The pulsating brain: a review of experimental and clinical studies of intracranial pulsatility. *Fluids and Barriers of the CNS*, 8(1):5.

Weerakkody, R. A., Czosnyka, M., Schuhmann, M. U., Schmidt, E., Keong, N., Santarius, T., Pickard, J. D., and Czosnyka, Z. (2011). Clinical assessment of cerebrospinal fluid dynamics in hydrocephalus. Guide to interpretation based on observational study. *Acta Neurologica Scandinavica*, 124(2):85–98.

Wilkinson, H. A., Schuman, N., and Ruggiero, J. (1979). Nonvolumetric methods of detecting impaired intracranial compliance or reactivity: pulse width and wave form analysis. *Journal of Neurosurgery*, 50(6):758–767.

Wilson, J. T., Pettigrew, L. E., and Teasdale, G. M. (1998). Structured interviews for the Glasgow Outcome Scale and the Extended Glasgow Outcome Scale: Guidelines for their use. *Journal of Neurotrauma*, 15(8):573–585.

Zakrzewska, A. P., Placek, M. M., Czosnyka, M., Kasprowicz, M., and Lang, E. W. (2021). Intracranial pulse pressure waveform analysis using the higher harmonics centroid. *Acta Neurochirurgica*, 163(12):3249–3258.

Zeiler, F. A., Ercole, A., Cabeleira, M., Beqiri, E., Zoerle, T., Carbonara, M., Stocchetti, N., Menon, D. K., Smielewski, P., Czosnyka, M., and CENTER-TBI High Resolution ICU Sub-Study Participants and Investigators, G. (2019). Compensatory-reserve-weighted intracranial pressure versus intracranial pressure for outcome association in adult traumatic brain injury: a CENTER-TBI validation study. *Acta Neurochirurgica*, 161(7):1275–1284.

Zeiler, F. A., Kim, D.-J., Cabeleira, M., Calviello, L., Smielewski, P., and Czosnyka, M. (2018). Impaired cerebral compensatory reserve is associated with admission imaging characteristics of diffuse insult in traumatic brain injury. *Acta Neurochirurgica*, 160(12):2277–2287.

Ziółkowski, A., Pudełko, A., **Kazimierska, A.**, Czosnyka, Z., Czosnyka, M., and Kasprowicz, M. (2021). Analysis of relative changes in pulse shapes of intracranial pressure and cerebral blood flow velocity. *Physiological Measurement*, 42(12):125004.

Zweifel, C., Hutchinson, P. J., and Czosnyka, M. (2011). Intracranial pressure. In Matta, B. F., Menon, D. K., and Smith, M., editors, *Core Topics in Neuroanesthesia and Neurointensive Care*, chapter 4, pages 45–62. Cambridge University Press, Cambridge, UK.

Appendix A

Full text of the papers:

- **Kazimierska, A.**, Kasprowicz, M., Czosnyka, M., Placek, M. M., Baledent, O., Smielewski, P., and Czosnyka, Z. (2021). Compliance of the cerebrospinal space: comparison of three methods. *Acta Neurochirurgica*, 163(7):1979–1989.

- Mataczyński, C.*, **Kazimierska, A.***, Uryga, A., Burzyńska, M., Rusiecki, A., and Kasprowicz, M. (2022). End-to-end automatic morphological classification of intracranial pressure pulse waveforms using deep learning. *IEEE Journal of Biomedical and Health Informatics*, 26(2):494–504. *joint first authorship

- **Kazimierska, A.**, Uryga, A., Mataczyński, C., Burzyńska, M., Ziółkowski, A., Rusiecki, A., and Kasprowicz, M. (2021). Analysis of the shape of intracranial pressure pulse waveform in traumatic brain injury patients. In: *43rd Annual International Conference of the IEEE Engineering in Medicine & Biology Society (EMBC 2021)*, pages 546–549, Mexico. IEEE.

- Mataczyński, C., **Kazimierska, A.**, Uryga, A., Kasprowicz, M., and CENTER-TBI high resolution sub-study participants and investigators (2022). Intracranial pressure pulse morphology-based definition of life-threatening intracranial hypertension episodes. Accepted for publication at *44th Annual International Conference of the IEEE Engineering in Medicine & Biology Society (EMBC 2022)*, 11–15 July 2022, Glasgow, United Kingdom.

Acta Neurochirurgica
https://doi.org/10.1007/s00701-021-04834-y

ORIGINAL ARTICLE - CSF CIRCULATION

Compliance of the cerebrospinal space: comparison of three methods

Agnieszka Kazimierska[1] · Magdalena Kasprowicz[1] · Marek Czosnyka[2,3] · Michał M. Placek[2] · Olivier Baledent[4] · Peter Smielewski[2] · Zofia Czosnyka[2]

Received: 3 December 2020 / Accepted: 26 March 2021

Abstract

Background Cerebrospinal compliance describes the ability of the cerebrospinal space to buffer changes in volume. Diminished compliance is associated with increased risk of potentially threatening increases in intracranial pressure (ICP) when changes in cerebrospinal volume occur. However, despite various methods of estimation proposed so far, compliance is seldom used in clinical practice. This study aimed to compare three measures of cerebrospinal compliance.

Methods ICP recordings from 36 normal-pressure hydrocephalus patients who underwent infusion tests with parallel recording of transcranial Doppler blood flow velocity were retrospectively analysed. Three methods were used to calculate compliance estimates during changes in the mean ICP induced by infusion of fluid into the cerebrospinal fluid space: (a) based on Marmarou's model of cerebrospinal fluid dynamics (C_{CSF}), (b) based on the evaluation of changes in cerebral arterial blood volume (C_{CaBV}), and (c) based on the amplitudes of peaks P1 and P2 of ICP pulse waveform ($C_{P1/P2}$).

Results Increase in ICP caused a significant decrease in all compliance estimates ($p < 0.0001$). Time courses of compliance estimators were strongly positively correlated with each other (group-averaged Spearman correlation coefficients: 0.94 [0.88–0.97] for C_{CSF} vs. C_{CaBV}, 0.77 [0.63–0.91] for C_{CSF} vs. $C_{P1/P2}$, and 0.68 [0.48–0.91] for C_{CaBV} vs. $C_{P1/P2}$).

Conclusions Indirect methods, C_{CaBV} and $C_{P1/P2}$, allow for the assessment of relative changes in cerebrospinal compliance and produce results exhibiting good correlation with the direct method of volumetric manipulation. This opens the possibility of monitoring relative changes in compliance continuously.

Keywords Intracranial pressure · Cerebrospinal compliance · Infusion test · Cerebral arterial blood volume · Pulse waveform

Introduction

In adults, the skull is a closed non-distensible box filled with three volume components: brain tissue, cerebral blood, and cerebrospinal fluid (CSF) [16]. According to the Monro–Kellie doctrine, in the long-term—and under normal conditions—increases in the volume of one component are compensated by decreases in the volume of another, maintaining the total volume at an approximately constant level [20]. However, in the short-term scale, considering pulsatile blood flow, for a part of the cardiac cycle, total blood volume increases and then decreases, leaving total volume changes equal to zero [2]. This produces rhythmic instability of the intracranial pressure (ICP) signal, known as 'pulse waveform'. The ability of the cerebrospinal space to accommodate changes in volume is quantified by a parameter called compliance which links changes in volume with corresponding changes in pressure [23]. Low compliance puts the system at risk of disproportionately large increases in ICP for even small increases in intracranial volume, potentially leading to intracranial hypertension [21]. To measure cerebrospinal compliance, external gradual volume addition into the cerebrospinal space is needed, which is a limitation preventing continuous

✉ Agnieszka Kazimierska
agnieszka.kazimierska@pwr.edu.pl

[1] Department of Biomedical Engineering, Faculty of Fundamental Problems of Technology, Wroclaw University of Science and Technology, Wroclaw, Poland

[2] Brain Physics Laboratory, Division of Neurosurgery, Department of Clinical Neurosciences, Addenbrooke's Hospital, University of Cambridge, Cambridge, UK

[3] Institute of Electronic Systems, Faculty of Electronics and Information Technology, Warsaw University of Technology, Warsaw, Poland

[4] Department of Medical Image Processing, CHU Amiens, University of Picardy Jules Verne, Amiens, France

Published online: 14 April 2021

monitoring. We aimed to examine and compare three methods of assessment of cerebrospinal compliance. One is a 'golden standard' based on external volume load, and two others rely on the evaluation of changes related to blood stroke volume over heart period. These two, if they are linked to 'gold standard' compliance, would allow for continuous monitoring in various clinical scenarios, for instance, hydrocephalus ICP monitoring or traumatic head injury (TBI) and subarachnoid haemorrhage neuro-intensive care monitoring.

The infusion study is a type of volume–pressure test based on the injection of additional volume into the cerebrospinal space that allows for the estimation of compensatory parameters, including cerebrospinal compliance, from a mathematical model of CSF circulation [13]. In the present work, we compared compliance estimates obtained with the model of CSF dynamics (the 'gold standard' method) during changes in the mean ICP induced by constant rate infusion of fluid into the CSF space in normal-pressure hydrocephalus (NPH) patients with two other measures: based on the estimation of changes in cerebral blood volume (CBV) in each cardiac cycle and based on the analysis of changes in the ratio of characteristic peaks P1 and P2 of ICP pulse waveform. The study offers new insight into the feasibility of using the P1/P2 ratio and evaluation of changes in CBV as a tool for continuous monitoring of compliance of the cerebrospinal space.

Materials and methods

Data acquisition

Data from patients who underwent infusion studies with simultaneous recording of ICP and cerebral blood flow velocity (CBFV) signals at Addenbrooke's Hospital (Cambridge, UK) between 1993 and 1998 were selected for retrospective analysis in this study. Selection of patients was made on a basis of good quality of ICP pulse waveform and CBFV recording, and only those tests where the shape of the pulse waveform of ICP presented both P1 and P2 peaks were classified as suitable for analysis. Out of the full group of 72 considered recordings, 36 were chosen. Sixteen recordings (22%) were excluded because of rounded ICP pulse waveform that did not allow for the identification of both characteristic peaks, and 20 recordings (28%) were excluded due to insufficient quality of either ICP or CBFV signals. The data were collected as part of routine clinical investigation following diagnosis of NPH. Ethics committee approval to record ICP and CBFV using transcranial Doppler (TCD) ultrasonography was obtained.

The computerized infusion test was performed with two hypodermic needles (25 gauges). One of the needles was used for ICP measurement and connected to a pressure transducer through a saline-filled tube. The second needle was used for infusion and connected to an infusion pump containing a pressure amplifier (Simonsen & Will, Sidcup, UK). The infusion of normal saline into the CSF space was performed at the rate of 1.5 ml/min. The test began with 10 min of baseline recording of ICP before the start of the infusion. Infusion continued until the increase in ICP reached either the plateau phase or the maximum acceptable level of 40 mm Hg, and the recordings were further collected until ICP returned to baseline level. CBFV in the middle cerebral artery was monitored during the test using a TCD unit (Neuroguard; MedaSonics, Fremont, CA, USA) with a 2-MHz probe locked in a stable position using a commercially available fixation system. Twenty-six recordings included also arterial blood pressure (ABP) monitored noninvasively using a photoplethysmographic system (Finapres; Finapres Medical Systems, the Netherlands).

An analogue-to-digital converter (DT 2814; Data Translation, Marlboro, USA) connected to an IBM AT laptop computer (Amstrad ALT 386 SX; Amstrad, Brentwood, UK) was used for the collection of data from the pressure monitors and the TCD system. The signals were sampled at frequency ranging from 30 to 50 Hz using custom software for waveform recording (WREC; W. Zabolotny, Warsaw University of Technology, Warsaw, Poland). An illustrative example of recorded signals is presented in Fig. 1.

Three methods of estimation of cerebrospinal compliance

The relationship between pressure and volume in the intracranial space is described by an exponential function known as the pressure–volume curve, which shows that changes in ICP increase progressively with the mean ICP [29]. Traditionally, measurement of the pressure response requires external manipulation of intracranial volume, such as bolus injection or constant rate infusion [18, 24]. A different approach to compliance estimation relies on the possibility of measuring changes in CBV alongside ICP. However, a method based on magnetic resonance imaging [1], although potentially accurate, is currently only applicable to the evaluation of instantaneous, or 'snapshot', values, and continuous estimation of changes in CBV using TCD recordings of CBFV in large cerebral arteries [19] does not allow for calibration of obtained values due to the unknown cross-sectional area of insonated vessels.

It has also been suggested that information about cerebral compliance may be extracted from the pulse waveform of ICP itself [6]. Three major features commonly used to characterize ICP pulse waveform are peaks P1, P2, and P3 [16]. Although the precise origin of those peaks is not universally agreed upon, the shape of the ICP waveform is believed to arise from

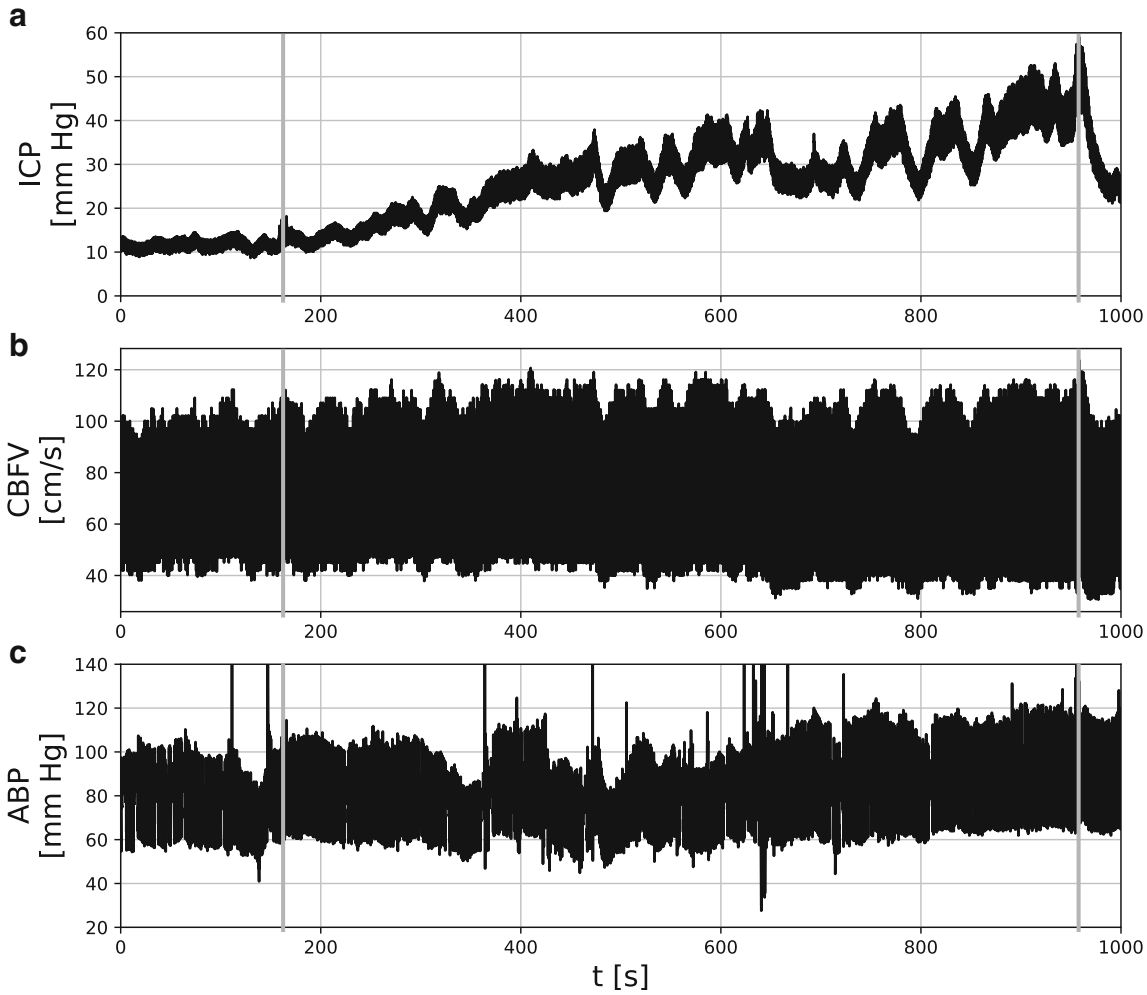

Fig. 1 Illustrative example of signals recorded during the infusion test for a single patient. Grey vertical lines indicate the start and end of constant rate (1.5 ml/min) infusion. **a** Intracranial pressure (ICP). **b** Cerebral blood flow velocity (CBFV). **c** Arterial blood pressure (ABP)

changes in both ABP and CBV [7]. Under normal circumstances, P1 dominates over the other two peaks, resulting in a saw-tooth appearance of the waveform (Fig. 2a). As the mean ICP increases, so does the amplitude of characteristic peaks. However, the change is not uniform, and rising prominence of P2 (Fig. 2b) eventually leads to a rounded or triangular waveform with indistinguishable P1 and P3 [9, 10]. Given the relatively larger changes in the magnitude of the P2 component, it has been suggested that the ratio of peak amplitudes, P1/P2, may provide information about cerebral compliance. Still, despite its potential as a means for long-term monitoring of the state of the cerebrospinal space, very little attention has been devoted to the application of this parameter in the evaluation of cerebral compensatory reserve.

In the present study, three methods were used to obtain estimates of cerebrospinal compliance: (a) based on a model of CSF dynamics, (b) based on evaluation of changes in CBV, and (c) based on the ICP pulse waveform. Assessment of model-based parameters describing CSF dynamics (a) was performed using built-in algorithms of specialized software (ICM+; Cambridge Enterprise, Cambridge, UK). All other analyses were performed using programmes custom-written in Python 3.8.

Model of cerebrospinal fluid dynamics

The first estimate of cerebrospinal compliance (denoted C_{CSF} from 'cerebrospinal fluid dynamics') was obtained from a mathematical model of CSF volume–pressure compensation [12]. Under normal conditions, in the absence of long-term fluctuations in cerebral blood volume, it is assumed that the production of CSF is balanced by its storage and reabsorption. Including external CSF infusion, this can be described by the following relationship:

$$\text{production of CSF} + \text{infusion} = \text{storage of CSF} + \text{reabsorption of CSF} \quad (1)$$

The rate of CSF production is assumed to be constant. $I(t)$ is the rate of the external volume infusion (e.g.,1.5 ml/min in

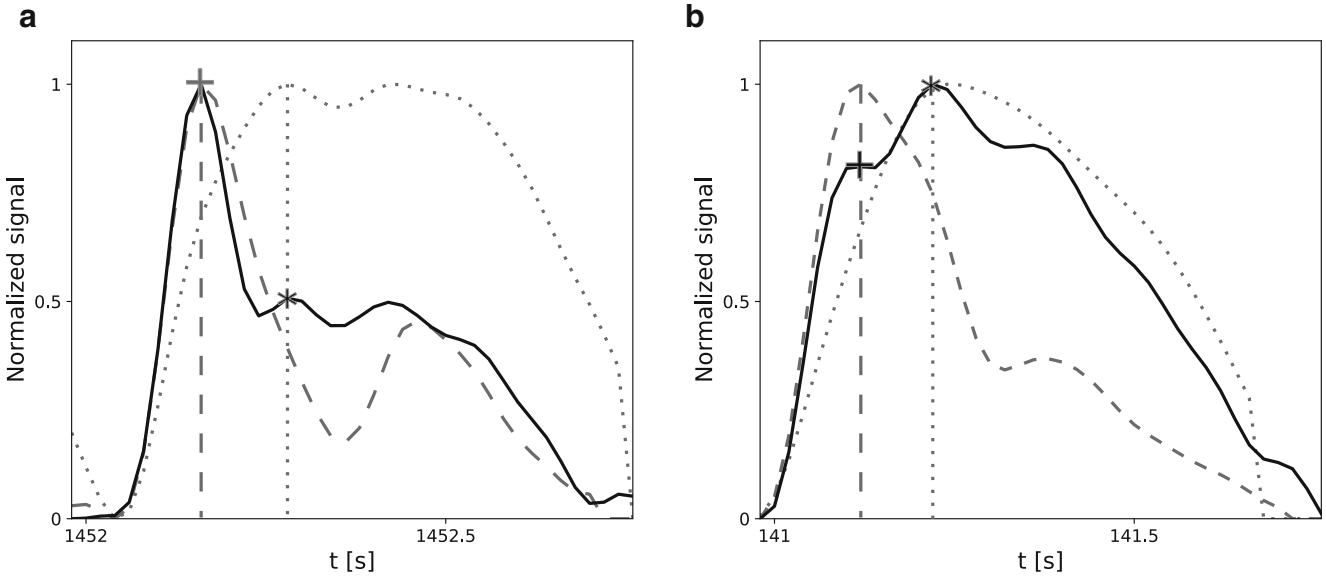

Fig. 2 Illustrative examples of intracranial pressure (ICP) pulse waveforms from two different patients. Location of peaks P1 and P2 is indicated by cross (P1) and star (P2) signs. ICP signals are plotted with solid black lines. Additional signals used in the process of peak detection are plotted as dashed (arterial blood pressure (ABP)) and dotted (cerebral arterial blood volume (CaBV)) lines. All signals are normalized and aligned with regard to pulse onset location. Vertical lines indicate the correlation between the position of peaks P1 and P2 and the local maxima of the ABP (dashed line) and CaBV (dotted line) waveforms, respectively

the present study). The rate of CSF storage (I_s) is proportional to cerebrospinal compliance (C) and depends on the derivative of CSF pressure (P) over time (dP/dt):

$$I_s = C\frac{dP}{dt} \tag{2}$$

Compliance is in turn inversely proportional to the gradient of CSF pressure and reference pressure (P_0):

$$C = \frac{1}{E(P-P_o)} \tag{3}$$

where E is cerebral elasticity. The rate of CSF reabsorption (I_r) is proportional to the gradient between CSF pressure P and pressure in the sagittal sinuses (P_{ss}):

$$I_r = \frac{P-P_{ss}}{R_{out}} \tag{4}$$

where R_{out} describes the resistance to CSF outflow. Relationship (3) is considered valid only above certain pressure level described as 'lower breakpoint pressure'. It is the pressure above which the cerebrospinal pressure–volume curve becomes exponential. Below this pressure, the pressure–volume relationship is linear. The combination of Eqs. (1) to (4) produces the final equation:

$$\frac{1}{E(P-P_0)}\frac{dP}{dt} + \frac{P-P_b}{R_{out}} = I(t) \tag{5}$$

where P_b is the baseline pressure.

Parameters R_{out}, E, and P_0 were estimated for ICP recordings used in this study based on the analytical solution of Eq. (5) for constant rate infusion. E and P_0 were then used to obtain estimates of cerebrospinal compliance over the course of the infusion test from Eq. (3). To maintain cohesion with the other two pulse-by-pulse methods of estimation, the mean ICP over each cardiac cycle was taken as $P(t)$.

Evaluation of pulsatile changes in cerebral blood volume

The second estimate of cerebrospinal compliance (denoted C_{CaBV} from 'cerebral arterial blood volume') was obtained from a mathematical model of cerebral blood circulation using the approach described by Kim et al. [19]. The change in CBV over a single cardiac cycle can be expressed as the difference between arterial inflow (CBF_a) and venous outflow (CBF_v):

$$\Delta CBV(t) = \int_{t_0}^{t}(CBF_a(s) - CBF_v(s))ds \tag{6}$$

where t_0, t are the beginning and end of the cardiac cycle, respectively, and s is the variable of integration. Given the assumption that venous outflow has low pulsatility compared to arterial inflow, the former can be approximated by a constant flow equal to averaged arterial inflow:

$$\Delta C_aBV(t) = \int_{t_0}^{t}(CBF_a(s) - meanCBF_a)ds \tag{7}$$

Furthermore, cerebral arterial blood flow can be expressed as cerebral blood flow velocity multiplied by cross-sectional area of the vessel. Using TCD recordings of CBFV in cerebral arteries and assuming that the cross-sectional area of insonated vessel remains constant, Eq. (7) can be approximated as

$$\Delta C_a BV(n) = S_a \cdot \sum_{i=1}^{n} (CBFV_a(i) - meanCBFV_a)\Delta t(i) \quad (8)$$

where n is the number of samples from the beginning of the cardiac cycle, Δt is the time interval between two consecutive samples, and S_a is the unknown cross-sectional area of insonated vessel.

Based on pulsatile signals CaBV and ICP, cerebrospinal compliance (C) can be estimated as

$$C = \frac{AMP_{C_aBV}}{AMP_{ICP}} \quad (9)$$

where AMP_{CaBV} and AMP_{ICP} are the amplitudes of fundamental components of CaBV and ICP, respectively. However, due to unknown S_a, resulting values of C cannot be calibrated in units of ml per mm Hg.

In this study, CaBV was estimated from Eq. (8) based on CBFV recordings in the middle cerebral artery. Peak-to-peak amplitudes of CaBV and ICP in each cardiac cycle were then used to obtain pulse-by-pulse estimates of cerebrospinal compliance using Eq. (9).

ICP waveform analysis

The third estimate of cerebrospinal compliance (denoted $C_{P1/P2}$ from the P1/P2 amplitude ratio) was based on the analysis of the ICP pulse waveform. Prior to the analysis, ICP, CBFV, and ABP (where available) signals were filtered using a low-pass filter with the cut-off frequency of 10 Hz. Individual pulses in the ICP signal were identified using a modified Scholkmann algorithm [4]; corresponding sections of CBFV and ABP signals were extracted based on pulse onset locations from ICP. For the purpose of peak annotation, each pulse was normalized and linearly detrended, and the three signals were aligned with regard to pulse onset in order to remove the phase shift resulting from distance between measurement sites.

A semi-automated algorithm based on the detection of the local maxima was used for peak identification. The algorithm incorporated information about the local maxima of ABP and CaBV (derived from the CBFV signal using Eq. (8)), taking into account observations from previous studies which showed that P1 is associated with the propagation of the pulse pressure wave through cerebral arteries and usually coincides with the systole of ABP, while P2 is derived from arterial blood volume load and coincides with the maximum of CaBV [8, 15]. In each pulse waveform, the local maxima of ICP corresponding to the position of maxima in ABP and CaBV were selected as candidates for P1 and P2, respectively. In the absence of the ABP signal, the first maximum of the CBFV signal was used instead to identify P1 candidates. Full detection results were reviewed and manually corrected in cases of insufficient detection accuracy, particularly in pathologically rounded waveforms. Pulses with distorted ICP waveform or unidentifiable P1 and P2 were excluded from further analyses. Illustrative examples of ICP pulse waveforms with peak annotations are presented in Fig. 2.

The amplitude of peaks P1 and P2 in each pulse was calculated as the vertical distance to the preceding local minimum identified as pulse onset. Pulse-by-pulse P1/P2 amplitude ratio was then used as a compliance estimate.

Statistical analysis

Statistical analyses were performed using Python 3.8 with the built-in methods included in the SciPy 1.5.0 package. The Shapiro–Wilk test with a significance level of 0.05 was used to assess normality of data distributions. Upon rejection of the normality hypothesis for most of the analysed variables, non-parametric methods were chosen to analyse the relationship between compliance estimates. Time courses of compliance estimates obtained for individual patients with each of the three methods were compared with each other and with ICP using the Spearman correlation coefficient. To reduce the effect of difference in time scales used in compliance estimation, 30-pulse moving averages were used.

In order to compare the ‘high’ and ‘low’ compliance states reflecting the baseline and plateau phase of the infusion test, 1-minute-long fragments of the recordings where all three compliance estimates could be obtained were selected manually. Due to significant distortion of the ICP pulse waveform during baseline in a number of recordings, the initial stage of infusion was selected instead as baseline. Two patients for whom baseline values were not available either due to low quality of the ICP signal or the lower breakpoint pressure limit used in estimation of C_{CSF} were excluded from this part of the analysis. Values averaged over the baseline and plateau phases of the infusion test were compared using the Wilcoxon signed rank test. The same methods were used to determine the significance of changes in amplitude of peaks P1 and P2.

A significance level of 0.05 was assumed in all statistical tests. All group-averaged values are presented as median [first quartile–third quartile].

Results

Patient characteristics

The mean age of the patients was 54 years (range, 27–76 years). The patients showed ventricular dilation marked by increased bicaudate index (mean, 0.27; range, 0.14–0.39), and 14% showed white matter ischemia. Initial ICP in the group was 8.7 [3.8–11.4] mm Hg. Group-averaged R_{out} and elasticity were 12.1 [8.9–15.8] mm Hg/(ml/min) and 0.19 [0.14–0.33] ml^{-1}, respectively.

Amplitude of peaks P1 and P2 during changes in mean ICP

Figure 3 shows an illustrative example of the time courses of P1 and P2 amplitude during infusion test for a single patient. The rise in the mean ICP during infusion resulted in an increase in amplitude of both P1 and P2 ($p < 10^{-6}$), with a visibly larger change for P2: up to 6.22 [4.44–8.35] mm Hg mm Hg from baseline amplitude of 3.52 [2.44–4.49] mm Hg vs. 4.23 [2.7–4.74] mm Hg from baseline of 2.51 [1.44–3.56] mm Hg for P1. While baseline P1/P2 ratio varied between patients, with some patients exhibiting pronounced P1 (P1/P2 > 1) and some already showing increased P2 (P1/P2 < 1), the P1/P2 ratio during plateau fell to around 1 and below. Time courses of both amplitudes were strongly correlated with changes in the mean ICP; however, slightly higher correlation was observed for P2 (group-averaged correlation coefficient equal 0.98 [0.93–0.99] vs. 0.95 [0.82–0.96] for P1). The magnitude of decrease in P1/P2 ratio between baseline and plateau phases was not correlated with either baseline ICP, change in ICP, or elasticity estimated based on the CSF dynamics model. It showed weak although statistically significant, inverse correlation with baseline P1/P2 ratio ($R = -0.38$, $p = 0.03$; Fig. 4), with largest changes observed in cases where baseline ICP waveform contained P1 dominating over P2. Figure 5 shows an example of changes in ICP waveform between baseline and plateau for patients with high and low baseline P1/P2 ratio.

Comparison of three estimates of cerebrospinal compliance

Figure 6 shows an illustrative example of the time courses of compliance estimates obtained with each of the three methods for a single patient. Compliance estimates were positively and statistically significantly ($p < 0.05$) correlated: 0.94 [0.88–0.97] for C_{CSF} vs. C_{CaBV}, 0.77 [0.63–0.91] for C_{CSF} vs. $C_{P1/P2}$, and 0.68 [0.48–0.91] for C_{CaBV} vs. $C_{P1/P2}$. Similarly, compliance estimates C_{CaBV} and $C_{P1/P2}$ showed inverse correlation with the mean ICP, although the correlation was stronger for C_{CaBV} (−0.82 [−0.71–−0.86]) than $C_{P1/P2}$ (−0.71 [−0.46–−0.79]); as C_{CSF} was calculated using the mean ICP itself, this pair of parameters was not compared.

Between baseline and plateau phase of the infusion test, group-averaged mean ICP increased from 13.4 [9.5–16.5] to 22.6 [18.7–28.0] mm Hg. Accordingly, all three methods showed a statistically significant decrease in compliance estimates between baseline and plateau (Wilcoxon signed rank test p-value < 10^{-4}) but with a varying degree of absolute changes, with the largest change observed for the values obtained with the CaBV model (baseline vs. plateau, 1.16 [0.71–1.75] cm/mm Hg vs. 0.72 [0.50–1.00] cm/mm Hg), smaller for the CSF dynamics model (0.67 [0.37–1.16] ml/mm Hg vs.

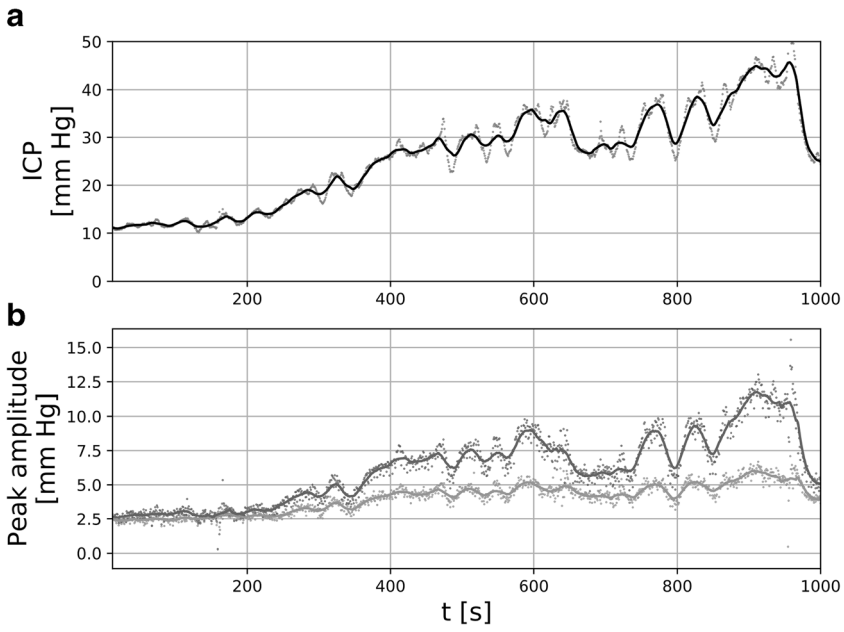

Fig. 3 Illustrative example of time courses of amplitude of peaks P1 and P2 for a single patient. Full pulse-by-pulse time courses are presented as dots while 30-pulse moving averages are presented as solid lines. **a** Mean intracranial pressure (ICP). **b** Amplitude of peaks P1 (light grey symbols) and P2 (dark grey symbols) of the ICP pulse waveform

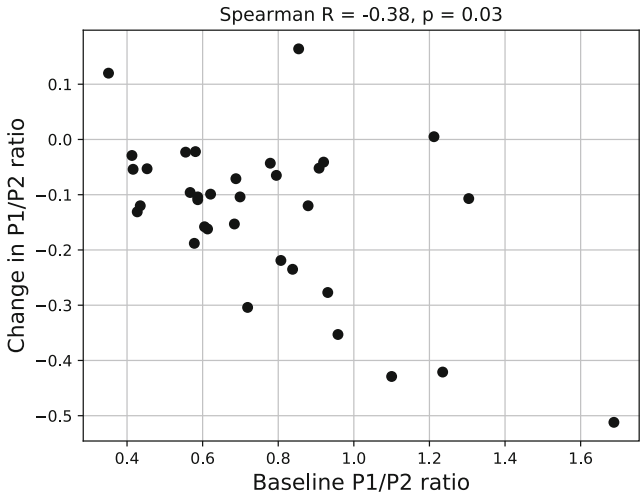

Fig. 4 Relationship between baseline P1/P2 ratio and change in P1/P2 ratio between baseline and plateau phases of infusion test. Values above the scatter plot indicate Spearman correlation coefficient and its *p*-value

0.27 [0.17–0.51] ml/mm Hg)), and smallest for the P1/P2 ratio (0.69 [0.58–0.90] vs. 0.57 [0.46–0.74]). Decrease in compliance estimates relative to baseline was 46.3% [36.5–65.1%], 41.0% [30.8–48.4%], and 16.4% [7.3–27.9%] for the C_{CSF}, C_{CaBV}, and $C_{P1/P2}$ method, respectively.

Discussion

The analysis of ICP pulse waveform, which relies on the assumption that variations in the pulsatile component of ICP reflect the pressure response to volume changes induced by the flow of cerebral blood in each cardiac cycle [2], has been the basis of various indirect methods of compensatory reverse estimation proposed over the years, such as the amplitude–pressure curve [31], high-frequency centroid [28], or RAP index [11]. The P1/P2 ratio, although suggested as a measure of cerebral compliance in the 1980s, so far has not been explored in much detail. A study by Cardoso et al. [6] showed that hyperventilation-induced reduction in the mean ICP is accompanied by a decrease in P2 and relatively small change in P1, while similar reduction caused by head elevation or CSF withdrawal has little to no effect on the shape of the pulse waveform. It was suggested that this would indicate the dependence of P2 on cerebral compliance. Results of the present study are in accordance with previously reported observations [6, 22]. Increase in the mean ICP caused by infusion of volume into the CSF space produced a noticeably larger change in the amplitude of P2 for similar baseline amplitudes of P1 and P2, resulting in decreases in the P1/P2 ratio. Individual time courses of the P1/P2 ratio followed the time courses of compliance estimated based on the CSF dynamics model relatively well, with mean correlation coefficient at the level of 0.75.

The differences in the time courses can be explained by the dependence of C_{CSF} on the trend in the mean ICP, used both in the estimation of elasticity and P_0 and further calculation of compliance, as the P1/P2 ratio is calculated only from the shape of the ICP waveform and on a pulse-by-pulse basis. However, this effect was partially mitigated by the use of moving averages in correlation analysis. The slightly weaker correlation with values of C_{CaBV} may in turn be the effect of inclusion of another signal, CBFV, in the model. Although the extent of

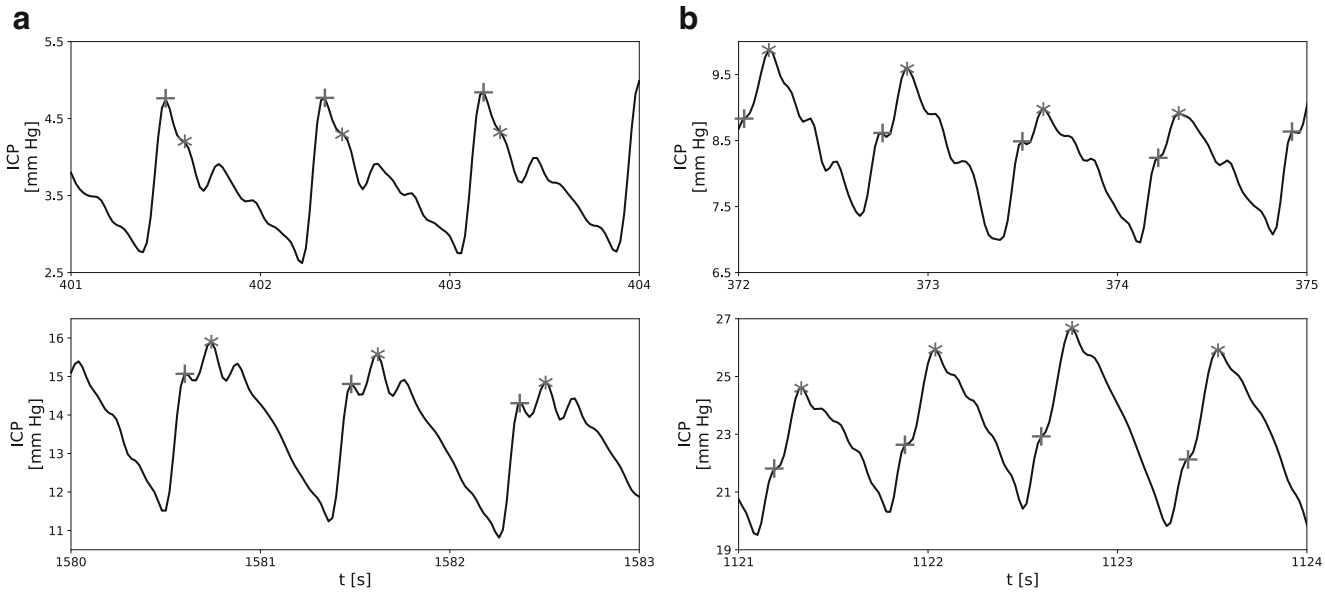

Fig. 5 Illustrative examples of changes in intracranial pressure (ICP) pulse waveform between baseline and plateau phases of infusion test. Baseline and plateau phases are presented in the top and bottom plots, respectively. Location of peaks P1 and P2 is indicated by cross (P1) and star (P2) signs. **a** Patient with high baseline P1/P2 ratio. **b** Patient with low baseline P1/P2 ratio

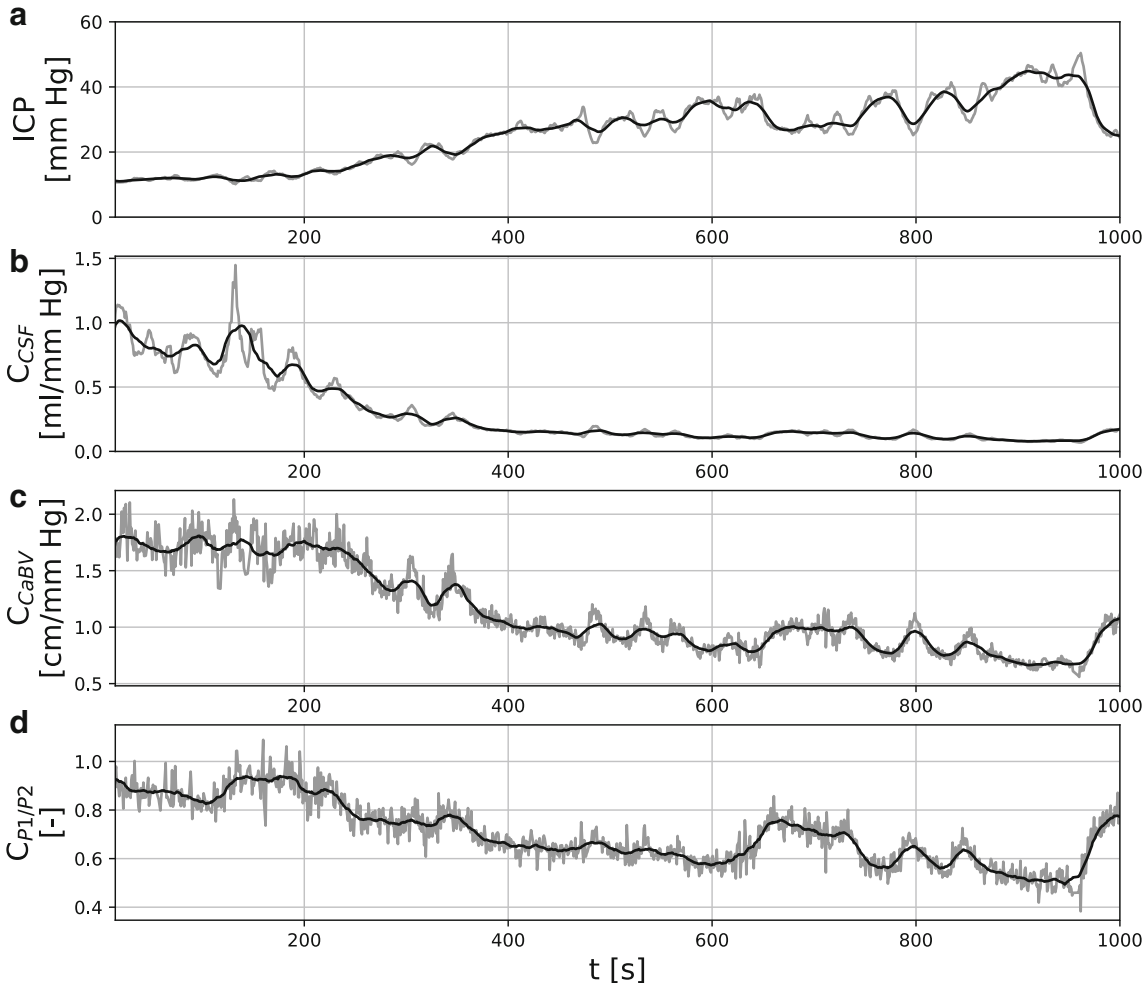

Fig. 6 Illustrative example of time courses of compliance estimates for a single patient. Full pulse-by-pulse time courses are presented as grey lines, while 30-pulse moving averages are presented as black lines. **a** Mean intracranial pressure (ICP). **b**–**d** Compliance estimates obtained with **b** CSF dynamics model (C_{CSF}), **c** cerebral blood volume model (C_{CaBV}) and **d** P1/P2 peak ratio of ICP pulse waveform ($C_{P1/P2}$)

decrease in compliance varied between methods, largely due to varying range of values obtained with each approach, all three methods allowed for statistically significant differentiation between the 'high' and 'low' compliance state associated with baseline and plateau phases of the infusion test. However, as the CaBV and P1/P2 methods examine the ICP pulse waveform resulting from unknown volume load, they are indirect measures that cannot be translated to units of compliance, and straightforward comparison of the values is not feasible. Table 1 outlines major features and limitations of each method of compliance estimation considered in this study.

One advantage of assessing cerebral compliance based on the P1/P2 ratio is the fact that it does not depend on external volumetric manipulation necessary to derive the pressure–volume curve. In principle, the method also does not require any additional signals beside ICP that are needed to estimate changes in CBV. It should be noted, however, that the major difficulty lies in reliable, fully automated detection of peaks P1 and P2. A number of algorithms of often impressive complexity have been proposed over the years for the task of ICP peak identification [5, 14, 17, 30]. Those methods remain a relatively recent development in the continuously advancing field of biomedical signal processing, and despite promising results reported so far, they are yet to find acceptance in the medical community and most importantly validation in large scale trials that would allow for introduction to standard clinical practice. Still, the ICP pulse waveform exhibits large inter- and intrapatient differences, with varying height and prominence of characteristic peaks that may not all be visible even in patients with normal compliance. Whereas the detection of P2 is usually possible despite pathological rounding of the pulse, the detection of P1 becomes unachievable. Incorporation of the ABP signal may improve general peak identification accuracy by allowing for better differentiation between P1 and P2 candidates. Nevertheless, the P1/P2 ratio approach relies heavily on the performance of the underlying detection algorithm, and that in turn requires that the signal is recorded with sufficiently good quality of ICP pulse waveform.

Table 1 Comparison of three methods of cerebrospinal compliance estimation

Characteristic	Method		
	Based on the model of CSF dynamics	Based on the evaluation of CaBV from TCD recordings	Based on the analysis of the P1/P2 ratio of ICP pulse waveform
Units	Absolute [ml/mm Hg]	Express compliance per unit of cross-sectional area of insonated vessel [cm/mm Hg]	Relative changes only [dimensionless]
Assessment	One-off measurement (based on a recording from entire infusion test)	Continuous but limited by positioning of TCD probes	Continuous
Accuracy	Good	Relative changes only	Relative changes only
Availability	Always when access to CSF space is possible	Requires TCD monitoring	Requires that P1 and P2 are detectable in the ICP pulse waveform
Additional requirements	Requires invasive ICP measurement	Requires invasive ICP measurement (with good quality of pulse waveform)	Requires invasive ICP measurement (with good quality of pulse waveform)

In the present study, in order to provide as reliable as possible assessment of the feasibility of using the P1/P2 ratio as an estimate of cerebrospinal compliance, P1 and P2 candidates identified by the algorithm using both the analysis of ICP pulse waveform and its relationship with ABP (where available), CBFV, and CaBV signals were manually reviewed and corrected in cases of insufficient detection accuracy. In order to consider validating this approach in the clinical setting, further work is required to refine the prototype and develop it into a fully automated method of peak identification. Moreover, a comprehensive solution would not only need to be capable of analysing in real time the large variety of ICP pulse waveform shapes encountered in patients with intracranial pathologies but also detecting artefacts and selecting pulses where the peaks, particularly P1, become impossible to distinguish due to the rounding of the waveform and not due to the low quality of the signal.

On the other hand, assuming that the peaks are identified reliably, it is theoretically possible to compare the results between separate measurements and between individuals. A previous study by Fan et al. [15] attempted to use the P2/P1 ratio (as opposed to the P1/P2 ratio used in the present study) as a predictor of disproportionate increases in ICP in TBI patients. Elevated P2 amplitude was signified by P2/P1 ratio equal to or exceeding 0.8. The study showed that the P2/P1 ratio, while not a unique predictor of intracranial hypertension episodes, was significantly higher in the group exhibiting ICP increases. A different study in paediatric hydrocephalus patients confirmed the applicability of the P2/P1 ratio in the identification of intracranial hypertension and assessment of the response to shunting [3]. It should be noted that other works focused on the classification of ICP pulse waveform patterns [14, 26] suggested that decrease in compliance is associated with P2 visibly dominating over P1. A threshold ratio of 0.8 could therefore potentially lead to the inclusion of normal waveforms in the elevated P2 group and influence the results.

Ultimately, the use of the P1/P2 ratio as an indicator of decreased buffering capacity of the cerebrospinal system would require further investigation with regard to the correlation between the value of P1/P2 ratio and the clinical status of the patient, as this measure cannot be directly converted to units of compliance. Given earlier reports on the relationship between measures of compliance and compensatory reserve and outcome in TBI patients [25, 27, 28, 32], combined with the possibility of continuously recording the ICP waveform in modern neuro-critical care units, this avenue of study seems nonetheless to be a promising one.

Limitations

Compliance estimation based on the evaluation of changes in CBV as used in this study is based on a number of assumptions, including constant diameter of insonated vessels during TCD recording. Due to unknown cross-sectional area of the vessels, C_{CaBV} values cannot be calibrated in units of compliance. The same applies to the P1/P2 ratio as changes in the ICP pulse waveform are analysed as a response to unknown blood stroke volume. Consequently, direct comparison between those two methods and the 'gold standard' approach based on the model of CSF dynamics was limited to the correlation between the time courses.

Moreover, this study was performed as a retrospective analysis of infusion test recordings of the ICP signal with the additional requirement of availability of simultaneously collected CBFV. As TCD measurements are not part of routine clinical investigation in NPH patients, the number of available recordings was limited, and given the size of the study group, the results of this study should be regarded as preliminary. Considered recordings were not collected with the explicit purpose of analysing the ICP pulse waveform in detail, which led to a relatively high

percentage of cases (almost 30% of the initial dataset) excluded on the basis of low signal quality.

However, even assuming sufficiently high quality of the signal, the visibility of peaks remains a significant limitation. On the other hand, pulses with indistinguishable P1 due to the rounding of the waveform constitute a separate class of signals. Whereas they do not allow for monitoring of relative changes over time, they could be incorporated as a form of low compliance indicator. This could be a viable solution especially in long-term monitoring aimed at detecting decreases in compensatory reserve, where peak visibility is expected to vary.

Conclusions

Apart from the 'gold standard' method, compliance of the cerebrospinal fluid system may be evaluated using pulse waveform of ICP and TCD recordings of blood flow velocity in the cerebral arteries. The latter two methods agree with the 'gold standard' approach based on volume addition. It potentially opens new perspectives for continuous brain compliance monitoring in various clinical scenarios.

List of abbreviations ABP, Arterial blood pressure [mm Hg]; CBFV, Cerebral blood flow velocity [cm/s]; CBV, Cerebral blood volume [ml]; CSF, Cerebrospinal fluid; ICP, Intracranial pressure [mm Hg]; NPH, Normal-pressure hydrocephalus; TBI, Traumatic brain injury; TCD, Transcranial Doppler

Funding AK received support from the Polish National Agency for Academic Exchange under the International Academic Partnerships programme. ZC, MC, PS and MP were supported by the European Union INTERREG Programme project REVERT 2020. The funders had no role in the study design, data collection and analysis, decision to publish or preparation of the manuscript.

Declarations

Ethical standards Data used in this study were collected with approval from the local ethics committee at Addenbrooke's Hospital, Cambridge, UK, and the study adhered to the tenets of the Declaration of Helsinki.

Conflict of interest MC and PS have a financial interest in part of licencing fee of ICM+ software (https://icmplus.neurosurg.cam.ac.uk) used in this study. Other authors declare that they have no conflict of interest.

References

1. Alperin N, Sivaramakrishnan A, Lichtor T (2005) Magnetic resonance imaging–based measurements of cerebrospinal fluid and blood flow as indicators of intracranial compliance in patients with Chiari malformation. J Neurosurg 103:46–52. https://doi.org/10.3171/jns.2005.103.1.0046
2. Ambarki K, Baledent O, Kongolo G, Bouzerar R, Fall S, Meyer M-E (2007) A new lumped-parameter model of cerebrospinal hydrodynamics during the cardiac cycle in healthy volunteers. IEEE Trans Biomed Eng 54:483–491. https://doi.org/10.1109/TBME.2006.890492
3. Ballestero MFM, Frigieri G, Cabella BCT, de Oliveira SM, de Oliveira RS (2017) Prediction of intracranial hypertension through noninvasive intracranial pressure waveform analysis in pediatric hydrocephalus. Childs Nerv Syst 33:1517–1524. https://doi.org/10.1007/s00381-017-3475-1
4. Bishop SM, Ercole A (2018) Multi-scale peak and trough detection optimised for periodic and quasi-periodic neuroscience data. Acta Nerochirurgica Suppl 126:189–195. https://doi.org/10.1007/978-3-319-65798-1_39
5. Calisto A, Galeano M, Serrano S, Calisto A, Azzerboni B (2013) A new approach for investigating intracranial pressure signal: filtering and morphological features extraction from continuous recording. IEEE Trans Biomed Eng 60:830–837. https://doi.org/10.1109/TBME.2012.2191550
6. Cardoso ER, Rowan JO, Galbraith S (1983) Analysis of the cerebrospinal fluid pulse wave in intracranial pressure. J Neurosurg 59:817–821. https://doi.org/10.3171/jns.1983.59.5.0817
7. Cardoso ER, Reddy K, Bose D (1988) Effect of subarachnoid hemorrhage on intracranial pulse waves in cats. J Neurosurg 69:712–718. https://doi.org/10.3171/jns.1988.69.5.0712
8. Carrera E, Kim D-J, Castellani G, Zweifel C, Czosnyka Z, Kasprowicz M, Smielewski P, Pickard JD, Czosnyka M (2010) What shapes pulse amplitude of intracranial pressure? J Neurotrauma 27:317–324. https://doi.org/10.1089/neu.2009.0951
9. Chopp M, Portnoy HD (1980) Systems analysis of intracranial pressure. Comparison with volume-pressure test and CSF-pulse amplitude analysis. J Neurosurg 53:516–527. https://doi.org/10.3171/jns.1980.53.4.0516
10. Contant CF, Robertson CS, Crouch J, Gopinath SP, Narayan RK, Grossman RG (1995) Intracranial pressure waveform indices in transient and refractory intracranial hypertension. J Neurosci Methods 57:15–25. https://doi.org/10.1016/0165-0270(94)00106-q
11. Czosnyka M, Guazzo E, Whitehouse M, Smielewski P, Czosnyka Z, Kirkpatrick P, Piechnik S, Pickard JD (1996) Significance of intracranial pressure waveform analysis after head injury. Acta Neurochir 138:531–542. https://doi.org/10.1007/BF01411173
12. Czosnyka M, Czosnyka Z, Momjian S, Pickard JD (2004) Cerebrospinal fluid dynamics. Physiol Meas 25:R51–R76. https://doi.org/10.1088/0967-3334/25/5/R01
13. Eklund A, Smielewski P, Chambers I, Alperin N, Malm J, Czosnyka M, Marmarou A (2007) Assessment of cerebrospinal fluid outflow resistance. Med Biol Eng Comput 45:719–735. https://doi.org/10.1007/s11517-007-0199-5
14. Elixmann IM, Hansinger J, Goffin C, Antes S, Radermacher K, Leonhardt S (2012) Single pulse analysis of intracranial pressure for a hydrocephalus implant. Conference Proceedings of the IEEE Engineering in Medicine and Biology Society, In, pp 3939–3942
15. Fan J-Y, Kirkness C, Vicini P, Burr R, Mitchell P (2008) Intracranial pressure waveform morphology and intracranial adaptive capacity. Am J Crit Care 17:545–554
16. Germon K (1988) Interpretation of ICP pulse waves to determine intracerebral compliance. J Neurosci Nurs 20:344–351. https://doi.org/10.1097/01376517-198812000-00004

17. Hu X, Glenn T, Scalzo F, Bergsneider M, Sarkiss C, Vespa P (2010) Intracranial pressure pulse morphological features improved detection of decreased cerebral blood flow. Physiol Meas 31:679–695. https://doi.org/10.1088/0967-3334/31/5/006
18. Katzman R, Hussey F (1970) A simple constant-infusion manometric test for measurement of CSF absorption. I. Rationale and Method. Neurology 20:534–544. https://doi.org/10.1212/wnl.20.6.534
19. Kim D-J, Kasprowicz M, Carrera E, Castellani G, Zweifel C, Lavinio A, Smielewski P, Sutcliffe MPF, Pickard JD, Czosnyka M (2009) The monitoring of relative changes in compartmental compliances of brain. Physiol Meas 30:647–659. https://doi.org/10.1088/0967-3334/30/7/009
20. Kim D-J, Czosnyka Z, Kasprowicz M, Smielewski P, Baledent O, Guerguerian A-M, Pickard JD, Czosnyka M (2012) Continuous monitoring of the Monro-Kellie doctrine: is it possible? J Neurotrauma 29:1354–1363. https://doi.org/10.1089/neu.2011.2018
21. Kirkness CJ, Mitchell PH, Burr RL, March KS, Newell DW (2000) Intracranial pressure waveform analysis: clinical and research implications. J Neurosci Nurs 32:271–277. https://doi.org/10.1097/01376517-200010000-00007
22. Kuramoto S, Moritaka K, Hayashi T, Honda E, Shojima T (1986) Non-invasive measurement in intracranial pressure and analysis of the pulse waveform. Neurol Res 8:93–96. https://doi.org/10.1080/01616412.1986.11739737
23. Marmarou A, Shulman K, LaMorgese J (1975) Compartmental analysis of compliance and outflow resistance of the cerebrospinal fluid system. J Neurosurg 43:523–534. https://doi.org/10.3171/jns.1975.43.5.0523
24. Marmarou A, Shulman K, Rosende R (1978) A nonlinear analysis of the cerebrospinal fluid system and intracranial pressure dynamics. J Neurosurg 48:332–344. https://doi.org/10.3171/jns.1978.48.3.0332
25. Maset AL, Marmarou A, Ward JD, Choi S, Lutz HA, Brooks D, Moulton RJ, DeSalles A, Muizelaar JP, Turner H, Young HF (1987) Pressure-volume index in head injury. J Neurosurg 67:832–840. https://doi.org/10.3171/jns.1987.67.6.0832
26. Nucci CG, De Bonis P, Mangiola A, Santini P, Sciandrone M, Risi A, Anile C (2016) Intracranial pressure wave morphological classification: automated analysis and clinical validation. Acta Neurochir 158:581–588. https://doi.org/10.1007/s00701-015-2672-5
27. Pillai S, Praharaj SS, Rao GSU, Kolluri VRS (2004) Cerebral perfusion pressure management of severe diffuse head injury: effect on brain compliance and intracranial pressure. Neurol India 52:67–71
28. Robertson CS, Narayan RK, Contant CF, Grossman RG, Gokaslan ZL, Pahwa R, Caram P, Bray RS, Sherwood AM (1989) Clinical experience with a continuous monitor of intracranial compliance. J Neurosurg 71:673–680. https://doi.org/10.3171/jns.1989.71.5.0673
29. Ryder HW, Espey FF, Kimbell FD, Penka EJ, Rosenauer A, Podolsky B, Evans JP (1953) The mechanism of the change in cerebrospinal fluid pressure following an induced change in the volume of the fluid space. J Lab Clin Med 41:428–435
30. Scalzo F, Asgari S, Kim S, Bergsneider M, Hu X (2012) Bayesian tracking of intracranial pressure signal morphology. Artif Intell Med 54:115–123. https://doi.org/10.1016/j.artmed.2011.08.007
31. Szewczykowski J, Śliwka S, Kunicki A, Dytko P, Korsak-Śliwka J (1977) A fast method of estimating the elastance of the intracranial system. J Neurosurg 47:19–26. https://doi.org/10.3171/jns.1977.47.1.0019
32. Zeiler FA, Ercole A, Cabeleira M, Beqiri E, Zoerle T, Carbonara M, Stocchetti N, Menon DK, Smielewski P, Czosnyka M, Anke A, Beer R, Bellander BM, Buki A, Chevallard G, Chieregato A, Citerio G, Czeiter E, Depreitere B, Eapen G, Frisvold S, Helbok R, Jankowski S, Kondziella D, Koskinen LO, Meyfroidt G, Moeller K, Nelson D, Piippo-Karjalainen A, Radoi A, Ragauskas A, Raj R, Rhodes J, Rocka S, Rossaint R, Sahuquillo J, Sakowitz O, Stevanovic A, Sundström N, Takala R, Tamosuitis T, Tenovuo O, Vajkoczy P, Vargiolu A, Vilcinis R, Wolf S, Younsi A (2019) Compensatory-reserve-weighted intracranial pressure versus intracranial pressure for outcome association in adult traumatic brain injury: a CENTER-TBI validation study. Acta Neurochir 161:1275–1284. https://doi.org/10.1007/s00701-019-03915-3

End-to-End Automatic Morphological Classification of Intracranial Pressure Pulse Waveforms Using Deep Learning

Cyprian Mataczyński, Agnieszka Kazimierska, Agnieszka Uryga, Małgorzata Burzyńska, Andrzej Rusiecki, and Magdalena Kasprowicz

***Abstract*—Objective. Mean intracranial pressure (ICP) is commonly used in the management of patients with intracranial pathologies. However, the shape of the ICP signal over a single cardiac cycle, called ICP pulse waveform, also contains information on the state of the craniospinal space. In this study we aimed to propose an end-to-end approach to classification of ICP waveforms and assess its potential clinical applicability. Methods. ICP pulse waveforms obtained from long-term ICP recordings of 50 neurointensive care unit (NICU) patients were manually classified into four classes ranging from normal to pathological. An additional class was introduced to simultaneously identify artifacts. Several deep learning models and data representations were evaluated. An independent testing dataset was used to assess the performance of final models. Occurrence of different waveform types was compared with the patients' clinical outcome. Results. Residual Neural Network using 1-D ICP signal as input was identified as the best performing model with accuracy of 93% in the validation and 82% in the testing dataset. Patients with unfavorable outcome exhibited significantly lower incidence of normal waveforms compared to the favorable outcome group even at ICP levels below 20 mm Hg (median [first-third quartile]: 9 [1–36]% vs. 63 [52–88] %, $p = 0.002$). Conclusions. Results of this study confirm the possibility of analyzing ICP pulse waveform morphology in long-term recordings of NICU patients. Proposed approach could potentially be used to provide additional information on the state of patients with intracranial pathologies beyond mean ICP.**

***Index Terms*—Deep neural networks, intracranial pressure, intensive care unit.**

Manuscript received February 11, 2021; revised April 22, 2021 and June 6, 2021; accepted June 6, 2021. Date of publication June 11, 2021; date of current version February 4, 2022. This work was supported by the National Science Centre, Poland under Grant UMO 2019/35/B/ST7/00500. Agnieszka Uryga receives a scholarship from the Foundation for Polish Science. *(Cyprian Mataczyński and Agnieszka Kazimierska contributed equally to this work.) (Corresponding author: Cyprian Mataczynski.)*

Cyprian Mataczyński and Andrzej Rusiecki are with the Department of Computer Engineering, Faculty of Electronics, Wroclaw University of Science and Technology, 50-370 Wroclaw, Poland (e-mail: cyprian.mataczynski@pwr.edu.pl; andrzej.rusiecki@pwr.edu.pl).

Agnieszka Kazimierska, Agnieszka Uryga, and Magdalena Kasprowicz are with the Department of Biomedical Engineering, Faculty of Fundamental Problems of Technology, Wroclaw University of Science and Technology, 50-370 Wroclaw, Poland (e-mail: agnieszka.kazimierska@pwr.edu.pl; agnieszka.uryga@pwr.edu.pl; magdalena.kasprowicz@pwr.edu.pl).

Małgorzata Burzyńska is with the Department of Anaesthesiology and Intensive Care, Wroclaw Medical University, 50-367 Wroclaw, Poland (e-mail: malgorzata.burzynska@umed.wroc.pl).

Digital Object Identifier 10.1109/JBHI.2021.3088629

I. Introduction

INTRACRANIAL pressure (ICP) is frequently monitored in patients with brain pathologies as elevated ICP puts the patient at risk of cerebral ischemia or herniation of structures within the cranial vault. However, the clinical state of the patient cannot be fully characterized by mean ICP alone as the changes in intracranial volume which influence ICP can be buffered to a certain degree [1]. The ability of the craniospinal system to tolerate or compensate for volume increases is quantified by a parameter called 'brain compliance' [2]. As long as the compensatory mechanisms for adapting to increased volume are intact and the compliance of the system is normal, small increases in intracranial volume result in small increases in ICP. When brain compliance is decreased and the compensatory mechanisms are exhausted, small increases in volume lead to disproportionately large increases in ICP. The pressure–volume curve, i.e., the exponential relationship between pressure and volume in the intracranial space, has long been regarded as a potential source of useful information on the state of the craniospinal system [3]. Despite promising results published on that subject, direct measurement of compliance has, however, proven difficult to implement in clinical practice on a larger scale [2].

On the other hand, it has long been known that the ICP signal contains much more information than can be captured by simple mean value [1]. ICP pulse morphology, which refers to the shape of the pressure signal over a single cardiac cycle, is believed to contain indirect information about brain compliance [4]. Under normal conditions, the ICP pulse is characterized by three distinct subpeaks, denoted P1, P2, and P3, arranged in a saw-tooth pattern. As brain compliance decreases and ICP increases, the subpeaks gradually become less pronounced, eventually resulting in a 'rounded' or sinusoidal wave [5]. Rounding of the pulse wave is often observed at elevated ICP levels; however, the rate of changes in pulse morphology varies both across patients and over time [6]. As the patients exhibit decreased compliance at different pressure levels, the analysis of the shape of ICP pulse waveform is key to characterizing the state of the intracranial space.

Due to high variability of the ICP pulse waveform, identification of characteristic peaks is a highly complex task, which in turn requires highly complex algorithms. Several attempts have been made to automatically analyze the changes in ICP pulse waveform based on detection of peaks and notches [7]–[11]. However, in addition to high complexity, limiting their understanding and acceptance in the medical community, those methods often rely on averaged pulses or fail in case of pathologically rounded signals. In recent years, deep learning rose to prominence in the field of biomedical signal processing, including pattern recognition tasks. Deep learning models have been successfully applied to remove artifacts from the ICP signal [12] and to detect ICP elevation [13] but as far as we know, a deep learning approach has never been used for the task of ICP pulse morphology classification not only in terms of valid vs. invalid pulses, but also with separate categories reflecting the changes in the configuration and visibility of characteristic peaks, i.e., the progression from normal, triphasic waveform to a rounded, sinusoidal shape.

Therefore, in this work we aimed to develop an automated method for morphological classification of different shapes of ICP pulse waveforms using deep neural networks. An end-to-end approach was proposed for the purpose of analyzing long-term recordings collected from neurointensive care unit (NICU) patients with intracranial pathologies, comprising stages responsible for single pulse detection, artifact detection, and classification of non-artifactual waveforms. Deep learning models were developed, evaluated, and compared in terms of their accuracy in identifying four types of ICP pulses as well as artifacts in the ICP signal. Additionally, we investigated the link between the occurrence of different morphological types of ICP pulse waveform and treatment outcomes of the patients to assess the potential clinical usefulness of the proposed approach.

II. Related Work

Nucci *et al.* [14] introduced the classification criteria for ICP pulse waveform analysis based on overall shape of the signal, reflecting the changes in the configuration of characteristic peaks of the ICP pulse. The authors used a small neural network with coefficients of radial basis function (RBF) kernel approximation of the ICP signal serving as network input, and reported accuracy of 88.3% in data collected in normal pressure hydrocephalus patients during infusion studies. We attempted to replicate this method but were unable to choose universal RBF midpoints for our dataset that would allow for representation of artifacts as well as valid ICP pulses. We hypothesize that differences in data acquisition and general aim of the system make it unsuitable for our study.

A similar approach to analysis of infusion study recordings was also previously proposed by Elixmann *et al.* [9] who identified five distinct waveform patterns. However, the study used a decision algorithm based on results of peak and notch detection, namely the number, relative height, and distance between subpeaks, to distinguish between waveform types. Various methods have also been presented for the task of binary classification of ICP waveforms into valid pulses versus artifacts, and multi-class classification as investigated in this study could theoretically be considered an extension of the previously proposed binary classification approaches. However, previous studies either also rely on peak identification [8], [10], [15], potentially producing higher number of false positives and false negatives related to difficulty in peak annotation in irregular but otherwise valid waveforms, are not a deep approach [16], or include a number of preprocessing steps that may significantly extend the computation time [12]. Consequently, in this study we propose a new approach taking into account recent developments in the field of deep learning. As we are not aware of any other studies that aimed to classify various pulse waveform patterns (i.e., beyond valid versus artifactual pulses) in long-term recordings obtained from NICU patients using deep neural networks, we compare our proposed model with the approach shown in [12], which was selected as the work with the most similar aim and methodology. However, it should be noted that [12] introduced a procedure for identification of artifacts in physiological signals, and for the purpose of comparison we used a modified version of that model allowing for multi-class instead of binary classification. Furthermore, we extended our analysis by investigating the possible relationship between the occurrence of different shapes of pulse ICP waves and clinical outcome in NICU patients.

III. Methodology

A. Problem Formulation

The aim of this study was to produce an end-to-end approach for detecting and annotating ICP pulse waveforms in long (i.e., lasting upwards of several hours) signals. Specifically, this means an algorithm capable of taking as input a raw, unprocessed recording and producing final results without manual preprocessing or human intervention during computations. The algorithm is therefore comprised of two steps: division of full signals into short pulse waveforms followed by classification of said pulse waveforms into one of five morphological classes: T1 – normal, T2 – potentially pathological, T3 – likely pathological, T4 – pathological, or A+E – artifacts and measurement errors (Figure 1). The classification expands upon criteria proposed previously by Nucci *et al.* [14] for analysis of infusion studies. First four classes reflect the changing relative height and visibility of characteristic subpeaks P1, P2, and P3 of the ICP pulse waveform, with class T1 (normal) representing the saw-tooth shape associated with normal compliance and class T4 (pathological) representing pathologically rounded pulse with unrecognizable peaks. The fifth class (A+E) was introduced to separate artifactual pulses related to loss of signal quality or failure to accurately identify pulse onset points without the need for introducing an additional step of artifact detection.

The problem can be formulated as obtaining a mapping m from full-length ICP signal to a set of tuples containing location and detected class of each of the pulses:

$$m : \mathbb{R}^L \rightarrow (Position, Class)^N$$

where $L \in \mathbb{N}$ is the number of data points in full-length ICP signal, $Position \in \{1, ..L\}$ is the number of data point in the full signal that marks the beginning of the pulse waveform, and

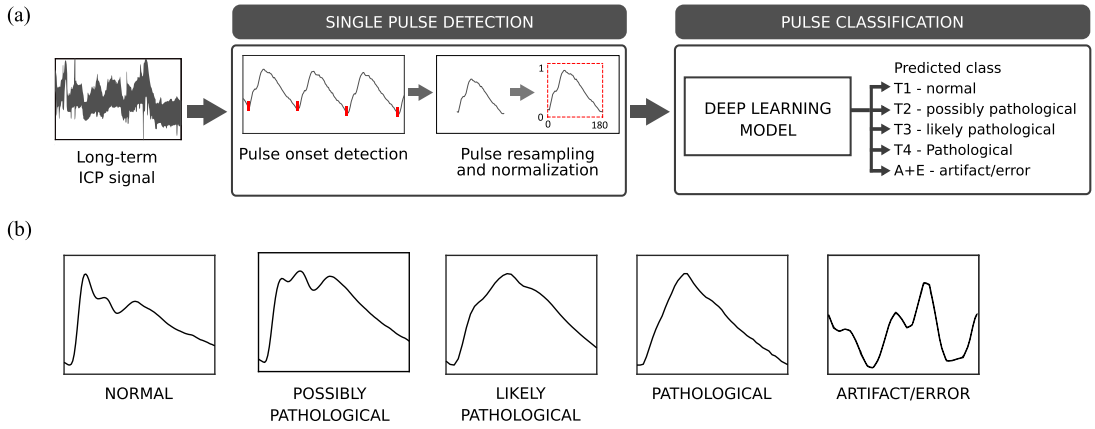

Fig. 1. (a) Overview of proposed approach to pulse waveform classification. (b) Illustrative examples of pulse waveform shapes in each of the five morphological classes.

TABLE I
PATIENT CHARACTERISTICS IN TOTAL GROUP OF 50 PATIENTS. DATA ARE PRESENTED AS N (% OF TOTAL GROUP) OR AS MEDIAN [FIRST-THIRD QUARTILE] UNLESS OTHERWISE INDICATED

Age	Mean: 45 years, Range: 20-85 years
Sex	Male: 32 (64%), Female: 18 (36%)
TBI	39 (78%)
aSAH	11 (22%)
GCS	7 [5-9]
GOS at discharge unfavourable (I-III): 40 (80%), favourable (IV-V): 10 (20%)	
GOS after 3 months unfavourable (I-III): 26 (52%), favourable (IV-V): 24 (48%)	

TABLE II
DETAILED PATIENT CHARACTERISTICS OF TBI PATIENTS (N=39). DATA ARE PRESENTED AS N (% OF TOTAL GROUP) OR AS MEDIAN [FIRST–THIRD QUARTILE]

ICU length of stay [days]	36 [16-63]
Marshall scale	3 [2-5]
Rotterdam scale	4 [3-4]
GOS at discharge	3 [2-3]
GOS after 3 months	3 [1-4]
30-days mortality	4 (10%)
ABP systolic [mm Hg]	105 [101-130]
ABP diastolic [mm Hg]	90 [70-101]
Arterial hypotension	17 (44%)
Pupils	anisocoria: 16 (41%), nonreactive: 13 (33%)
Hematoma	subdural: 13 (33%), epidural: 5 (13%), cerebral: 12 (31%)
Edema/cerebral contusion	23 (59%)
Axonal trauma	5 (13%)
Isolated head trauma	13 (33%)

$Class \in \{T1, T2, T3, T4, A+E\}$ is the morphological class to which that pulse waveform belongs. The end of each pulse is also the beginning of a subsequent pulse, thus only one positional argument is required to unambiguously mark the whole pulse waveform location.

B. Data Collection

Data from 50 patients admitted to the Neurointensive Care Unit (NICU) of University Hospital in Wroclaw, Poland between 2014 and 2019 were chosen for retrospective analysis in this study. The patients were selected out of all patients admitted to the NICU during this period on the basis of availability and acceptable quality of ICP recordings. The study was conducted with approval from the Bioethics committee at the Wroclaw Medical University, Poland (approvals no KB–624/2014 and KB–134/2014). All patients were adults over 18 years of age.

Out of the entire group of 50 patients (see Table I), 39 patients suffered from traumatic brain injury (TBI) and 11 had confirmed aneurysmal subarachnoid haemorrhage (aSAH). TBI and aSAH are two distinct clinical entities with different pathophysiology. However, both conditions are associated with changes in mean ICP and the shape of ICP pulse waveform due to disturbances in the intracranial volume equilibrium, and are subject to the same method of assessing the patient's outcome. As a result, previous studies on ICP pulse morphology combined various groups to increase the number of available recordings [7], [8]. In this study, the aSAH patients were selected in order to introduce a second, independent set of data that would allow for evaluation of final model performance.

TBI patients were treated according to the American Brain Trauma Foundation guidelines applicable at the time of admission [17], [18]. Patients with aSAH were treated according to guidelines from the American Heart Association/American Stroke Association [19]. The patients were classified in the NICU using the Glasgow Coma Scale (GCS). Outcome was assessed at discharge from the hospital and after three months using the Glascow Outcome Scale (GOS), with scores IV-V representing favourable outcome and scores I-III unfavourable outcome. The patient cohort was homogenous with regard to severity of the injury and treatment protocol. Table II presents detailed characteristics of the TBI group used in the assessment

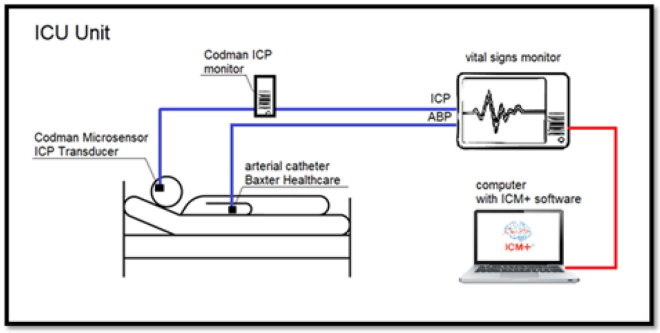

Fig. 2. Measurement setup. Intracranial pressure (ICP) was measured invasively using intraparenchymal probes. Arterial blood pressure (ABP) was measured invasively in the radial or femoral artery using standard monitoring kits. The blood pressure transducer was calibrated at the phlebostatic axis. Signals were monitored using standard bedside vital signs monitors and recorded on a portable computer using ICM+ software with custom-written measurement profile.

of the relationship between classification results and clinical outcome.

ICP was measured invasively using intraparenchymal probes (Codman MicroSensor ICP Transducer, Codman & Shurtleff, Randolph, MA, USA) inserted into the frontal cortex. Although the parenchymal ICP sensor is considered more invasive than the ventricular sensor due to implantation into the brain tissue, it was found to be more accurate, as the calibration and zeroing process only needs to be done once before insertion and the readings are not dependent on the patient's position in relation to the transducer. Arterial blood pressure (ABP) was measured in the radial or femoral artery using standard monitoring kits (Baxter Healthcare, CardioVascular Group, Irvine, CA, USA). The signals were recorded continuously and synchronously (Figure 2) using ICM+ software (Cambridge Enterprise Ltd, Cambridge, U.K.) with sampling frequency ranging from 50 Hz to 300 Hz. The signals were resampled to 50 Hz prior to further analyses in order to reduce computation time, but taking into account the minimum sampling frequency requirements reported in previous experimental studies [20].

The signals were monitored and recorded continuously starting on day 1 or day 2 after admission to the hospital, depending on the date of surgery, and in most cases the day of admission was the same date the injury occurred. Patients were monitored throughout their ICU stay with average recording length of 5 $\pm$ 3 days. In each case the decision to remove the sensor was made by the neurosurgeon and/or intensivist based on medical indications, particularly low mean value and stability of the ICP signal and progressive improvement of the patient's conditions.

C. Single Pulse Detection

A modified Scholkmann algorithm proposed by Bishop and Ercole [21] for analysis of neuroscience data was used for the purpose of single pulse detection. Pulse detection was performed in full long-term signals low-pass filtered with a cutoff frequency of 10 Hz. Individual ICP pulse onset points were defined as local minima preceding the first peak of the waveform occurring at intervals corresponding to the length of the cardiac cycle (i.e., around 1 s).

D. Classification Datasets

The full group of 50 patients was divided between the training/validation and test datasets, with 39 TBI patients assigned to the training and validation datasets and 11 aSAH patients assigned to the test dataset.

In the training and validation datasets, full long-term ICP signals from TBI patients were divided into pulse waveforms (see III-C), and a total of 21 390 pulses were randomly selected from all recordings. In addition to ICP, corresponding ABP pulse waves were selected to aid in manual classification as it has been previously shown that the systolic part of an ABP pulse correlates with the position of peak P1 in ICP pulse waveform and the slopes of ABP and ICP become increasingly divergent with higher waveform type [22]. Each example was then annotated by an expert researcher.

As pulses from the same patient within one waveform class are largely similar and could therefore influence generalization, in order to mitigate the correlation between examples the patients in the training set were selected in such a way that the group did not intersect with the validation dataset. A simple binary genetic algorithm was set up to divide the patients into two sets where one includes 2/3 of the total number of examples in each class and the other includes the remaining pulses. This created a split of the data into the training set consisting of 14 578 pulses and the validation set consisting of 6812 pulses.

The testing dataset was in turn extracted from 11 aSAH patients. Full ICP signals were again divided into pulse waveforms, and 650 pulses were randomly selected from all recordings. The examples were annotated by a panel of three expert researchers using ICP and corresponding ABP pulses. In cases of ambiguous waveform type (particularly signals exhibiting features of two adjacent classes) or disagreement between the experts' assessment, an additional label, the 'possible type', was added. This label was later used in an alternative scoring method (see III-F) and to test multi-label classification described in Appendix II. Inter-rater agreement between the three experts' primary type annotations was tested using Fleiss' kappa test [23] with significance level of 0.05. The reference classification provided by the experts showed statistically significant substantial agreement κ=0.700 (95% CI, 0.672 to 0.728), $p < 0.001$.

As shown in the class distribution in Figure 3, the resulting datasets were not balanced, making the classification task more challenging for smaller models. This issue is discussed in Appendix II.

E. Data Representations

Cubic resampling was used to unify the length of pulses to 180 samples. The pulses were then scaled to an interval between 0 and 1. This step was introduced to test classification based purely on the shape of the waveform and to remove the influence of ICP pulse amplitude which is strongly correlated with mean ICP level and may therefore vary across patients despite comparable pulse morphology. Other types of data representations, such as Fourier

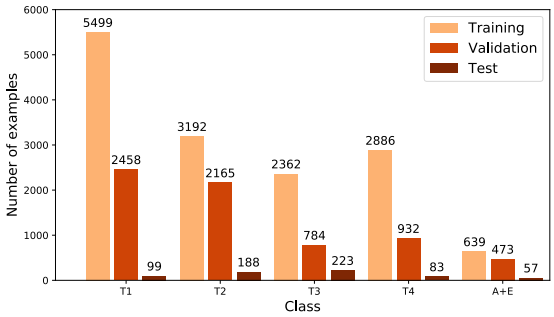

Fig. 3. Number of examples in each dataset.

transform coefficients or time-frequency representations, were investigated but did not result in improved classification accuracy (see Appendix II); therefore, only 1-D vectors of normalized signal samples were used as input. We did, however, investigate the generalization of the models using univariate ICP time series versus multivariate input including both ICP and ABP, as ABP was used in the process of manual annotation.

F. Classification Models and Evaluation

A number of different models were investigated in this study; however, this paper focuses on models identified as best performing: 1-D Residual Neural Network (ResNet) [24], its two variants: dual channel network with joint ICP and ABP signal input or Siamese feature extractors, and Long-Short Term Memory Fully Convolutional Network (LSTM-FCN) [25]. The fully connected neural network was selected as the baseline for our results. Additionally, the approach introduced in [12] was adapted for multi-class classification for the purpose of comparison with proposed models and trained in the same way as the other models.

Convolutional neural networks (CNN) extract information based not only on a single sample but also on the sample's neighborhood, which allows them to easily extract morphological features and therefore makes them a perfect fit for the task of morphological classification. Additionally, in this case, due to the relatively short duration of processed signals (mostly less than 1 s in length), the networks are not required to overcome the challenge of modelling the long term dependencies. ResNets are deep convolutional models that use residual connections between layers for more stable error propagation. The hyperparameters were chosen through the empirical choice method across many conducted experiments with each of the proposed models. The architecture of residual models used in this study is presented in Figure 4, and the hyperparameters of the models are shown in Appendix I.

In addition to changing the number of channels in the first layer of the network, a Siamese architecture with residual feature extractors was tested (however, the latter was not trained on contrastive loss function as in the original paper [26], but through standard procedures). This approach was used to emulate the behaviour of manual annotators who used features of both ICP and ABP signals in the decision making process.

The LSTM-FCN models were employed to test the possibility that long-term dependencies are more relevant to the classification problem. The networks are composed of two different feature extractors, one with a CNN-based architecture, and the second consisting of LSTM cells. Based on the concatenated output of the two arms, an embedding is created and used by the fully connected network to make the final prediction. The main difference from the residual network lies in the LSTM layer which allows the embedding to consider the whole signal, as the memory cell of the LSTM is affected by all previous observations. The structure and hyperparameters of LSTM-FCN models used in this study are presented in Appendix I.

The model proposed in [12] is a combination of a stacked convolutional autoencoder (SCAE) and a CNN that takes 2-D images generated from 1-D signals as input. The first part converts segmented pulse waveforms into representative images. In the original paper, the second part classifies the input as either artifactual or valid. In our reproduction, the SCAE part was preserved while the last layer of the CNN classifier was modified to produce multinomial instead of binary classification.

An universal training loop using Python's PyTorch [27] package was created for all the models to ensure fair comparison of their scoring (see Appendix I). Additionally, taking into account that discrete classification employed in this study does not fully capture the gradual changes in the shape of the ICP pulse waveform cause by physiological and pathophysiological processes, two approaches to evaluation of the models' performance were investigated. First, the standard single-label accuracy score, denoted 'strict accuracy', and the second, denoted 'best accuracy', where the prediction is considered correct in the same cases as strict accuracy but also if it matches the class marked as 'possible' in manual annotations. The second scoring was proposed to test the models' performance in cases where it is acceptable to classify a waveform as belonging to more than one type.

G. Analysis of the Relationship Between Waveform Type and Outcome

Classification results were obtained from long-term recordings of 35 TBI patients. 4 patients from the original TBI group were excluded due to gaps in their recordings that did not have any impact on single ICP pulse classification but could influence the results of the analysis of the relationship between occurrence of ICP waveform types in long-term recordings and the patients' outcome. Each ICP pulse was assigned a waveform type based on classification results and mean ICP calculated as the average over the whole pulse. Classification results were compared with outcome assessed by GOS score after three months. GOS at discharge from the hospital was not used due to significant inequality of favourable versus unfavourable outcome groups that would have prevented reliable statistical analysis. Occurrence of different waveform types was calculated as the percentage of pulses classified as types T1-T4 in the recording. Pulses classified as artifacts (class A+E) were treated as noise and excluded from analysis.

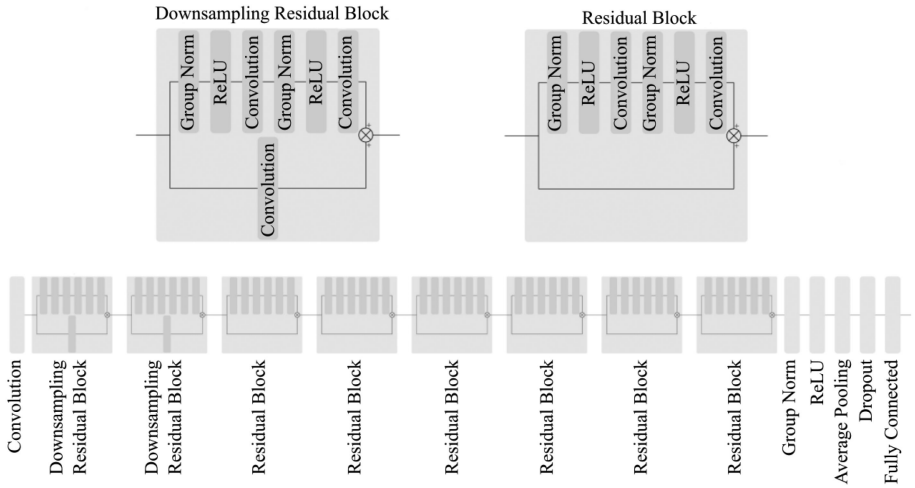

Fig. 4. Model of used Residual Network. The hyperparameters of the model are presented in Appendix I. The convolution nodes are one-dimensional convolution. The initial downsampling residual blocks are used to reduce the size of the processed tensors.

TABLE III
TRAINING RESULTS OF SELECTED MODELS IN DIFFERENT DATASETS. ALL OF THE MODELS SHOWN HERE USED SINGLE LABEL CLASSIFICATION (SEE APPENDIX II)

	N = 650		N = 6812		N = 14578	
	Test		Validation		Train	
Model	Best Accuracy [%]	Strict Accuracy [%]	Best Accuracy [%]	Strict Accuracy [%]	Best Accuracy [%]	Strict Accuracy [%]
Single channel ResNet	**86.00**	**81.85**	**95.17**	**92.95**	98.45	97.78
Siamese ResNet	83.54	80.62	94.10	92.18	98.15	97.24
Dual channel ResNet	81.69	78.92	94.85	92.56	**99.14**	**98.74**
Single channel LSTM-FCN	80.62	77.69	91.18	89.09	95.51	94.17
Reproduction of the approach from [12]	68.00	64.62	81.55	81.44	98.65	98.48
Single channel fully connected (baseline)	72.46	69.38	81.25	74.35	92.59	91.38

In order to separately analyze areas of the recordings where ICP falls within normal or increased range, the range of ICP values was subsequently divided into areas with ICP $<=$ 20 mm Hg and ICP $>$ 20 mm Hg based on moving average (window length: 5 minutes, window shift: 30 s) of single pulse mean ICP values.

Normality of all parameters used in the analyses was tested using the Shapiro-Wilk test. Upon rejection of the normality hypothesis for most of analyzed variables, non-parametric statistical tests were used to assess the difference between groups where applicable. Significance level of 0.05 was used in all analyses. All group-averaged results are presented as median [first-third quartile].

H. Analysis of the Potential for Real-Time Processing

Finally, in order to assess if proposed end-to-end approach could be realistically used to process ICP signals in real-time, an additional experiment was performed using a single illustrative ICP recording and the best performing 1-D ResNet model. In order to simulate real-life continuous measurement, but taking into account that the classification stage requires individual pulses to be detected first, the recording was divided into 10-seconds-long chunks. Each chunk was then processed with the hardware specification described in Appendix I. and the computation times for both single pulse detection and classification step were recorded.

IV. RESULTS

A. Classification Results

Table III shows classification accuracy of selected best performing models compared to baseline accuracy of the fully connected network. The results shown are the best results obtained for each model after empirically choosing hyperparameters through a series of experiments. All three variants of the ResNet model as well as the LSTM-FCN model outperformed the fully connected network, with the highest accuracy registered for the single channel ResNet using only the ICP signal as input. The addition of the ABP signal in the dual channel and Siamese ResNet did not improve classification accuracy in the validation and test datasets, although dual channel ResNet achieved the highest accuracy in the training dataset. As discussed in Appendix II, the single channel ResNet model also retained the highest accuracy in experiments including addition of artificially created A+E examples, weighing of the gradients, or unsupervised pretraining. The modified version of the model proposed in [12] achieved comparable accuracy in the training dataset, but performed considerably worse than the ResNet models in the other two datasets.

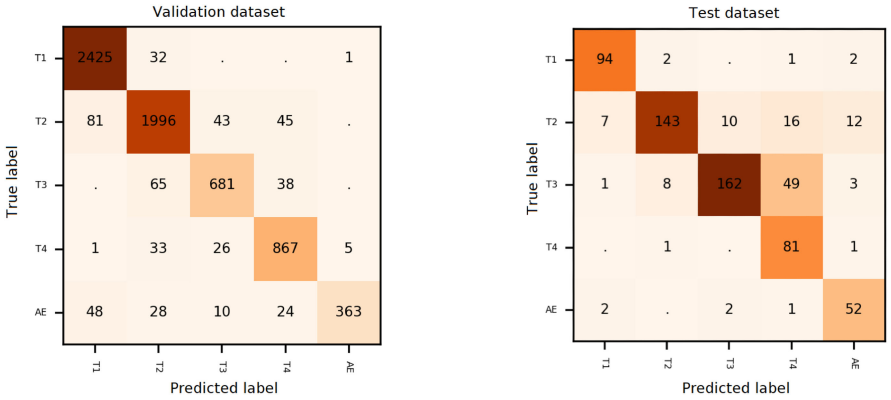

Fig. 5. Confusion matrices for the best performing ResNet model. The number in each tile shows how many examples with given true label were classified as given predicted label.

TABLE IV
DETAILED CLASSIFICATION SCORES FOR THE BEST-PERFORMING RESNET MODEL

Class	T1	T2	T3	T4	A+E
Validation dataset N = *6812*					
Precision	0.95	0.94	0.75	0.76	0.73
Recall	0.95	0.72	0.90	0.93	0.99
F1-score	0.95	0.82	0.82	0.84	0.84
Specificity	0.97	0.88	0.99	0.99	0.99
Test dataset N = *650*					
Precision	0.95	0.76	0.73	0.98	0.91
Recall	0.90	0.93	0.93	0.55	0.74
F1-score	0.93	0.84	0.82	0.70	0.82
Specificity	0.98	0.98	0.97	0.88	0.97

The use of best accuracy scoring instead of standard strict accuracy showed improved classification accuracy of all models (e.g., from 82% to 86% in the test dataset in case of the best performing single channel ResNet). However, attempts at multi-label classification did not boost the models' performance (see Appendix II). The confusion matrices for the single channel ResNet model (Figure 5) show that while in the validation dataset the main problem was presented by the artifact class characterized by the lowest number of examples, in the test dataset the errors primarily concern likely pathological and pathological pulses (types T3 and T4), and detailed classification scores (Table IV) in the latter dataset show that type T4, although characterized by high precision, showed markedly lower recall compared to other types.

B. Relationship Between Waveform Type and Outcome

Mean ICP and ICP waveform type. Figure 6 shows average ICP in each waveform class based on data from patients separated into favourable and unfavourable outcome groups. In both cases, mean ICP increased with progressively more pathological waveform type. There were no statistically significant differences in mean ICP between patients with favourable and unfavourable outcome. However, while mean ICP was slightly lower in the favourable outcome group in waveform type T1, it grew to higher values than in the unfavourable outcome group in more pathological types T3 and T4.

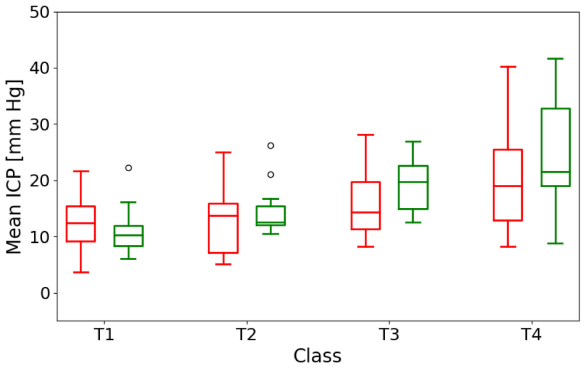

Fig. 6. Mean ICP in each ICP waveform type for unfavourable (red, left-hand side boxes) vs. favourable (green, right-hand side boxes) outcome groups. Central box line: median, box edges: first-third quartile, whiskers: most extreme data points not including outliers (circle signs).

TABLE V
GROUP-AVERAGED OCCURRENCE OF ICP WAVEFORM TYPES FOR UNFAVOURABLE VS. FAVOURABLE OUTCOME GROUPS. RESULTS ARE PRESENTED AS MEDIAN [FIRST-THIRD QUARTILE] WITH P-VALUE OF MANN-WHITNEY U TEST. NS - RESULTS NOT STATISTICALLY SIGNIFICANT

ICP <= 20 mm Hg			
Class	Unfavourable outcome	Favourable outcome	p-value
T1 [%]	9 [1-36]	63 [52-88]	0.002
T2 [%]	27 [6-49]	25 [11-36]	ns
T3 [%]	5 [0-41]	5 [0-8]	ns
T4 [%]	1 [0-38]	0 [0-0]	0.032
ICP > 20 mm Hg			
Class	Unfavourable outcome	Favourable outcome	p-value
T1 [%]	2 [0-9]	34 [10-39]	< 0.001
T2 [%]	11 [2-47]	43 [31-54]	ns
T3 [%]	29 [0-40]	16 [2-26]	ns
T4 [%]	13 [1-46]	2 [0-7]	0.028

Occurrence of different ICP waveform types. Occurrence of different waveform types in the favourable and unfavourable outcome groups is presented in Table V. Significantly higher

incidence of normal waveforms (type T1) as well as lower incidence of pathological waveforms (type T4) was observed in patients with favourable outcome for ICP $<=$ 20 mm Hg. An inverse relationship was found for ICP $>$ 20 mm Hg, with markedly increased occurrence of pathological waveforms in the unfavourable outcome group.

C. Potential for Real-Time Processing

In a subset of 1000 chunks of length equal 10 seconds extracted from an illustrative ICP recording the average processing time was 0.027 [0.026-0.029] seconds per pulse for full analysis, with 0.020 [0.019-0.021] seconds per pulse for single pulse detection and 0.0075 [0.0070-0.0080] seconds per pulse for waveform shape classification.

V. Discussion

In this work we investigated the feasibility of using deep neural networks for identification of different shapes of ICP pulse waveform as well as artifacts in recordings obtained from patients with intracranial pathologies. Given the small number of previous studies on the subject of morphological classification of ICP pulse waveforms, none of which–to the best of our knowledge–used deep learning methods, we tested different approaches to solving this task, including different models, data representations, and training and evaluation methods. The single channel ResNet model using 1-D vector of ICP signal samples as input was identified as the best performing model, achieving best classification accuracy of 86% (82% strict accuracy) in an independent test dataset which suggests good generalization ability. This shows the potential of classifying ICP pulse waveform with relatively high accuracy. Additionally, proposed approach is robust to recordings of different length than the ones used in this study as ICP waveform classification is performed on a single-pulse level and does not require information about the position of each pulse in the full recording. Assessment of changes in pulse morphology over time (i.e., changes in the occurrence of different waveform classes) is secondary to classification of individual pulses and could therefore be performed on both short and long-term measurements.

The fact that neither different models nor alternative data representations resulted in further improvement in accuracy could be to a certain degree explained by the complexity of the task. Despite the use of four distinct non-artifactual classes of ICP pulse waveforms in this study, it should be noted that the changes in brain compliance represented by changes in the shape of the waveform are continuous rather than discrete. As a result, some of the pulses may exhibit the features of more than one class or fall into the 'gray area' between two classes. This phenomenon is visible in the test dataset confusion matrix of the single channel ResNet model where the majority of classification errors occurred between two adjacent classes, and very few were observed between types that are far apart. While this reduces the accuracy score of the models, from the viewpoint of clinical utility this type of mistake is less severe than erroneous classification of normal pulses as pathological or vice versa. Additionally, the increase in best accuracy score compared to strict accuracy shows that a number or errors stems from ambiguity of the waveform shape that has also been noted by the experts performing manual annotations. Taking into account the accuracy recorded in the validation set (best accuracy of over 95% for the single channel ResNet model), we hypothesize that classification accuracy of the model could be further improved by providing a bigger and more balanced training dataset. It should be noted that the test dataset was not only independent from the training and validation datasets, but included data from a different distribution. Whereas all datasets were selected to provide examples of different shapes of ICP pulse waveforms, the test dataset was collected in a separate group of patients for the purpose of assessing the models' real-life applicability. Therefore, despite the decrease in accuracy between the validation and test datasets, the models' performance can still be considered acceptable as the model correctly classifies a large percentage of pulses from a completely different data distribution.

Interestingly, while manual classification of ICP pulses by expert researchers was based on the ICP signal as well as corresponding ABP signal, taking into account previous studies which showed the correlation between the systolic part of ABP and the P1 portion of ICP pulse waveform [22], inclusion of the ABP signal did not improve the performance of deep learning models, and single channel ResNet outperformed both its dual channel and Siamese counterpart. As indicated by comparison of results achieved in the training and test datasets, the use of an additional signal only made the models prone to overfitting. This, however, is an advantage, as a simpler model means that the computation time is lower, and the classification could theoretically be performed in a continuous and real-time manner.

The potential for real-time processing is further supported by the use of an end-to-end pipeline including single pulse detection and artifact exclusion steps in addition to pulse waveform classification. ICP recordings are subject to a variety of disturbances that manifest, for instance, as very short spikes in mean value or waveform deformations. Those disturbances do not carry clinically useful information but instead are related to the purely technical aspect of collecting the signal. It has been shown that artifacts are the cause of a significant number of false positive alarms in the intensive care units [28] and that artifact removal improves the performance of other measures used in TBI management [12]. Various methods of reducing the impact of artifacts on ICP signal analysis have been proposed so far [29], [30], also using deep learning models [12]. Our approach, instead of introducing further algorithms for artifact detection, treats it as part of the classification stage, with artifacts such as noise, sensor calibration signal, or distorted waveforms regarded as an additional class. This also allows for mitigation of false positives resulting from errors in the single pulse detection step. Furthermore, within the proposed pipeline average processing time of a single 10-seconds-long fragment of the ICP signal is over 10 times shorter than the collection time. This shows that the algorithm is capable of effectively working in real-time if adapted to process the full signal in smaller chunks as soon as they are recorded. Given the large difference between computation and collection time, the windows could also be

overlapping, removing the potential problem of losing data from pulses located at the edges of the window that would be discarded by the single pulse detection step.

To investigate the potential clinical applicability of proposed approach we obtained classification results in a group of patients with intracranial pathologies using the best performing single channel ResNet model. In accordance with the relationship described by the pressure–volume curve, higher waveform types were associated with progressively higher mean ICP. While within each waveform class we did not register statistically significant differences in mean ICP between the favourable and unfavourable outcome groups, in the favourable outcome group mean ICP rose more steeply. Given the assumption that higher waveform types are associated with decreasing compliance, this suggests that reduction of the compensatory reserve occurs more slowly in patients with favourable outcome. On the other hand, in patients with unfavourable outcome larger variance of results in each waveform type suggests weaker dependence on mean ICP.

The latter is supported by further analysis of results divided between two ICP levels. The threshold used in this study to separate low and high ICP ranges, 20 mm Hg, reflects the value adopted in the clinical setting as the level above which therapeutic interventions should be introduced [31]. In our study the difference between outcome groups was already pronounced at ICP levels below the threshold for clinical intervention, where the unfavourable outcome group exhibited significantly lower incidence of type 1 waveforms in favour of higher waveform types suggesting diminished compensatory reserve. Over the threshold both groups moved towards higher waveform types, although in terms of average number of pulses of given type the change was more pronounced in patients with unfavourable outcome, with markedly increased incidence of pathological waveforms.

The occurrence of pathologically changed waveforms at lower ICP should be treated as a warning sign, indicating that despite normal levels of pressure the compensatory reserve is already reduced and the system may not be able to tolerate further increases in volume. Evaluation of intracranial compliance based on analysis and interpretation of ICP pulse morphology would also represent a method free of any additional risks to the patient as it is not additionally invasive. In most clinical settings, ICP is monitored continuously (as recommended by The American Brain Trauma Foundation guidelines [18]) and at sufficiently high sampling frequency to analyze the pulse shape in detail. Furthermore, in contrast to imaging techniques, monitoring of cerebral compliance by means of ICP pulse morphology analysis can be performed in a continuous manner during the entire time of ICP monitoring. Consequently, this approach would avoid the frequently cited constraints of the standard method of assessing the full pressure–volume curve by injection or withdrawal of fluid from the cerebrospinal fluid space, namely the intermittent nature of the procedure and the risk of causing potentially dangerous increases in ICP through changes in intracranial volume [32].

It has to be noted, however, that this work was conducted as a retrospective study in a relatively small group of patients and with certain limitations. During identification of ICP ranges in full recordings we did not differentiate patients with continuous hypertensive episodes from patients with high instability of the signal, and information about medical interventions affecting mean ICP was not included. The length of analyzed recordings was not standardized and although patients who did not exhibit values in both ICP ranges were excluded from further analysis, no lower length limit for low/high ICP portion of the recording was used. Furthermore, the parameter used to assess the occurrence of different waveform types, i.e., the percentage of all pulses, was global in nature, derived from all data points in given ICP range, not taking into consideration whether they occurred prior to or following ICP increases or at which stage of monitoring. Finally, outcome as assessed by the Glasgow Outcome Scale provides information on the patient's general condition following injury and is a commonly accepted metric [33], but it does not take into account the diverse character of brain injury in terms of type, severity, and comorbidities. Specifically, it may be influenced by extracranial injury, such as damage to the spinal cord or limb amputations [34] which will not result in changes in ICP pulse morphology, and it assigns a disproportionate weight to physical disability over cognitive impairment [35]. The GOS scores were chosen in this study taking into account its pilot nature in order to assess the potential utility of proposed method of ICP pulse analysis and with full awareness that a more exhaustive description of the patient cohort, with regard to both clinical assessment and other physiological factors, would be required to definitively show the benefits of this approach in the clinical setting.

TABLE VI
HYPERPARAMETERS OF USED RESNET ARCHITECTURE. BOTH RESIDUAL AND DOWNSAMPLING RESIDUAL BLOCKS ARE STANDARD RESIDUAL BLOCKS WITH CONVOLUTIONS OF SIZE 3 AND GROUP NORMALIZATION WITH 32 GROUPS. THE DOWNSAMPLING BLOCK IS ALSO SCALING THE OUTPUT BY ADDING STRIDE 2 TO THE FIRST CONVOLUTION IN THE MAIN BRANCH WHILE ADDING SIZE 1 CONVOLUTION WITH THE SAME NUMBER OF FILTERS AS MAIN BRANCH AND STRIDE 2 TO TO THE SKIP CONNECTION BRANCH

Layer Number	Layer Type	Hyperparameters
1	1D-Convolution	input_channels, filters=64, window=3, stride=1
2 - 3	Downsampling Residual Block	filters=64, stride=2
4 - 9	Residual Block	filters=64, stride=1
10	Group Normalization	groups=32, channels=64
11	ReLU	-
12	Average Pooling	Adaptive to size 1
13	Dropout	0.6 probability during training
14	Fully connected layer	64 inputs, 5 neurons

APPENDIX I

The hyperparameters of used networks are shown in Tables VI (ResNet) and VII (LSTM-FCN). The fully connected baseline network consisted of 3 Layers with 64, 32 and 5 neurons with dropout between layers with small probability of 0.3 and ReLU activation functions between hidden layers. The models were trained on a machine with AMD's Ryzen 9 3900XT (3.8 - 4.7 GHz) 12 core CPU and Nvidia's GeForce RTX 3090 GPU with 24 GB of VRAM. The training was performed for 100

TABLE VII
HYPERPARAMETERS OF USED LSTM-FCN ARCHITECTURE. ARCHITECTURE PRESENTED IN THE TABLE PRODUCES THE EMBEDDING WHICH IS LATER CLASSIFIED BY A FULLY CONNECTED LAYER OF 128 INPUTS AND 5 NEURONS

Convolutional branch		Recurrent branch	
Layer type	Hyperparameters	Layer Type	Hyperparameters
1D-Convolution	channels=32, size=8, stride=1	LSTM	hidden_size = 64, layers=1
Batch Norm.	-		
ReLU	-		
1D-Convolution	channels=64, size=5, stride=1		
Batch Norm.	-		
ReLU	-	Dropout	probability = 0.8
1D-Convolution	channels=64, size=3, stride=1		
Batch Norm.	-		
ReLU	-		
Global Average Pooling	-		

epochs optimized by Stochastic Gradiant Descent with Nesterov momentum of 0.95 and starting learning rate of 0.01. Learning rate was lowered to 0.001 on epoch 33 and to 0.0001 in epoch 66. Training times were relatively short - around 4 minutes for ResNet, 2 minutes for LSTM-FCN and less than 1 minute for fully connected baseline. Single label classfication and multi-label classification experiments used Cross Entropy Loss and Binary Cross Entropy, respectively. Model performance in the validation dataset was logged at the end of every epoch and running averages of the training dataset every 10 steps. Batch training with batch size of 256 was used. The source code used for analysis is available https://github.com/MaczekO/ICP_NN in this GitHub repository.

APPENDIX II

This section describes alternative approaches to the classification task that did result in improved accuracy.

Models. In an attempt to simplify the model without a reduction in accuracy, networks based on Long-Short Term Memory cell (LSTMs) [36], Gated Recurrent Unit cell (GRUs) [37], and Shallow Convolutional Neural Networks (CNNs) [38] with different configurations were tested. However, the results were not satisfactory, showing at least 5% drop in accuracy scores.

Data representations. In an attempt to boost the performance of the models, different representations of ICP pulse waveforms were tested: Fourier transform coefficients, spectrograms, approximation by orthogonal Chebyshev polynomials, empirical mode decomposition, and RBF approximation coefficients. However, none of the methods resulted in an improvement over the 1-D vector of signal samples, and some of them resulted in loss of information during the approximation step, posing an additional challenge for the model.

Secondly, the effect of using the ABP signal as a second input was tested by attaching the signal as a second channel for input to convolutional layers and by training a shared weights model of two univariate feature extractors, then concatenating the results and performing classification through a fully connected network. Neither method, however, improved the classification accuracy.

Addressing class imbalance. To reduce the great imbalance between the A+E class and non-artifactual classes, artificial examples were created by choosing a number of examples from other classes and heavily obscuring them with a composition of multiple sine waves with different parameters, as it is similar to the experimental data. This did not improve the results, possibly due to the fact that the method of creating artificial examples introduced new distribution of data into the class that did not match the distribution of existing examples.

Pretraining. The possibility of pretraining on a large, unannotated dataset was investigated in place of starting the classification from a random distribution of weights. A dataset consisting of all pulses from all patients in the training dataset was created and used in pretraining based on an autoencoder structure with a ResNet model without the classfication layer as encoder and a simple fully connected network as decoder. The pretraining lasted 15 epochs with Adam as optimizer, reducing the MSE of signal reconstruction. Unfreezing of only the classification layer during supervised training resulted in a large reduction in accuracy (66% in the validation dataset), probably due to high correlation between pulses from the same patient. Unfreezing of all layers with trained weights used as a starting point for the network resulted in slightly lower (90.24% in the validation dataset) accuracy than starting from random weights.

Multi-label classification. The multi-label approach was based on the same types of networks but with separate sigmoids instead of softmax as output. The classification threshold was unified to 0.5 for all classes. Binary cross entropy for minimization with SGD optimizer was used. Achieved results were similar to single label classification, e.g., ResNet with multi-label output achieved Jaccard score of 82.44% and best accuracy of 95.59% in the validation dataset.

ResNet depth ablation. In a second attempt to reduce the complexity of the network, additional experiments with ResNet architecture were performed. The change in the number of residual blocks lowered the number of parameters as well the complexity of the network. While this procedure did not affect the results in the validation dataset, it significantly affected the generalization to the test dataset, with removal of blocks resulting in a decrease of 4 to 6% in best accuracy and 3 to 6% in strict accuracy. This indicates that all of the layers are important for the generalization ability of used ResNet.

REFERENCES

[1] K. Germon, "Interpretation of ICP pulse waves to determine intracerebral compliance," *J. Neurosci. Nurs.*, vol. 20, no. 6, pp. 344–351, 1988.
[2] M. Czosnyka and G. Citerio, "Brain compliance: The old story with a new 'et cetera'," *Intensive Care Med.*, vol. 38, no. 6, pp. 925–927, 2012.
[3] A. Marmarou, K. Shulman, and J. Lamorgese, "Compartmental analysis of compliance and outflow resistance of the cerebrospinal fluid system," *J. Neurosurg.*, vol. 43, no. 5, pp. 523–534, 1975.
[4] E. R. Cardoso, J. O. Rowan, and S. Galbraith, "Analysis of the cerebrospinal fluid pulse wave in intracranial pressure," *J. Neurosurg.*, vol. 59, no. 5, pp. 817–821, 1983.
[5] J.-Y. Fan, C. Kirkness, P. Vicini, R. Burr, and P. Mitchell, "Intracranial pressure waveform morphology and intracranial adaptive capacity," *Amer. J. Crit. Care*, vol. 17, no. 6, pp. 545–554, 2008.

[6] T. Ellis, J. McNames, and B. Goldstein, "Residual pulse morphology visualization and analysis in pressure signals," in *Proc. IEEE 27th Annu. Conf. Eng. Med. Biol.*, 2006, pp. 3966–3969.
[7] F. Scalzo, P. Xu, M. Bergsneider, and X. Hu, "Nonlinear regression for sub-peak detection of intracranial pressure signals," in *Proc. 30th Annu. Int. Conf. IEEE Eng. Med. Biol. Soc.*, 2008, pp. 5411–5414.
[8] X. Hu, P. Xu, F. Scalzo, P. Vespa, and M. Bergsneider, "Morphological clustering and analysis of continuous intracranial pressure," *IEEE Trans. Biomed. Eng.*, vol. 56, no. 3, pp. 696–705, Mar. 2009.
[9] I. M. Elixmann, J. Hansinger, C. Goffin, S. Antes, K. Radermacher, and S. Leonhardt, "Single pulse analysis of intracranial pressure for a hydrocephalus implant," in *Proc. Annu. Int. Conf. IEEE Eng. Med. Biol. Soc.*, 2012, pp. 3939–3942.
[10] A. Calisto, M. Galeano, S. Serrano, A. Calisto, and B. Azzerboni, "A new approach for investigating intracranial pressure signal: Filtering and morphological features extraction from continuous recording," *IEEE Trans. Biomed. Eng.*, vol. 60, no. 3, pp. 830–837, Mar. 2013.
[11] H.-J. Lee, E.-J. Jeong, H. Kim, M. Czosnyka, and D.-J. Kim, "Morphological feature extraction from a continuous intracranial pressure pulse via a peak clustering algorithm," *IEEE Trans. Biomed. Eng.*, vol. 63, no. 10, pp. 2169–2176, Oct. 2016.
[12] S.-B. Lee *et al.*, "Artifact removal from neurophysiological signals: Impact on intracranial and arterial pressure monitoring in traumatic brain injury," *J. Neurosurgery*, vol. 132, no. 6, pp. 1952–1960, 2019.
[13] B. Quachtran, R. Hamilton, and F. Scalzo, "Detection of intracranial hypertension using deep learning," in *Proc. 23 rd Int. Conf. Pattern Recognit.*, 2016, pp. 2491–2496.
[14] C. G. Nucci *et al.*, "Intracranial pressure wave morphological classification: Automated analysis and clinical validation," *Acta Neurochirurgica*, vol. 158, no. 3, pp. 581–588, 2016.
[15] P. K. Eide, "A new method for processing of continuous intracranial pressure signals," *Med. Eng. Phys.*, vol. 28, no. 6, pp. 579–587, 2006.
[16] M. Megjhani *et al.*, "An active learning framework for enhancing identification of non-artifactual intracranial pressure waveforms," *Physiol. Meas.*, vol. 40, no. 1, 2019, Art. no. 0 15002.
[17] T. F. Brain *et al.*, "Guidelines for the management of severe traumatic brain injury. introduction," *J. Neurotrauma*, vol. 24, p. S 1, 2007, doi: 10.1089/neu.2007.9999.
[18] N. Carney *et al.*, "Guidelines for the management of severe traumatic brain injury," *Neurosurgery*, vol. 80, no. 1, pp. 6–15, 2017.
[19] E. S. Connolly Jr. *et al.*, "Guidelines for the management of aneurysmal subarachnoid hemorrhage: A guideline for healthcare professionals from the American Heart Association/American Stroke Association," *Stroke*, vol. 43, no. 6, pp. 1711–1737, 2012.
[20] S. Holm and P. K. Eide, "Impact of sampling rate for time domain analysis of continuous intracranial pressure (ICP) signals," *Med. Eng. Phys.*, vol. 31, no. 5, pp. 601–606, 2009.
[21] S. M. Bishop and A. Ercole, "Multi-scale peak and trough detection optimised for periodic and quasi-periodic neuroscience data," in *Proc. Intracranial Press. Neuromonitoring XVI*, 2018, pp. 189–195.
[22] E. Carrera *et al.*, "What shapes pulse amplitude of intracranial pressure?," *J. Neurotrauma*, vol. 27, no. 2, pp. 317–324, 2010.
[23] R. Artstein and M. Poesio, "Inter-coder agreement for computational linguistics," *Comput. Linguistics*, vol. 34, no. 4, pp. 555–596, 2008.
[24] K. He, X. Zhang, S. Ren, and J. Sun, "Deep residual learning for image recognition," in *Proc. IEEE Conf. Comput. Vis. Pattern Recognit.*, 2016, pp. 770–778.
[25] F. Karim, S. Majumdar, H. Darabi, and S. Chen, "LSTM fully convolutional networks for time series classification," *IEEE Access*, vol. 6, pp. 1662–1669, 2017.
[26] R. Hadsell, S. Chopra, and Y. LeCun, "*Dimensionality reduction by learning an invariant mapping*," in *Proc. IEEE Comput. Soc. Conf. Comput. Vis. Pattern Recognit.*, vol. 2, 2006, pp. 1735–1742.
[27] A. Paszke *et al.*, "Pytorch: An imperative style, high-performance deep learning library," in *Advances in Neural Information Processing Systems* vol. 32 (H. H. Wallach, A. Larochelle Beygelzimer, F. d Alché-Buc, E. Fox, and R. Garnett, Eds.), pp. 8024–8035, Curran Associates, Inc., 2019.
[28] M. Imhoff and S. Kuhls, "Alarm algorithms in critical care monitoring," *Anesth. Analg.*, vol. 102, no. 5, pp. 1525–1537, 2006.
[29] M. Feng, L. Y. Loy, F. Zhang, and C. Guan, "Artifact removal for intracranial pressure monitoring signals: A robust solution with signal decomposition," in *Proc. Annu. Int. Conf. IEEE Eng. Med. Biol. Soc.*, 2011, pp. 797–801.
[30] F. Scalzo, D. Liebeskind, and X. Hu, "Reducing false intracranial pressure alarms using morphological waveform features," *IEEE Trans. Biomed. Eng.*, vol. 60, no. 1, pp. 235–239, Jan. 2012.
[31] C. Hawthorne and I. Piper, "Monitoring of intracranial pressure in patients with traumatic brain injury," *Front. Neurol.*, vol. 5, pp. 121–137, 2014.
[32] C. S. Robertson *et al.*, "Clinical experience with a continuous monitor of intracranial compliance," *J. Neurosurg.*, vol. 71, no. 5, pp. 673–680, 1989.
[33] T. McMillan, L. Wilson, J. Ponsford, H. Levin, G. Teasdale, and M. Bond, "The glasgow outcome scale-40 years of application and refinement," *Nature Rev. Neurol.*, vol. 12, no. 8, pp. 477–485, 2016.
[34] N. Stocchetti and E. R. Zanier, "Chronic impact of traumatic brain injury on outcome and quality of life: A narrative review," *Critical Care*, vol. 20, no. 1, pp. 1–10, 2016.
[35] S. I. Anderson, A. M. Housley, P. A. Jones, J. Slattery, and J. D. Miller, "Glasgow outcome scale: An inter-rater reliability study," *Brain Inj.*, vol. 7, no. 4, pp. 309–317, 1993.
[36] S. Hochreiter and J. Schmidhuber, "Long short-term memory," *Neural Comput.*, vol. 9, no. 8, pp. 1735–1780, 1997.
[37] J. Chung, C. Gulcehre, K. Cho, and Y. Bengio, "Empirical evaluation of gated recurrent neural networks on sequence modeling," *NIPS 2014 Workshop Deep Learning*, Dec. 2014, *arXiv:1412.3555*.
[38] Y. LeCun, L. Bottou, Y. Bengio, and P. Haffner, "Gradient-based learning applied to document recognition," *Proc. IEEE*, vol. 86, no. 11, pp. 2278–2324, Nov. 1998.

2021 43rd Annual International Conference of the
IEEE Engineering in Medicine & Biology Society (EMBC)
Oct 31 - Nov 4, 2021. Virtual Conference

2021 43rd Annual International Conference of the IEEE Engineering in Medicine & Biology Society (EMBC) | 978-1-7281-1179-7/21/$31.00 ©2021 IEEE | DOI: 10.1109/EMBC46164.2021.9630516

Analysis of the Shape of Intracranial Pressure Pulse Waveform in Traumatic Brain Injury Patients

Agnieszka Kazimierska[1], Agnieszka Uryga [1], Cyprian Mataczyński[2], Małgorzata Burzyńska[3], Arkadiusz Ziółkowski[1], Andrzej Rusiecki[2], and Magdalena Kasprowicz[1]

***Abstract*— Intracranial pressure (ICP) pulse waveform, i.e., the shape of the ICP signal over a single cardiac cycle, is regarded as a potential source of information about intracranial compliance. In this study we aimed to compare the results of automatic classification of ICP pulse shapes on a scale from normal to pathological with other ICP pulse–derived metrics. Additionally, identification of artifacts was performed simultaneously with pulse classification to assess the effect of artifact removal on the results. Data from 35 traumatic brain injury (TBI) patients were analyzed retrospectively in terms of dominant waveform shape, mean ICP, mean amplitude of ICP (AmpICP), mean index of compensatory reserve (RAP index), and their association with the patient's clinical outcome. Our results show that patients with poor outcome exhibit more pathological waveform shape than patients with good outcome. More pathological ICP pulse shape is associated with higher mean ICP, mean AmpICP, and RAP.**

***Clinical relevance*— In the clinical setting, ICP pulse waveform analysis could potentially be used to complement the commonly monitored mean ICP and improve the assessment of intracranial compliance in TBI patients. Artifact removal from the ICP signal could reduce the frequency of false positive detection of clinically adverse events.**

I. INTRODUCTION

Traumatic brain injury (TBI) is considered an important public health concern because of its high incidence and significant socioeconomic costs [1]. In the clinical setting, monitoring of mean intracranial pressure (ICP) is often used in the management of TBI patients due to the association between increases in ICP and higher mortality and worse outcome [2]. However, pressure (P) and volume (V) in the intracranial space are nonlinearly related (mathematically modelled as an exponential P-V curve), and a reduction in brain compliance (i.e., the cerebrospinal system's ability to compensate changes in volume without potentially threatening increases in ICP) may occur before a rise in mean ICP is detected [3].

Various studies have been conducted to develop tools for the assessment of intracranial compliance. A number of such studies included the analysis of ICP pulse waveform, i.e., the ICP signal over a single cardiac cycle. Notably, there have been attempts to derive that information from changes in the amplitude of the ICP pulse (AmpICP) and its relationship with changes in the mean value [4], [5] or from changes in the configuration of peaks and notches of ICP pulse contour [6], [7]. The RAP index [5], which is the correlation coefficient between changes in mean ICP and AmpICP, is a clinically accepted method of assessing cerebral compensatory reserve that provides an estimation of the patient's position along the P-V curve. However, peak detection methods proposed so far are yet to gain widespread clinical application. More recently, a different approach was suggested, which is based on classification of different shapes of the ICP pulse waveform using a neural network [8] instead of relying on the results of peak identification. In this work we aimed to compare the results of pulse waveform classification using a previously developed deep learning model with other metrics used to describe TBI patients and to assess the possible relationship between ICP pulse type and the patients' outcome.

II. MATERIALS AND METHODS

A. Data collection

This study was performed as a retrospective single-center trial at Wroclaw University Hospital (Wroclaw, Poland) with approval from the local Ethics Committee (approval no. KB-624/2014) and in adherence to the Declaration of Helsinki. 35 patients suffering from TBI were selected for analysis. All patients were treated according to guidelines applicable at the time of admission [9]. The study group was homogenous with regard to severity of the injury and treatment protocol. The patients' condition was assessed using the Glasgow Coma Scale (GCS), Marshall scale, and Rotterdam scale. The patients' outcome was assessed using the Glasgow Outcome Scale (GOS) at 3 months after discharge from the hospital, with poor outcome represented by scores I–III and good outcome by scores IV–V.

ICP was measured invasively using an intraparenchymal sensor (Codman MicroSensor ICP Transducer, Codman & Shurtleff, MA, USA) inserted into the frontal cortex. The

*Research supported by the National Science Centre, Poland (grant no. UMO-2019/35/B/ST7/00500). A. Uryga is supported by the Foundation for Polish Science. The funders had no role in study design or preparation of this submission.

[1]A. Kazimierska (corresponding author; phone: +48 71 320 46 65; agnieszka.kazimierska@pwr.edu.pl), A. Uryga, A. Ziółkowski, and M. Kasprowicz are with the Department of Biomedical Engineering, Wroclaw University of Science and Technology, 27 Wybrzeże Wyspiańskiego street, 50-370 Wroclaw, Poland. agnieszka.uryga@pwr.edu.pl, arkadiusz.ziolkowski@pwr.edu.pl, magdalena.kasprowicz@pwr.edu.pl

[2]C. Mataczyński and A. Rusiecki are with the Department of Computer Engineering, Wroclaw University of Science and Technology, 27 Wybrzeże Wyspiańskiego street, 50-370 Wroclaw, Poland. cyprian.mataczyński@pwr.edu.pl, andrzej.rusiecki@pwr.edu.pl

[3]M. Burzyńska is with the Department of Anaesthesiology and Intensive Care, Wroclaw Medical University, 213 Borowska street, 50-556 Wroclaw, Poland. malgorzata.burzynska@umed.wroc.pl

signal was recorded with sampling frequency of 200 Hz using ICM+ software (Cambridge Enterprise Ltd, Cambridge, UK). The patients were monitored continuously, starting in day 1 or day 2 after admission to the hospital, depending on the date of surgery. On average, the patients were monitored for 5 $\pm$ 3 days.

B. Signal analysis and ICP pulse waveform classification

All analyses were performed using programs custom written in Python 3.8 with PyTorch package. A residual neural network (ResNet) model using 1-D vector of signal samples (standardized to an interval between 0 and 1 and resampled to uniform length of 180 samples) was trained to classify ICP pulse waveforms into four morphological classes: 1– normal, 2 – possibly pathological, 3 – likely pathological, 4 – pathological, reflecting the changes in the configuration and visibility of characteristic peaks P1, P2, and P3 of the waveform (Fig. 1) [8]. An additional class (A+E) was introduced to identify invalid pulses in the signal, such as artifacts or errors in pulse onset detection. Pulse detection was performed using modified Scholkmann algorithm [10]. The model was trained using 23252 waveforms (divided into training and validation datasets of 17011 and 6241 pulses, respectively) randomly selected from full recordings of TBI patients and manually classified by an expert researcher. All waveforms from the same patient were assigned to only one of the datasets to prevent correlation between datasets that could limit the model's generalization ability.

The model was then tested in an independent dataset of 650 pulses extracted from 11 aneurysmal subarachnoid hemorrhage patients and manually classified by a panel of three experts (who showed significant agreement as tested by Fleiss kappa test, κ=0.700 (95% CI: 0.672 to 0.728), $p < 0.001$) to ensure its applicability to patient cohorts with different data distributions. In cases with waveform type at the border between two classes two labels were allowed, and during assessment of classification accuracy the label produced by the model was considered correct if it matched either of the two. A detailed description of model development and evaluation methodology is presented in our earlier paper [11].

Classification results were obtained for all pulses in the full recordings of TBI patients using the ResNet model with each patient characterized by dominant pulse type (i.e., the pulse type occurring most frequently in the whole recording with pulses classified as artifacts excluded from analysis). The long-term recordings were also used to obtain RAP index [5] with AmpICP calculated as the amplitude of the fundamental component of the ICP signal in range 0.6–1.8 Hz using Fast Fourier Transform. The interpretation of the RAP index is as follows: values around 0 indicate good compensatory reserve whereas values increasing to +1 indicate poor compensatory reserve; negative values are associated with cessation of blood flow due to the collapse of cerebral arterial bed at very high ICP [12]. Mean ICP and mean AmpICP were calculated in 10-second-long windows and the correlation coefficient between them was calculated in 5-minute-long windows shifted every 10 seconds. The calculations were performed for each raw recording and for modified recordings where the pulses identified by the model as artifacts were removed. Finally, episodes of mean ICP exceeding 20 mm Hg and episodes of RAP exceeding 0.6 (with minimum length of each episode no less than 5 minutes) were identified in each recording before and after artifact removal. The thresholds reflect values used in clinical practice to identify intracranial hypertension [9] and reduced compensatory reserve [13], respectively. Total duration of all identified episodes was analyzed as well as the number of individual episodes and mean duration of a single episode.

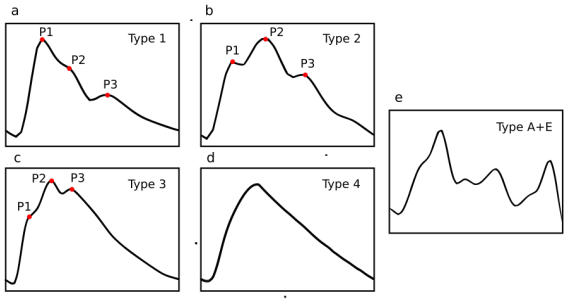

Fig. 1. Illustrative examples of ICP pulse waveform shapes in each class: a) 1 – normal, b) 2 – possibly pathological, c) 3 – likely pathological, d) 4 – pathological, e) A+E – artifact or error.

C. Statistical analysis

Statistical analysis was performed using Statistica software (v13.1, Tibco, Palo Alto, CA, USA). Statistical significance level of 0.05 was assumed in all analyses. Data distributions were tested for normality using the Kolmogorov-Smirnov test with Lillefors correction. Difference between two independent outcome groups was assessed using Mann-Whitney U test and difference between metrics derived from recordings before and after artifact removal (i.e., dependent variables) using Wilcoxon singed rank test. The Fisher-Freeman-Halton exact test of independence was used to determine the association between two categorical variables (outcome vs. dominant pulse waveform type) with 2x4 contingency table, where the effect size was assessed using V Cramer's coefficient. The relationships between pulse type and mean ICP, mean AmpICP, and mean RAP averaged over the whole recording were calculated using multiple linear or linearized regression analysis with subjects treated as categorical factors using dummy variables (with respect to the inter-subject variability) and using partial coefficient (Rp) between analyzed variables. All results are presented as median $\pm$ interquartile range unless otherwise indicated.

III. RESULTS

A. Patient characteristics

The study group consisted of 26 men and 9 women with median age of 38 $\pm$ 29 years. All patients had comparable GCS score with median 6 $\pm$ 4. Detailed patient characteristics are presented in Table I.

TABLE I

PATIENT CHARACTERISTICS

Clinical feature	**Number of patients / Value** total group n = 35 (100%)
GCS on admission n (%)	**3-8:** 30 (86%), **9-12:** 3 (8%), **13-15:** 2 (6%)
Marshall score median ± IQR	3 ± 3
Rotterdam score median ± IQR	4 ± 1
30-days mortality n (%)	4 (10%)
GOS (3 months) n (%)	**I-III:** 20 (57%), **IV-V:** 15 (43%)

B. Classification results

The ResNet model achieved classification accuracy of 95% in the validation dataset and 81% in the independent test dataset. Detailed scores for each pulse type are presented in Table II.

TABLE II

RESNET MODEL PERFORMANCE

	Validation dataset n = 6241		**Test dataset** n = 650	
Pulse type	**Precision**	**Recall**	**Precision**	**Recall**
1	0.97	0.96	0.86	0.93
2	0.90	0.94	0.71	0.92
3	0.89	0.87	0.71	0.95
4	0.85	0.91	0.84	0.57
A+E	0.99	0.92	0.98	0.46

C. Relationship between outcome, ICP pulse type, and other metrics

There were no statistically significant differences in mean ICP, mean AmpICP, or mean RAP between good and poor outcome groups (see Table III). Dominant ICP pulse type was significantly lower (Z = 2.93, p = 0.003) in the good outcome group (1.0 ± 1.0) compared to the poor outcome group (2.0 ± 2.0). Additionally, there was a significant association between ICP pulse type and the following parameters: mean ICP (Rp = 0.63, $p < 0.001$), mean AmpICP (Rp = 0.61, $p < 0.001$), and mean RAP (Rp = 0.26, p = 0.004), as presented in Fig. 2.

Dominant ICP pulse type (see Fig. 3) was significantly associated with outcome: $\chi^2(3) = 10.11$, p = 0.011, with V Cramer's coefficient of 0.56 indicating a strong effect of this relationship. Patients in the good outcome group frequently exhibited dominant ICP pulse type 1 (73.3% of patients) and rarely types 3 or 4 (7.3% and 0.0%, respectively). On the other hand, a significant number of patients with poor outcome exhibited pulse types 3 (15.0%) and 4 (30.0%).

TABLE III

MEAN ICP, AMPICP, RAP INDEX AND DOMINANT ICP PULSE TYPE FOR PATIENTS WITH POOR AND GOOD OUTCOME. NS - RESULT NOT STATISTICALLY SIGNIFICANT

GOS after 3 months	**Poor outcome** n = 20	**Good outcome** n = 15	***p***
ICP [mm Hg]	13.88 ± 5.69	12.31 ± 4.52	ns
AmpICP [mm Hg]	1.15 ± 0.74	0.87 ± 0.54	ns
RAP [a.u.]	0.32 ± 0.23	0.46 ± 0.27	ns
Dominant pulse type	2.0 ± 2.0	1.0 ± 1.0	0.003

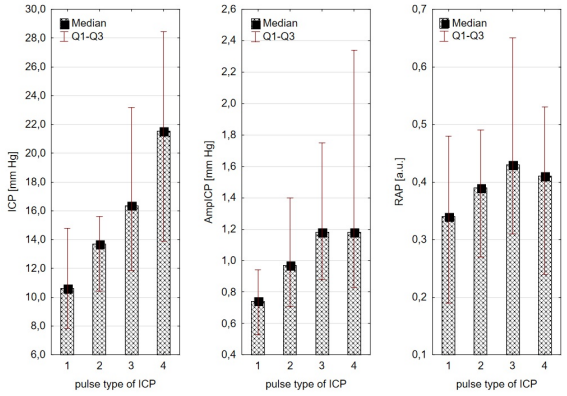

Fig. 2. The relationship between dominant ICP pulse type and mean ICP (left), mean AmpICP (middle), and RAP index (right).

D. Effect of artifact removal

For episodes of RAP > 0.6, artifact removal resulted in a statistically significant decrease in the total duration of the episodes (from 29.7 ± 37.6 hours to 25.3 ± 38.2 hours, $p << 0.001$) and in the number of individual episodes (from 141 ± 135 to 125 ± 156, $p < 0.001$). For episodes of intracranial hypertension (ICP > 20 mm Hg), artifact removal resulted in a decrease in the total duration of the episodes (from 174 ± 804 minutes to 160 ± 750 minutes, p = 0.006).

IV. DISCUSSION

In this work we aimed to use a deep learning model to classify different shapes of ICP pulse waveforms and compare them with other ICP pulse–derived indices in order to further explore the meaning of ICP pulse morphology.

Our results show that in TBI patients dominant ICP pulse type is associated with the patients' outcome. Patients in the good outcome group more frequently exhibit normal waveforms (type 1) with dominant peak P1. In the poor outcome group the number of normal waveforms decreases in favor of pathologically changed pulses, particularly rounded pulses with no identifiable peaks (type 4). In the clinical setting, ICP–guided management mostly relies on a set threshold for mean ICP above which therapeutic interventions should be introduced [15]. The application of a general

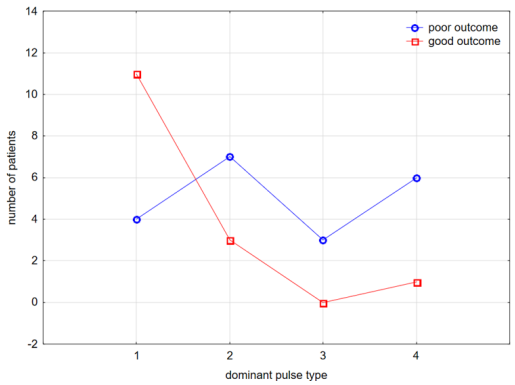

Fig. 3. The interaction between dominant ICP pulse type and the number of patients with poor or good outcome.

threshold in all TBI patients remains controversial [16], and attention has been called to the fact that the relationship between the state of the craniospinal system and mean ICP is not straightforward [3]. Accordingly, our results show that despite comparable mean ICP, the poor and good outcome groups show differences in dominant pulse type, and pulse type is the only parameter whose changes reach statistical significance when compared against outcome. Furthermore, ICP pulse types are significantly correlated with both ICP and AmpICP, reflecting the trends expressed by the pressure–volume and amplitude–pressure curves. Statistically significant but weak correlation between ICP pulse shape and RAP index may be explained by their different interpretation, as ICP pulse shape is more related to intracranial compliance while RAP provides information on the patient's position on the P-V curve. We also found that identification of artifacts simultaneously with the classification of valid pulses changes the total duration of detected episodes of increased ICP and RAP, which is in line with previous studies highlighting the role of artifacts in generating false alarms in the clinical setting [17].

Presented observations are based on the results of a preliminary study conducted in a small patient cohort and with a simple neural network model. Performance of the model can potentially be further improved by providing a more balanced training and validation dataset or by introducing modifications to the classification criteria which in their current form were derived from patients with a different type of intracranial pathology.

V. CONCLUSION

Analysis of brain compliance by means of automatic ICP pulse shape classification is a promising approach to continuous monitoring of the state of the compensatory reserve that could be used in patients with intracranial pathologies alongside standard mean ICP measurement and improve the assessment of the state of the intracranial space. Results of this study suggest an association between dominant ICP waveform type and the clinical outcome of TBI patients. Clinical significance of proposed approach should be confirmed in a larger set of patients.

REFERENCES

[1] M. C. Dewan, A. Rattani, S. Gupta, R. E. Baticulon, Y. Hung, M. Punchak, A. Agrawal, A. O. Adeleye, M. G. Shrime, A. M. Rubiano, J. V. Rosenfeld, and K. B. Park, "Estimating the global incidence of traumatic brain injury," J. Neurosurg., vol. 130, no. 4, pp. 1080–1097, Apr. 2019, doi: 10.3171/2017.10.JNS17352.

[2] S. Badri, J. Chen, J. Barber, N. R. Temkin, S. S. Dikmen, R. M. Chesnut, S. Deem, N. D. Yanez, and M. M. Treggiari, "Mortality and long-term functional outcome associated with intracranial pressure after traumatic brain injury," Intensive Care Med., vol. 38, no. 11, pp. 1800–1809, Nov. 2012, doi: 10.1007/s00134-012-2655-4.

[3] T. Heldt, T. Zoerle, D. Teichmann, and N. Stocchetti, "Intracranial pressure and intracranial elastance monitoring in neurocritical care," Annu. Rev. Biomed. Eng., vol. 21, pp. 523–551, June 2019, doi: 10.1146/annurev-bioeng-060418-052257.

[4] J. Szewczykowski, S. Sliwka, A. Kunicki, P. Dytko, and J. Korsak-Sliwka, "A fast method of estimating the elastance of the intracranial system," J. Neurosurg., vol. 47, no. 1, pp. 19–26, July 1977, doi: 10.3171/jns.1977.47.1.0019.

[5] M. Czosnyka, E. Guazzo, M. Whitehouse, P. Smielewski, Z. Czosnyka, P. Kirkpatrick, S. Piechnik, and J. D. Pickard, "Significance of intracranial pressure waveform analysis after head injury," Acta Neurochir. (Wien)., vol. 138, no. 5, pp. 531–542, 1996, doi: 10.1007/BF01411173.

[6] E. R. Cardoso, J. O. Rowan, and S. Galbraith, "Analysis of the cerebrospinal fluid pulse wave in intracranial pressure," J. Neurosurg., vol. 59, no. 5, pp. 817–821, Nov. 1983, doi: 10.3171/jns.1983.59.5.0817.

[7] C. S. Robertson, R. K. Narayan, C. F. Contant, R. G. Grossman, Z. L. Gokaslan, R. Pahwa, P. Caram Jr, R. S. Bray, and A. M. Sherwood, "Clinical experience with a continuous monitor of intracranial compliance," J. Neurosurg., vol. 71, no. 5 Pt 1, pp. 673–680, Nov. 1989, doi: 10.3171/jns.1989.71.5.0673.

[8] C. G. Nucci, P. De Bonis, A. Mangiola, P. Santini, M. Sciandrone, A. Risi, and C. Anile, "Intracranial pressure wave morphological classification: automated analysis and clinical validation," Acta Neurochir. (Wien)., vol. 158, no. 3, pp. 581–588, Mar. 2016, doi: 10.1007/s00701-015-2672-5.

[9] Brain Trauma Foundation, American Association of Neurological Surgeons, Congress of Neurological Surgeons, "Guidelines for the management of severe traumatic brain injury," J. Neurotrauma, vol. 24 Suppl 1, pp. S1-106, doi: 10.1089/neu.2007.9999.

[10] S. M. Bishop and A. Ercole, "Multi-scale peak and trough detection optimised for periodic and quasi-periodic neuroscience data," Acta Nerochirurgica Suppl., vol. 126, pp. 189–195, 2018, doi: 10.1007/978-3-319-65798-1_39.

[11] C. Mataczynski, A. Kazimierska, A. Uryga, M. Burzynska, A. Rusiecki, and M. Kasprowicz, "End-to-end automatic morphological classification of intracranial pressure pulse waveforms using deep learning," IEEE J. Biomed. Health Inform., June 2021, published online ahead of print, doi: 10.1109/JBHI.2021.3088629.

[12] L. Calviello, J. Donelly, D. Cardim, C. Robba, F. A. Zeiler, P. Smielewski, and M. Czosnyka, "Compensatory-reserve-weighted intracranial pressure and its association with outcome after traumatic brain injury," Neurocrit. Care, vol. 28, no. 2, pp. 212–220, Apr. 2018, doi: 10.1007/s12028-017-0475-7.

[13] L. A. Steiner, M. Balestreri, A. J. Johnston, J. P. Coles, P. Smielewski, J. D. Pickard, D. K. Menon, M. Czosnyka, "Predicting the response of intracranial pressure to moderate hyperventilation'," Acta Neurochir. (Wien)., vol. 147, no. 5, pp. 477–483, May 2005, doi: 10.1007/s00701-005-0510-x.

[14] M. Czosnyka and G. Citerio, "Brain compliance: the old story with a new 'et cetera,'" Intensive Care Med., vol. 38, no. 6, pp. 925–927, June 2012, doi: 10.1007/s00134-012-2572-6.

[15] C. Hawthorne and I. Piper, "Monitoring of intracranial pressure in patients with traumatic brain injury," Front. Neurol., vol. 5, pp. 121, July 2014, doi: 10.3389/fneur.2014.00121.

[16] M. Czosnyka, P. Smielewski, I. Timofeev, A. Lavinio, E. Guazzo, P. Hutchinson, and J. D. Pickard, "Intracranial pressure: more than a number," Neurosurg. Focus, vol. 22, no. 5, p. E10, May 2007, doi: 10.3171/foc.2007.22.5.11.

[17] M. Imhoff and S. Kuhls, "Alarm algorithms in critical monitoring," Anesth. Analg., vol. 102, no. 5, pp. 1525–1537, May 2006, doi: 10.1213/01.ane.0000204385.01983.61.

Intracranial Pressure Pulse Morphology-based Definition of Life-threatening Intracranial Hypertension Episodes

Cyprian Mataczyński[1], Agnieszka Kazimierska[2], Agnieszka Uryga[2], Magdalena Kasprowicz[2], and CENTER-TBI High-resolution substudy participants and investigators

***Abstract*— Intracranial hypertension (IH) is associated with poor outcome in traumatic brain injury (TBI) patients and must be avoided to prevent secondary brain injury. In clinical practice the most common method of IH detection is the calculation of the mean value of intracranial pressure (ICP) and the therapeutic intervention is usually introduced when the mean exceeds a certain threshold. This threshold, however, is rather individual for each patient than universal for all. Impaired cerebrovascular reactivity and reduced intracranial compliance are associated with raised ICP. This work explores a new definition of life-threatening hypertension (LTH) which accounts for the state of cerebral compliance. In the proposed method, changes in compliance are analysed through identification of likely pathological and/or pathological shapes of ICP pulse waveforms using a neural network. In terms of predictive power for mortality in TBI, detection of both shape clasess of ICP pulse waveforms during raised ICP offers similar results to previously proposed LTH definition accounting for the state of cerebrovascular reactivity (77.8% vs 76.9% accuracy, respectively). On the other hand, the fully pathological shapes of ICP pulses are present during ICP rises almost only in recordings of patients who died: out of 216 analysed patients only 6% of surviving and as many as 42% of deceased patients developed this type of LTH event. The stricter definition of LTH events including only pathological shape of ICP pulses presents the highest accuracy among the analysed approaches for mortality prediction (87.9%).**

***Clinical relevance*—Reliable detection of potentially life-threatening episodes of ICP elevation offers the possibility of improving clinical management of TBI by identifying the patients at risk of unfavourable outcome.**

I. INTRODUCTION

Intracranial hypertension (IH) is usually defined as sustained elevation of intracranial pressure (ICP) above a certain threshold (20 or 22 mm Hg) lasting more than 5 minutes. However, an increase in mean ICP above a fixed value does not always indicate the need for immediate intervention as the precise ICP threshold and event length above which the patient requires treatment are still unknown.

As recent studies demonstrated that both the magnitude of ICP elevation and its duration are associated with worse outcome [1], a metric that accounts for the cumulative extent of IH episodes has been proposed [2]. In this approach, the pressure-time dose (PTD) is calculated as the area under the ICP curve above a certain threshold. It has also been shown that IH is poorly tolerated in patients with impaired cerebrovascular autoregulation and cerebrovascular reactivity status should be considered jointly with ICP levels [3]. Consequently, Lee et al. [4] introduced a new concept of life-threatening hypertension (LTH) that accounts for the findings described above. In order to recognize potentially dangerous IH events, the proposed method incorporates identification of IH and evaluation of cerebrovascular reactivity based on the pressure reactivity index (PRx) calculated from relative slow changes in mean arterial blood pressure (ABP) and mean ICP [5].

However, impaired cerebrovascular reactivity is not the only complication accompanying ICP elevation. Reduced cerebrospinal compliance, defined as diminished ability of the craniospinal system to buffer changes in volume, is a major risk factor for disproportionate ICP increases in TBI patients [6]. As patients with decreased compliance may be exposed to greater increase in ICP from a given increase in volume than patients with normal compliance, the combined analysis of PTD and intracranial compliance may be crucial in detecting LTH episodes. Although several approaches have been proposed so far for compliance estimation, direct assessment requires potentially dangerous modification of intracranial volume and does not allow for continuous evaluation [7], [8]. In this study we used an indirect method based on the analysis of cardiac-induced oscillations in the ICP signal, called the ICP pulse waveform. In this approach, a naturally occurring pulsatile increment in cerebral blood volume associated with each heartbeat is used as a substitute for volumetric manipulation and the change in ICP pulse shape is analysed as the system's response to the change in volume. This method is free of any added risks to the patient as it is not additionally invasive and it has been validated in studies on cerebrospinal compliance [9], [10]. Using a recently developed deep learning algorithm for morphological classification of ICP pulse waveforms based on artificial neural network [11], we tested the hypothesis that an LTH event can be detected by simultaneous analysis of ICP rises and the state of cerebrospinal compliance

This work was supported by the National Science Centre, Poland (grant no UMO-2019/35/B/ST7/00500). Data used in preparation of this manuscript were obtained in the context of CENTER-TBI, a large collaborative project with the support of the European Union 7th Framework program (EC grant 602150). The funders had no role in study design or preparation of this submission.

[1]Cyprian Mataczyński (corresponding author) is with the Department of Computer Engineering, Faculty of Information and Communication Technology, Wroclaw University of Science and Technology, Wroclaw, Poland. cyprian.mataczynski@pwr.edu.pl

[2]A. Kazimierska, A. Uryga, and M. Kasprowicz are with the Department of Biomedical Engineering, Faculty of Fundamental Problems of Technology, Wroclaw University of Science and Technology, Wroclaw, Poland. agnieszka.kazimierska@pwr.edu.pl, agnieszka.uryga@pwr.edu.pl, magdalena.kasprowicz@pwr.edu.pl

estimated based on changes in ICP pulse shape. Pressure reactivity- and morphology-based LTH definitions as well as their combination were investigated in the context of their association with mortality in TBI patients.

II. METHODOLOGY

A. Data acquisition

Data collected in 282 TBI patients as part of the high-resolution CENTER-TBI project [12], [13] was selected for analysis in the presented work (version CENTER Core 3.0). The use of these data has been approved officially by the CENTER-TBI committee (approval number 359). 37 patients (13%) were excluded due to external ventricular drains and 29 patients (10%) because of craniectomy performed before the start of monitoring. Aditionally, one patient was removed due to very short ICP recording (less than 5 minutes). Final dataset included 216 recordings of ICP and ABP signals. ICP was acquired using an intraparenchymal strain gauge probe (Codman ICP MicroSensor, Codman & Shurtleff Inc., Raynham, MA) or parenchymal fiber optic pressure sensor (Camino ICP Monitor, Integra Life Sciences, Plainsboro, NJ). ABP was obtained through either radial or femoral arterial lines connected to pressure transducers (Baxter Healthcare Corp. CardioVascular Group, Irvine, CA). All signals were recorded with sampling frequency of 100 Hz or higher using ICM+ software (Cambridge Enterprise Ltd., Cambridge, UK) or Moberg CNS Monitor (Moberg Research Inc., Ambler, PA). Data for the CENTER-TBI study has been collected through the Quesgen e-CRF (Quesgen Systems Inc, USA), hosted on the INCF platform and extracted via the INCF Neurobot tool (INCF, Sweden).

The CENTER-TBI study (EC grant 602150) has been conducted in accordance with all relevant laws of the EU if directly applicable or of direct effect and all relevant laws of the country where the Recruiting sites were located, including but not limited to, the relevant privacy and data protection laws and regulations (the "Privacy Law"), the relevant laws and regulations on the use of human materials, and all relevant guidance relating to clinical studies from time to time in force including, but not limited to, the ICH Harmonised Tripartite Guideline for Good Clinical Practice (CPMP/ICH/135/95) ("ICH GCP") and the World Medical Association Declaration of Helsinki entitled "Ethical Principles for Medical Research Involving Human Subjects". Informed Consent by the patients and/or the legal representative/next of kin was obtained, accordingly to the local legislations, for all patients recruited in the Core Dataset of CENTER-TBI and documented in the e-CRF. Ethical approval was obtained for each recruiting site and the list of approvals is available on `https://www.center-tbi.eu/project/ethical-approval`.

The analysed cohort included 50 females and 166 males with median age of 51 [29–62] years. 13 patients (6%) underwent craniectomy after the start of monitoring; in those patients only the part of the signals recorded before surgery was analysed. The patients were divided into surviving and deceased group based on their ICU discharge status. In the final dataset, 26 patients (12%) died in the ICU. Median recording time was 135 [114–207] hours.

B. Signal processing and morphological classification of ICP pulse waveforms

Prior to analysis, all recordings were cut to include only those parts where both the ICP and ABP signals were available. Manually annotated artifacts and invalid values within the data were replaced by the median of their immediate surroundings.

Modified Scholkmann algorithm [14] was used for ICP pulse onset detection and resulting pulses were scaled to interval 0–1 and resampled to uniform length of 180 samples before classification. Classification of ICP pulse waveforms was performed using a Residual Neural Network model trained to assign individual pulse waveforms to one of five types: four morphological classes or artifacts (see Figure 1). The first four classes (as proposed in [15]) represent the progressive change from normal waveform with three characteristic local maxima to pathologically rounded waveform associated with decreased brain compliance. The last class is reserved for local artifacts such as distorted waveforms or errors in pulse onset detection and serves as an additional filtering tool. The algorithm is described in detail in [11].

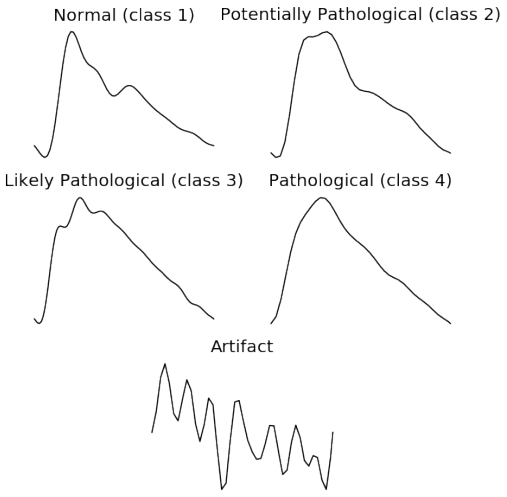

Fig. 1: Examples of intracranial pressure pulse waveforms annotated by the classification model

C. Identification of IH and LTH episodes

IH episodes were identified as parts of the recording where mean ICP in 5 minute window was greater than 20 mm Hg. If the IH episode started within 5 minutes of the end of the previous episode, both episodes were merged into one. The following metrics were calculated for each detected IH episode: PTD, dominant class of ICP pulse waveform, and mean PRx. PTD measured in $mmHg*hour$, was defined as the area between the constant threshold line of 20 mm Hg and the raw ICP curve for the whole IH event [1]. Dominant class of ICP pulse waveform was defined as the class with the highest incidence within the IH event excluding pulses

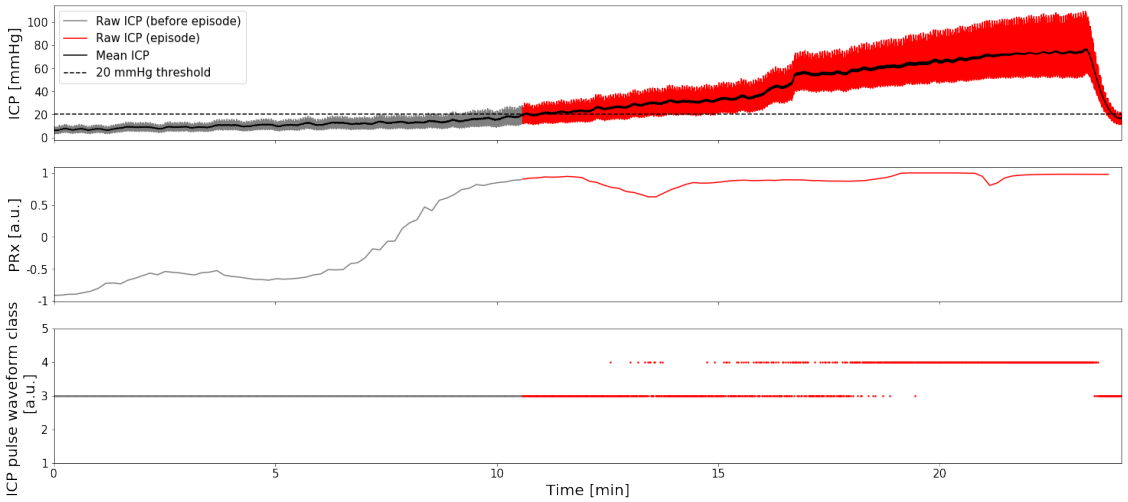

Fig. 2: Illustrative example of an IH episode identified as PTD >5 and class 3+4.

marked by the model as artifacts. PRx was calculated in 5 minute windows (window shift: 10 seconds) as the Pearson correlation coefficient between mean ICP and mean ABP obtained from non-overlapping 10-seconds-long windows [5].

LTH episodes were identified using three approaches. The reference definition was based only on PTD >5. The second approach, described in [4], defined the LTH event as an IH episode with PTD >5 and PRx >0. In the third approach we defined the morphology-based LTH event as an IH episode with PTD >5 and pathologically changed ICP pulse waveform. Two versions of this approach were tested: one including both likely pathological and pathological waveforms (class 3 and 4) and the second including only pathological waveforms of class 4. An illustrative example of an LTH episode with traces of PRx and ICP pulse waveform class is presented in Figure 2. All LTH definitions were compared in terms of event incidence in surviving versus deceased patient groups. Additionally, the influence of adding a PRx threshold of 0 (previously identified as having the most predictive power [4]) on morphology-based LTH detection was analysed. Statistical analysis was performed using MedCalc Software Ltd [16].

III. RESULTS

In the full dataset, at least one IH episode was detected in 193 patients (90%). Out of 23 patients (10%) who did not exhibit any IH events throughout the whole recording, 4 (2%) died in the ICU.

The incidence of different LTH events, assessed as the percentage of patients who presented at least one LTH event of given type during the whole recording, is presented in Figure 3a. LTH events defined as PTD >5 and class 3+4, while less frequent than PTD >5 and PRx >0, showed a similar performance in distinguishing between surviving and deceased patients. LTH episodes identified using the stricter morphological definition (PTD >5 and only pathological waveforms of class 4) were almost non-existent in the data from surviving patients, amounting to less than 1% of all IH episodes in that group (Figure 3b). This is confirmed by the data shown in Table I. While all prediction scores were similar for PTD >5 with PRx >0 and PTD >5 with class 3+4, the comparison with PTD >5 and class 4 shows that not only did the stricter definition have higher overall accuracy, but also much higher specificity.

The addition of PRx >0 to PTD >5 and PTD >5 with class 3+4 definitions led to an increase in accuracy in predicting the patient's ICU outcome of approximately 5%, associated with increased specificity and little to no change in sensitivity. On the other hand, the inclusion of PRx >0 resulted in only marginal changes for PTD >5 with class 4 (mainly, 0.5% increase in accuracy).

IV. DISCUSSION

In this study we compared the performance of reactivity-based LTH definition in predicting mortality of TBI patients with a different approach that includes information about the state of cerebrospinal compliance represented by the shape of ICP pulse waveform. Our results show that the incidence of LTH events identified using either the reactivity- or morphology-based definition distinguished deceased vs. surviving patients with over 70% accuracy. However, while the episodes detected with the reactivity-based and morphology-based definition including two ICP pulse waveform classes were balanced predictors with comparable sensitivity and specificity, the stricter morphology-based definition which considered only pathological ICP waveforms of class 4 as an indicator of decreased compliance allowed for high confidence in declaring the IH episode as life-threatening as this type of events rarely occured in patients who survived in the ICU. Furthermore, its predictive power was not influenced significantly by the inclusion of PRx which has a practical implication on potential real-time monitoring as this definition requires only the ICP signal.

One of the acknowledged limitations of existing methods of predicting elevated ICP is their reliance on relatively

a

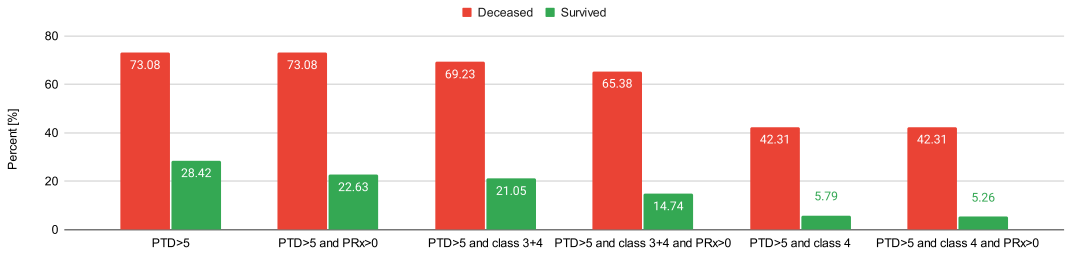

b

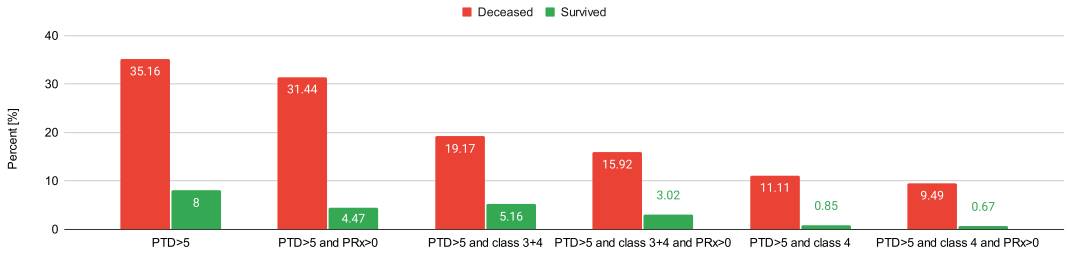

Fig. 3: Comparison of incidence of each LTH event type found in patients' ICP recordings in the survived vs deceased group. The values were obtained as the percentage of patients who developed at least one LTH event in the whole dataset (a) and as the percentage of events identified as LTH in the whole set of detected IH episodes aggregated from all patients (b).

TABLE I: Performance of each LTH event type as predictor of mortality in the ICU. A true positive is defined as a patient who exhibited at least one LTH episode and died in the ICU. Data are expressed as percentages with 95% confidence intervals. SE – Sensivity, SP – Specificity, PPV – Positive Predictive Value, NPV – Negative Predictive Value, Acc – Accuracy.

	PTD>5	PTD>5 and PRx>0	PTD>5 and class 3+4	PTD>5 and class 3+4 and PRx>0	PTD>5 and class 4	PTD>5 and class 4 and PRx>0
SE	73.1 (52.2–88.4)	73.1 (52.2–88.4)	69.2 (48.2–85.7)	65.4 (44.3–82.8)	42.3 (23.4–63.1)	42.3 (23.6–63.1)
SP	71.6 (64.6–77.9)	77.4 (70.8–83.1)	78.9 (72.5–84.5)	85.3 (79.4–89.9)	94.2 (89.9–97.1)	94.7 (90.5–97.5)
PPV	26.0 (20.3–32.7)	30.7 (23.7–38.6)	31.0 (23.6–39.6)	37.8 (28.1–48.6)	50.0 (32.6–67.4)	52.4 (34.2–70.0)
NPV	95.1 (91.1–97.4)	95.5 (91.7–97.6)	94.9 (91.3–97.1)	94.7 (91.4–98.8)	92.3 (89.6–94.3)	92.3 (89.6–94.4)
Acc	71.8 (65.3–77.7)	76.9 (70.7–82.3)	77.8 (71.6–83.1)	82.9 (77.2–87.6)	87.9 (82.9–91.9)	88.4 (83.4–92.4)

simple IH definitions with set thresholds for mean ICP and episode duration which in turn makes them prone to false alarms. The combination of the PTD-based approach with morphological analysis of the ICP pulse waveform could potentially be used as a basis for a more sophisticated model predicting the occurrence of clinically-relevant IH events and therefore improve the chances of preventing secondary insults leading to worse outcomes.

However, it has to be noted that this work was performed as a retrospective analysis in a highly unbalanced dataset with low percentage of patients who died in the ICU. Further prospective studies are required to fully assess the performance of proposed LTH definitions in predicting mortality in TBI patients. Additionally, as we did not investigate in detail the influence of PTD and PRx thresholds on morphology-based LTH detection but used the thresholds proposed for reactivity-based analysis for comparison purposes, this factor should be examined. Our previous study showed that normalization of ICP pulse waveforms improves classification accuracy. However, the potential usefullness of ICP pulse amplitude as an additional parameter in LTH detection should also be explored in further studies. Lastly, in this study we did not consider the effect of ageing on the shape of ICP pulse waveforms.

CONTRIBUTIONS

CM, MK contributed to the study conception and design. Data analysis and results interpretation was performed by AK, AU, CM, MK. The first draft of the article was written by CM, AK and all authors contributed to article editing. All authors read and approved the final manuscript.

ACKNOWLEDGMENTS

We acknowledge the work of The Collaborative European Neurotrauma Effectiveness Research in Traumatic Brain Injury (CENTER-TBI) High-resolution substudy participants and investigators:

Audny Anke[1], Ronny Beer[2], BoMichael Bellander[3], Erta Beqiri[4], Andras Buki[5], Manuel Cabeleira[6], Marco Carbonara[7], Arturo Chieregato[4], Giuseppe Citerio[8,9], Hans Clusmann[10], Endre Czeiter[11], Marek Czosnyka[6], Bart Depreitere[12], Ari Ercole[13], Shirin Frisvold[14], Raimund Helbok[2], Stefan Jankowski[15], Daniel Kondziella[16], Lars-Owe Koskinen[17], Ana Kowark[18], David Menon[13], Geert Meyfroidt[19], Kirsten Moeller[20], David Nelson[3], Anna Piippo-Karjalainen[21], Andreea Radoi[22], Arminas Ragauskas[23], Rahul Raj[21], Jonathan Rhodes[24], Saulius Rocka[23], Rolf Rossaint[18], Juan Sahuquillo[22], Oliver Sakowitz[25,26], Peter Smielewski[6], Nino Stocchetti[27], Nina Sundström[28], Riikka Takala[29], Tomas Tamosuitis[30], Olli Tenovuo[31], Andreas Unterberg[26], Peter Vajkoczy[32], Alessia Vargiolu[8], Rimantas Vilcinis[33], Stefan Wolf[34], Alexander Younsi[26], Frederick A. Zeiler[13,35].

[1]Department of Physical Medicine and Rehabilitation, University hospital Northern Norway [2]Department of Neurology, Neurological Intensive Care Unit, Medical University of Innsbruck, Innsbruck, Austria [3]Department of Neurosurgery & Anesthesia & intensive care medicine, Karolinska University Hospital, Stockholm, Sweden [4]NeuroIntensive Care, Niguarda Hospital, Milan, Italy [5]Department of Neurosurgery, Medical School, University of Pécs, Hungary and Neurotrauma Research Group, János Szentágothai Research Centre, University of Pécs, Hungary [6]Brain Physics Lab, Division of Neurosurgery, Dept of Clinical Neurosciences, University of Cambridge, Addenbrooke's Hospital, Cambridge, UK [7]Neuro ICU, Fondazione IRCCS Cà Granda Ospedale Maggiore Policlinico, Milan, Italy [8]NeuroIntensive Care Unit, Department of Anesthesia & Intensive Care, ASST di Monza, Monza, Italy [9]School of Medicine and Surgery, Università Milano Bicocca, Milano, Italy [10]Department of Neurosurgery, Medical Faculty RWTH Aachen University, Aachen, Germany [11]Department of Neurosurgery, University of Pécs and MTA-PTE Clinical Neuroscience MR Research Group and János Szentágothai Research Centre, University of Pécs, Hungarian Brain Research Program (Grant No. KTIA 13 NAP-A-II/8), Pécs, Hungary [12]Department of Neurosurgery, University Hospitals Leuven, Leuven, Belgium [13]Division of Anaesthesia, University of Cambridge, Addenbrooke's Hospital, Cambridge, UK [14]Department of Anesthesiology and Intensive care, University Hospital Northern Norway, Tromso, Norway [15]Neurointensive Care, Sheffield Teaching Hospitals NHS Foundation Trust, Sheffield, UK [16]Departments of Neurology, Clinical Neurophysiology and Neuroanesthesiology, Region Hovedstaden Rigshospitalet, Copenhagen, Denmark [17]Department of Clinical Neuroscience, Neurosurgery, Umeå University, Umeå, Sweden [18]Department of Anaesthesiology, University Hospital of Aachen, Aachen, Germany [19]Intensive Care Medicine, University Hospitals Leuven, Leuven, Belgium [20]Department Neuroanesthesiology, Region Hovedstaden Rigshospitalet, Copenhagen, Denmark [21]Helsinki University Central Hospital, Helsinki, Finland [22]Department of Neurosurgery, Vall d'Hebron University Hospital, Barcelona, Spain [23]Department of Neurosurgery, Kaunas University of technology and Vilnius University, Vilnius, Lithuania [24]Department of Anaesthesia, Critical Care & Pain Medicine NHS Lothian & University of Edinburg, Edinburgh, UK [25]Klinik für Neurochirurgie, Klinikum Ludwigsburg, Ludwigsburg, Germany [26]Department of Neurosurgery, University Hospital Heidelberg, Heidelberg, Germany [27]Department of Pathophysiology and Transplantation, Milan University, and Neuroscience ICU, Fondazione IRCCS Cà Granda Ospedale Maggiore Policlinico, Milano, Italy [28]Department of Radiation Sciences, Biomedical Engineering, Umeå University, Umeå, Sweden [29]Perioperative Services, Intensive Care Medicine, and Pain Management, Turku University Central Hospital and University of Turku, Turku, Finland [30]Neuro-intensive Care Unit, Kaunas University of Health Sciences, Kaunas, Lithuania [31]Rehabilitation and Brain Trauma, Turku University Central Hospital and University of Turku, Turku, Finland [32]Neurologie, Neurochirurgie und Psychiatrie, Charité – Universitätsmedizin Berlin, Berlin, Germany [33]Department of Neurosurgery, Kaunas University of Health Sciences, Kaunas, Lithuania [34]Department of Neurosurgery, Charité – Universitätsmedizin Berlin, corporate member of Freie Universität Berlin, Humboldt-Universität zu Berlin, and Berlin Institute of Health, Berlin, Germany [35]Section of Neurosurgery, Department of Surgery, Rady Faculty of Health Sciences, University of Manitoba

REFERENCES

[1] A. Vik, T. Nag, O. A. Fredriksli, T. Skandsen, K. G. Moen, K. Schirmer-Mikalsen, and G. T. Manley, "Relationship of "dose" of intracranial hypertension to outcome in severe traumatic brain injury," *Journal of neurosurgery*, vol. 109, no. 4, pp. 678–684, 2008.

[2] S. Kahraman, R. P. Dutton, P. Hu, Y. Xiao, B. Aarabi, D. M. Stein, and T. M. Scalea, "Automated measurement of "pressure times time dose" of intracranial hypertension best predicts outcome after severe traumatic brain injury," *Journal of Trauma and Acute Care Surgery*, vol. 69, no. 1, pp. 110–118, 2010.

[3] C. A. Åkerlund, J. Donnelly, F. A. Zeiler, R. Helbok, A. Holst, M. Cabeleira, F. Güiza, G. Meyfroidt, M. Czosnyka, P. Smielewski, *et al.*, "Impact of duration and magnitude of raised intracranial pressure on outcome after severe traumatic brain injury: A center-tbi high-resolution group study," *PloS one*, vol. 15, no. 12, p. e0243427, 2020.

[4] H.-J. Lee, H. Kim, Y.-T. Kim, K. Won, M. Czosnyka, and D.-J. Kim, "Prediction of life-threatening intracranial hypertension during the acute phase of traumatic brain injury using machine learning," *IEEE journal of biomedical and health informatics*, vol. 25, no. 10, pp. 3967–3976, 2021.

[5] M. Czosnyka, Z. Czosnyka, and P. Smielewski, "Pressure reactivity index: journey through the past 20 years," *Acta neurochirurgica*, vol. 159, no. 11, pp. 2063–2065, 2017.

[6] T. Heldt, T. Zoerle, D. Teichmann, and N. Stocchetti, "Intracranial pressure and intracranial elastance monitoring in neurocritical care," *Annual review of biomedical engineering*, vol. 21, pp. 523–549, 2019.

[7] A. Marmarou, K. Shulman, and J. Lamorgese, "Compartmental analysis of compliance and outflow resistance of the cerebrospinal fluid system," *Journal of neurosurgery*, vol. 43, no. 5, pp. 523–534, 1975.

[8] J. Miller and J. Garibi, "Intracranial volume/pressure relationships during continuous monitoring of ventricular fluid pressure," in *Intracranial pressure*, pp. 270–274, Springer, 1972.

[9] A. Kazimierska, M. Kasprowicz, M. Czosnyka, M. M. Placek, O. Baledent, P. Smielewski, and Z. Czosnyka, "Compliance of the cerebrospinal space: comparison of three methods," *Acta Neurochirurgica*, vol. 163, no. 7, pp. 1979–1989, 2021.

[10] A. Ziółkowski, A. Pudełko, A. Kazimierska, M. Czosnyka, Z. Czosnyka, and M. Kasprowicz, "Analysis of relative changes in pulse shapes of intracranial pressure and cerebral blood flow velocity during infusion test," *Physiological Measurement*, 2021.

[11] C. Mataczynski, A. Kazimierska, A. Uryga, M. Burzynska, A. Rusiecki, and M. Kasprowicz, "End-to-end automatic morphological classification of intracranial pressure pulse waveforms using deep learning," *IEEE Journal of Biomedical and Health Informatics*, pp. 1–1, 2021.

[12] A. I. Maas, D. K. Menon, E. W. Steyerberg, G. Citerio, F. Lecky, G. T. Manley, S. Hill, V. Legrand, and A. Sorgner, "Collaborative european neurotrauma effectiveness research in traumatic brain injury (center-tbi) a prospective longitudinal observational study," *Neurosurgery*, vol. 76, no. 1, pp. 67–80, 2015.

[13] E. W. Steyerberg, E. Wiegers, C. Sewalt, A. Buki, G. Citerio, V. De Keyser, A. Ercole, K. Kunzmann, L. Lanyon, F. Lecky, *et al.*, "Case-mix, care pathways, and outcomes in patients with traumatic brain injury in center-tbi: a european prospective, multicentre, longitudinal, cohort study," *The Lancet Neurology*, vol. 18, no. 10, pp. 923–934, 2019.

[14] S. M. Bishop and A. Ercole, "Multi-scale peak and trough detection optimised for periodic and quasi-periodic neuroscience data," in *Intracranial Pressure & Neuromonitoring XVI*, pp. 189–195, Springer, 2018.

[15] C. G. Nucci, P. De Bonis, A. Mangiola, P. Santini, M. Sciandrone, A. Risi, and C. Anile, "Intracranial pressure wave morphological classification: automated analysis and clinical validation," *Acta neurochirurgica*, vol. 158, no. 3, pp. 581–588, 2016.

[16] "Medcalc software ltd. diagnostic test evaluation calculator.." `https://www.medcalc.org/calc/diagnostic_test.php`. (Version 20.023; accessed January 4, 2022).

Appendix B

CURRICULUM VITAE

EDUCATION

Doctoral studies in Biomedical engineering **October 2016–present**
Wrocław University of Science and Technology

Master of Science in Biomedical engineering **February 2015–July 2016**
Wrocław University of Science and Technology
Graduated with distinctions

Bachelor of Science in Biomedical engineering **October 2011–January 2015**
Wrocław University of Science and Technology
Graduated with distinctions

RESEARCH PROJECTS

Investigator in research grant (PhD student) **October 2020–present**
Development of brain compliance monitoring methods by means of intracranial pressure pulse waveform analysis in traumatic brain injury
Project leader: Magdalena Kasprowicz, PhD, DSc
National Science Centre, Poland
OPUS grant no UMO-2019/35/B/ST7/00500

Investigator in research grant (Master's student) **October 2015–June 2016**
Analysis of dynamic cerebral autoregulation in joint time and frequency domain
Project leader: Magdalena Kasprowicz, PhD, DSc
National Science Centre, Poland
SONATA BIS grant no UMO-2013/10/E/ST7/00117

INTERNSHIPS

Academic internship at Brain Physics Laboratory
University of Cambridge, Cambridge, United Kingdom

- 1–19.03.2020 (suspended due to the COVID-19 pandemic; continued online)
- 15.11.2021–04.02.2022 (continuation)

Supervisor: prof. Marek Czosnyka
Funded by the International Academic Partnerships programme
National Agency for Academic Exchange, Poland

INTERNATIONAL COLLABORATION

- **University of Cambridge, Cambridge, United Kingdom**
  Brain Physics Laboratory: prof. Marek Czosnyka and team
- **Toulouse University Hospital, Toulouse, France**
  dr Eric Schmidt and team

ARTICLES IN PEER REVIEWED JOURNALS

1. Mataczyński, C.*, **Kazimierska, A.***, Uryga, A., Burzyńska, M., Rusiecki, A., and Kasprowicz, M. (2022). End-to-end automatic morphological classification of intracranial pressure pulse waveforms using deep learning. *IEEE Journal of Biomedical and Health Informatics*, 26(2):494–504. ***joint first authorship**; IF: 5.772, MEiN: 140 points

   Input: selected retrospective data and prepared the training datasets; contributed to preparation of classification models and computational algorithms; contributed to results analysis, including statistical analysis; contributed to preparation and editing of the manuscript; prepared response to reviewers and manuscript revisions according to reviewers' comments

2. Ziółkowski, A., Pudełko, A., **Kazimierska, A.**, Czosnyka, Z., Czosnyka, M., and Kasprowicz, M. (2021). Analysis of relative changes in pulse shapes of intracranial pressure and cerebral blood flow velocity. *Physiological Measurement*, 42(12):125004. IF: 2.833, MEiN: 100 points

   Input: contributed to preparation of computational algorithms and results analysis; contributed to preparation and editing of the manuscript; contributed to preparation of response to reviewers

3. **Kazimierska, A.***, Ziółkowski, A.*, Kasprowicz, M., Lalou, D. A., Czosnyka, Z., and Czosnyka, M. (2021). Mathematical modelling in hydrocephalus. *Neurology India*, 69 (Supplement):S275–S282. ***joint first authorship**; IF: 2.117, MEiN: 40 points

   Input: performed literature review; prepared and edited the manuscript

4. **Kazimierska, A.**, Kasprowicz, M., Czosnyka, M., Placek, M. M., Baledent, O., Smielewski, P., and Czosnyka, Z. (2021). Compliance of the cerebrospinal space: comparison of three methods. *Acta Neurochirurgica*, 163(7):1979–1989. IF: 2.216, MEiN: 100 points

   Input: selected retrospective data; prepared computational algorithms and performed results analysis, including statistical analysis; prepared and edited the manuscript (corresponding author); prepared response to reviewers and manuscript revisions according to reviewers' comments

5. **Kazimierska, A.**, Placek, M. M., Uryga, A., Wachel, P., Burzyńska, M., and Kasprowicz, M. (2019). Assessment of baroreflex sensitivity using time–frequency analysis during postural change and hypercapnia. *Computational and Mathematical Methods in Medicine*, 2019:4875231. IF: 1.770, MEiN: 40 points

   Input: selected retrospective data; prepared computational algorithms and performed results analysis, including statistical analysis; prepared and edited the manuscript (corresponding author); prepared response to reviewers and manuscript revisions according to reviewers' comments

6. Uryga, A., Burzyńska, M., Tabakow, P., Kasprowicz, M., Budohoski, K. P., **Kazimierska, A.**, Smielewski, P., Czosnyka, M., and Goździk, W. (2018). Baroreflex sensitivity and heart rate variability are predictors of mortality in patients with aneurysmal subarachnoid haemorrhage. *Journal of the Neurological Sciences*, 394:112–119. IF: 2.651, MEiN: 70 points

   Input: contributed to results analysis; contributed to preparation and editing of the manuscript

ARTICLES IN PEER REVIEWED CONFERENCE PROCEEDINGS

1. Mataczyński, C., **Kazimierska, A.**, Uryga, A., Kasprowicz, M., and CENTER-TBI high resolution sub-study participants and investigators. Intracranial pressure pulse morphology-based definition of life-threatening intracranial hypertension episodes. Accepted for publication at *44th Annual International Conference of the IEEE Engineering in Medicine & Biology Society (EMBC 2022)*, 11–15.07.2022, Glasgow, United Kingdom

   Input: contributed to results analysis; contributed to preparation and editing of the manuscript, including revisions according to reviewers' comments

2. **Kazimierska, A.**, Mataczyński, C., Uryga, A., Burzyńska, M., Rusiecki, A., and Kasprowicz, M. (2022). Analysis of the relationship between intracranial pressure pulse waveform and outcome in traumatic brain injury. In: Piaseczna, N., Gorczowska, M., Łach, A. (eds) *Innovations and Developments of Technologies in Medicine, Biology and Healthcare. EMBS ISC 2020* (p. 52–57). Springer, Cham. MEiN: 20 points

Input: selected retrospective data; contributed to preparation of classification models and computational algorithms; contributed to results analysis, including statistical analysis; prepared and edited the manuscript (corresponding author)

3. **Kazimierska, A.**, Uryga, A., Mataczyński, C., Burzyńska, M., Ziółkowski, A., Rusiecki, A., and Kasprowicz, M. (2021). Analysis of the shape of intracranial pressure pulse waveform in traumatic brain injury patients. In: *2021 43rd Annual International Conference of the IEEE Engineering in Medicine & Biology Society (EMBC)* (p. 546–549). IEEE. MEiN: 20 points

   Input: selected retrospective data; prepared computational algorithms; performed results analysis and contributed to statistical analysis; prepared and edited the manuscript (corresponding author)

4. **Kazimierska, A.**, Kasprowicz, M., Placek, M. M., and Czosnyka, M. (2021). Cerebrovascular impedance during hemodynamic change in rabbits: a pilot study. In: Depreitere, B., Meyfroidt, G., Guiza, F. (eds) *Intracranial Pressure and Neuromonitoring XVII. Acta Neurochirurgica Supplement*, 131 (p. 283–288). Springer, Cham. MEiN: 20 points

   Input: selected retrospective data; prepared computational algorithms; performed results analysis; prepared and edited the manuscript (corresponding author)

5. Kaczmarska, K., Smielewski, P., Kasprowicz, M., **Kazimierska, A.**, Grzanka, A., Czosnyka, Z., and Czosnyka, M. (2021). Analysis of intracranial pressure pulse–pressure relationship: experimental validation. In: Depreitere, B., Meyfroidt, G., Guiza, F. (eds) *Intracranial Pressure and Neuromonitoring XVII. Acta Neurochirurgica Supplement*, 131 (p. 279–282). Springer, Cham. MEiN: 20 points

   Input: contributed to preparation and editing of the manuscript

6. Ziółkowski, A., **Kazimierska, A.**, Czosnyka, M., and Kasprowicz, M. (2021). Analiza zmian podatności mózgowej u pacjentów po urazie czaszkowo–mózgowym podczas umiarkowanej hipokapnii. In: Maciąg, K., Maciąg, M. (eds) *Zdrowie człowieka — profilaktyka, rozpoznawanie i leczenie chorób* (p. 234–258). Wydawnictwo Naukowe TYGIEL, Lublin. MEiN: 20 points

   Input: contributed to results analysis; contributed to preparation and editing of the manuscript

INTERNATIONAL CONFERENCE PRESENTATIONS

1. **Kazimierska, A.**, Uryga, A., Mataczyński, C., Czosnyka, M., Kasprowicz, M., and CENTER-TBI high resolution sub-study participants and investigators. Intracranial pressure pulse shape correlates with outcome in traumatic brain injury: a CENTER-TBI study. Accepted for presentation at *15th International Neurotrauma Symposium (INTS 2022)*, 17–20.07.2022, Berlin, Germany [presenting author]

2. **Kazimierska, A.**, Uryga, A., Mataczyński, C., Burzyńska, M., Ziółkowski, A., Rusiecki, A., and Kasprowicz, M. Analysis of the shape of intracranial pressure pulse waveform in traumatic brain injury patients. *43rd Annual International Conference of the IEEE Engineering in Medicine & Biology Society (EMBC 2021)*, 1–5.11.2021, online [presenting author]

3. Ziółkowski, A., Pudełko, A., **Kazimierska, A.**, Czosnyka, Z., Czosnyka, M., and Kasprowicz, M. Analysis of intracranial pressure pulse waveforms during infusion test. *13th Meeting of the Hydrocephalus Society (Hydrocephalus 2021)*, 10–13.09.2021, online

4. **Kazimierska, A.**, Mataczyński, C., Uryga, A., Burzyńska, M., Rusiecki, A., and Kasprowicz, M. Analysis of the relationship between intracranial pressure pulse waveform and outcome in traumatic brain injury. *IEEE EMBS International Student Conference 2020*, 11–12.12.2020, online [presenting author]

5. **Kazimierska, A.**, Kasprowicz, M., Czosnyka, M., Placek, M. M., Baledent, O., Smielewski, P., and Czosnyka, Z. Assessment of cerebrospinal compliance. *66th Annual Meeting of the Society for Research into Hydrocephalus and Spina Bifida*, 06.11.2020, online [presenting author]

6. **Kazimierska, A.**, Mataczyński, C., Uryga, A., Burzyńska, M., Wachel, P., and Kasprowicz, M. Automated classification of intracranial pressure pulse waveforms. *42nd Annual International Conference of the IEEE Engineering in Medicine & Biology Society (EMBC 2020)*, 20–24.07.2020, online [presenting author]

7. **Kazimierska, A.**, Kasprowicz, M., Placek, M. M., and Czosnyka, M. Cerebrovascular impedance during hemodynamic change in rabbits: a pilot study. *17th International Symposium on Intracranial Pressure and Neuromonitoring (ICP 2019)*, 8–11.09.2019, Leuven, Belgium [presenting author]

8. Kaczmarska, K., Smielewski, P., Kasprowicz, M., **Kazimierska, A.**, Grzanka, A., Czosnyka, Z., and Czosnyka, M., Analysis of intracranial pressure pulse–pressure relationship: experimental validation. *17th International Symposium on Intracranial Pressure and Neuromonitoring (ICP 2019)*, 8–11.09.2019, Leuven, Belgium

9. Uryga, A., Mielczarek, A., Placek, M. M., **Kazimierska, A.**, Wachel, P., and Kasprowicz, M. Influence of respiratory rate on the cerebral autoregulation. *38th Annual International Conference of the IEEE Engineering in Medicine and Biology Society (EMBC 2016)*, 16–20.08.2016, Orlando, FL, USA

NATIONAL CONFERENCE PRESENTATIONS

1. Ziółkowski, A., **Kazimierska, A.**, Czosnyka, M., and Kasprowicz, M. Analiza zmian podatności mózgowej u pacjentów po urazie czaszkowo-mózgowym podczas umiarkowanej hipokapnii. *VII Ogólnopolskie Sympozjum Biomedyczne ESKULAP*, 28–29.11.2020, online

2. **Kazimierska, A.**, Michta, F., Placek, M. M., Uryga, A., Wachel, P., Burzyńska, M., and Kasprowicz, M. Ocena czułości baroreceptorów tętniczych za pomocą analizy czasowo-częstotliwościowej podczas zmiany pozycji ciała w hiperkapnii. *IX Sympozjum Współczesna myśl techniczna w naukach medycznych i biologicznych*, 22–23.06.2018, Wrocław, Poland [presenting author]

3. **Kazimierska, A.**, Uryga, A., Placek, M. M., Wachel, P., and Kasprowicz, M. Baroreflex sensitivity estimation during postural change in joint time and frequency domain. *XX Polish Conference on Biocybernetics and Biomedical Engineering (PCBBE)*, 2022.09.2017, Kraków, Poland [presenting author]

4. Uryga, A., **Kazimierska, A.**, Mielczarek, A., Placek, M. M., Wachel, P., and Kasprowicz, M. The relationship between baroreflex sensitivity and cerebral autoregulation during controlled breathing. *XX Polish Conference on Biocybernetics and Biomedical Engineering (PCBBE)*, 20–22.09.2017, Kraków, Poland

5. Uryga, A., **Kazimierska, A.**, Kasprowicz, M., and Burzyńska, M. Wpływ nadciśnienia tętniczego oraz lokalizacji tętniaka na czułość baroreceptorów tętniczych u osób po krwotoku podpajęczynówkowym z pękniętego tętniaka. *VI Wrocławska Konferencja Studentów Nauk Technicznych i Ścisłych Puzzel 2017*, 1–2.04.2017, Wrocław, Poland

6. **Kazimierska, A.**, Uryga, A., Kasprowicz, M., and Danielewska, M. E. Autoregulation of blood flow in glaucoma. *VI Wrocławska Konferencja Studentów Nauk Technicznych i Ścisłych Puzzel 2017*, 1–2.04.2017, Wrocław, Poland [presenting author]

7. Uryga, A. and **Kazimierska, A.** Effect of body position on baroreflex sensitivity. *14th Students' Science Conference*, 22–25.09.2016, Wrocław, Poland [presenting author]

8. Uryga, A., **Kazimierska, A.**, Burzyńska, M., and Kasprowicz, M. Pomiar czułości baroreceptorów tętniczych u osób po krwotoku podpajęczynówkowym z wykorzystaniem metod czasowo-częstotliwościowej analizy sygnałów. *Innowacyjne Projekty Badawcze*, 2.09.2016, Wrocław, Poland

9. Uryga, A., **Kazimierska, A.**, Placek, M. M., Wachel, P., and Kasprowicz, M. Zależność pomiędzy podatnością naczyń mózgowych a czułością baroreceptorów tętniczych. *VII Sympozjum Współczesna Myśl Techniczna w naukach medycznych i biologicznych*, 24–25.06.2016, Wrocław, Poland

10. Uryga, A., Placek, M. M., **Kazimierska, A.**, Mielczarek, A., Wachel, P., and Kasprowicz, M. Metody czasowo-częstotliwościowe w badaniach autoregulacji mózgowej. *III Ogólnokrajowa Konferencja Młodzi Naukowcy w Polsce — Badania i Rozwój*, 13.04.2016, Wrocław, Poland

11. **Kazimierska, A.**, Uryga, A., Kasprowicz, M., and Wachel, P. Comparison of different methods of baroreflex sensitivity estimation. *V Wrocławska Konferencja Studentów Nauk Technicznych i Ścisłych Puzzel 2016*, 16–17.04.2016, Wrocław, Poland [presenting author]

AWARDS AND DISTINCTIONS

1. Best E-teacher award in the Teacher Award competition organised by the Student Council of the Faculty of Fundamental Problems of Technology, Wrocław University of Science and Technology (2021)

2. Scientific Committee distinction for presentation Kazimierska A., Uryga A., Kasprowicz M., and Danielewska M.E. Autoregulation of blood flow in glaucoma. *VI Wrocławska Konferencja Studentów Nauk Technicznych i Ścisłych Puzzel*, Wrocław, Poland (2017) [presenting author]

3. Scientific Committee distinction for presentation Uryga, A., Kazimierska, A., Kasprowicz, M., Burzyńska, M. Wpływ nadciśnienia tętniczego oraz lokalizacji tętniaka na czułość baroreceptorów tętniczych u osób po krwotoku podpajęczynówkowym z pękniętego tętniaka. *VI Wrocławska Konferencja Studentów Nauk Technicznych i Ścisłych Puzzel*, Wrocław, Poland (2017)

4. Award for best presentation in category *Advancement in biosciences* for presentation Uryga A. and Kazimierska A. Effect of body position on baroreflex sensitivity. *14th Students' Science Conference*, Wrocław, Poland (2016) [presenting author]

5. 7th place in the TOP10 competition for best alumni of the Faculty of Fundamental Problems of Technology, Wrocław University of Science and Technology (2016)

6. Dean's Award for best students of the Faculty of Fundamental Problems of Technology, Wrocław University of Science and Technology (2016)

7. Dean's Distinction for best students of the Faculty of Fundamental Problems of Technology, Wrocław University of Science and Technology (2015)